Parametric Study of Timber Shear Walls

by

Maurice Walter White

Dissertation submitted to the Faculty of the

Virginia Polytechnic Institute and State University

in partial fulfillment of the requirements for the degree of

DOCTOR OF PHILOSOPHY

IN

CIVIL ENGINEERING

APPROVED:

James D. Dolan, Chairman

Siegfried M. Holzer

Joseph R. Loferski

Thomas M. Murray

Frank E. Woeste

August 1995

Blacksburg, Virginia

Key words: Shear wall, seismic, finite element, aspect ratio, openings

PARAMETRIC STUDY OF TIMBER SHEAR WALLS

by

Maurice Walter White

James D. Dolan, Chairman

Civil Engineering

(ABSTRACT)

Timber shear walls comprise the vertical element of the lateral force resisting system in many low–rise buildings in North America. A typical shear wall consists of a solid panel product connected to a light timber frame with either a dowel–type fastener, such as nails, or elastomeric adhesives. Shear walls vary in size, depending on their use in a structure, and sometimes contain openings for windows and doors. These changes in wall configuration have an effect on the response of shear walls.

A parametric study was performed to determine the effect that aspect ratio (ratio of wall length to height) and openings have on the response of timber shear walls subjected to monotonic and seismic loading. Twenty–five shear wall models of various aspect ratios and opening configurations were created and then analyzed using WALSEIZ, a program developed by the author which utilizes finite element analysis to analyze shear wall models. The maximum resistance, initial stiffness, distribution of forces in the wall and at the reactions, and maximum relative drift (ratio of displacement at the top of the wall to wall height), seismic base shear, and velocity and acceleration at the top of the wall were recorded and examined for each model. The results from the parametric study were used to develop a modified design procedure for timber shear walls.

Acknowledgements

It is with the effort of many that the completion of my dissertation was made possible. Therefore, I would like to express my appreciation the persons who assisted me during my doctoral studies.

I would like to first thank my advisor, Dr. James D. Dolan, for all of the support and guidance that he provided and for challenging me during my studies.

I would also like to thank the members of my committee, Dr. Siegfried Holzer, Dr. Joseph Loferski, Dr. Thomas Murray, Dr, Frank Woeste for the advice and assistance they provided.

The assistance provided by Les Fuller and Lon Weber pertaining to computers was greatly appreciated.

Alan Kolba and Dr. Keith Faherty at Marquette University are thanked for providing much needed data for validation of the program used to analyze the shear walls models in the parametric study.

The National Consortium for Graduate Degrees for Minorities in Engineering and Science, Inc. (GEM) and the Charles Minor fellowship committee are thanked first for selecting me as a recipient of their respective fellowships, which I truly consider to be an honor, and also for providing financial support during my studies along with information to enhance my career development.

The United States Department of Agriculture (USDA) is to be thanked for providing financial support for the research project.

Finally, but not least, I would like to thank all of the family, friends, and colleagues for providing the support to make all of this possible.

Dedication

This is dedicated to my parents, Everett and Audrey White, who taught me to always be the best that I can be; to my grandfather, Carthon W. Giles, who showed me that the seemingly impossible can be done; and to all of the people who made this possible.

Table of Contents

List of Tables

List of Figures

List of Variables

$\mathbf{A}$ = Cross–sectional area of framing element.

$\mathbf{a_{1-4}}$ = The ratio of the load intercept to the peak displacement of the hysteresis, $\frac{F_i}{u_i}$.

$\mathbf{b}$ = One–half length of sheathing element in x–direction.

$\mathbf{\tilde{B}_{1-4x}}$ = Derivatives of shape functions with respect to x for the sheathing elements.

$\mathbf{\tilde{B}_{1-4y}}$ = Derivatives of shape functions with respect to y for the sheathing elements.

$\mathbf{\bar{B}_{1-6}}$ = Derivatives of shape functions with respect to x for the framing elements.

$[\mathbf{B}]$ = Matrix of shape functions derivatives for sheathing element.

$[\mathbf{\bar{B}}]$ = Matrix of shape functions derivatives for framing element.

$\mathbf{C}$ = Factor in seismic base shear equation that accounts for natural frequency of the structure and soil conditions at the site.

$[\mathbf{c}]$ = Element viscous damping matrix.

$[\mathbf{C}]$ = System viscous damping matrix.

$\mathbf{D_i}$ = Components of system displacement vector.

$\mathbf{\ddot{D}_g}$ = Ground acceleration.

$\mathbf{\Delta \ddot{D}_g}$ = Change in ground acceleration over time step.

$\{\mathbf{d}\}$ = Displacements at element nodes.

$\{\mathbf{\dot{d}}\}$ = Velocities at element nodes.

$\{\mathbf{\ddot{d}}\}$ = Accelerations at element nodes.

$\{\delta \mathbf{d}\}$ = Virtual displacements at element nodes.

$\{\mathbf{D}\}$ = Displacements at system nodes.

$\{\mathbf{\dot{D}}\}$ = Velocities at system nodes.

$\{\ddot{\mathbf{D}}\}$ = Accelerations at system nodes.

$\{\mathbf{\Delta D}\}$ = Change in displacement over iteration or time step.

$\{\mathbf{\Delta \dot{D}}\}$ = Change in velocity over time step.

$\{\mathbf{\Delta \ddot{D}}\}$ = Change in acceleration over time step.

$\mathbf{E}$ = Modulus of elasticity for framing element.

$\mathbf{E_x}$ = Modulus of elasticity in x–direction for sheathing element.

$\mathbf{E_y}$ = Modulus of elasticity in y–direction for sheathing element.

$\mathbf{F_{con}}$ = Force in connector subjected to monotonic loading.

$\mathbf{F_{con(i)}}$ = Force in connector on leg 'i' of the hysteresis curve.

$\mathbf{F_{1,2}}$ = Maximum or minimum load on hysteresis curve.

$\{\mathbf{f}\}$ = Element forces.

$\{\mathbf{f_t}\}$ = Vector containing nodal and distributed load for element.

$\{\mathbf{F}\}$ = System forces.

$\{\hat{\mathbf{F}}\}$ = Effective system force vector.

$\mathbf{G(t)}$ = External energy input to system.

$\mathbf{G_{xy}}$ = Shear modulus of elasticity for sheathing element.

$[\mathbf{G}]$ = Vector containing material properties for sheathing element.

$\mathbf{h}$ = One–half length of sheathing element in y–direction.

$\mathbf{H}$ = 1 - $\nu_{xy}\nu_{yx}$.

$\mathbf{I}$ = Importance factor used in the calculation of base shear or moment of inertia for framing.

$\{\mathbf{I}\}$ = Influence vector.

$\mathbf{k_{bear}}$ = Stiffness of bearing element.

$\mathbf{k_{con}}$ = Tangent stiffness of connector element.

$\mathbf{K(t)}$ = Kinetic energy of system.

$\mathbf{K_1}$ = Initial stiffness on the monotonic curve for the sheathing–to–framing connector.

$\mathbf{K_2}$ = Stiffness of the sheathing–to–framing connector subjected to monotonic loading at Δ_{max}.

$\mathbf{K_3}$ = Stiffness of the sheathing–to–framing connector subjected to monotonic loading when Δ exceeds Δ_{max}.

$\mathbf{K_4}$ = Slope of the hysteretic curve at zero deflection.

$[\mathbf{k}]$ = Element stiffness matrix.

$[\mathbf{K}]$ = System stiffness matrix.

$[\hat{\mathbf{K}}]$ = Effective system stiffness matrix.

$[\mathbf{K_t}]$ = System tangent stiffness matrix.

$\mathbf{l}$ = Length of framing element.

$[\mathbf{m}]$ = Element mass matrix.

$[\mathbf{M}]$ = System mass matrix.

$\tilde{\mathbf{N}}_{\mathbf{1-4}}$ = Shape functions for sheathing elements.

$\bar{\mathbf{N}}_{\mathbf{1-6}}$ = Shape functions for framing elements.

$[\tilde{\mathbf{N}}]$ = Matrix of shape functions for sheathing elements.

$[\bar{\mathbf{N}}]$ = Matrix of shape functions for framing elements.

$\mathbf{ncc}$ = Total number of connectors in wall model.

$\mathbf{p(x)}$ = Distributed load acting on framing element.

$\mathbf{P(t)}$ = Energy dissipated through viscous damping.

$\mathbf{P_o}$ = The load–intercept of the K_2 line on the monotonic connector curve.

$\mathbf{P_1}$ = The load–intercept of the hysteretic curve.

$\{\mathbf{Q}\}$ = Array of applied nodal loads at given displacement used in Newton–Raphson method.

$\mathbf{R_w}$ = Ductility factor used in the seismic base shear equation.

$\{\mathbf{R}\}$ = Residual force vector used in Newton–Raphson method.

$\{\mathbf{r^{int}}\}$ = Internal force vector for element.

$\{\mathbf{R^{int}}\}$ = Internal force vector for system.

$\mathbf{S(t)}$ = Strain energy.

$\mathbf{t}$ = Time.

$\mathbf{\Delta t}$ = Finite change in time (i.e. time step).

$\mathbf{u_{1,2}}$ = Maximum or minimum displacement on hysteresis curve.

$\tilde{\mathbf{u}}$ = Displacement of sheathing element in x–direction at a point.

$\bar{\mathbf{u}}$ = Axial displacement of framing element at a point.

$\tilde{\mathbf{u}}_{\mathbf{1-4}}$ = Nodal displacements of sheathing element in x–direction.

$\bar{\mathbf{u}}_{\mathbf{i,j}}$ = Axial displacement of framing element at the nodes.

$\mathbf{\Delta u}$ = Displacement of connector element in X–direction.

$\bar{\mathbf{U}}$ = Displacement of framing element in X–direction.

$\mathbf{\delta U}$ = Virtual work done by internal forces or strain energy.

$\tilde{\mathbf{v}}$ = Displacement of sheathing element in y–direction at a point.

$\bar{\mathbf{v}}$ = Transverse displacements of framing element.

$\tilde{\mathbf{v}}_{\mathbf{1-4}}$ = Nodal displacements of sheathing element in y–direction.

$\bar{\mathbf{v}}_{\mathbf{i,j}}$ = Transverse displacements of framing element at nodes i and j.

$\mathbf{V}$ = Design seismic base shear.

$\bar{\mathbf{V}}$ = Displacement of framing element in Y–direction.

$\mathbf{\Delta v}$ = Displacement of connector element in Y–direction.

$\mathbf{W}$ = The weight of the wall.

$\mathbf{\delta W}$ = Virtual work of a system.

$\mathbf{\delta W_e}$ = Virtual work done by external forces acting on a system.

$\mathbf{x}(\tau)$ = Generalized displacement variable.

$\dot{\mathbf{x}}(\tau)$ = Generalized velocity variable.

$\ddot{\mathbf{x}}(\tau)$ = Generalized acceleration variable.

$\mathbf{\Delta X}$ = Distance between adjacent sheathing elements in X–direction.

$\mathbf{\Delta Y}$ = Distance between adjacent sheathing elements in Y–direction.

$\mathbf{Z}$ = Variable used to calculate base shear which is a function of the seismic activity of a region.

α = Angle between x–axis of the framing and the system X–axis.

β = Constant used in the Newmark–Beta method.

γ = Constant used in the Newmark–Beta method.

δ = Change in connector element displacement over time step.

$\mathbf{\Delta}$ = Displacement of connector element.

$\mathbf{\Delta_{bear}}$ = Displacement of bearing element.

$\mathbf{\Delta_{max}}$ = Maximum connector displacement before load carrying capacity decreases.

$\{\mathbf{\Delta}\}$ = Vector of connector element displacements.

$\{\mathbf{\Delta_{bear}}\}$ = Vector of displacements between adjacent sheathing panels.

$\epsilon_{\mathbf{a}}$ = Axial strain in the framing element.

$\epsilon_{\mathbf{b}}$ = Bending strain in the framing element.

$\epsilon_{\mathbf{x}}$ = Strain in the sheathing element in x–direction.

$\epsilon_{\mathbf{y}}$ = Strain in the sheathing element in y–direction.

$\epsilon_{\mathbf{xy}}$ = Shear strain in the sheathing element.

$\{\epsilon\}$ = Vector of element strains.

ζ = Viscous damping factor.

η = Dimensionless coordinate along y–axis for sheathing element.

$\theta_{\mathbf{i,j}}$ = Rotation of framing element at the nodes.

ν_{xy} = Poisson's ratio giving strain in x–direction given stress in y–direction.

ν_{yx} = Poisson's ratio giving strain in y–direction given stress in x–direction.

ξ = Dimensionless coordinate along x–axis for framing and sheathing elements.

ρ = Density of framing or sheathing element.

$\{\sigma\}$ = Vector of element stresses.

σ_a = Axial stress in the framing element.

σ_b = Bending stress in the framing element.

σ_x = Stress in the sheathing element in x–direction.

σ_y = Stress in the sheathing element in y–direction.

σ_{xy} = Shear stress in the sheathing element.

ω_n = Natural frequency of wall model.

Chapter 1

Introduction

1.1 Background

Timber is one of the oldest and most extensively used building materials for low–rise buildings in North America. It is a desirable building material because of its high strength to weight ratio, relatively good fire retardance in large cross–sections, and abundance. It is an especially good material for use in seismic zones because of the many redundancies in wood structures and because most connections in wood structures provide ductility and dissipate significant quantities of energy through hysteretic damping and friction.

Shear walls, which provide the resistance to lateral forces along with providing some resistance to gravity loads and partitions, are one use of timber in low–rise buildings. A typical shear wall in North America, shown in Figure 1.1, has three primary components: the framing, sheathing, and connectors that attach the sheathing to the framing. The sheathing, which is a structural panel product such as plywood or oriented strandboard (OSB), is attached to the framing, usually made from 38x89 mm or 38x140 mm (2x4 in or 2x6 in nominal) lumber, with dowel–type fasteners such as nails and screws, although elastomeric adhesives are sometimes used.

There has been a substantial amount of research conducted on the subject of shear walls, however, there remain some areas that have not been adequately covered. One area is the effect that the aspect ratio (ratio of wall length to height) of a shear wall

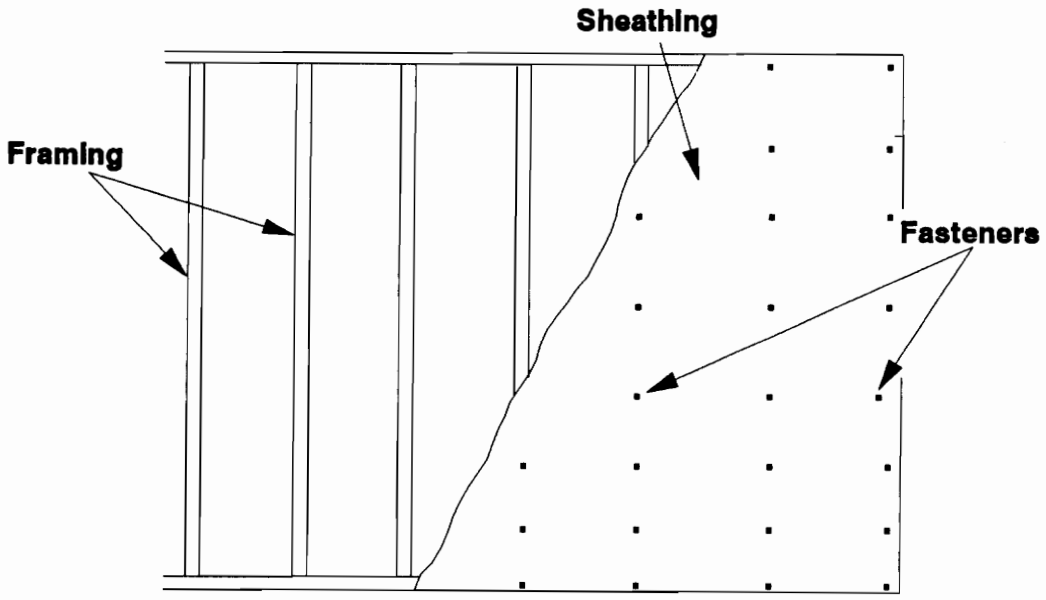

Figure 1.1: Components of Typical Shear Wall

has on the distribution of the loading through the wall. The load that is applied along the top of the wall is distributed to the base of the wall by the diaphragm action of the sheathing and the framing. The exact manner in which the loading is distributed is dependent on, among other things, the geometry of the wall. However, the exact manner in which the aspect ratio of the shear wall will affect the load distribution has yet to be fully understood. Also, the aspect ratio may have an effect on the magnitude of the overturning moment that is experienced by a structure. A structure with a low aspect ratio (i.e. a tall, narrow structure) is expected to generate a higher overturning moment than a structure with a higher aspect ratio. This difference in overturning moment would affect the forces experienced at the base of the structure which would in turn affect the design of the anchorage connections. Also, as the length of the wall increases, the effects of shear on the wall may become greater (analogous to a simple beam increasing in depth). This could affect the magnitude of the deformations experienced by the wall and change the mode of failure.

It is often necessary that openings are present in shear walls for windows and doors. The openings reduce the strength and stiffness of a shear wall, with strength and stiffness decreasing as the length of the opening increases. This reduction in strength and stiffness is accounted for by assuming that the strength and stiffness of these walls is the same as that of a wall without openings of the same effective length (total length of the wall less the length of the openings). This is a conservative estimate of the strength and stiffness of the wall because it assumes that the wall above and/or below the opening does not provide any resistance, although this portion of the wall does provide added resistance (Ge et. al, 1991). The design base shear of a wall with openings subjected to seismic loading is assumed to equal that of a shear wall of the same total length without openings. This assumption was made although there have been no studies done for shear walls with openings subjected to cyclic or seismic loading.

1.2 Objectives and Scope

The objectives of this project are to determine how variations in configuration affect the response of timber shear walls subjected to monotonic and seismic loading and to then use this knowledge to develop an improved design methodology. Specifically, the following characteristics of timber shear walls are examined:

- The effect that aspect ratio has on the dynamic response characteristics and load distribution in timber shear walls and the associated anchorage connections.
- The effect of wall openings on the dynamic response characteristics and load distribution in timber shear walls and the associated anchorage connections.

The objectives were achieved by analyzing shear wall models of varying aspect ratio and opening configurations using a finite element program and then developing a

modified design methodology based on the analysis results. The program is a modification of the shear wall analysis program developed by Dolan (1989), which was enhanced by expanding its capabilities to include the analysis of larger walls and by incorporating load–controlled monotonic analysis and the calculation of internal forces and stresses. The program, which has the capability to analyze shear walls subjected to static, monotonic, or dynamic loading, was validated by analyzing shear wall models corresponding to shear walls tested experimentally and comparing the program results with the experimental results. The program was used to analyze the shear wall models, which were subjected to monotonic and seismic loading, after validation was completed.

1.3 Significance

The current design practice for shear walls with different aspect ratios and openings configurations subjected to seismic loading is based on data from monotonic shear walls tests. The results from the parametric study will provide quantitative results that indicate whether aspect ratio and openings have an effect on the response of shear walls subjected to seismic loading. The results will also provide in–depth information on the distribution of forces throughout the wall and at the connections. These results will then be used to develop a modified design methodology that accurately predicts the shear at the base of the wall, forces in the components, and forces due to the overturning moment present in the wall more accurately. With the importance of seismic design, it is imperative that an adequate basis for the procedures be developed.

Chapter 2

Literature Review

2.1 Introduction

The base of knowledge concerning timber shear walls has increased greatly since their inception as a structural component. This chapter provides a summary of the research that has been performed concerning timber shear walls. First, research in the area of monotonic loading will be reviewed. This will include information on connections, modeling of the walls, openings, and aspect ratio. Next, research in the area of dynamic loading will be presented, covering the areas of connections and modeling. Finally, research in the area of walls as part of a system will be examined. This will include information on how individual wall response is affected when it is part of a system of walls.

2.2 Background

The primary purpose of a shear wall is to provide the resistance to lateral loads for a structure. The majority of low–rise light–frame timber structures use shear walls for this purpose instead of other systems such as moment frames or braced frames. The load path for a structure with shear walls subjected to lateral loading, such as a constant wind pressure, is as follows. The load is applied to a vertical side wall, which is a shear wall perpendicular to the direction of the loading. The load is

then transferred to a horizontal diaphragm, such as a floor or roof, and from there it is transferred to the shear walls at the ends of the diaphragms, and in turn to the foundation (Diekmann, 1989). The load path is similar for seismic loading, for the resultant horizontal load occurs at the horizontal diaphragm because of its high concentration of mass.

An ideal wall deflects in a manner similar to that shown in Figure 2.1 when a load is applied, with the framing deforming as a parallelogram and the sheathing

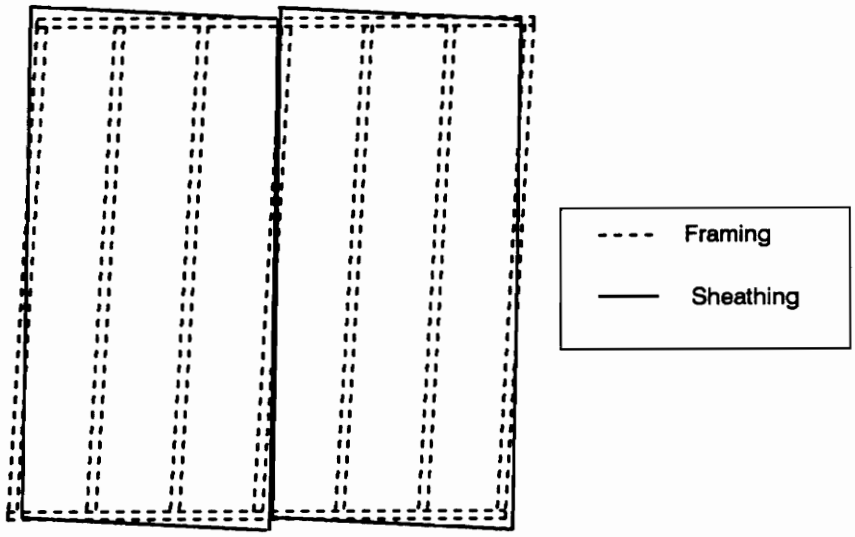

Figure 2.1: Typical Deflection Configuration of a Shear Wall

remaining rectangular and rotating slightly. The external load is resisted by the energy dissipated by the nails as they distort (Tuomi and McCutcheon, 1978). The sheathing in a shear wall provides a majority of the shear resistance, while the framing provides a majority of the bending resistance and the connectors transfer the load between the framing and sheathing. The shear force at the top of the wall produces an overturning moment. In design, this moment is resolved into a force–couple, and the forces from the couple are resisted by the end chords, which are the vertical framing members located at either end of a shear panel. The moment will sometimes cause

one end of the wall to lift up slightly.

2.3 Monotonic Loading

The most elementary case of shear wall analysis is the case of a wall subjected to monotonic loading. Monotonic loads are applied slowly in one direction over relatively long periods of time, and therefore inertia effects are not significant. An example of a monotonic load is a load due to constant wind pressure. The most important characteristics of shear walls subjected to monotonic loading are in–plane strength and stiffness. Strength, which is a measure of the magnitude of load that the wall can resist before a limit state (excessive deflection, catastrophic failure, etc.) occurs, is important for determining the resistance potential of a wall. Stiffness, which is a measure of the relative deformability of a material under load (Davis et al., 1982), is vital for determining the extent of architectural damage that could occur in a structure. Factors that affect the strength and stiffness include the structural properties of sheathing materials, fastener size and spacing, framing density and spacing, wall length, opening size and number (Solitis et al., 1981), and the interaction between the sheathing, the framing, and the anchorage (Griffiths, 1984).

2.3.1 Connections

The connections that are focused on in this research are those used to attach the sheathing to the framing, and in particular dowel–type fasteners such as nails. The most important properties of a connection are its shear strength and load–deflection characteristics. The shear strength of a connection is important for determining the overall racking strength of a wall. The strength of a connection in single shear (sheathing–to–framing connections are in single shear) is a function of the diameter and yield strength of the connector and the bearing strength of the members (McLain,

1991 and NDS, 1991). Loading rate is another factor that affects the strength of a connector. A fast loading rate increases the failure load of the connection, similar to the effect that an increased loading rate has on the strength capacity of a beam in bending. Girhammar and Andersson (1988) examined this effect and found that the increase in ultimate load is linearly dependent on the logarithmic deformation rate and that the deformation rate is much greater for the wood than it is for the nails. Bodig and Farquhar (1988) similarly found a semi–logarithmic relationship between ultimate load of a connector and loading rate. Along these same lines, Jenkins et al. (1979) examined the effect that long term lateral loads (creep) have on the characteristics of nails joints and developed a method for the evaluation of joint moduli under long–term loads.

Determination of the ultimate strength and load–displacement characteristics of connectors has been attempted by several researchers. Walford (1976) developed a relationship to characterize the allowable loads on nailed joints in diaphragms and concluded that an optimum point of comparison of nailed fastenings appeared to be at a slip of 1.5 to 2.0 mm rather than the customary (at that time) 0.4 mm. Polensek (1978) also performed experimental tests in order to determine the strength of joints for shear walls and proposed recommended joint moduli and developed experimental load–deflection curves for the joints tested. The load–displacement characteristics of the connection are important because the racking behavior of a shear wall is dependent upon them (McCutcheon, 1985; Zagajeski et al., 1979). Development of a monotonic load–displacement curve has been examined by some researchers. Foschi (1977) developed one of the earliest numerical models of a nailed connection by fitting a curve to experimental data. The model is nonlinear and contains both a linear and exponential component. Dolan (1989) modified the model by adding a linear segment to model the portion of the load–deflection curve after maximum load had been reached. Smith et al. (1986) developed an integrated program to predict

the load–slip behavior of timber joints with dowel–type fasteners. It can predict the behavior under short–term and long–term loading.

In recent years, elastomeric adhesives have been used for attaching the sheathing to the framing. Nails are used along with the adhesive, but only to hold the sheathing and framing in place until the adhesive cures; the nails are not intended to provide additional lateral resistance due to the difference in stiffness between the nails and adhesive. The properties of these connectors have been examined by researchers to determine how they compare to nailed connections. Wernersson and Gustafsson (1988) studied the strength and constitutive properties of adhesive joints and found that adhesive bond lines experience gradual softening, major deformations occur in the plastic hardening and softening region, and that the elastic deformation of a bond line appears negligible compared to the plastic deformation. Pellicane and Schmidt (1988) also studied the strength and load-slip characteristics of wood joints with elastomeric construction adhesives and found that adhesive type has an effect on joint behavior and that the presence of glue in a nailed joint accounts for a substantial increase in strength and stiffness over joints without glue. Pellicane (1991b) would later use this information to develop a model to predict the ultimate strength and load–displacement curve, based on concepts involving superposition.

A method for designing joints with nails and elastomeric adhesives was developed by Hoyle (1987). In the method, the joint capacity for a given slip is computed by adding together the resistance of the nails and adhesive acting independently, and the overall joint strength is chosen so that the joint slip will not exceed that considered acceptable in mechanically fastened joints in general. However, one must remember that some adhesives are stiffer and stronger than the mechanical fasteners; therefore, the mechanical fasteners may never experience significant load until the failure of the adhesive, by which time the load is too high for the mechanical fastener to provide sufficient resistance.

2.3.2 Modeling

Apart from the basic mechanism models stated previously, many shear wall models have been developed that predict deformation of a wall for a given load. There are two general categories of models: closed-form models and finite element models. These models are important because they provide insight into the characteristics of shear walls without having to use experimental testing, which can sometimes prove to be very costly. The closed–form models usually employ an energy method or strain–displacement relationship as their basis and provide information concerning overall wall behavior, but do not provide detailed analysis of the components of a wall. Tuomi and McCutcheon (1978) developed an analytical method for predicting the racking performance of shear walls which is independent of panel size. The strength equation was derived by an energy formulation whereby the externally applied load is resisted by the internal energy dissipated by the fasteners. Interior or field nails, however, were not considered in the derivation. Easley et al. (1982) developed formulas for the analysis of typical timber shear walls with sheathing attached by nails or other types of discrete fasteners. The formulas are based on force and moment equilibrium for a panel and are valid only if no separation occurs in the framing member joints or between the studs and the header or sill when a wall is loaded. Akerlund (1987) developed a method of modeling wood-framed shear walls. The derivations are based on assumptions which include a hinged frame of stiff framing members, stiff sheathing, linear load-slip relation for a single nail, and rigid top and bottom sole plates.

The finite element method, which is based on the work–energy principle, can be used to determine more localized information concerning the shear wall performance. Foschi (1977) developed a nonlinear finite element model which contained four elements: a cover (sheathing) element, a frame element, the connections between frame members, and the cover-to-frame connections. The program incorporated orthotropic

plate action for the cover and nonlinear connection behavior. The program was later modified by Dolan (1989) to include the modified load–displacement curve for the connector discussed previously and an element to simulate bearing between adjacent sheathing elements. Gupta and Kuo (1985) developed a model to predict the response of timber shear walls based on equating the strain energies of the studs, nails, and sheathing with the work done by the external force and later, in 1987, they developed a model that took into account uplift of the wall. McCutcheon (1988) developed a computer program to calculate the response of a shear wall subjected to in-plane loads. Falk and Itani (1988) formulated a nonlinear finite element that accounted for the stiffness of fasteners connecting the sheathing to the framing. Falk and Itani (1989) improved on the modeling of the wood diaphragms by formulating a nonlinear finite element that accounts for the distribution and stiffness of fasteners connecting the sheathing to the framing. Gutkowski and Castillo (1988) developed a computer program (WANELS) that incorporated elements for the framing, sheathing, and connectors. The program was also among the first programs with the capability to analyze walls with openings. Itani and Cheung (1984) developed a model for predicting the quasi-static load-deflection behavior of diaphragms. The model is formulated for the general case, where the joint element is assumed to exhibit elastic behavior while the beam and plane stress elements are assumed to be linearly elastic throughout the analysis. Kasal and Leichti (1992) developed a nonlinear finite–element model for shear wall analysis and also developed an equivalent model for the wall, which had a reduced number of degrees–of–freedom, for possible use in the analysis of a full structure. The model was used for determining out–of–plane (buckling) deflections.

2.3.3 Openings

Openings are often needed in shear walls for doors as windows. The openings have an effect on the walls, reducing their racking strength and stiffness when compared to walls of similar size without openings (Falk and Itani, 1987). The necessity arose to quantify the strength and stiffness reduction and to develop design criteria to reflect this phenomena. Dean et al. (1984) developed a design procedure for shear walls with rectangular openings that was based on simple equilibrium analysis and the shear transfer method. Patton-Mallory et al. (1985) found that the proportionate effective wall length, which is the total length of the wall less the total length of the openings, can be conservatively used as a measure of the racking strength of shear walls with door and window openings, although it tends to overestimate the stiffness of the walls. This is the methodology that is currently used. Yasumura (1986) developed a theoretical means of determining the yield strength and lateral stiffness of shear walls with openings. Ge et al. (1991) proposed a method to consider the effect of the wall area above and below an opening on the stiffness of the wall. The method, which is similar to superposition, consists of treating the wall as if it had no openings, then making adjustments due to the presence of a cutout. Sugiyama and Matsumoto (1993,1994) have proposed a method for determining the strength of a plywood-sheathed shear wall with openings. The method is based on assuming a deflection pattern, determining the resulting relationship between nail slip and shear forces, dividing the wall into panel groups, and finally solving a series of simultaneous equations to determine the magnitude of the forces and displacements.

2.3.4 Aspect Ratio

The aspect ratio of a shear wall is the ratio of the length of the wall to the height of the wall. The characteristics of shear walls with different aspect ratios have been

examined to determine its effect, if any, on the response of the wall. Suzuki et al. (1978) performed racking tests on shear walls of various lengths and found that the maximum shear load is almost linearly proportional to wall length. Patton–Mallory et al. (1985) determined that racking strength is linearly proportional to wall length and that the racking stiffness increases as wall length increases for walls with aspect ratios between 1 and 4. This was similar to the conclusions from research by Patton–Mallory et al. (1984) in which experimental tests on shear walls with sheathing on two sides were performed and the strength was found to be proportional to wall length. Although not the focus of the research, Naik et al. (1984) found that lateral stiffness and strength of a shear wall is more dependent on the number of nails and nail spacing than on wall height. McDowall and Halligan (1989) studied the racking resistance of short lengths of particleboard sheathed timber framed wall panels 2600 mm high and found that for short lengths of walls (between 300 mm and 600 mm), the failure load varies linearly as a function of wall length.

2.4 Dynamic Loading

Loading that is dynamic in nature is applied at a frequency that is sufficiently high that the effects of inertia cannot be neglected (Cook et al., 1989). Wood is a material that is good for use in seismic areas because of its high strength–to–weight ratio, the redundancies found in light–frame construction, and the energy dissipation that occurs at its connections. The basic mechanism of the wall remains the same as for monotonic loading, with the framing resisting the bending stresses and the sheathing resisting the shear stresses (Anderson, 1988). The difference between dynamic and monotonic loading, other than the introduction of inertial forces, is the importance of ductility over stiffness because it prevents loads from becoming excessively high. Displacement ductility can be defined as the ratio of the maximum

to the yield displacements (Zahran and Hall, 1984). A material that is truly linear elastic will experience higher loads up to the point at which failure occurs, while a system with substantial ductility will experience higher loads only up to a yield load. Therefore, the loads experienced by the ductile system will be lower than those of the of the elastic system after the yield point, if the displacements and initial stiffnesses are equal. It is important to remember, however, that walls with excessive ductility are subject to extensive displacements and costly architectural damage for earthquakes of high magnitude. Stiffness prevents excessive displacements from occurring in the wall, and thereby reduces the extent of architectural damage. Therefore, there must be a balance between stiffness and ductility in a shear wall.

The load–deflection envelope pattern for shear walls subjected to seismic loads was assumed to be perfectly elastic–plastic for the design code criteria. However, it has been shown that deflection envelope for the walls is nonlinear (Thurston and Hutchinson, 1984; Stewart et al., 1984). Also, the strength and stiffness was found to be proportional to the nail spacing; differences in sheathing material (between plywood and waferboard) were not found to have a significant effect on wall response (Dolan and Madsen, 1991), although Thurston and Hutchinson (1984) found particle board sheathed walls to be stiffer than plywood walls; and wall strength and stiffness increased as the rate of loading increased (Stewart et al., 1988).

Different methods have been used to try and improve the performance of shear walls subjected to dynamic loading. One method, which has been applied to all types of structures, involves base isolation. This usually involves using a flexible interface between the structure and the ground in order to minimize the lateral load acing on a building during a seismic event. This is done by shifting the fundamental period of the structure to a range outside the energy–containing periods of the earthquake ground motion and providing supplemental damping (Shenton and Lin, 1993). Purely sliding friction mechanisms, which dissipate energy through friction, can also be used as base

isolation mechanisms (Koh and Kelly, 1990). Friction has been used by Filiatrault (1990), who incorporated a friction damper in the wall diagonal, and by Sakamoto et al. (1984), who combined friction plates with a damper in base isolation systems for shear walls. Efforts to model base isolation systems have been undertaken by Koh and Kelly (1990), Ahn and Gould (1992), and Tsai and Lee (1993).

2.4.1 Connections

Connections are very important when walls are subjected to dynamic loading because a great deal of energy dissipation in a structure occurs either through the inelastic deformation of the components of the connection or through the friction between the connector and the wood (Polensek and Bastendorff, 1987). Typically, cyclic loading of a connection produces a load–deflection curve which is commonly referred to as a hysteresis loop. A typical hysteresis loop for a nailed timber connection, shown in Figure 2.2, exhibits the characteristic nonlinear, inelastic deformation;

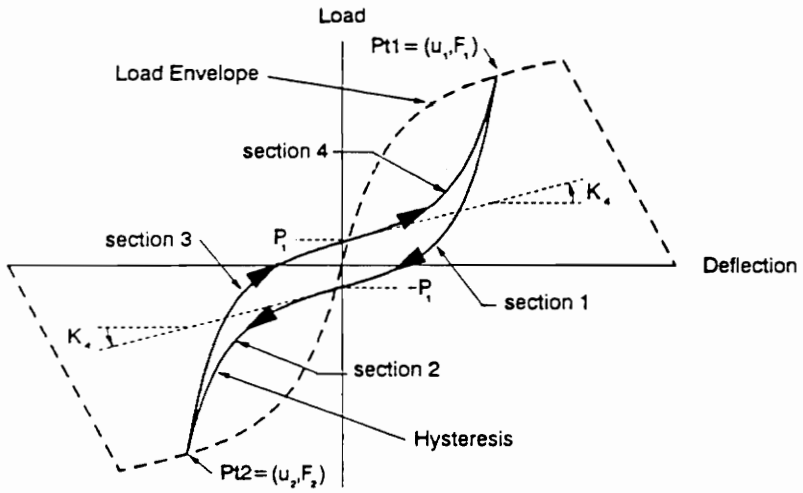

Figure 2.2: Typical Hysteresis Loop for 8d Nail (Dolan, 1989)

pinched loops; and stiffness degradation. Another important feature, not observed in the figure, is that the response of a joint is dependent on the loading and response

history of the joint (Foliente, 1993). The area contained in a loop reflects the energy loss in a loading cycle. There is a decrease in the overall resistance of a joint at large deformations and numbers of cycles (Soltis and Mtenga, 1985) when compared to identical connections subjected to static loading. Fatigue is also a consideration of nails subjected to cyclic loading, although this phenomena rarely occurs in shear walls.

There have been various attempts to model the hysteretic behavior of nailed timber joints. Ewing et al. (1980) developed a model based on experimental data that followed a trilinear path from the maximum to minimum load–displacement. Kivell et al. (1981) proposed a model based on the modified Takeda model, which had been previously used for concrete models. Stewart (1987) developed a model consisting of a series of linear components by utilizing idealized pinching and stiffness degradation and a set of force–history rules. Dolan (1989) performed cyclic tests on nailed connections and used the resulting data to model a hysteretic curve. The curve is broken into four sections, each section governed by a superimposed linear and exponential equation. Foliente et al. (1993) used the Buoc–Wen–Baber–Noori (BWBN) model in order to fashion a hysteretic curve. The hysteretic relationship incorporates pinching and stiffness degradation, which are common in wood joints. However, the model is extremely general and several special parameters need to be determined using trial and error methods before its use.

As stated previously, the adhesives approved for structural use have a higher stiffness and lower ductility than traditional nailed connections. Although only one unpublished study (Kalkert, 1992) has focused specifically on the load–displacement characteristics of adhesive joints subjected to reverse cyclic loading, others have examined the system behavior of walls with adhesive connections. Buchanan (1984) studied the relationship between wood properties and the seismic design of timber structures and found that failure of a glued connection will be similar to failure of

solid timber. The most extensive study on the characteristics of a timber shear wall with adhesive connections was performed by Foschi and Filiatrault (1990). They found that the adhesive shear wall was much stiffer than the walls constructed with dowel-type fasteners. This was found to be both good and bad. The stiffer, stronger adhesive walls are better suited for applied loadings where stiffness and ductility do not play an important role in load magnitude. However, in situations in which seismic loads are acting on the wall, the adhesive shear wall generated larger shear forces because of their increased stiffness and reduced ductility (Dolan and White, 1992). Also, the adhesive shear walls tended to fail in a brittle manner, which is not a good characteristic for building design.

2.4.2 Modeling and Design

There have been a few attempts to model the behavior of shear walls subjected to dynamic loading. Adeli et al. (1978) investigated several numerical techniques in order to determine the most efficient for nonlinear dynamic analysis of structures modeled by finite elements and found that in general, explicit methods are more unstable for nonlinear dynamic analysis than implicit methods. Dolan (1989) developed a closed form mathematical model for the response of shear walls subjected to a harmonic excitation. The shear wall was modeled as a single degree–of–freedom non–linear oscillator with no viscous damping and an idealized hysteresis loop which consists of six line segments. Diekmann (1989) studied the possible methods for the analysis of shear walls for solid walls and walls with openings based on the equilibration of forces in the wall components. Stewart and Dean (1989) use the capacity design procedure as a basis for the design of earthquake resistant sheathed shear walls. Hoyle (1988) established design criteria for wood shear joints fastened with nails and structural elastomeric adhesives. The criteria include that the allowable

design load; nail slip; glue line stress; shear stress for the lumber, plywood, particleboard, or hardboard; and the glue line slip at the allowable stress must not be exceeded. Tembulkar and Nau (1987) investigated the role of hysteretic modeling in earthquake energy dissipation and concluded that the bilinear model is the simplest model to use to simulate nonlinear force-deformation behavior for analytical studies (the model is justified for low frequencies with displacement ductilities greater than or equal to three) and hysteretic action occurs in the case of inelastic structures.

Also, Cheung and Itani (1984) used the equivalent viscous damping method along with a finite element model to develop a theoretical procedure for determining the damping ratio in sheathed diaphragms. Sakamoto et al. (1984) performed a study in which the stiffness degradation and hysteretic bearing walls were modeled by making use of a combination of a BI-LINEAR element and a SLIP element. The results are limited because several important factors which affect the response of timber shear walls were not studied. Potter (1989) used the elastic shear distribution method, produced by Kiyoshi Muto, in order to develop a program to calculate the distribution of shear load within a building. Dolan (1989) developed a finite element model for a shear wall subjected to dynamic loading. The model includes nonlinearities in the nail connection between the sheathing and the framing, nonlinearities due to the bearing between adjacent sheathing panels, and the out–of–plane bending of the sheathing material. The bearing between adjacent shearing panels is modeled using a bilinear spring with a low stiffness in tension and high stiffness in compression. Filiatrault et al. (1990) developed a single degree–of–freedom shear wall analysis program based on Dolan's (1989) hysteresis that incorporated reliability methods. Potter (1989) used the elastic shear distribution method in order calculate the distribution of shear load within a building. Yasumura (1992) developed a relationship to determine the yield load of a shear wall subjected to dynamic loads.

2.5 System Behavior

Shear walls are only one component in a structure. They function along with vertical side walls and horizontal diaphragms to resist the lateral loads. The research cited to this point has focused on the performance of shear walls or its components separately. However, a few researchers have looked into behavior of shear walls in a structure. Phillips et al. (1993) conducted tests on a one story structure and found that the roof diaphragm affected the distribution of lateral load to the shear walls and that vertical side walls carried between 8 % to 25 % of the total lateral load. Nelson et al. (1985) found that interior shear walls located on the windward side of an assembly have higher ultimate strengths. Soltis (1984) studied the seismic performance of light-framed wood buildings and found that bad performance for the racking resistance occurs when there is a lack of shear walls, a lack of wall sheathing under the siding, large openings, or nonsymmetric arrangement of shear walls. He also found that a large number of fasteners provides immense energy–dissipating capacity. Freeman (1977) ran a series of tests on wall panels to determine the response to different loads. Findings from the study included the fact that interstory drift and damage can be limited in two general ways: stiffening the structure or providing details that will allow large deflections to occur without causing damage.

Arima et al. (1990) performed nondestructive testing using vibration generator to test the frequency-response curve of a full-scale house and evaluate the relationship between the natural frequency and the racking resistance of a house. They found that the frequency-response curve and natural frequency depend on the number of stories, elevation, and components (lining and cladding) of the house. They also found that the existence of an unbalanced amount of wall and openings in the floor of the structure could cause torsion in the horizontal plane. Sugiyama et al. (1988) performed full scale tests on houses subjected to lateral loads and found that wall

sheathing and/or wall covering applied on the wall spaces above and below window and door openings provides some increase in the racking resistance, although the amount of added resistance was not quantified. Other findings are that a symmetrical arrangement of shear walls is the most efficient layout (Thorson, 1989; Polensek and Schimel, 1986), the exterior walls resist most ($\approx$ 70 %) of the earthquake load (Kawachi et al., 1990), cross–walls (walls perpendicular to the load) contribute to the stiffness of walls by preventing rotation of the bearing walls, and that maximum strength and stiffness is achieved by fully restraining the top plate against bending out of plane (McDowall, 1984).

An important characteristic of systems is the distribution of forces. This has been examined by Kawai et al. (1990) and Stewart et al. (1989). They found that the participation of interior shear walls in resisting lateral loads is a function of the behavior of the composite structural system, which includes the roof and floor diaphragms, and the shear walls. The behavior of a base isolated wood structure was examined by Sakamoto et al. (1990) and the results showed that the isolators reduced the maximum acceleration experienced by the building. A model of the structure with the base isolator was also developed.

Ultimately, it is important that the information on systems be used to design a reliable structure. Manahey and Kehoe (1988) developed a procedure for the design of multi–story buildings with horizontal and vertical wood diaphragms subjected to seismic loading. Schmidt and Moody (1989) developed a model (RACK3D) to predict the nonlinear response to lateral loading of three–dimensional light–frame structures. The model included shear wall and horizontal diaphragm elements. Leichti and Kasal (1992) developed a three–dimensional, nonlinear finite–element model of a light–frame wood building to examine the effects of load sharing in a structure. Gupta and Kuo (1987) developed one of the first models for analyzing entire wood frame houses subjected to lateral loads and earthquakes. It is a finite element model

with elements representing shear and flange walls, roof and ceiling diaphragms, and gable end trusses. Boughton and Reardon (1984) modeled house behavior subjected to monotonic loading by assuming that the roof and ceiling diaphragms were stiff, thereby ensuring transfer of lateral loads to the transverse walls. Anderson and Reinhold (1990) developed a design procedure based on the assumption that the load carried by the diaphragm is equal to the reaction at the eave necessary to prevent eave deflection. Bulleit (1987) incorporated a probability model (Markov model) to determine the ultimate capacity reliability for a wood system. An assumption in the model, which could turn out to be unconservative, is that only one member can fail per loading cycle. Hayashi (1990) proposed several formulas to determine the performance of shear walls with vertical slit openings.

Chapter 3

Shear Wall Analysis Program

3.1 Introduction

A program that is capable of performing static, monotonic, or dynamic analysis on shear wall models was developed in order to analyze wall models for the parametric study. The program, titled WALSEIZ, is a modification of DYNWAL, a shear wall analysis program developed by Dolan (1989). WALSEIZ utilizes the finite element method for analysis. Elements corresponding to the framing, sheathing, connectors attaching the sheathing to the framing, and the effect of bearing between adjacent sheathing panels are used to model a shear wall. WALSEIZ has the capability to analyze shear walls up to 4.9 m by 12.2 m (16 ft by 40 ft) in size, calculate displacements at the nodes and forces and stresses in the elements for user specified nodes and elements, and determine the maximum and minimum displacements and forces and stresses for all of the nodes and elements. The derivation of the elements and solution techniques are covered in considerable detail in this chapter to accommodate anyone without a strong background in finite element analysis.

3.2 Background

WALSEIZ is a program that is capable of performing static, load–controlled monotonic, or dynamic analysis on shear wall models. It has its basis in DYNWAL, a program developed by Dolan (1989). WALSEIZ utilizes finite element analysis, which involves applying compatibility, constitutive laws, and equilibrium to a discretized continuum in order to develop relationships between the applied forces and the internal resistance (Holzer, 1990). Four different elements are used to model a shear wall in WALSEIZ: a two node linear elastic element to model the framing (henceforth referred to as a framing element), a four node plane rectangular element to model the sheathing (henceforth referred to as a sheathing element), two nonlinear spring elements to model the connectors that attach the sheathing to the framing (henceforth referred to as a connector element), and a bi–linear spring element to model the effect of adjacent sheathing panels bearing on one another (henceforth referred to as a bearing element).

3.2.1 Modifications

Several modification were made to DYNWAL in its transformation to WALSEIZ, including:

- Reduction of the degrees–of–freedom of the sheathing element from 48 to 8, which in turn reduced the degrees–of–freedom associated with the connector element from 56 to 14 and those associated with the bearing element from 96 to 16 because these elements utilize the degrees–of–freedom of the sheathing element. The change was prompted because out–of–plane deflections of the sheathing is not significant when the sheathing is 9.5 mm (3/8 in) or thicker and studs are spaced a maximum of 610 mm (24 in) on center (Dolan, 1989).

This change significantly reduced the computation time required for analysis of a model and therefore enabled the maximum model size to be increased.

- The addition of force and stress calculations, which enables the state of forces and stresses to be calculated in the framing and sheathing at any time during the analysis.

- Alteration of the logic for the hysteresis loop so that the re–loading curves have a shape similar to that of the load envelope instead of the linear re–loading curves found in DYNWAL.

- The incorporation of load–controlled monotonic analysis. This was accomplished by adding code which allowed the program to perform successive static analysis with the applied loading incremented after each analysis. This modification to ease the development of a load–displacement curve by allowing a series of static analyses to be performed without having to modify the data file.

- Incorporation of hinges for the framing elements, which were used to model the connections between the studs and the sill and sole plates and the connection between the studs and the opening header in the framing of a shear wall. This modification was made to provide a more accurate and conservative model of the nail connections, which resemble more of a pinned connection than a rigid connection in shear walls.

- Imposition of boundary conditions at the element level in order to reduce the analysis time for the program to run because the stiffness elements are "mapped" directly to the proper location in the stiffness matrix and therefore the boundary conditions do not need to be imposed on the global stiffness matrix.

3.2.2 Assumptions

It is important to take into account all of the idiosyncrasies when modeling an actual system. However, assumptions are often included in the model in order to simplify the model. The following assumptions were made in the development of WALSEIZ:

- The shear wall does not deflect in the out–of–plane direction. This assumption was made because out–of–plane displacements were previously determined to be insignificant for sheathing of thickness greater than 9.5 mm (3/8 in) and studs spaced a maximum of 610 mm (24 in) on–center (Dolan, 1989).

- The shear deformation in the framing is minimal and is therefore neglected in the formulation of the framing element. This assumption was made because the majority of the shear force is resisted by the sheathing.

- Layered sheathing materials are modeled as non–layered orthotropic materials. This assumption was made to simplify the element, and since the sheathing is loaded in its plane, the effect of layering is negligible.

- The framing and sheathing components exhibit linear–elastic material behavior. All non–linear behavior is assumed to be due to yielding of the connectors.

- The effect of the eccentricity of a shear wall sheathed on one side only is not present. Shear walls sheathed on one side only are not symmetric and the load applied to the wall does not pass through the shear center, thereby creating the possibility for the wall to twist. However, some type of support is often used in experimental tests of shear walls to reduce or eliminate this effect.

- Framing members are isotropic, linear–elastic, and homogeneous; the sheathing is orthotropic, linear–elastic, and homogeneous; and failure does not occur in

the framing or sheathing elements. This assumption was made because the failure of the sheathing–to–framing connector is the primary mode of failure in a shear wall (Dolan, 1989) and because it is assumed that the framing or sheathing do not yield or fail. The magnitude of the stresses can be manually checked to determine if the allowable design stress is reached for any of the wood materials.

3.3 Description and Formulation of Elements

The framing and sheathing elements were formulated by approximating a displacement field for each element, applying compatibility (strain–displacement) relationships and constitutive (stress–strain) laws using the approximated displacement field, and then imposing equilibrium by utilizing the principle of virtual work along with D'Alembert's principle. The principle of virtual work was applied directly in the formulation of the connector and bearing elements. The principle of virtual work states that the virtual work of a system, δW, is equal to the difference between the virtual work done by external forces acting on the system, δW_e, and the virtual work done by the internal forces or the strain energy, δU. The system is in equilibrium if the net virtual work done on the system is zero, or

$$\delta W = \delta W_e - \delta U = 0 \tag{3.1}$$

Substitution of the external and internal virtual work terms into Equation 3.1 results in equations of the form

$$\{f\} = \{r^{int}\} + [m]\{\ddot{d}\} + [c]\{\dot{d}\} \tag{3.2}$$

where $\{f\}$ are the loads acting on the element, $\{r^{int}\}$ is the internal force vector due to straining of the material, $[c]$ is the viscous damping matrix for the element, $\{\dot{d}\}$ are

the velocities at the element nodes, $[m]$ is the mass matrix of the element, and $\{\ddot{d}\}$ are the accelerations at the element nodes. The internal force vector, $\{r^{int}\}$, is equivalent to $[k]\{d\}$ for a linear system, where $[k]$ is the stiffness matrix for the element and $\{d\}$ are the displacements at the element nodes.

3.3.1 Framing Element

The framing element, shown in Figure 3.1, is a common two node linear elas-

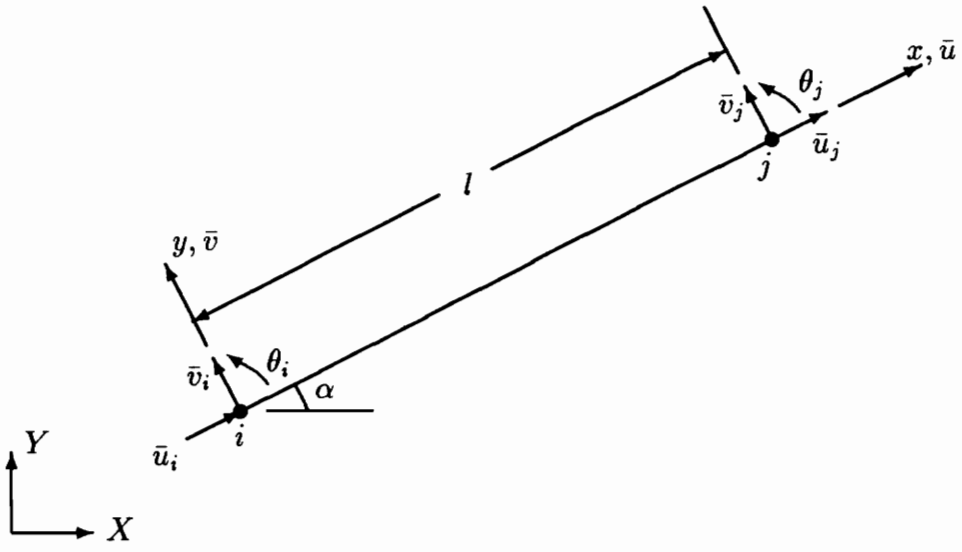

Figure 3.1: Framing Element

tic element with a linear displacement field for the axial displacements and a cubic displacement field for the transverse displacements. The coordinate system located directly on the element is the local coordinate system, which is oriented such that the x–axis is the axial direction and the y–axis is the transverse direction. Angle α is the angle between the x–axis and the global X–axis. The element has a total of six degrees–of–freedom with axial, transverse, and rotational degrees–of–freedom at each node. The displacement field for the axial displacement is

$$\bar{u} = \bar{N}_1 \bar{u}_i + \bar{N}_4 \bar{u}_j \tag{3.3}$$

where $\bar{u}$ is the axial displacement at a point along the element, the $\bar{N}_{i's}$ are the shape functions, and $\bar{u}_i$ and $\bar{u}_j$ are the axial displacements at nodes i and j. The displacement field for the transverse displacement is

$$\bar{v} = \bar{N}_2\bar{v}_i + \bar{N}_3\theta_i + \bar{N}_5\bar{v}_j + \bar{N}_6\theta_j \tag{3.4}$$

where $\bar{v}$ is the transverse displacement at a point along the element and $\bar{v}_i$, $\bar{v}_j$, θ_i, and θ_j are the transverse displacements and rotations at nodes i and j. The shape functions are

$$\begin{aligned} \bar{N}_1 &= 1-\xi \\ \bar{N}_2 &= 1-3\xi^2+2\xi^3 \\ \bar{N}_3 &= l(\xi-2\xi^2+3\xi^3) \\ \bar{N}_4 &= \xi \\ \bar{N}_5 &= 3\xi^2-2\xi^3 \\ \bar{N}_6 &= l(-\xi^2+\xi^3) \end{aligned} \tag{3.5}$$

where ξ is the ratio of $\frac{x}{l}$, x is the distance from node i to the point of interest, and l is the length of the element.

The governing strain–displacement relationships for the element are

$$\begin{aligned} \epsilon_a &= \frac{d\bar{u}}{dx} \\ \epsilon_b &= -y\frac{d^2\bar{v}}{dx^2} \end{aligned} \tag{3.6}$$

where ϵ_a is the axial strain, ϵ_b is the bending strain, and y is the distance from the cross-sectional neutral axis of the beam to a point on the cross–section of the beam. Substituting the displacement fields from Equations 3.3 and 3.4 into the strain–displacement relationships results in the following expressions

$$\begin{aligned} \epsilon_a &= \bar{B}_1\bar{u}_i + \bar{B}_4\bar{u}_j \\ \epsilon_b &= \bar{B}_2\bar{v}_i + \bar{B}_3\theta_i + \bar{B}_5\bar{v}_j + \bar{B}_6\theta_j \end{aligned} \tag{3.7}$$

where the $\bar{B}_{i's}$ are derivatives of shape functions with respect to x and are given by

$$\begin{aligned}
\bar{B}_1 &= \frac{-1}{l} \\
\bar{B}_2 &= -6yl^2(2\xi - 1) \\
\bar{B}_3 &= -2yl(3\xi - 2) \\
\bar{B}_4 &= \frac{1}{l} \\
\bar{B}_5 &= -6yl^2(1 - 2\xi) \\
\bar{B}_6 &= -2yl(3\xi - 1)
\end{aligned} \tag{3.8}$$

The constitutive law for the element is Hooke's law, or

$$\sigma = E\epsilon \tag{3.9}$$

where σ is the element stress, ϵ the element strain, and E is the modulus of elasticity. Substituting the strain–displacement relations from Equation 3.7 into the constitutive laws produces the following expressions

$$\begin{aligned}
\sigma_a &= E(\bar{B}_1\bar{u}_i + \bar{B}_4\bar{u}_j) \\
\sigma_b &= E(\bar{B}_2\bar{v}_i + \bar{B}_3\theta_i + \bar{B}_5\bar{v}_j + \bar{B}_6\theta_j)
\end{aligned} \tag{3.10}$$

where σ_a is the axial stress and σ_b is the bending stress. These equations can be written in matrix form as

$$\begin{Bmatrix} \sigma_a \\ \sigma_b \end{Bmatrix} = E \begin{bmatrix} \bar{B}_1 & 0 & 0 & \bar{B}_4 & 0 & 0 \\ 0 & \bar{B}_2 & \bar{B}_3 & 0 & \bar{B}_5 & \bar{B}_6 \end{bmatrix} \begin{Bmatrix} \bar{u}_i \\ \bar{v}_i \\ \theta_i \\ \bar{u}_j \\ \bar{v}_j \\ \theta_j \end{Bmatrix}$$

This is analogous to $\{\sigma\} = E[\bar{B}]\{d\}_{bm}$ where $\{\epsilon\} = [\bar{B}]\{d\}_{bm}$.

The external virtual work is comprised of the virtual work done by the applied loads less the virtual work absorbed by the inertial and viscous damping loads. The virtual work done by the applied loads is a product of the virtual displacements and the loads acting on the element; the virtual work per unit volume absorbed by the inertial loads a product of the virtual displacements, mass, and acceleration of the element; and the virtual work per unit volume absorbed by the damping loads a product of the virtual displacements, equivalent viscous damping, and velocity of the element. The viscous damping is modeled using the mass–proportional damping term from the Rayleigh damping scheme, which eliminates the need to re–calculate the damping term throughout the analysis. Therefore, the external virtual work is given by

$$\begin{aligned} \delta W_e &= \{\delta d\}_{bm}^T(\{f\}_{bm} + \int_0^l [\bar{N}]^T p(x)\,dx) \\ &\quad - \iiint_{vol} \{\delta d\}_{bm}^T [\bar{N}]^T \rho [\bar{N}] \{\ddot{d}\}_{bm}\, d\,vol \\ &\quad - \iiint_{vol} \{\delta d\}_{bm}^T [\bar{N}]^T 2\omega_n \zeta \rho [\bar{N}] \{\dot{d}\}_{bm}\, d\,vol \end{aligned} \tag{3.11}$$

where $\{\delta d\}_{bm}^T$ is a vector containing the virtual displacements at the nodes, $\{f\}_{bm}$ is a vector of the nodal loads acting on the element, $p(x)$ is a distributed load acting on the element, ρ is the density of an element, and $2\omega_n\zeta\rho$ is a term representing viscous damping per unit volume of an element for mass–proportional Rayleigh damping, where ω_n is the natural frequency of the wall and ζ is the viscous damping factor. The natural frequency for a model is determined using the Vianello–Stodola method (Brebbia and Ferrante, 1978). The internal virtual work is equal to the strain energy, which is given by the virtual strain multiplied by the stress, or

$$\delta U = \iiint_{vol} \{\delta d\}_{bm}^T [\bar{B}]^T E [\bar{B}] \{d\}_{bm}\, d\,vol \tag{3.12}$$

Substituting Equations 3.11 and 3.12 into Equation 3.1 and setting

$$[k]_{bm} = \iiint_{vol} [\bar{B}]^T E [\bar{B}]\, d\,vol \tag{3.13}$$

$$[m]_{bm} = \iiint_{vol} [\bar{N}]^T \rho [\bar{N}] \, d\, vol \tag{3.14}$$

$$[c]_{bm} = 2\omega_n \zeta [m]_{bm} \tag{3.15}$$

results in the equation

$$\{f_t\}_{bm} = [k]_{bm}\{d\}_{bm} + [m]_{bm}\{\ddot{d}\}_{bm} + 2\omega_n\zeta[m]_{bm}\{\dot{d}\}_{bm} \tag{3.16}$$

where $\{f_t\}_{bm}$ is a vector containing both the nodal and distributed applied loads. The stiffness matrix, $[k]_{bm}$, is given by

$$\begin{bmatrix} \frac{EA}{l} & 0 & 0 & -\frac{EA}{l} & 0 & 0 \\ 0 & \frac{12EI}{l^3} & \frac{6EI}{l^2} & 0 & -\frac{12EI}{l^3} & \frac{6EI}{l^2} \\ 0 & \frac{6EI}{l^2} & \frac{4EI}{l} & 0 & -\frac{6EI}{l^2} & -\frac{2EI}{l} \\ -\frac{EA}{l} & 0 & 0 & \frac{EA}{l} & 0 & 0 \\ 0 & -\frac{12EI}{l^3} & -\frac{6EI}{l^2} & 0 & \frac{12EI}{l^3} & -\frac{6EI}{l^2} \\ 0 & \frac{6EI}{l^2} & \frac{2EI}{l} & 0 & -\frac{6EI}{l^2} & \frac{4EI}{l} \end{bmatrix}$$

where A is the cross–sectional area of the element and I is the moment of inertia of the element. The mass matrix, $[m]$, is calculated by multiplying out Equation 3.14 or using a lumped mass formulation.

3.3.2 Sheathing Element

The sheathing element, shown in Figure 3.2, is a four node plane rectangular bilinear element (Cook, 1989). The element has a total of eight degrees–of–freedom with degrees–of–freedom at each node modeling displacement along the x– and y–axes. The element has a linear displacement field along each axis and does not deflect in the out–of–plane direction. The displacement field in the x–direction is

$$\tilde{u} = \tilde{N}_1\tilde{u}_1 + \tilde{N}_2\tilde{u}_2 + \tilde{N}_3\tilde{u}_3 + \tilde{N}_4\tilde{u}_4 \tag{3.17}$$

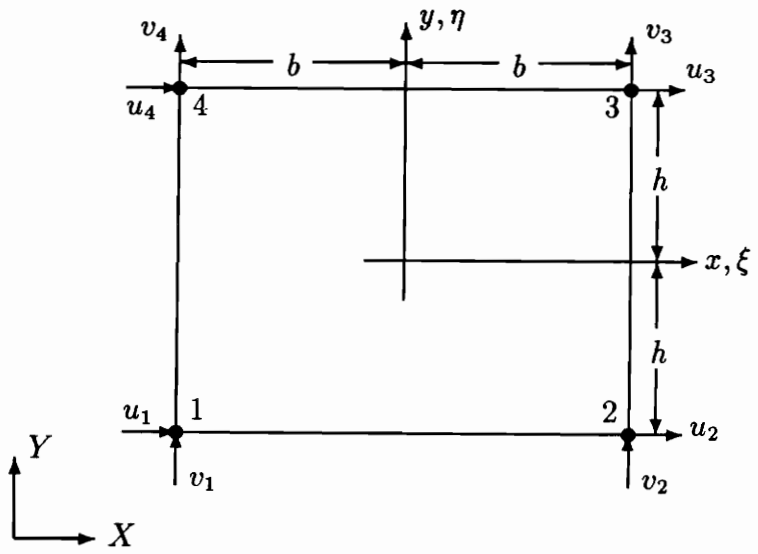

Figure 3.2: Sheathing Element

where $\tilde{u}$ is the displacement at a point on the element in the x–direction, the $\tilde{N}_{i's}$ are the shape functions, and the $\tilde{u}_{i's}$ are the nodal displacements in the x–direction. The displacement field in the y–direction is

$$\tilde{v} = \tilde{N}_1\tilde{v}_1 + \tilde{N}_2\tilde{v}_2 + \tilde{N}_3\tilde{v}_3 + \tilde{N}_4\tilde{v}_4 \tag{3.18}$$

where $\tilde{v}$ is the displacement at a point on the element in the y–direction and the $\tilde{v}_{i's}$ the nodal displacements in the y–direction. The shape functions are

$$\begin{aligned} \tilde{N}_1 &= 0.25(1-\xi)(1-\eta) \\ \tilde{N}_2 &= 0.25(1-\xi)(1+\eta) \\ \tilde{N}_3 &= 0.25(1+\xi)(1+\eta) \\ \tilde{N}_4 &= 0.25(1+\xi)(1-\eta) \end{aligned} \tag{3.19}$$

where ξ is the ratio of $\frac{x}{b}$, η is the ratio of $\frac{y}{h}$, and b and h are half the length of the side of the element, as shown in Figure 3.2.

The compatibility relationships for the sheathing element are derived from Kirchhoff plate theory and are

$$\begin{aligned} \epsilon_x &= \frac{\partial \tilde{u}}{\partial x} \\ \epsilon_y &= \frac{\partial \tilde{v}}{\partial y} \\ \epsilon_{xy} &= \frac{\partial \tilde{u}}{\partial y} + \frac{\partial \tilde{v}}{\partial x} \end{aligned} \tag{3.20}$$

where ϵ_x is the strain in the x–direction, ϵ_y is the strain in the y–direction, and ϵ_{xy} is the shear strain. Substitution of the displacement functions from Equations 3.17 and 3.18 into the strain–displacement relations results in

$$\begin{aligned} \epsilon_x &= \tilde{B}_{1x}\tilde{u}_1 + \tilde{B}_{2x}\tilde{u}_2 + \tilde{B}_{3x}\tilde{u}_3 + \tilde{B}_{4x}\tilde{u}_4 \\ \epsilon_y &= \tilde{B}_{1y}\tilde{v}_1 + \tilde{B}_{2y}\tilde{v}_2 + \tilde{B}_{3y}\tilde{v}_3 + \tilde{B}_{4y}\tilde{v}_4 \\ \epsilon_{xy} &= \tilde{B}_{1y}\tilde{u}_1 + \tilde{B}_{2y}\tilde{u}_2 + \tilde{B}_{3y}\tilde{u}_3 + \tilde{B}_{4y}\tilde{u}_4\tilde{B}_{1x}\tilde{v}_1 + \tilde{B}_{2x}\tilde{v}_2 + \tilde{B}_{3x}\tilde{v}_3 + \tilde{B}_{4x}\tilde{v}_4 \end{aligned} \tag{3.21}$$

where the $\tilde{B}_{i's}$, which are derivatives of shape functions with respect to x or y, are given by

$$\begin{aligned} \tilde{B}_{1x} &= -\frac{1}{4b}(1-\eta) \\ \tilde{B}_{2x} &= -\frac{1}{4b}(1+\eta) \\ \tilde{B}_{3x} &= \frac{1}{4b}(1+\eta) \\ \tilde{B}_{4x} &= \frac{1}{4b}(1-\eta) \\ \tilde{B}_{1y} &= -\frac{1}{4h}(1-\xi) \\ \tilde{B}_{2y} &= \frac{1}{4h}(1-\xi) \\ \tilde{B}_{3y} &= \frac{1}{4h}(1-\xi) \\ \tilde{B}_{4y} &= -\frac{1}{4h}(1-\xi) \end{aligned} \tag{3.22}$$

The constitutive laws are given by

$$\begin{aligned} \sigma_x &= \frac{E_x}{H}\epsilon_x + \frac{E_x\nu_{xy}}{H}\epsilon_y \\ \sigma_y &= \frac{E_y\nu_{yx}}{H}\epsilon_x + \frac{E_y}{H}\epsilon_y \\ \sigma_{xy} &= G_{xy}\epsilon_{xy} \end{aligned} \tag{3.23}$$

where E_x is the modulus of elasticity in the x–direction, E_y is the modulus of elasticity in the y–direction, ν_{xy} is poisson's ratio giving the strain in the x–direction given a stress in the y–direction, ν_{yx} is the poisson's ratio giving the strain in the y–direction given a stress in the x–direction, G_{xy} is the shear modulus of elasticity, and $H = 1 - \nu_{xy}\nu_{yx}$. Substituting the strain–displacement relationships from Equation 3.21 into the constitutive laws and writing the resulting equation in matrix form

$$\begin{Bmatrix} \sigma_x \\ \sigma_y \\ \sigma_{xy} \end{Bmatrix} = \begin{bmatrix} \frac{E_x}{H} & \frac{E_x\nu_{xy}}{H} & 0 \\ \frac{E_y\nu_{yx}}{H} & \frac{E_y}{H} & 0 \\ 0 & 0 & G_{xy} \end{bmatrix} \begin{bmatrix} \tilde{B}_{1x} & 0 & \tilde{B}_{1y} \\ 0 & \tilde{B}_{1y} & \tilde{B}_{1x} \\ \tilde{B}_{2x} & 0 & \tilde{B}_{2y} \\ 0 & \tilde{B}_{2y} & \tilde{B}_{2x} \\ \tilde{B}_{3x} & 0 & \tilde{B}_{3y} \\ 0 & \tilde{B}_{3y} & \tilde{B}_{3x} \\ \tilde{B}_{4x} & 0 & \tilde{B}_{4y} \\ 0 & \tilde{B}_{4y} & \tilde{B}_{4x} \end{bmatrix}^T \begin{Bmatrix} \tilde{u}_1 \\ \tilde{v}_1 \\ \tilde{u}_2 \\ \tilde{v}_2 \\ \tilde{u}_3 \\ \tilde{v}_3 \\ \tilde{u}_4 \\ \tilde{v}_4 \end{Bmatrix}$$

which is analogous to $\{\sigma\} = [G][\tilde{B}]\{d\}_{sh}$ where $\{\epsilon\} = [\tilde{B}]\{d\}_{sh}$.

The external virtual work is comprised of the virtual work done by the applied loads less the virtual work absorbed by the inertial and viscous damping loads. The virtual work done by the applied loads is a product of the nodal virtual displacements and the loads acting on the element; the virtual work absorbed by the inertial loads a product of the virtual displacements, mass, and acceleration of the element; and the virtual work absorbed by the damping loads a product of the virtual displacements, equivalent viscous damping, and velocity of the element. The viscous damping

is modeled using the mass–proportional damping term from the Rayleigh damping scheme, which eliminates the need to re–calculate the damping term throughout the analysis. Therefore, the external virtual work is given by

$$\begin{aligned} \delta W_e &= \{\delta d\}_{sh}^T \{f\}_{sh} - \iiint_{vol} \{\delta d\}_{sh}^T [\tilde{N}]^T \rho [\tilde{N}] \{\ddot{d}\}_{sh} \, d\,vol \\ &\quad - \iiint_{vol} \{\delta d\}_{sh}^T [\tilde{N}]^T 2\omega_n \zeta \rho [\tilde{N}] \{\dot{d}\}_{sh} \, d\,vol \end{aligned} \tag{3.24}$$

where $\{\delta d\}_{sh}^T$ is a vector containing the nodal virtual displacements, $\{f\}_{sh}$ is a vector of the nodal loads acting on the element, ρ is the density of an element, and $2\omega_n\zeta\rho$ is a term representing viscous damping per unit volume of an element. The internal virtual work per unit volume is equal to the strain energy, which is given by the virtual strain multiplied by the stress, or

$$\delta \bar{U} = \{\delta d\}_{sh}^T [\tilde{B}]^T [G] [\tilde{B}] \{d\}_{sh} \tag{3.25}$$

Substituting Equations 3.24 and 3.25 into Equation 3.1 and setting

$$[k]_{sh} = \iiint_{vol} [\tilde{B}]^T [G] [\tilde{B}] \, d\,vol \tag{3.26}$$

$$[m]_{sh} = \iiint_{vol} [\tilde{N}]^T \rho [\tilde{N}] \, d\,vol \tag{3.27}$$

$$[c]_{bm} = 2\omega_n \zeta [m]_{bm} \tag{3.28}$$

results in the equation

$$\{f\}_{sh} = [k]_{sh} \{d\}_{sh} + [m]_{sh} \{\ddot{d}\}_{sh} + [c]_{sh} \{\dot{d}\}_{sh} \tag{3.29}$$

where $[k]_{sh}$ is calculated using Gauss quadrature and $[m]_{sh}$ is calculated using Gauss quadrature or a lumped mass formulation.

3.3.3 Connector Element

Two independent nonlinear springs, one acting parallel to the global X–axis and the other parallel to the global Y–axis, are used to model the response of the connectors that attach the sheathing to the framing in a shear wall. The element has no

independent degrees–of–freedom but instead utilizes the degrees–of–freedom of the framing and sheathing elements it connects. The element operates in the following manner. A force applied to a connector element passing through concurrent points on the sheathing and framing causes a displacement between the points, as is shown in Figure 3.3. The components of this displacement, Δu and Δu, are calculated by

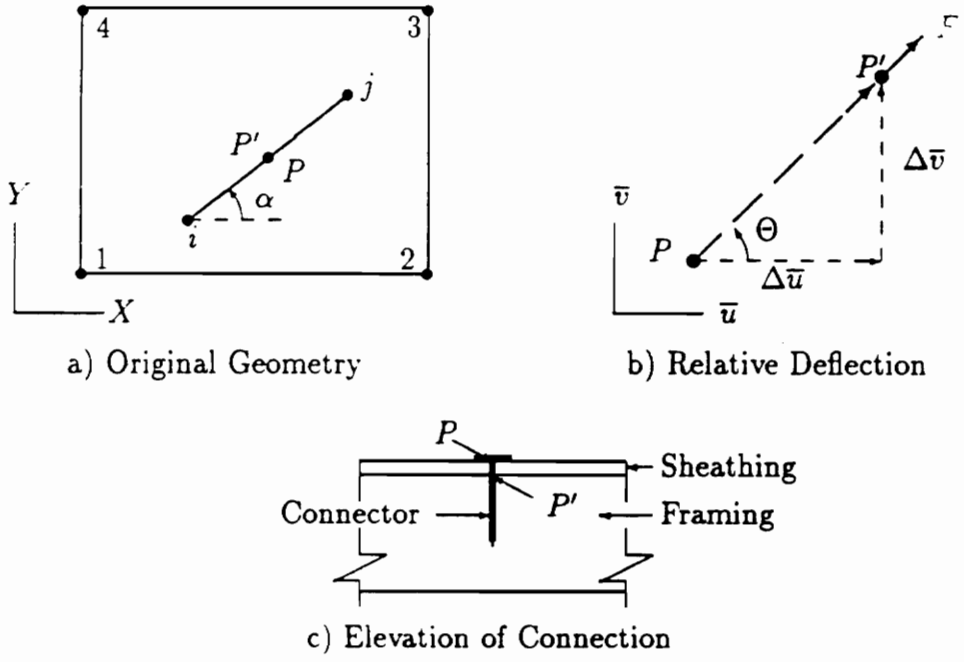

Figure 3.3: Mechanism for a Connector Element (Dolan, 1989)

determining the axial and transverse displacements of the framing element at the point, transforming these displacements from the coordinate system of the framing to that of the system, and subtracting the sheathing displacements at that point. The transformation of frame displacements from local to global coordinates is done using the following relationship

$$\begin{Bmatrix} \bar{U} \\ \bar{V} \end{Bmatrix} = \begin{bmatrix} cos\alpha & sin\alpha \\ -sin\alpha & cos\alpha \end{bmatrix} \begin{Bmatrix} \bar{u} \\ \bar{v} \end{Bmatrix}$$

where $\bar{U}$ and $\bar{V}$ are the frame displacements along the global $X-$ and $Y-$ axes. This leads to the relationships

$$\begin{aligned} \bar{U} &= \bar{u}cos\alpha + \bar{v}sin\alpha \\ \bar{V} &= -\bar{u}sin\alpha + \bar{v}cos\alpha \end{aligned} \tag{3.30}$$

Substituting the expressions from Equations 3.3 and 3.4 into Equation 3.30 and subtracting Equations 3.17 and 3.18 results in the following expressions governing the components of the connector displacement

$$\begin{aligned} \Delta\bar{u} &= \bar{N}_1\bar{u}_i cos\alpha + \bar{N}_2\bar{v}_i sin\alpha + \bar{N}_3\bar{\theta}_i sin\alpha + \bar{N}_4\bar{u}_j cos\alpha + \bar{N}_5\bar{v}_j sin\alpha + \bar{N}_6\bar{\theta}_j sin\alpha \\ &\quad -\tilde{N}_1\tilde{u}_1 - \tilde{N}_2\tilde{u}_2 - \tilde{N}_3\tilde{u}_3 - \tilde{N}_4\tilde{u}_4 \end{aligned} \tag{3.31}$$

$$\begin{aligned} \Delta\bar{v} &= -\bar{N}_1\bar{u}_i sin\alpha + \bar{N}_2\bar{v}_i cos\alpha + \bar{N}_3\bar{\theta}_i cos\alpha - \bar{N}_4\bar{u}_j sin\alpha + \bar{N}_5\bar{v}_j cos\alpha + \bar{N}_6\bar{\theta}_j cos\alpha \\ &\quad -\tilde{N}_1\tilde{v}_1 - \tilde{N}_2\tilde{v}_2 - \tilde{N}_3\tilde{v}_3 - \tilde{N}_4\tilde{v}_4 \end{aligned}$$

which can be written in matrix form as

$$\begin{Bmatrix} \Delta\bar{u} \\ \Delta\bar{v} \end{Bmatrix} = \begin{bmatrix} \bar{N}_1 cos\alpha & -\bar{N}_1 sin\alpha \\ \bar{N}_2 sin\alpha & \bar{N}_2 cos\alpha \\ \bar{N}_3 sin\alpha & \bar{N}_3 cos\alpha \\ \bar{N}_4 cos\alpha & -\bar{N}_4 sin\alpha \\ \bar{N}_5 sin\alpha & \bar{N}_5 cos\alpha \\ \bar{N}_6 sin\alpha & \bar{N}_6 cos\alpha \\ \tilde{N}_1 & 0 \\ 0 & \tilde{N}_1 \\ \tilde{N}_2 & 0 \\ 0 & \tilde{N}_2 \\ \tilde{N}_3 & 0 \\ 0 & \tilde{N}_3 \\ \tilde{N}_4 & 0 \\ 0 & \tilde{N}_4 \end{bmatrix}^T \begin{Bmatrix} \bar{u}_i \\ \bar{v}_i \\ \theta_i \\ \bar{u}_j \\ \bar{v}_j \\ \theta_j \\ -\tilde{u}_1 \\ -\tilde{v}_1 \\ -\tilde{u}_2 \\ -\tilde{v}_2 \\ -\tilde{u}_3 \\ -\tilde{v}_3 \\ -\tilde{u}_4 \\ -\tilde{v}_4 \end{Bmatrix}$$

This is analogous to $\{\Delta\}_{con} = [N]\{d\}_{con}$ where $\{\Delta\}_{con}$ is a vector containing the displacement of the connector in the X–direction and the Y–direction.

The relationship between the load applied to the connector element and the resulting displacement were determined from curve–fitting of experimental data. The load–displacement relationship for a connector subjected to monotonic loading is characterized by the curve shown in Figure 3.4. The curve is governed by the following equation developed by Foschi (1977) when $|\Delta| \leq |\Delta_{max}|$

$$|F_{con}| = (P_o + K_1|\Delta|)[1 - exp(\frac{-K_2|\Delta|}{P_o})] \tag{3.32}$$

and by the following modification of Equation 3.32 developed by Dolan (1989) when $|\Delta| > |\Delta_{max}|$

$$|F_{con}| = (P_o + K_1|\Delta_{max}|)[1 - exp(\frac{-K_2|\Delta_{max}|}{P_o})] - K_3(|\Delta| - |\Delta_{max}|) \tag{3.33}$$

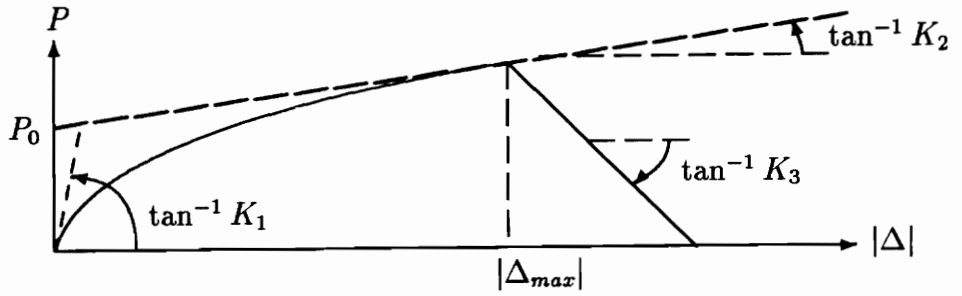

Figure 3.4: Load–Displacement Relationship for Connector Element Subjected to Monotonic Loading (Dolan, 1989)

where Δ is the connector displacement (in either the X– or Y–direction), Δ_{max} is the displacement at which the maximum resistance of the connector occurs, K_1 is the slope of the curve at the origin, K_2 is the slope of the curve at Δ_{max}, P_o is the load–intercept of the line tangent to the curve at Δ_{max}, and K_3 is the slope of the curve for displacements greater than Δ_{max}.

The load–displacement relationship for a connector subjected to dynamic loading is characterized by the curve shown in Figure 3.5. The curve is divided into four segments, which are governed by the following equations (Dolan, 1989):

$$\begin{aligned} F_{con(1)} &= -P_1 + K_4\Delta + [exp(a_1\Delta) - 1] \\ a_1 &= \frac{ln(F_1 + P_1 - K_4u_1 + 1)}{u_1} \end{aligned} \tag{3.34}$$

$$\begin{aligned} F_{con(2)} &= -P_1 + K_4\Delta - [exp(a_2|\Delta|) - 1] \\ a_2 &= \frac{ln(-F_2 - P_1 + K_4u_2 + 1)}{u_2} \end{aligned} \tag{3.35}$$

$$\begin{aligned} F_{con(3)} &= P_1 + K_4\Delta - [exp(a_3|\Delta|) - 1] \\ a_3 &= \frac{ln(-F_2 + P_1 + K_4u_2 + 1)}{u_2} \end{aligned} \tag{3.36}$$

$$\begin{aligned} F_{con(4)} &= P_1 + K_4\Delta + [exp(a_4\Delta) - 1] \\ a_4 &= \frac{ln(F_1 - P_1 - K_4u_1 + 1)}{u_1} \end{aligned} \tag{3.37}$$

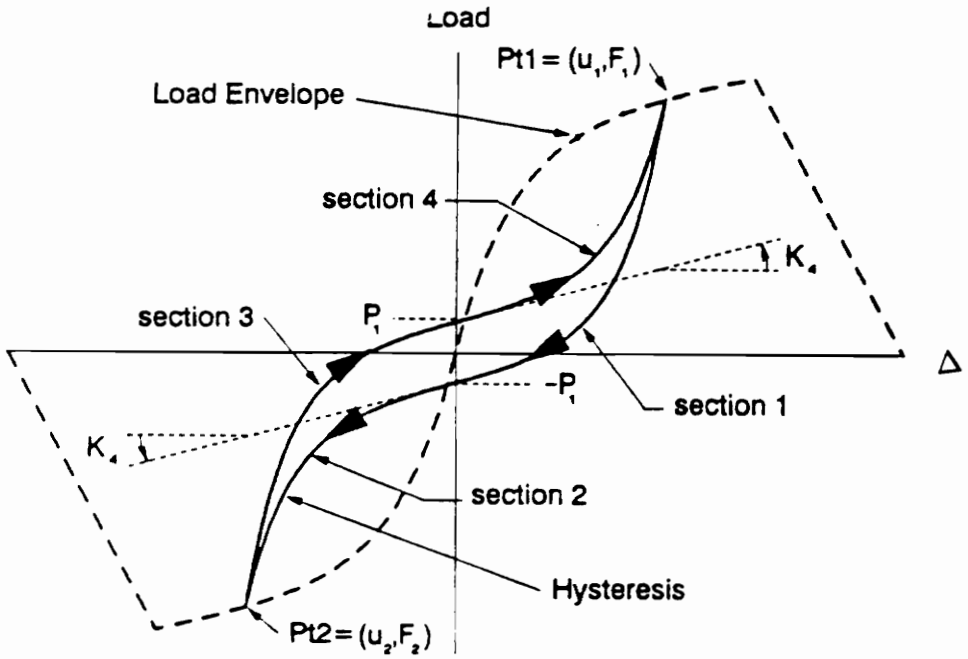

Figure 3.5: Load–Displacement Relationship for Connector Element Subjected to Dynamic Loading (Dolan, 1989)

where $F_{con(i)}$ is the force of the connector in segment i, P_1 is the load at zero deflection, K_4 is the stiffness at zero deflection, and $u_{1,2}$ and $F_{1,2}$ are the maximum and minimum deflections loads that the connector has experienced. The load envelope, which is denoted by the dashed line in Figure 3.5, is governed by the relationships for the connector subjected to monotonic loading.

The external virtual work is equal to the virtual displacements multiplied by the corresponding nodal or effective nodal loads, or

$$\delta W_e = \{\delta d\}_{con}^T \{f_t\}_{con} \tag{3.38}$$

where $\{\delta d\}_{con}^T$ are the nodal virtual displacements and $\{f_t\}_{con}$ the distributed and nodal loads acting on the framing and sheathing elements to which the connector is attached. The internal virtual work of the connectors is a product of the virtual

displacement, stiffness, and displacement of the element. This can be written as

$$\delta U = \{\delta d\}_{con}^{T}[N]^{T}k_{con}[N]\{\delta d\}_{con} \tag{3.39}$$

where k_{con} is a function of displacement. Substituting Equations 3.38 and 3.39 into Equation 3.1 results in

$$\{\delta d\}_{con}^{T}\{f_t\}_{con} - \{\delta d\}_{con}^{T}\{r^{int}\} = 0 \tag{3.40}$$

where $\{r^{int}\}$, which is the internal force vector, is equal to $[N]^{T}k_{con}[N]\{\delta d\}_{con}$. Rearranging Equation 3.40 results in the equation

$$\{f_t\}_{con} = \{r^{int}\} \tag{3.41}$$

which cannot be solved explicitly because of the nonlinearity in the element.

3.3.4 Bearing Element

A bi–linear spring is used to model the effect of two sheathing panels bearing on each other. The element has no independent degrees–of–freedom but instead utilizes the degrees–of–freedom of the adjacent sheathing elements. This element is included because models that neglect the effect of bearing underestimate the sheathing stiffness because the plate elements will be able to mathematically overlap each other with no resistance (Dolan, 1989). The element has a low stiffness in tension, which permits free movement of the sheathing panels when they are not bearing on one–another, and a high stiffness in compression, which allows the effect of bearing to be included when the panels are in contact (see Figure 3.6). The relative displacement of the adjacent nodes is used to determine if the plates overlap. Given nodes k and s on sheathing elements 1 and 2, as shown in Figure 3.7, the displacements for the nodes is determined using Equation 3.17 if the vertical edges of the sheathing bear against one–another (i.e., the bearing force is in the X–direction) or Equation 3.18 if the

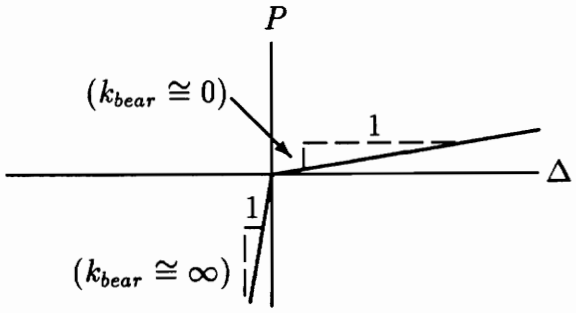

Figure 3.6: Stiffness of Bearing Element (Dolan, 1989)

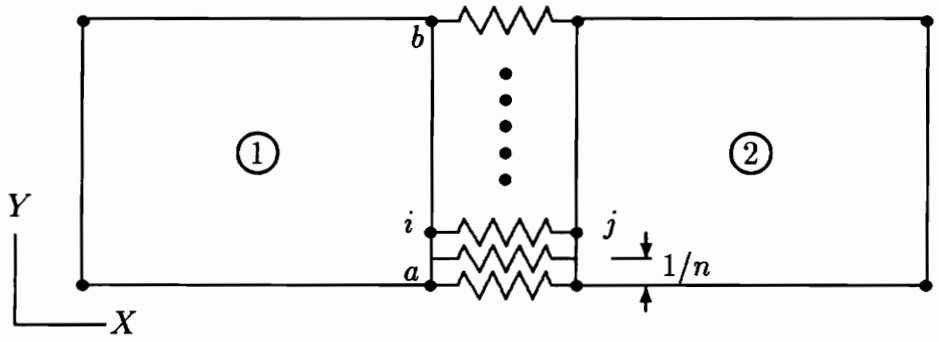

Figure 3.7: Schematic of Bearing Element (Dolan, 1989)

horizontal edges of the sheathing bear against one–another. Therefore, the relative displacement of the sheathing panels in the $X-$ and $Y-$ directions are given by

$$\begin{aligned} \Delta X &= \tilde{N}_1\tilde{u}_{1(1)} + \tilde{N}_2\tilde{u}_{2(1)} + \tilde{N}_3\tilde{u}_{3(1)} + \tilde{N}_4\tilde{u}_{4(1)} \\ &\quad -\tilde{N}_1\tilde{u}_{1(2)} - \tilde{N}_2\tilde{u}_{2(2)} - \tilde{N}_3\tilde{u}_{3(2)} - \tilde{N}_4\tilde{u}_{4(2)} \end{aligned} \tag{3.42}$$

$$\begin{aligned} \Delta Y &= \tilde{N}_1\tilde{v}_{1(1)} + \tilde{N}_2\tilde{v}_{2(1)} + \tilde{N}_3\tilde{v}_{3(1)} + \tilde{N}_4\tilde{v}_{4(1)} \\ &\quad -\tilde{N}_1\tilde{v}_{1(2)} - \tilde{N}_2\tilde{v}_{2(2)} - \tilde{N}_3\tilde{v}_{3(2)} - \tilde{N}_4\tilde{v}_{4(2)} \end{aligned}$$

where the numbers in parenthesis indicate the sheathing panel. Equation 3.42 can be written in matrix form as

$$\begin{Bmatrix} \Delta X \\ \Delta Y \end{Bmatrix} = \begin{bmatrix} \tilde{N}_1 & 0 \\ 0 & \tilde{N}_1 \\ \tilde{N}_2 & 0 \\ 0 & \tilde{N}_2 \\ \tilde{N}_3 & 0 \\ 0 & \tilde{N}_3 \\ \tilde{N}_4 & 0 \\ 0 & \tilde{N}_4 \\ \tilde{N}_1 & 0 \\ 0 & \tilde{N}_1 \\ \tilde{N}_2 & 0 \\ 0 & \tilde{N}_2 \\ \tilde{N}_3 & 0 \\ 0 & \tilde{N}_3 \\ \tilde{N}_4 & 0 \\ 0 & \tilde{N}_4 \end{bmatrix}^T \begin{Bmatrix} \tilde{u}_{1(1)} \\ \tilde{v}_{1(1)} \\ \tilde{u}_{2(1)} \\ \tilde{v}_{2(1)} \\ \tilde{u}_{3(1)} \\ \tilde{v}_{3(1)} \\ \tilde{u}_{4(1)} \\ \tilde{v}_{4(1)} \\ -\tilde{u}_{1(2)} \\ -\tilde{v}_{1(2)} \\ -\tilde{u}_{2(2)} \\ -\tilde{v}_{2(2)} \\ -\tilde{u}_{3(2)} \\ -\tilde{v}_{3(2)} \\ -\tilde{u}_{4(2)} \\ -\tilde{v}_{4(2)} \end{Bmatrix}$$

which is analogous to $\{\Delta\}_{bear} = [\hat{N}]\{d\}_{bear}$ where $\{\Delta\}_{bear}$ is a vector containing the relative displacement between the sheathing elements in the X–direction and/or the Y–direction.

The external virtual work is equal to the virtual work of the nodal loads multiplied by the corresponding nodal virtual displacements, or

$$\delta W_e = \{\delta d\}^T_{bear}\{f\}_{bear} \tag{3.43}$$

where $\{\delta d\}^T_{bear}$ are the nodal virtual displacements of and $\{f\}_{bear}$ the nodal loads acting on the sheathing elements upon which the bearing element acts. The internal

virtual work is a product of the virtual displacement, stiffness, and displacement of the element. This can be written as

$$\delta U = \{\delta d\}^T_{bear}[N]^T k_{bear}[N]\{d\}_{bear} \tag{3.44}$$

where k_{bear} is the stiffness of the element. Substituting Equations 3.43 and 3.44 into Equation 3.1 results in

$$\{\delta d\}^T_{bear}\{f\}_{bear} - \{\delta d\}^T_{bear}[N]^T k_{bear}[N]\{d\}_{bear} = 0 \tag{3.45}$$

Rearranging Equation 3.45 and setting

$$[k]_{bear} = [N]^T k_{bear}[N] \tag{3.46}$$

results in the equation

$$\{f\}_{bear} = [k]_{bear}\{d\}_{bear} \tag{3.47}$$

where $[k]_{bear}$ is calculated by multiplying the right side of Equation 3.46.

3.4 Formulation of Shear Wall Model

The relationship between the applied loads and the internal, viscous damping, and inertial loads for the entire shear wall model is developed by merging the mass and stiffness matrices from each of the individual elements and forming the mass–proportional viscous damping matrix and the applied load vector. The same principles used to formulate the elements (constitutive laws, compatibility, and equilibrium) are used to formulate the mass and stiffness matrices for the wall model. The constitutive laws are inherent in the element models and therefore are already imposed for the system model (Holzer, 1990). The conditions of compatibility and equilibrium were imposed by using the member code technique developed by Tezcan (1963). The technique involves relating the degrees–of–freedom of the individual elements to those

of the system and then adding the components of the element matrices to the proper locations in the system matrices. Applying the technique to the mass and stiffness matrices of the elements and using mass–proportional damping for the entire system results in the equation

$$[M]\{\ddot{D}\} + [C]\{\dot{D}\} + \{R^{int}\} = \{F(t)\} \tag{3.48}$$

where $[M]$ is the mass matrix for the system; $\{\ddot{D}\}$ is the vector containing the acceleration at the degrees–of–freedom; $[C]$ is the viscous damping matrix for the system, which is equal to $2\omega\zeta[M]$; $\{\dot{D}\}$ is the vector containing the velocity at the degrees–of–freedom; $\{R^{int}\}$ is the internal force vector for the system; and $\{F(t)\}$ is a vector containing the applied loads.

The seismic loading is applied to the model in the following manner. As will be discussed later, the majority (over 99%) of the mass in the models is distributed along the sill plate, which reflects the mass of the upper story. This is analogous to a structure with the majority of the mass concentrated at the floor levels. Therefore, the applied loads for seismic loading are (Clough and Penzien, 1975):

$$\{F(t)\} = -[M]\{I\}\ddot{D}_g \tag{3.49}$$

where $\{I\}$ is the influence vector and $\ddot{D}_g$ is the ground acceleration. Substituting this expression into Equation 3.48 results in

$$[M]\{\ddot{D}\} + [C]\{\dot{D}\} + \{R^{int}\} = -[M]\{I\}\ddot{D}_g \tag{3.50}$$

which is the equation–of–motion for the shear wall model subjected to seismic loads. The inertial and damping effects are neglected for static or monotonic loading applied at a slow rate, which reduces Equation 3.48 to

$$\{R^{int}\} = \{F\} \tag{3.51}$$

where the internal forces and applied load are not functions of time.

3.5 Solution Methods

Two solution methods are used in the program to solve the equations of equilibrium: the Newton–Raphson method for models subjected to static or monotonic loads and the Newmark–Beta method for models subjected to dynamic loads. Different methods are used because of the differences in solution techniques needed for each.

3.5.1 Static or Monotonic Loading

Analysis of a wall model subjected to static or monotonic loading is performed using the Newton–Raphson method (Cook, 1989) because of the nonlinearity of the connector elements. The method proceeds as follows. First, the global tangent stiffness matrix, $[K_t]_n$, for the shear wall is determined, where n is the iteration number. This is the matrix containing the stiffnesses from the framing, sheathing, and bearing elements and the tangent of the load–displacement curve for the connector elements. Next, the residual applied load vector, $\{R\}_n$, is determined. The residual force is governed by the equation

$$\{R\}_n = \{F\} - \{Q\}_{n-1} \tag{3.52}$$

where $\{Q\}_{n-1}$ is a vector of the force at the displacement from the previous iteration, or $\{D\}_{n-1}$. The tangent stiffness matrix and residual applied load vector are then substituted into the relationship

$$[K_t]_n\{\Delta D\}_n = \{R\}_n \tag{3.53}$$

which is then solved for the change in displacement $\{\Delta D\}_n$.

$$\{\Delta D\}_n = \{D\}_n - \{D\}_{n-1} \tag{3.54}$$

Equation 3.53 is solved for $\{\Delta D\}_n$ using Gauss elimination. Determination of the solution convergence is done by summing the change in displacements for each of the

degrees–of–freedom and determining if the change exceeds a specified tolerance. This is summarized by the expression

$$\sqrt{\sum_{i=1}^{dof}[(D_i)_n - (D_i)_{n-1}]^2} \leq TOL \sqrt{\sum_{i=1}^{dof}(D_i)_{n-1}^2} \tag{3.55}$$

If the conditions of Equation 3.55 are not satisfied, a modified residual load vector is determined and the process is repeated until the tolerance requirement is satisfied. If the value of $\{\Delta D\}_n$ falls below a user specified tolerance, the analysis is completed. The small tolerance corresponds to a low residual force. In summary, the analysis is performed as follows:

1. Form the tangent stiffness matrix, $[K_t]_n$
2. Form the residual load vector, $\{R\}_n$, using Equation 3.52.
3. Solve Equation 3.53 for $\{\Delta D\}_n$.
4. Calculate $\{D\}_n$ using Equation 3.54.
5. Determine if the solution tolerance is satisfied using Equation 3.55.
   (a) If tolerance is met, calculate stresses and forces for the framing and sheathing elements using Equations 3.11, 3.16, 3.24, and 3.29. If a monotonic analysis is being performed, increment the load vector, $\{F\}$, go to Step 1, and repeat analysis.
   (b) If tolerance is not met, goto step 1 and continue analysis with next iteration.

3.5.2 Dynamic Loading

Analysis of a shear wall model subjected to dynamic loading is performed using the Newmark–Beta method, which is an implicit direct integration method (Cook, 1989).

The relationships utilized in the method are derived as follows. A discretized equation is formed by taking the difference between the equation of motion (Equation 3.50) at time $t + \Delta t$ and at time t. The resulting discretized equation is given by

$$[M]\{\Delta\ddot{D}\} + [C]\{\Delta\dot{D}\} + [K_t]\{\Delta D\} = -[M]\{I\}\Delta\ddot{D}_g \tag{3.56}$$

where $\{\Delta\ddot{D}\}$, $\{\Delta\dot{D}\}$, $\{\Delta D\}$, and $\Delta\ddot{D}_g$ are the changes in acceleration, velocity, displacement, and ground acceleration over a time step and (Cook, 1989)

$$\{R^{int}(t + \Delta t)\} - \{R^{int}(t)\} = [K_t]\{\Delta D\} \tag{3.57}$$

where $[K]_t$ is the tangent stiffness matrix. Assuming that the acceleration over a time step remains constant, the acceleration, velocity, and displacement at any time during the step can be characterized by the following expressions

$$\begin{aligned} \ddot{x}(\tau) &= \frac{\ddot{x}_{t+\Delta t} + \ddot{x}_t}{2} \\ \dot{x}(\tau) &= \dot{x}_t + \int_t^\tau \ddot{x}(\tau)\, d\tau \\ x(\tau) &= x_t + \int_t^\tau \dot{x}(\tau)\, d\tau \end{aligned} \tag{3.58}$$

where $t \leq \tau \leq t + \Delta t$. Integrating Equations 3.58, solving for $\Delta\ddot{x}$ and $\Delta\dot{x}$, and substituting $\{D's\}$ for the $x's$ results in the following relationships for the changes in acceleration and velocity over a time step

$$\{\Delta\ddot{D}\} = \{\ddot{D}(t + \Delta t)\} - \{\ddot{D}(t)\} = \frac{1}{\beta(\Delta t)^2}\{\Delta D\} - \frac{1}{\beta\Delta t}\{\dot{D}(t)\} - \frac{1}{2\beta}\{\ddot{D}(t)\} \tag{3.59}$$

$$\{\Delta\dot{D}\} = \{\dot{D}(t + \Delta t)\} - \{\dot{D}(t)\} = \Delta t\{\ddot{D}(t)\} + \frac{\gamma}{\beta\Delta t}\{\Delta D\} - \frac{\gamma}{\beta}\{\dot{D}(t)\} - \frac{\gamma\Delta t}{2\beta}\{\ddot{D}(t)\} \tag{3.60}$$

where β and γ represent the constants generated from the integrations and are 0.25 and 0.5, respectively, for the assumption of constant acceleration during a time step. Using these values of β and γ also ensures an inherently stable solution. Substituting Equations 3.59 and 3.60 into Equation 3.56 leads to the following relationship:

$$[\hat{K}]\{\Delta D\} = \{\hat{F}\} \tag{3.61}$$

where $[\hat{K}]$ is the effective stiffness matrix, which is given by

$$[\hat{K}] = \frac{1}{\beta(\Delta t)^2}[M] + \frac{\gamma}{\beta \Delta t}[C] + [K_t] \tag{3.62}$$

and $\{\hat{F}\}$ is the effective load vector, which is given by

$$\begin{aligned} \{\hat{F}\} &= [M](-\{I\}\Delta\ddot{D}_g(t) + \frac{1}{2\beta}\{\ddot{D}(t)\} + \frac{1}{\beta\Delta t}\{\dot{D}(t)\}) + \\ & [C]((\frac{\gamma}{2\beta} - 1)\Delta t\{\ddot{D}(t)\} + \frac{\gamma}{\beta}\{\dot{D}(t)\}) \end{aligned} \tag{3.63}$$

Equation 3.61 is solved to determine the change in displacements, $\{\Delta D\}$, during a given time step, which can then be used to determine the changes in velocity and acceleration over the time step.

3.5.3 Residual Force Check

The nonlinear behavior of the connector elements in a wall model allows for the occurrence of residual forces, which must be monitored for the models subjected to seismic loading to ensure that the forces do not become excessive. The check for excessive residual forces is done only on the connector elements in WALSEIZ because they are the only nonlinear element in the shear wall models. The residual force, as shown in Figure 3.8, is the difference between the load on the hysteretic curve at time $t + \Delta t$ and the load approximated at time $t + \Delta t$ using the tangent stiffness at time t, or

$$Residual = F_{con}^{t+\Delta t} - (F_{con}^{t} + \delta k_{con}^{t}) \tag{3.64}$$

The acceptability of the residual force in the connector elements is monitored using two criteria. The criteria are are imposed for the system and not individual connectors so that a large error in a single connector will not cause the tolerance to be exceeded. The first criterion, governed by the relationship

$$\sqrt{\sum_{i=1}^{ncc}[(F_{con}^{t+\Delta t} - (F_{con}^{t} + \delta k_{con}^{t})/(F_{con}^{t} + \delta k_{con}^{t})]^2/ncc} \leq TOL \tag{3.65}$$

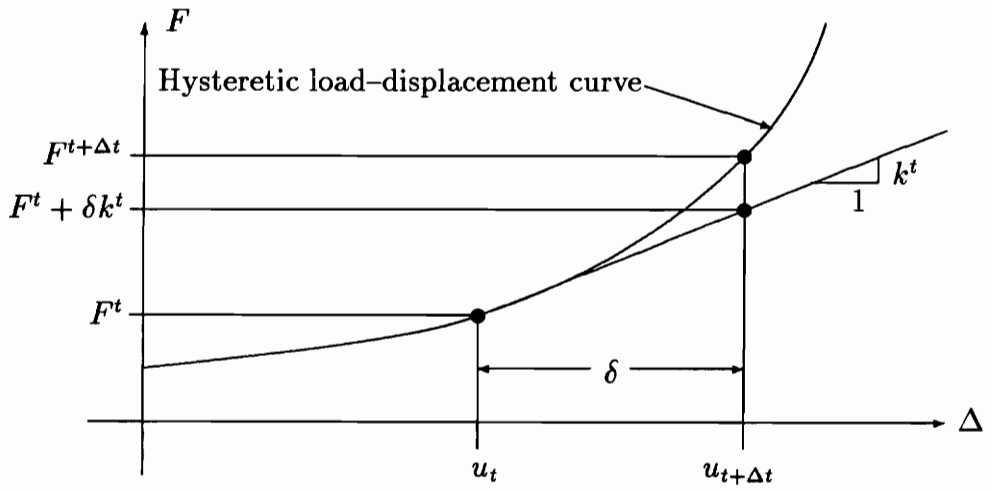

Figure 3.8: Schematic of Residual Force in a Connector Element

where *ncc* is the total number of connectors in the wall model and TOL is the desired tolerance, which is set by the user, is used to determine if the average relative residual force for all of the connectors is excessive. The second criterion, governed by the relationship

$$\sqrt{\sum_{i=1}^{ncc}[(F_{con}^{t+\Delta t} - (F_{con}^{t} + \delta k_{con}^{t})/P_1]^2/ncc} \leq TOL \tag{3.66}$$

where P_1 is the load–intercept of the hysteretic curve, is used to determine if a high relative residual force in the connectors is due to a residual force of low magnitude.

The residual force is excessive if both criteria are not satisfied. An excessive residual force results in re–analysis at time t with the time–step, Δt, cut in half. Analyzing a model with a reduced time step reduces the residual force in the connectors because of the smaller change in the connector force. The connectors are again subjected to the error criteria to determine if further re–analysis, with an even smaller time step, is required. This continues until either one of the criteria is satisfied or the length of the time–step falls below a specified value (for this case, 0.005 seconds). A very small time step is avoided to prevent round off error in the global equations from becoming too large.

3.5.4 Energy Balance Formulation

Performing an energy balance check when using explicit dynamic analysis methods is important to help ensure stable and accurate computation (Cook, 1989). The balance of energy shows that all sources of internal and external energy have been accounted and that the energy imparted into a system equals the internal energy of the system. There are four energy components in the model:

- The energy imparted into the structure by the external applied loads (denoted by G(t)).
- The energy due to the straining of the material and includes the energy dissipated by hysteretic damping (denoted by S(t)).
- The energy dissipated by the structure through all forms of damping except for hysteretic damping (denoted by P(t)).
- The kinetic energy of the system (denoted by T(t)).

The components of energy are determined by pre–multiplying Equation 3.50 by the nodal velocities ($\{\dot{D}\}^T$) and integrating over time. This produces the following expressions for the energy balance

$$\begin{aligned} \int_o^t \{\dot{D}\}^T [M]\{\ddot{D}\}\, d\tau &+ \\ \int_o^t \{\dot{D}\}^T [C]\{\dot{D}\}\, d\tau &+ \\ \int_o^t \{\dot{D}\}^T \{R^{int}(\tau)\}\, d\tau &= -\int_o^t \{\dot{D}\}^T [M]\{I\}\ddot{D}_g(\tau)\, d\tau \end{aligned} \tag{3.67}$$

where

$$\begin{aligned} G(t) &= -\int_o^t \{\dot{D}\}^T [M]\{I\}\ddot{D}_g(\tau)\, d\tau \\ T(t) &= \int_o^t \{\dot{D}\}^T [M]\{\ddot{D}\}\, d\tau \end{aligned} \tag{3.68}$$

$$
\begin{aligned}
P(t) &= \int_o^t \{\dot{D}\}^T [C]\{\dot{D}\}\, d\tau \\
S(t) &= \int_o^t \{\dot{D}\}^T \{R^{int}(\tau)\}\, d\tau
\end{aligned}
$$

Integrating the expressions from Equation 3.68 using the trapezoidal rule results in

$$
\begin{aligned}
G(t+\Delta t) &= G(t) - \frac{\Delta t}{2}[\{\Delta\dot{D}\}^T [M]\{I\}\Delta\ddot{D}_g] \\
T(t+\Delta t) &= \{\dot{D}\}^T [M]\{\dot{D}\} \\
P(t+\Delta t) &= P(t) + \frac{\Delta t}{2}[\{\Delta\dot{D}\}^T [C]\{\Delta\dot{D}\}] \\
S(t+\Delta t) &= S(t) + \frac{\Delta t}{2}[\{\dot{D}(t+\Delta t)\}^T \{R^{int}(t+\Delta t)\} \\
&\quad -\{\dot{D}(t)\}^T \{R^{int}(t)\}]
\end{aligned}
\tag{3.69}
$$

In summary, the dynamic analysis is performed as follows:

1. Perform static analysis on the shear wall model using the procedure outlined in Section 3.5.1. The results from this solution are used as the initial conditions ($\{\ddot{D}(0)\}$, $\{\dot{D}(0)\}$, and $\{D(0)\}$) of the dynamic solution.

2. Form the mass ($[M]$)and viscous damping ($[C]$) matrices for the shear wall model using the method outlined in Section 3.4.

3. Form the tangent stiffness matrix ($[K_t(t)]$) for the shear wall model at time t. This is the matrix containing the stiffnesses from the framing, sheathing, and bearing connector elements and the tangent stiffness from the sheathing connector elements. This is the step in which the error in the connector elements is determined and the hysteretic path on which a connector follows is determined. Excessive error in the connectors or a significant number of connectors changing paths can cause the analysis to backup a step in order to help ensure an accurate solution. If the error in the connectors exceeds the tolerance the following procedure is followed.

(a) Backup all pertinent values to their value at time $t - \Delta t$. This includes displacement, velocity, acceleration, and parameters used to define the shape of the hysteretic curve.

(b) Divide the current length of the time step in half. The time step will remain at this reduced length until the analysis reaches time $t + \Delta t$.

(c) Goto Step 3 and re–calculate ($[K_t(t)]$) for $t = t - \Delta t$ and with modified time step.

If a significant number of connectors change direction the following procedure is implemented.

(a) Backup all pertinant values to their values at time $t - \Delta t$. This includes displacement, velocity, acceleration, and parameters used to define the shape of the hysteretic curve.

(b) Calculate the stiffness of the connectors at the time $t - \Delta t$. This new stiffness will be used for calculating the error on the new path.

(c) Goto Step 3 and re–calculate $[K_t]$ at time $t = t - \Delta t$.

4. Form the effective stiffness matrix ($[\hat{K}]$) and effective load vector ($\{\hat{F}\}$) following Equations 3.62 and 3.63.

5. Solve Equation 3.61 for the change in nodal displacements ($\{\Delta D\}$) and then calculate the displacements at the end of the time step ($\{D(t + \Delta t)\}$).

6. Calculate the acceleration ($\{\ddot{D}(t + \Delta t)\}$) and velocity ($\{\dot{D}(t + \Delta t)\}$) at the end of the time step using Equations 3.59 and 3.60.

7. Calculate the forces and stresses in the framing elements using Equations 3.16 and 3.11 and the forces and stresses in the sheathing elements using Equations 3.29 and 3.24.

8. Calculate the total energy and energy balance.

9. Go to Step 3 and repeat process. Repeat until all of the desired time has been analyzed.

3.6 Summary

A program that is capable of performing static, monotonic, or dynamic analysis on shear wall models was developed to analyze wall models for the parametric study. The program, WALSEIZ, is a modification of DYNWAL, a shear wall analysis program developed by Dolan (1989). WALSEIZ utilizes the finite element method for analysis. Elements corresponding to the framing, sheathing, connectors attaching the sheathing to the framing, and the effect of bearing between adjacent sheathing panels are used to model a shear wall. WALSEIZ has the capability to analyze shear walls up to 4.9 m by 12.2 m (16 ft by 40 ft) in size, calculate displacements at the nodes and forces and stresses in the elements for user specified nodes and elements, and determine the maximum and minimum displacements and forces and stresses for all of the nodes and elements.

Chapter 4

Program Verification and Validation

4.1 Introduction

Verification, which is the process of determining that a simulation program performs as intended, and validation, which is the process of determining if a simulation model is an accurate representation of the system under study (Law and Kelton, 1991), are important steps in the development of a computer program. Verification and validation of WALSEIZ was done to ensure that the program could be used to accurately model the response of a timber shear wall. Verification consisted of analyzing the components of a wall model and an entire shear wall model using WALSEIZ and comparing the results with theoretical and experimental results to ensure that the algorithms are coded properly. Validation consisted of analyzing three shear wall models using WALSEIZ and comparing the results to experimental data obtained from corresponding shear wall tests to determine the capability of the program to accurately model the response of a shear wall.

4.2 Verification

The following tests were performed to verify the elements used in WALSEIZ. Several simple framing configurations (cantilever beam, simple frame, etc.) were constructed and analyzed using WALSEIZ and the resulting displacements and forces compared to existing theoretical results in order to verify the framing elements. Verification of the sheathing element involved performing a patch test in order to ensure that the element is converging to the correct solution. Also, similar to the framing element, several simple configurations were constructed and analyzed using WALSEIZ and the results compared to results from similar configurations analyzed using ABAQUS[1]. The connector elements were verified in the following manner. A 61 cm (24 in) long framing element was attached to a 122 cm by 122 cm (48 in by 48 in) sheathing element with two connectors spaced eqi–distant from each other (see Figure 4.1). Two connectors were used because using only one connector is an unstable

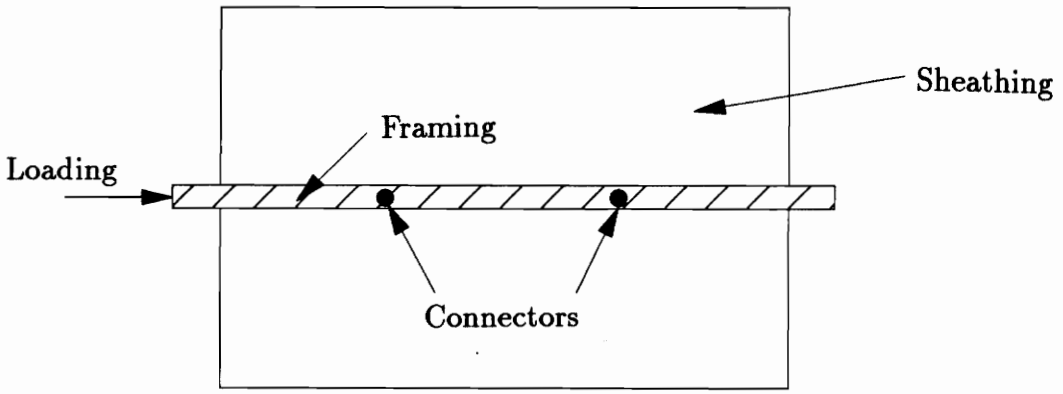

Figure 4.1: Configuration Used for Verification of Connector Element

configuration. The framing element was subjected to both a concentrated monotonic load increasing at increments of 44.5 N (10 lb) for verification of the connector

[1]ABAQUS is a widely used finite element program developed by Hibbitt, Karlsson, and Sorensen, Inc..

element subjected to monotonic loading and a sinusoidal acceleration record with increasing amplitude and a maximum acceleration of 51 in/sec^2 (20 in/sec^2), shown in Figure 4.2, to verify the connector element when subjected to dynamic loading. Two

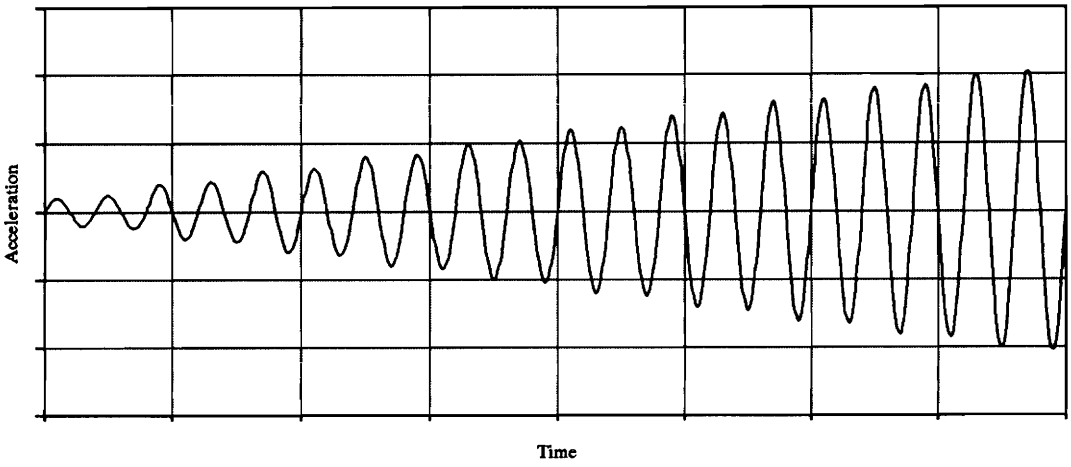

Figure 4.2: Load Profile Used for Verification of Connector Element Subjected to Dynamic Loading

systems were analyzed, one oriented such that the loading displaced the connectors in the X–direction, the other oriented such that the loading displaced the connectors in the Y–direction. All of the degrees–of–freedom of the sheathing element were fixed, and all of the degrees–of–freedom in the framing element were fixed except for those corresponding to the direction of the loading. A correlation of the load–deflection curves generated from WALSEIZ for the connectors and load–displacement curves obtained in experimental tests by Kalkert (1992) was performed to check for validity. The results were also plotted so that a visual check of the shape of the curves could be performed.

Verification of a shear wall model consisted of constructing and analyzing identical 2.4 m by 2.4 m (8 ft by 8 ft) models using WALSEIZ and ABAQUS and comparing the results. The layout of the framing and sheathing elements for the wall models is shown in Figure 4.3. Note the coordinate system shown in Figure 4.3a. All of

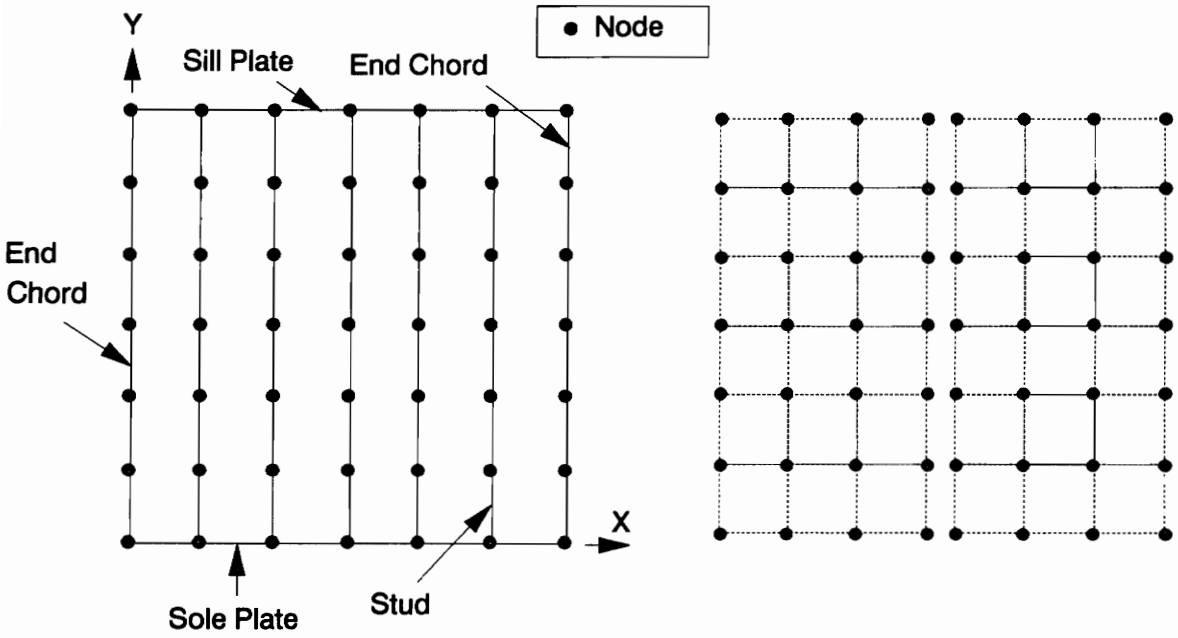

Figure 4.3: Configuration of Wall Models Used to Verify WALSEIZ

the models used for the verification and validation of WALSEIZ, and also the models used in the parametric study, utilized a similar coordinate system. The models were oriented using coordinate axes positioned such that the Y–axis, which corresponds to the vertical direction, coincides with one of the end chords (designated as the "left" chord), and the X–axis which corresponds to the horizontal direction, coincides with the sole plate. The framing of the wall models consisted of two series of elements each 41 cm (16 in) long which extend the length of the model, one series forming the sill plate and the other the sole plate, and six 41 cm (16 in) long framing elements forming each stud and end chord. The ends of the studs and end chords share common nodes with the sill and sole plates. The B23 element was used in ABAQUS to model the framing, which is identical to the framing element in WALSEIZ. Each of the two 2.4 m by 1.2 m (8 ft by 4 ft) sheathing panels consisted of eighteen elements, each measuring 41 cm by 41 cm (16 in by 16 in), with six elements extending vertically and

three elements horizontally. The CPS4 element was used in ABAQUS to model the sheathing, which is identical to the sheathing element in WALSEIZ. The sheathing was attached to the framing with connectors located at the coincident nodes of the framing and sheathing elements. The connectors, which were spaced 41 cm (16 in) apart, were modeled in the ABAQUS model using a nonlinear spring element that corresponds to the shape of the connector element subjected to monotonic loading used in WALSEIZ. This element is similar to the connector element in WALSEIZ, with the difference being that the shape of the element in ABAQUS is defined by a series of load–displacement points instead of a continuous curve. The boundary conditions for the wall models is that the sole plate is fixed to the foundation and allows for no uplift. The material properties for the framing and sheathing elements and the constants defining the force of the connector element as a function of displacement were identical for both of the models. The wall models were subjected to a static distributed load of 1.8 N/cm (1.0 lb/in) applied along the elements that make up the sill plate.

4.2.1 Results

The results from the verification tests for the framing and sheathing elements analyzed using WALSEIZ were identical to the theoretical results, which indicates that the elements are coded properly. The load–displacement curves for a connector element generated using WALSEIZ, which are shown in Figure 4.4 for one series of tests, were identical to the load–displacement equations for either monotonic and dynamic loading. Therefore the correlation between actual load–displacement curve and the curve traced in the program is 0.95, which is correlation between the load–displacement experimental data from Kalkert (1992) and the load–displacement relationships given in Chapter 3.

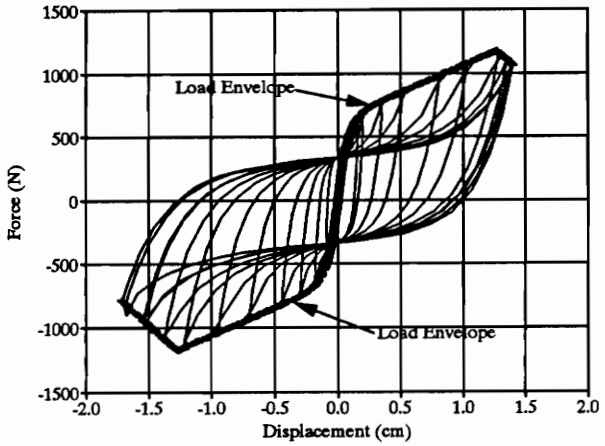

Figure 4.4: Load–Displacement Curve from Connector Element Verification

The load–relative drift[2] curves generated for the model using WALSEIZ and ABAQUS , shown in Figure 4.5, were almost identical. The correlation between the results from the two programs was 0.9999. The lowest natural frequency for the two wall models was also calculated and compared. The difference between the frequency for the two wall models, which was 1.78 Hz for the model analyzed using ABAQUS and 1.77 Hz for the model analyzed using WALSEIZ, was less than 1%. However, WALSEIZ did not converge to a solution for the natural frequency for some of the wall models with openings analyzed for the parametric study. In these cases, the natural frequency was assumed to be equal that of the 2.4 m by 3.7 m (8 ft by 12 ft) wall model for formulating the viscous damping term. The differences found in the verification of the wall models are due to the fact that the relationship for the element modeling the connector in ABAQUS is discretized. All of the verification results indicate that the program is coded properly.

[2]Relative drift is the ratio of the displacement at the top of the wall (or model) to the height of the wall.

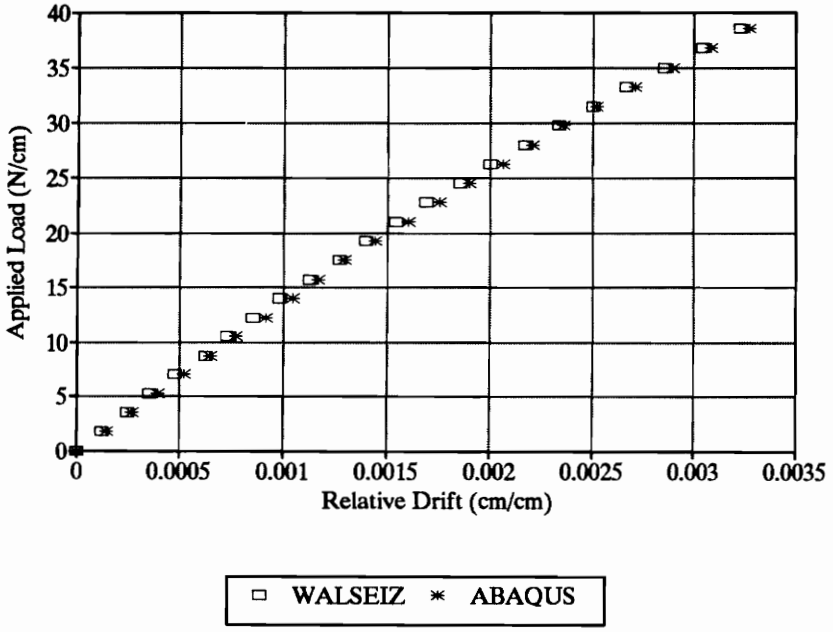

Figure 4.5: Load–Relative Drift Curves from Model Verification

4.3 Validation

Validation of WALSEIZ consisted of creating three wall models, two without openings and the other containing a window opening, corresponding to walls tested experimentally, analyzing the models using WALSEIZ, and comparing the results from WALSEIZ with the experimental results. The specific wall models and simulations that were performed are shown in Table 4.1. The wall models without openings corresponded to 2.4 m by 2.4 m (8 ft by 8 ft) shear walls tested by Dolan (1989). A diagram of the walls is shown in Figure 4.6. The framing of the walls consisted of studs spaced 61 cm (24 in) apart, which were attached to the header and sill framing members by nailing through the header or sill plate into the end–grain of the stud using 2–76 mm (10d or 3 in) common nails. All of the framing was made of 38 x 89 mm (2 x 4 in nominal) Spruce–Pine–Fir ranging in moisture content from 9–14%. One wall was sheathed with 9.5 mm (3/8 in) A–5 Exterior CF BC 142 grade Canadian

Table 4.1: Validation Tests for WALSEIZ

Sheathing Material	Nail Schedule		Loading	Earthquake Record
	Perimeter cm (in)	Interior cm (in)		
Plywood	10.2 (4)	15.2 (6)	Monotonic	N/A
			Seismic	Taft[1]
Waferboard	10.2 (4)	15.2 (6)	Monotonic	N/A
			Seismic	Taft[1]
OSB (Opening)	15.2 (6)	30.5 (12)	Monotonic	N/A

[1]S69E component of 1954 Kern County, California, earthquake.

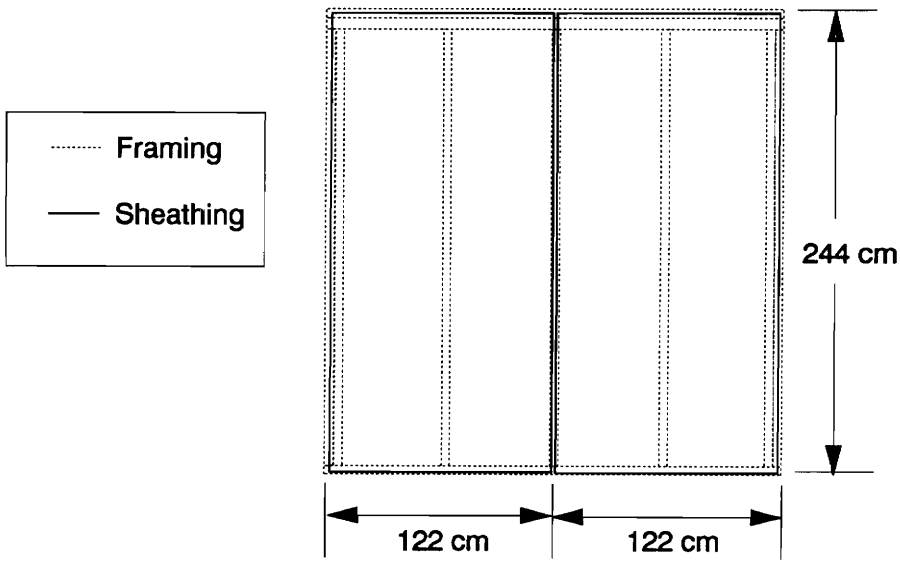

Figure 4.6: Diagram of Shear Wall Without Opening Used for Validation of WALSEIZ

softwood plywood (CSP) sheathing and the other wall with 9.5 mm (3/8 in) solid exterior grade waferboard[3].

The sheathing was attached to the framing with 8d or 63.5 mm (2.5 in) hot dipped galvanized common nails spaced 10 cm (4 in) along the perimeter of a sheathing panel and 15 cm (6 in) along the interior of a sheathing panel. A couple of 101.6 x 76.2 x 6.4 mm (4 x 3 x 1/4 in) hot rolled, mild structural steel angles attached to the end chords and the sill in the uppermost corners using 4 x 38 mm (No. 8 x 1.5 in) drywall screws. The walls were anchored using steel hold–down connections located at the bottom of the end chords The walls were tested using a four–hinge steel frame that provided no lateral resistance (therefore all of the resistance is provided by the wall) but did provide vertical resistance so that loading modeling vertical or inertial loading could be applied. A reaction column was part of the frame that restrained the top of the wall during the loading of the wall (i.e., moving of the shaketable). The asymmetry, due to the sheathing being applied on one side, was not a factor because the wall was restrained by steel tubes at the top and bottom of the wall, which prevented any twisting of the wall.

The layout of the framing and sheathing elements for the models without openings is shown in Figure 4.7. The framing of the wall models consisted of two series of framing elements each 61 cm (24 in) long which extended the length of the model, one series forming the sill plate and the other the sole plate. The studs and end chords were formed using four framing elements, each 61 cm (24 in) long. A hinge was located at the end of each of the studs in the model to simulate the relatively low resistance found at the joint. The geometric and material properties for the different categories of elements are shown in Table 4.2, where the width of the element is the dimension perpendicular to the face of the sheathing and the depth of the dimension parallel to the face of the sheathing. These dimensions and material properties were

[3]Waferboard is a sheathing material which is not currently manufactured

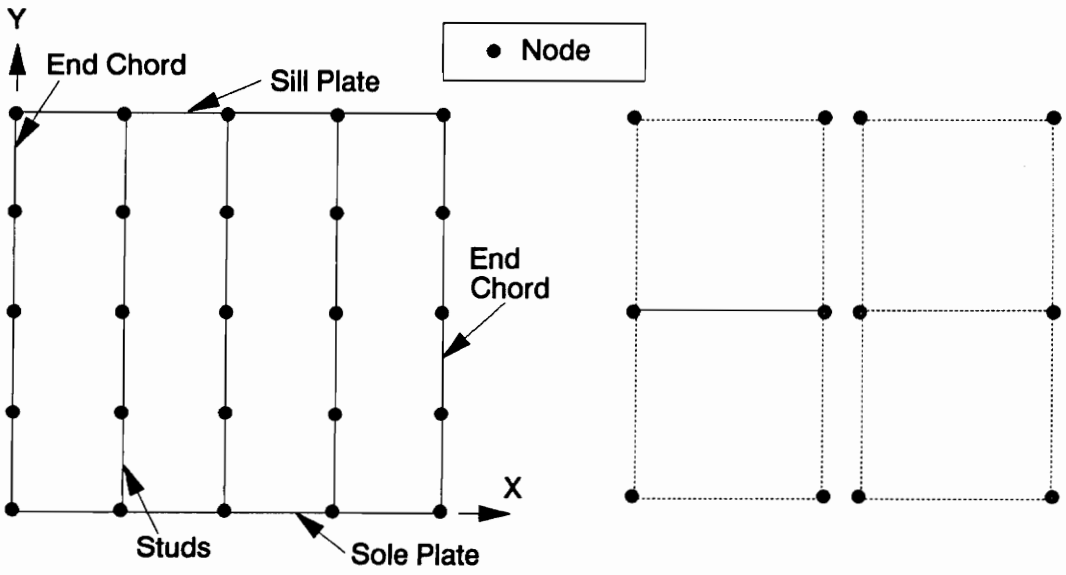

a).Framing b).Sheathing

Figure 4.7: Configuration of Wall Models Without Opening Used for Validation of WALSEIZ

Table 4.2: Geometric and Material Properties of Framing Elements in Wall Models Without Openings

Framing Component	Width	Depth	Modulus of Elasticity	Density
	cm (in)	cm (in)	N/cm^2 (lb/in^2)	kg/cm^3 (sl/in^3)
Sill plate	8.9 (3.5)	7.6 (3.0)	$1.09E^6$ ($1.58E^6$)	$*3.29E^{-1}$ ($3.70E^{-1}$)
Sole plate, Studs	8.9 (3.5)	3.8 (1.5)	$1.09E^6$ ($1.58E^6$)	$2.07E^{-4}$ ($2.32E^{-4}$)
End chords	8.9 (3.5)	7.6 (3.0)	$1.09E^6$ ($1.58E^6$)	$2.07E^{-4}$ ($2.32E^{-4}$)

*:The high density for the sill plate represents the inertial mass of the upper story.

chosen to best represent the framing used in the shear wall tests. The sole plate of each model was fixed at the base of each of the studs and the chords. The high density of the sill plate modeled the inertial mass associated with the upper stories of a structure. A mass of identical magnitude was used in the experimental tests.

Each sheathing panel consisted of two 1.2 m by 2.4 m (4 ft by 8 ft) sheathing elements that were 9.1 mm (0.361 in) thick. The material properties for the sheathing elements, shown in Table 4.3, were similar for monotonic and seismic loading and based on the design properties for the two materials. The connectors attaching the

Table 4.3: Material Properties for Sheathing Elements

Sheathing Material	$E_x t$ N/cm^2 (lb/in^2)	$E_y t$ N/cm^2 (lb/in^2)	$\frac{E_x \nu_{xy} t}{H}$ N/cm^2 (lb/in^2)	$\frac{E_y \nu_{yx} t}{H}$ N/cm^2 (lb/in^2)	$G_{xy} t$ N/cm^2 (lb/in^2)	Density kg/cm^3 (slugs/in^3)
Plywood	241306.5 (349991.0)	171497.5 (248740.0)	7862.9 (11404.4)	7862.9 (11404.4)	24889.7 (36100.0)	6.00E^{-5} (6.74E^{-5})
Waferboard	128573.8 (186483.4)	128573.8 (186483.4)	30214.8 (43823.6)	30214.8 (43823.6)	20254.0 (29376.4)	6.00E^{-5} (6.74E^{-5})
OSB	192407.9 (279053.0)	171497.5 (248740.0)	63494.3 (92087.0)	63494.3 (92087.0)	42314.8 (61370.0)	6.00E^{-5} (6.74E^{-5})

sheathing to the framing, spaced 10 cm (4 in) along the perimeter of the sheathing and 15 cm (6 in) along the interior of the sheathing, were modeled using connector elements governed by the properties shown in Table 4.4. The properties of the

Table 4.4: Values Used to Define Monotonic and Hysteretic Connector Curves

Sheathing Material	K_1 N/cm (lb/in)	P_o N (lb)	K_2 N/cm (lb/in)	Δ_{max} cm (in)	K_3 N/cm (lb/in)	P_1 N (lb)
Plywood	9559.8 (5458.8)	1035.2 (232.7)	372.1 (212.4)	1.27 (0.5)	-875.6 (-500)	333.6 (75)
Waferboard	8305.2 (4742.4)	800.7 (180.0)	353.8 (202.0)	1.27 (0.5)	-875.6 (-500)	333.6 (75)
OSB	9717.7 (5549.0)	1003.1 (225.5)	424.3 (242.3)	1.27 (0.5)	-875.6 (-500)	– –

connectors for the walls were based on experimental tests performed by Dolan (1989).

The wall models were subjected to load–controlled monotonic distributed loading applied to the sill plate at increments of 0.88 kN/m (5.0 lb/in). This load increment was chosen in order to provide approximately ten to twenty points for the load–displacement curves. The models were also subjected to the acceleration record from the S69E component of the 1954 Kern County, California, earthquake, which was the record used for seismic analysis in the experimental tests. Loading is in the plane of the walls, as shown in Figure 4.8. The following comparisons were performed in order to validate the shear wall model:

- A correlation between the load–displacement curves from the experimental data and the model simulation to determine how accurately the model predicts the reponse of a shear wall subjected to monotonic loading.

- A comparison of the maximum loads from the experimental data and the model simulation to determine how accurately the model predicts the maximum load.

- A comparison between the load calculated at the reactions and the applied load to determine the accuracy of the force calculation algorithm in WALSEIZ.

- A correlation between the time–displacement curves from the experimental data and the model simulation to determine how accurately the model predicts the reponse of a shear wall subjected to seismic loading.

- A comparison of the peaks of the fast fourier transform (FFT) from the experimental data and the model simulation to determine the accuracy of frequency prediction.

The model with an opening corresponds to a wall tested by Kolba (unpublished)[4].

[4]Alan Kolba is a graduate student at Marquette University performing tests on shear walls with openings.

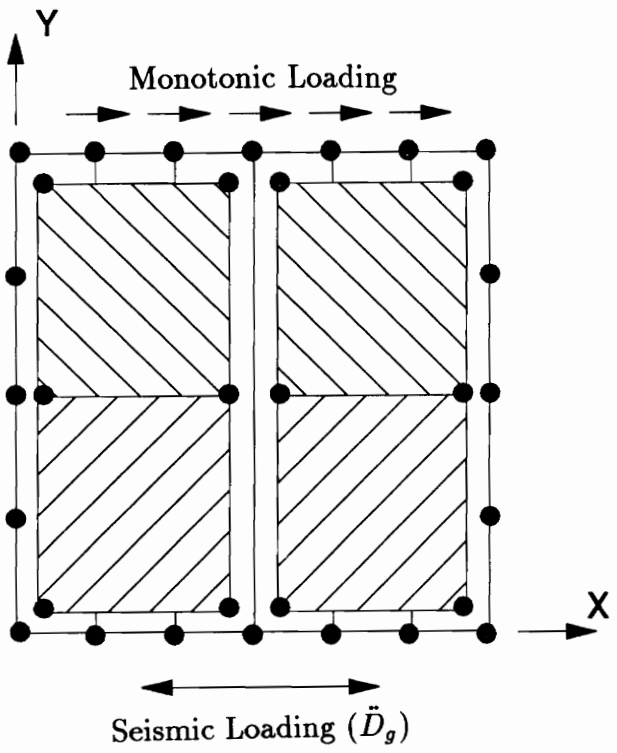

Figure 4.8: Loading Applied to Wall Models

The wall, shown in Figure 4.9, was 2.4 m (8 ft) long and 3.7 m (12 ft) high with an opening 81 cm (32 in) long and 122 cm (48 in) high located 81 cm (32 in) from the left edge and 80 cm (31.5 in) from the bottom of the wall. The framing of the wall

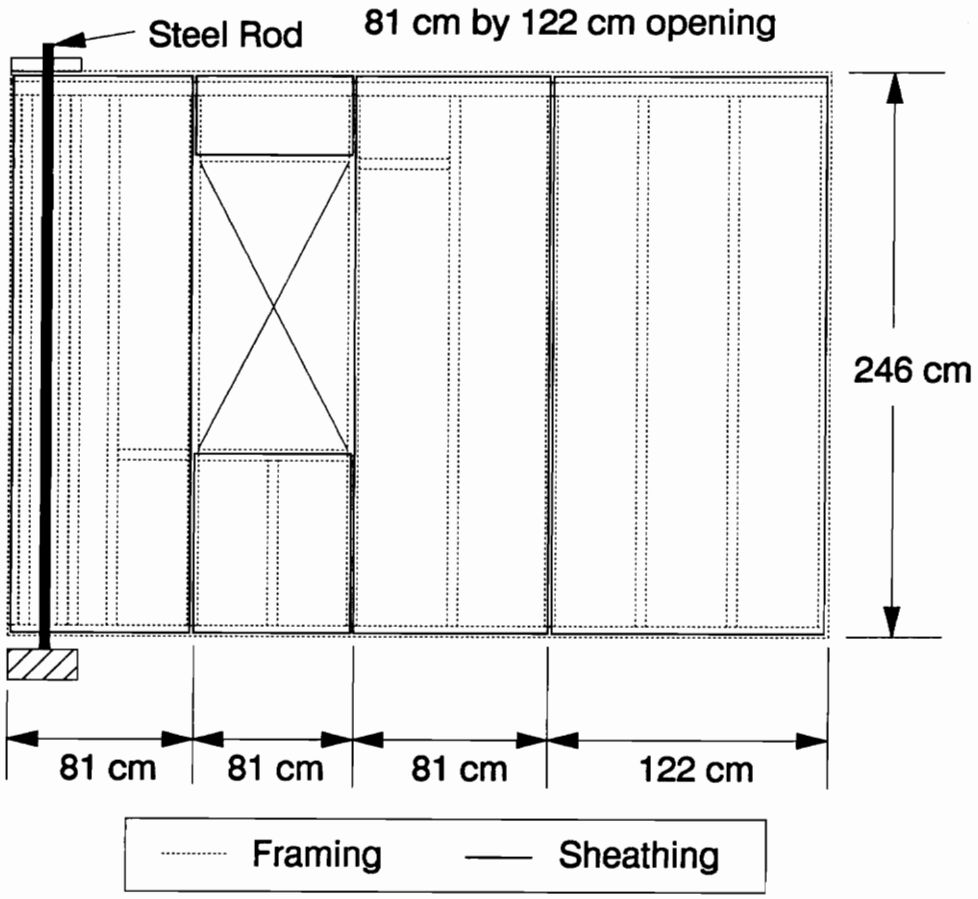

Figure 4.9: Diagram of Shear Wall with Opening Used for Validation of WALSEIZ

consisted of studs spaced 41 cm (16 in) apart except at the extreme left end of the wall, where two sets of doubled studs spaced 11 cm (4.5 in) apart are located. The studs were attached to the header and sill framing members by nailing through the header or sill plate into the end-grain of the stud. A 0.635 cm (0.25 in) diameter steel rod that is screwed into a plate at the top of the wall and screwed into the floor is located between the doubled studs. There was also blocking and straps present in the vicinity of the top and bottom of the openings, and a header above the opening

which consisted of two 2x12's nailed together. The wall was sheathed with 0.435 cm (7/16 in) thick Oriented Strandboard (OSB), the boundaries of which are outlined with dash lines in Figure 4.9. The sheathing was attached to the framing with nails spaced on average 15 cm (6 in) along the perimeter of a sheathing panel and 31 cm (12 in) along the interior of a sheathing panel.

The layout of the framing and sheathing elements for the models without openings is shown in Figure 4.10. There were five broad classes of framing elements that existed in the models without openings; the sill plate (which includes the double studs), sole plate (which includes the studs), header, steel rod, and straps. The location of the elements is shown in Figure 4.10. The geometric and material properties for these classes of elements are shown in Table 4.5. These dimensions and material properties

Table 4.5: Geometric and Material Properties of Framing Elements in Wall Model with Opening

Framing Component	Width	Depth	Modulus of Elasticity	Density
	cm (in)	cm (in)	N/cm^2 (lb/in^2)	kg/cm^3 (sl/in^3)
Sill plate	8.9 (3.5)	7.6 (3.0)	$1.10E^6$ ($1.60E^6$)	$*3.29E^{-1}$ ($3.70E^{-1}$)
Sole plate	8.9 (3.5)	3.8 (1.5)	$1.10E^6$ ($1.60E^6$)	$2.07E^{-4}$ ($2.32E^{-4}$)
Header	7.6 (3.0)	28.6 (11.25)	$1.10E^6$ ($1.60E^6$)	$2.07E^{-4}$ ($2.32E^{-4}$)
Steel Rod	0.64 (0.25)	0.64 (0.25)	$2.00E^7$ ($2.90E^7$)	$6.07E^{-4}$ ($8.80E^{-3}$)
Straps	0.34 (0.13)	1.59 (0.63)	$1.09E^6$ ($1.58E^6$)	$2.32E^{-4}$ ($2.32E^{-4}$)

*:The high density for the sill plate represents the inertial mass of the upper story.

were chosen to best represent the framing used in the shear wall tests, which was made from Douglas–Fir. The sole plate of the model was fixed at the base of each of the studs and the chords.

Each of the solid sheathing panels consisted of three elements. The elements are

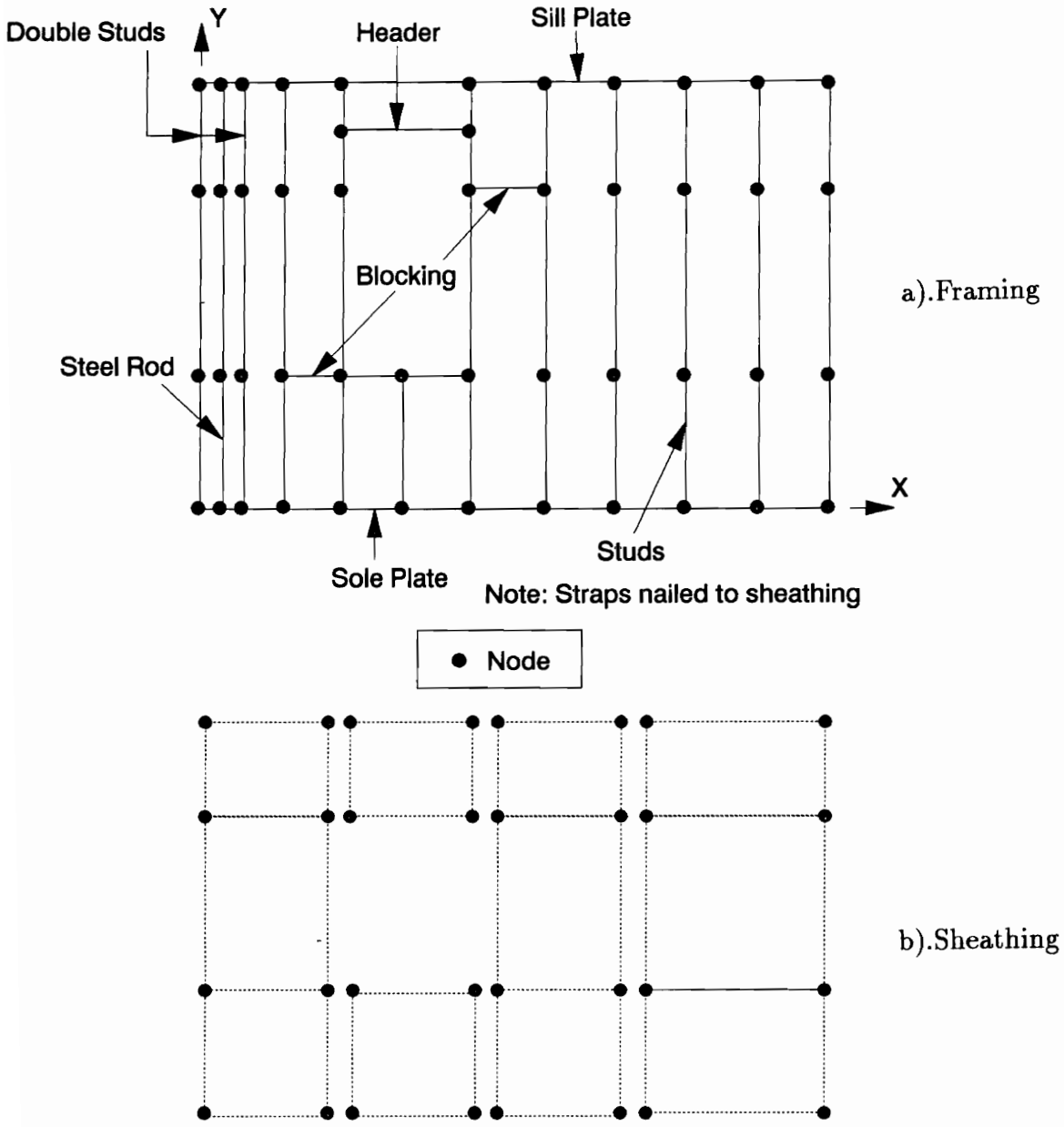

a).Framing

b).Sheathing

Figure 4.10: Configuration of Shear Wall Model with Opening

either 81.3 cm (32 in) wide or 121.9 cm (48 in) wide, depending on their location in the wall. The bottom element is 80.0 cm (31.5 in) in height, the middle element 123.8 cm (48.75 in) in height, and the uppermost element 36.2 cm (14.25 in) in height. The sheathing element below the opening is 80 cm by 81.3 cm (31.5 in by 32 in) while the sheathing element above the opening is 36.2 cm by 81.3 cm (14.25 in by 32 in). The properties of the sheathing elements, shown in Table 4.3, were selected based on the design properties of OSB. The connectors attaching the sheathing to the framing, spaced on average 15 cm (6 in) along the perimeter of a sheathing panel and 31 cm (12 in) along the interior of a sheathing panel, were modeled using connector elements governed by the properties shown in Table 4.4.

The model was subjected to load–controlled monotonic distributed loading applied to the sill plate at increments of 0.88 kN/m (5.0 lb/in). A visual correlation of the experimental load–displacement curve for the wall with an opening was compared with the results from the program because the relatively low number of experimental data points.

4.3.1 Results

The results from the shear wall models without openings compared favorably to the experimental results. The load–displacement curves generated from the monotonic analysis of the wall models without openings are shown along with the corresponding experimental data in Figure 4.11 for the walls with plywood sheathing and Figure 4.12 for the walls with waferboard sheathing. The solid lines in the figures are the results from the experimental tests and the symbols are the results from the program. The plots, along with the numerical comparisons from the wall validation results shown in Table 4.6, indicate a good correlation (greater than 0.99) between the program generated and experimental load–displacement curves, as well as a very

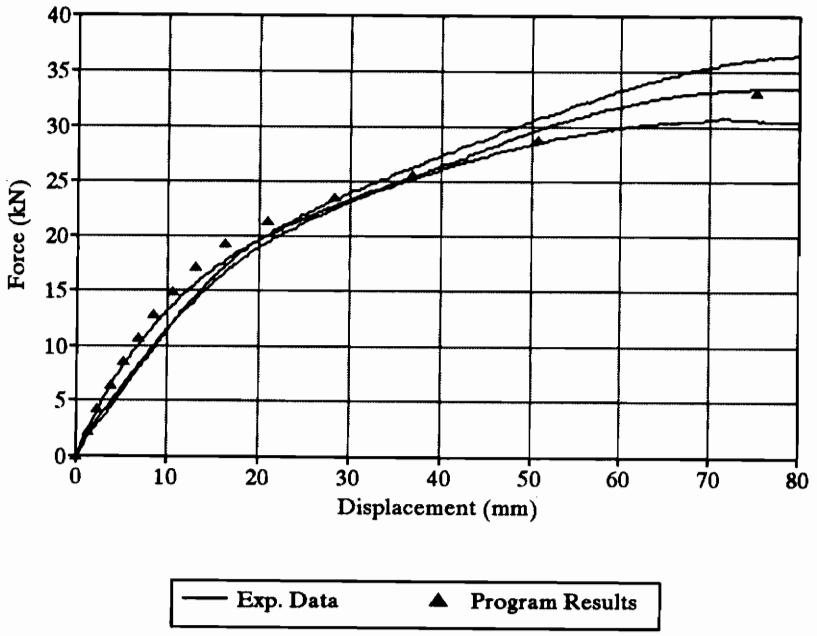

Figure 4.11: Load–Displacement Curves for Walls With Plywood Sheathing Used to Validate WALSEIZ

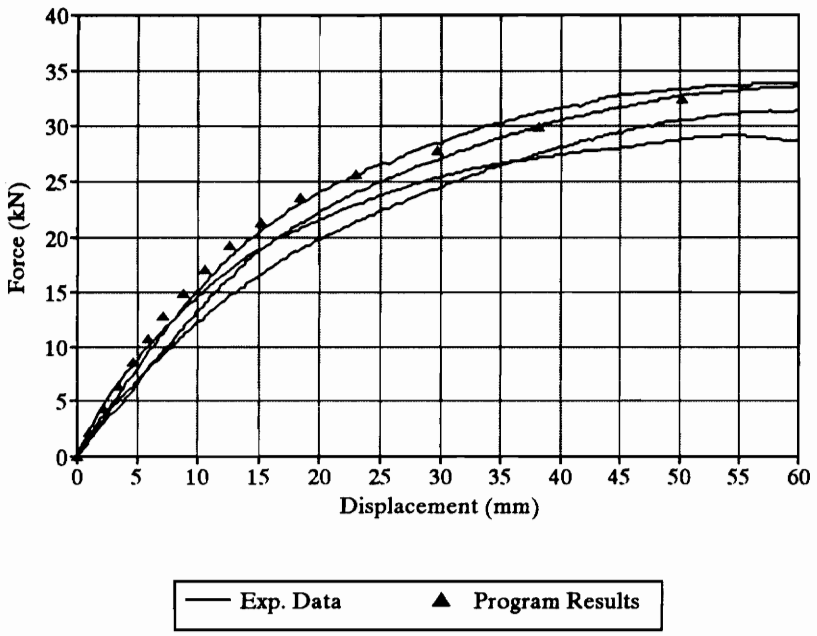

Figure 4.12: Load–Displacement Curves for Walls With Waferboard Sheathing Used to Validate WALSEIZ

Table 4.6: Results of Monotonic Shear Wall Validation Tests

Sheathing Material	Maximum Strength			Correlation Coefficient for Monotonic Curve
	Experimental Results	Program Results	Percentage Difference	
	kN (kips)	kN (kips)		
Plywood	33.5 (7.54)	32.4 (7.29)	1.1	0.9938
Waferboard	31.8 (7.16)	33.1 (7.45)	1.8	0.9965

small difference between the maximum load (within 2%) calculated using the program and the average maximum load determined experimentally. The differences could be due to the fact that average nail parameters were used or localized bearing failure occurring around the framing connectors during the experiments. The results of the comparison between the applied load and the forces at the reactions, shown in Table 4.7 indicate that the program accurately calculates the vertical and horizontal

Table 4.7: Comparison of Theoretical and Computed Base Shear and Overturning Moment for Wall Models Subjected to Monotonic Loading

Sheathing Material	Applied Load	Base Shear	Percentage Difference	Overturning Moment	Resisting Moment	Percentage Difference
	kN (kips)	kN (kips)		kN*m (kips*ft)	kN*m (kips*ft)	
Waferboard	19.2 (4.32)	18.5 (4.16)	3.3	46.8 (34.6)	47.1 (34.8)	0.6
Plywood	19.2 (4.32)	19.1 (4.30)	0.4	46.8 (34.6)	47.6 (35.2)	1.6

forces at the reactions.

The first 10 seconds of the time–displacement curves generated from the seismic analysis of the wall models without openings are plotted along with the corresponding experimental data in Figure 4.13 for the walls with plywood sheathing and Figure 4.14 for the walls with waferboard sheathing. The remainder of the curves are located

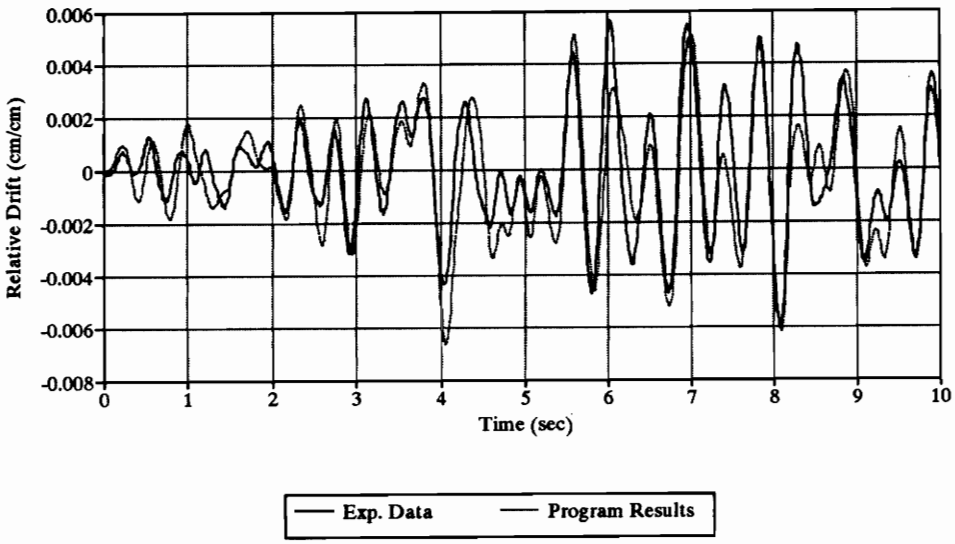

Figure 4.13: Time–Displacement Curves for Walls With Plywood Sheathing Used to Validate WALSEIZ (0–10 sec)

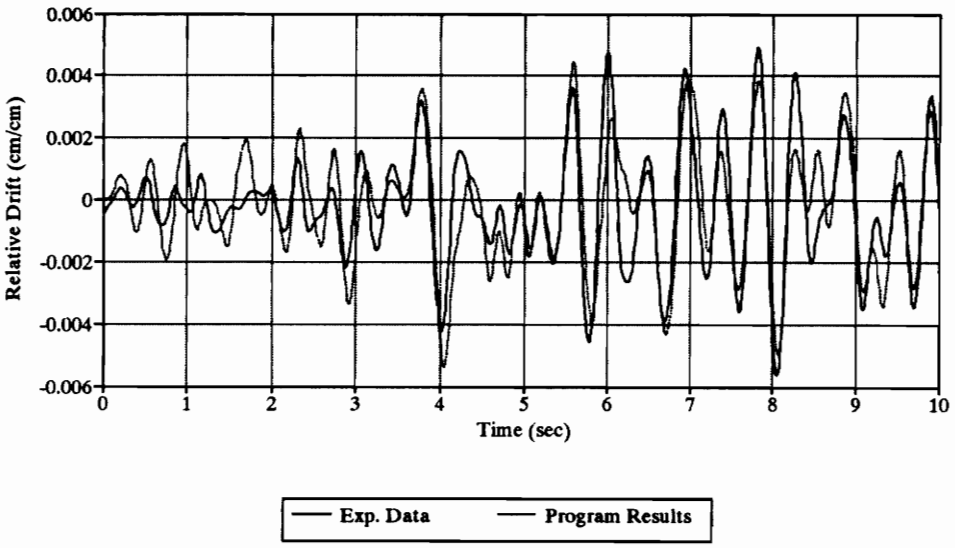

Figure 4.14: Time–Displacement Curves for Walls With Waferboard Sheathing Used to Validate WALSEIZ (0–10 sec)

in the Appendix. These figures show a close correlation between the experimental and time–displacement time histories. The observed correlation is supported by the correlation results shown in Table 4.8, in which the correlation for either of the wall

Table 4.8: Results of Validation Test for Shear Walls Subjected to Seismic Loading

Sheathing Material	Correlation Coefficient for Displacement Trace	Correlation Coefficient for FFT
Plywood	0.8456	0.9998
Waferboard	0.8345	0.9990

types is no worse than 0.83. Plots containing the peaks of the FFT curves from the experimental data and program results, shown in Figure 4.15 for the plywood walls and Figure 4.16 for the waferboard walls, show a good correlation between the two

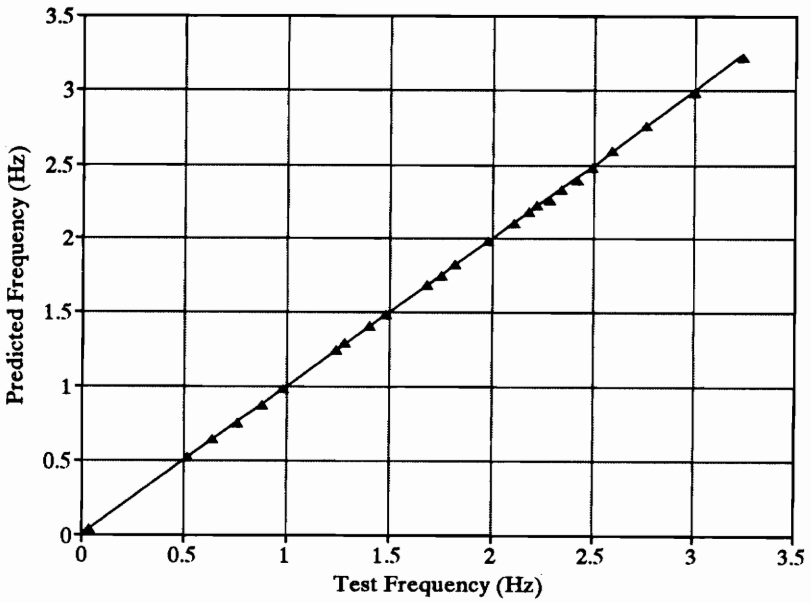

Figure 4.15: FFT Results for Walls With Plywood Sheathing Used to Validate WALSEIZ

parameters. The results of the correlation, shown in Table 4.8, indicate that there is a good correlation between the experimental and program results (greater than 0.99).

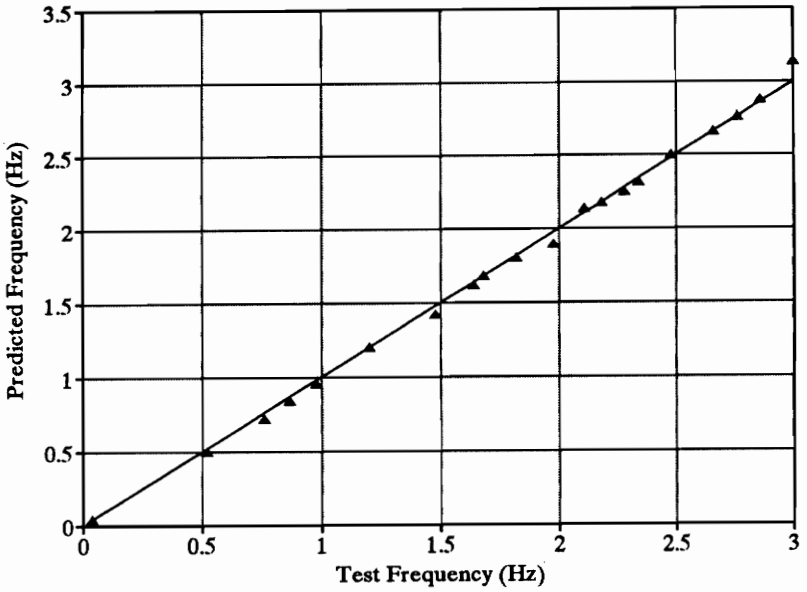

Figure 4.16: FFT Results for Walls With Waferboard Sheathing Used to Validate WALSEIZ

The load–displacement curve from the monotonic analysis of the 2.4 m by 3.7 m (8 ft by 12 ft) wall model with a window opening is plotted along with the corresponding experimental data in Figure 4.17. The plot shows a good correlation between the results from the program and the experimental data up to approximately two times the design load. However, the program exhibits some difficulty in determining the ultimate load that a shear wall with openings experiences. The difficulty that the program has for obtaining the maximum load could be due to the role that the bearing elements play. A few of the wall models analyzed in the study were unable to sustain significant deflections until an optimum bearing stiffness was used, which was determined through trial and error. This could indicate that a nonlinear spring element, as opposed to a bi–linear spring element, should be used to model the effect of bearing between adjacent sheathing panels. However, this phenomena did not seem to affect the capability of the program to calculate maximum base shear and deflections for wall models in the parametric study subjected to seismic loading.

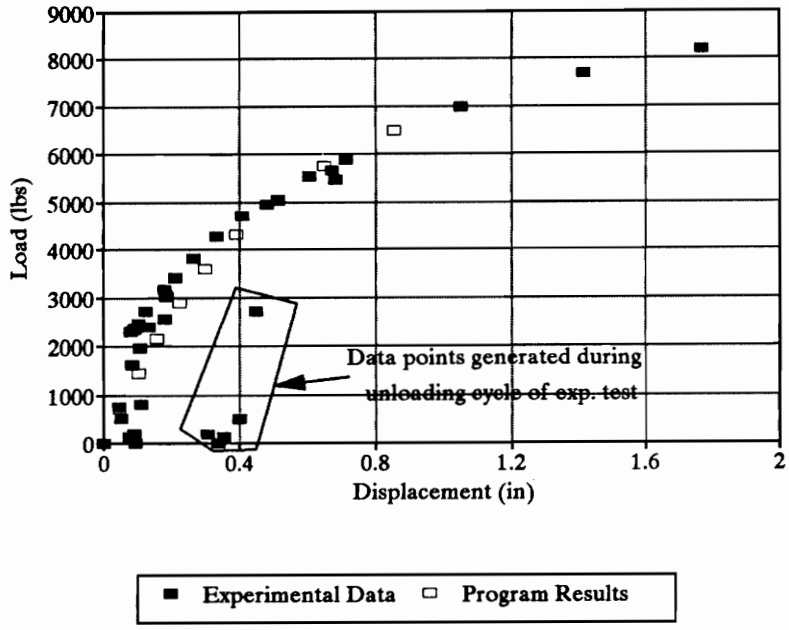

Figure 4.17: Load–Displacement Curves for Walls With an Opening Used to Validate WALSEIZ Validation Results for Wall with Opening Subjected to Monotonic Loading

4.4 Summary

Verification and validation of WALSEIZ was performed to ensure that the program adequately modeled the response of a shear wall subjected to monotonic or seismic loads. Verification of the elements in WALSEIZ consisted of analyzing the framing, sheathing, and connector elements separately and comparing the results to theoretical and experimental results. Verification of the wall system in WALSEIZ consisted of analyzing equivalent shear walls in WALSEIZ and ABAQUS and comparing the results. The results from the verification compared favorably, indicating that the program was coded properly. Validation of WALSEIZ consisted of comparing the results from monotonic and seismic tests of two shear walls without openings and the results from a monotonic test of a shear wall with an opening to the results from equivalent shear wall models analyzed using WALSEIZ. The items compared favorably, except when determining the maximum load for the wall with a window

opening subjected to monotonic loading, indicating that WALSEIZ did an excellent modeling shear walls.

Chapter 5

Overview of Parametric Study

5.1 Introduction

A parametric study was performed in order to determine the effect that aspect ratio (ratio of wall length to height) and openings have on the response of timber shear walls subjected to either monotonic or dynamic loads. A total of twenty–five shear wall models, fourteen models of various sizes that did not contain openings and eleven models of the same total length with various opening sizes and types, were utilized in the study. The models, which were subjected to monotonic and dynamic loading, were analyzed using WALSEIZ, the shear wall analysis program outlined in Chapter 3. The relative drift (ratio of displacement at the top of the wall to wall height) of a wall model as a function of applied load and maximum relative drift, resistance, forces at the reactions, and forces in the elements were recorded for the wall models subjected to monotonic loading. The relative drift of a wall model as a function of time and maximum total relative drift, base shear, forces in the models at the reactions, and element forces were collected for the wall models subjected to seismic loading. The information collected from the study is used to characterize the behavior of shear walls and to develop a modified design methodology for shear walls.

5.2 Shear Wall Models

The shear wall models analyzed in the study fall under two categories: models of various aspect ratios that do not contain openings and models of the same overall length that contain openings of various sizes and configurations. Models of both 2.4 m (8 ft) and 4.9 m (16 ft) in height were analyzed in each category. The models correspond to common light–frame shear walls with 9.5 mm (3/8 in) A–5 Exterior CF BC 142 grade Canadian softwood plywood (CSP) sheathing attached to one side of the framing, which is made of Spruce–Pine–Fir, with 8d or 63.5 mm (2.5 in) hot dipped galvanized common nails spaced 10 cm (4 in) along the perimeter of a sheathing panel and 15 cm (6 in) along the interior of a sheathing panel. The framing of the walls consists of studs spaced 41 cm (16 in) apart (except for wall less than 1.2 m (4 ft) long, which have studs spaced 30 cm (12 in) apart), which are attached to the sole plate, header, and sill framing members by nailing through the header or sill plate into the end–grain of the stud using 2–76 mm (10d or 3 in) common nails. The headers are attached to the chords adjacent to the openings by nailing through the chord into the end–grain of the stud. The 4.9 m high walls have blocking at mid–height because most sheathing material is sold in 2.4 m by 4.9 m sections, and the blocking provides a nail base for the one of the edges of a sheathing panel. The sole plate is snugly attached to the foundation using anchor bolts, and hold–down connections are used at all of the chords.

The following assumptions are made in the models:

- The effect of structural components adjacent to the wall, such as adjacent walls, are neglected. This simulates the conditions found for the current testing of most shear walls, in which single shear walls are tested.

- The load–displacement properties of all the connectors are identical. This is based on the assumption that the effect of the individual connectors in a wall should "average out" due to the large number present in any given wall, and therefore the use of average nail properties for all of the connectors should provide adequate results.

- The anchorage connections do not yield or displace vertically. This assumption implies that efficient anchorages are used.

5.2.1 Aspect Ratio

Fourteen shear wall models of various aspect ratios that do not contain openings were created and analyzed for the parametric study. The overall dimensions of these models are listed in Table 5.1. The heights and aspect ratios were selected in order to cover a wide variety of wall sizes often used in buildings. Program array sizes limit the maximum model size to 4.9 m by 12.2 m (16 ft by 40 ft) if each sheathing panel is modeled with two plate elements.

The layout of the framing and sheathing elements for all the 2.4 m (8 ft) high wall models adhere to the same general pattern, which is shown in Figure 5.1 for a 2.4 m by 2.4 m (8 ft by 8 ft) model. The framing of the wall models consisted of two series of framing elements each 41 cm (16 in) long (31 cm (12 in) long for the models less than 1.2 m in length) which extend the length of the model, one series forming the sill plate and the other the sole plate, and three 81 cm (32 in) long framing elements forming each stud and end chord. A hinge is located at each end of the studs and chords on all wall models in order to simulate the relatively low resistance found at the joint.

Each sheathing panel consisted of two elements, each measuring 1.2 m by 1.2 m (4 ft by 4 ft), except for the 0.6 m (2 ft) long wall model, which had two sheathing

Table 5.1: Overall Dimensions of Shear Wall Models Without Openings

Wall Height m (ft)	Wall Length m (ft)	Aspect Ratio
2.4 (8)	0.6 (2)	0.25
4.9 (16)	1.2 (4)	
2.4 (8)	0.9 (3)	0.33
2.4 (8)	1.2 (4)	0.5
4.9 (16)	2.4 (8)	
2.4 (8)	2.4 (8)	1
4.9 (16)	4.9 (16)	
2.4 (8)	4.9 (16)	2
4.9 (16)	9.8 (32)	
2.4 (8)	6.1 (20)	2.5
4.9 (16)	12.2 (40)	
2.4 (8)	7.3 (24)	3
	9.8 (32)	4
	12.2 (40)	5

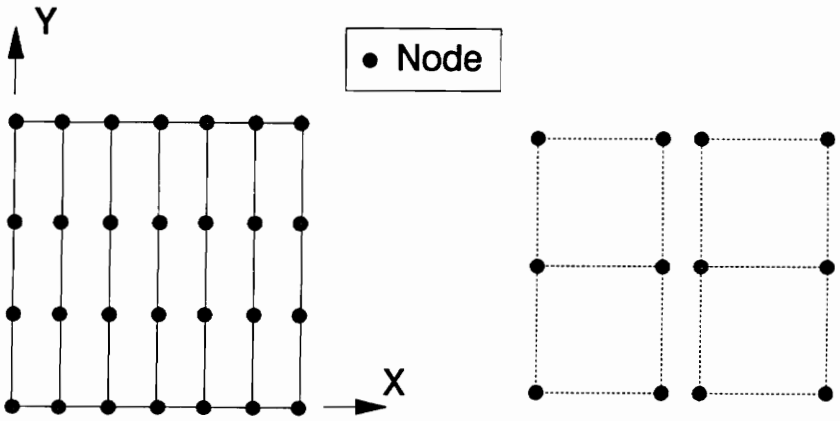

a).Framing b).Sheathing

Figure 5.1: Configuration of 2.4 m by 2.4 m (8 ft by 8 ft) Shear Wall Model Without Openings

elements measuring 0.6 m by 1.2 m, and the 0.9 m (3 ft) long wall, which had two sheathing elements measuring 0.9 m by 1.2 m. Two elements were used to model each sheathing panel in order to obtain force and stress values along the interior of a sheathing panel. The connector elements are spaced at 10 cm (4 in) intervals along the exterior of the sheathing and 15 cm (6 in) along the interior of the sheathing. The boundary conditions for all of the wall models is that the sole plate is fixed to the foundation and allows for no uplift, which represents effective anchorage connections.

The layout of the framing and sheathing elements for all the 4.9 m (16 ft) high wall models, shown in Figure 5.2 for a 4.9 m by 2.4 m (16 ft by 8 ft) model, is similar to that of the 2.4 m (8 ft) high wall models. The only differences between the 2.4 m and 4.9 m high models are that six elements are used for the studs and end chords instead of three and that a series of horizontal framing elements the same length as the sill and sole plates are present at mid-height to model the blocking.

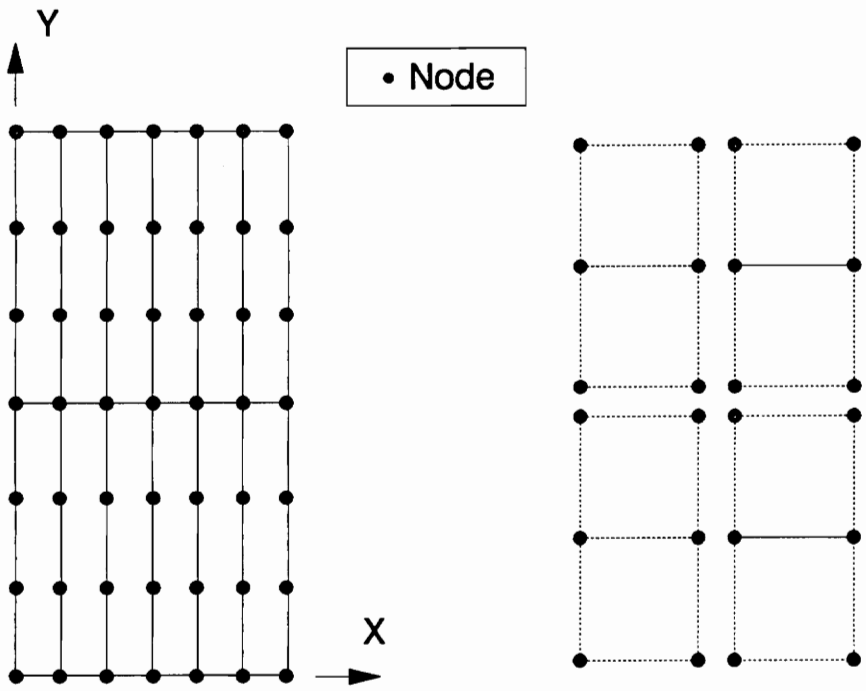

Figure 5.2: Configuration of 2.4 m by 4.9 m (8 ft by 16 ft) Shear Wall Model Without Openings

5.2.2 Openings

Eleven shear wall models with various opening configurations were created and analyzed for the parametric study. The overall dimensions of the models and size and type of openings present are listed in Table 5.2. The opening sizes were selected because they cover a wide range of sizes often used in buildings. These models can

Table 5.2: Dimensions for Shear Wall Models with Openings[1]

Opening Type	Wall Height m (ft)	Opening Height m (ft)	Opening Length m (ft)	Effective Aspect Ratio
Window	2.4 (8)	1.2 (4)	1.2 (4)	2.5
			2.4 (8)	2
			3.7 (12)	1.5
			4.9 (16)	1
Door	2.4 (8)	2.0 (6.4)	1.2 (4)	2.5
			2.4 (8)	2
			3.7 (12)	1.5
			4.9 (16)	1
	4.9 (16)	3.3 (10.7)	2.4 (8)	1
			3.7 (12)	0.75
			4.9 (16)	0.5

[1]All models have total length of 7.3 m (24 ft)

be divided into three groups. The first group consists of four wall models, shown in Figure 5.3, that are 2.4 m (8 ft) high and 7.3 m (24 ft) long with window openings. The openings extend 1.2 m (4 ft) in the positive Y–direction and from 1.2 m (4 ft) to 4.9 m (16 ft), in increments of 1.2 m (4 ft), in the positive X–direction from a

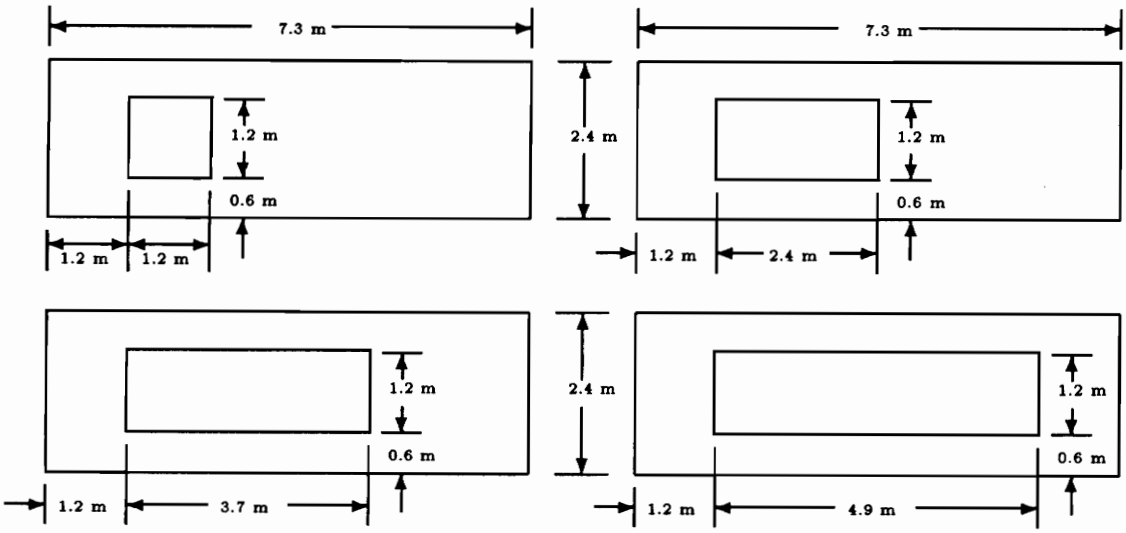

Figure 5.3: Dimensions of 2.4 m (8 ft) High Wall Models with Window Openings

location 1.2 m (4 ft) from the left edge of the wall and 0.6 m (2 ft) from the bottom of the wall.

The layout of the framing and sheathing elements for these models adhere to the same general pattern, which is shown in Figure 5.4 for a model with a 2.4 m (8 ft) long window opening. The element length and arrangement for the sill plate, sole plate, studs, and end chords are identical to those used for the 2.4 m (8 ft) high wall models without openings. The window header, which is the framing located directly above and/or below the opening, consisted of a series of 41 cm (16 in) long framing elements. The chords adjacent to the opening consist of four 61 cm (24 in) long framing elements and the studs above and below the opening consist of one 61 cm (24 in) framing element each. Each sheathing panel in the solid portion of the wall consists of four 1.2 m by 0.6 m (4 ft by 2 ft) sheathing elements, while each sheathing panel above and below the opening consists of one 1.2 m by 0.6 m (4 ft by 2 ft) sheathing element. The connector elements were spaced at intervals of 10 cm (4 in) along the exterior of the sheathing and 15 cm (6 in) along the interior of the sheathing

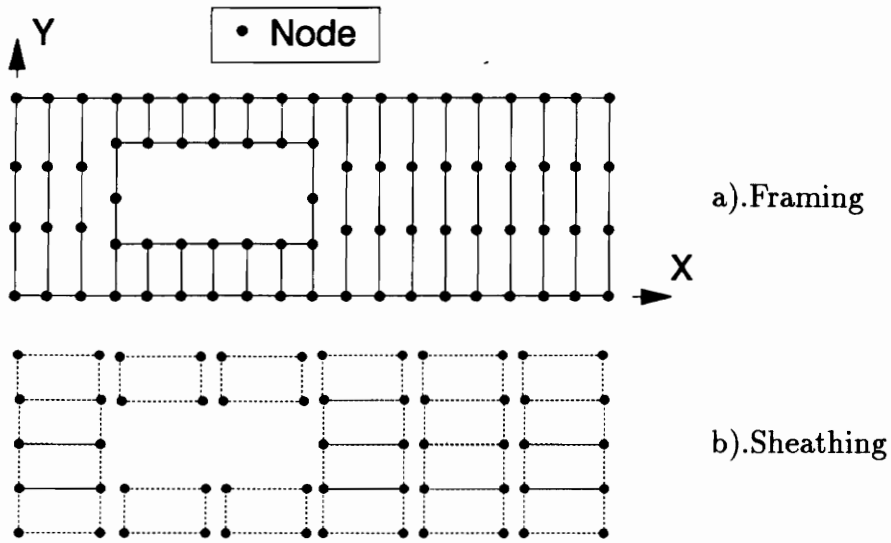

Figure 5.4: Configuration of 2.4 m (8 ft) High Shear Wall Model with 2.4 m (8 ft) Long Window Opening

for all of the sheathing panels.

The second group consists of four wall models, shown in Figure 5.5, that are 2.4 m (8 ft) high and 7.3 m (24 ft) long with door openings. The openings extend 2.0 m (6.4 ft) in the positive Y–direction and from 1.2 m (4 ft) to 4.9 m (16 ft), in increments of 1.2 m, in the positive X–direction from a location 1.2 m (4 ft) from the left edge of the wall. The layout of the framing and sheathing elements for these models adhere to the same general pattern which is shown in Figure 5.6 for a model with a 2.4 m (8 ft) long door opening. The element length and arrangement for the sill plate, sole plate, studs, and end chords are identical to those used for the 2.4 m (8 ft) high wall models without openings, with the exception that the sole plate exists only in the portion of the wall that does not contain the opening. The window header, which is the framing located directly above and/or below the opening, consisted of a series of 41 cm (16 in) long framing elements. The chords adjacent to the opening were composed of five 49 cm (19.2 in) long framing elements, while the studs over the

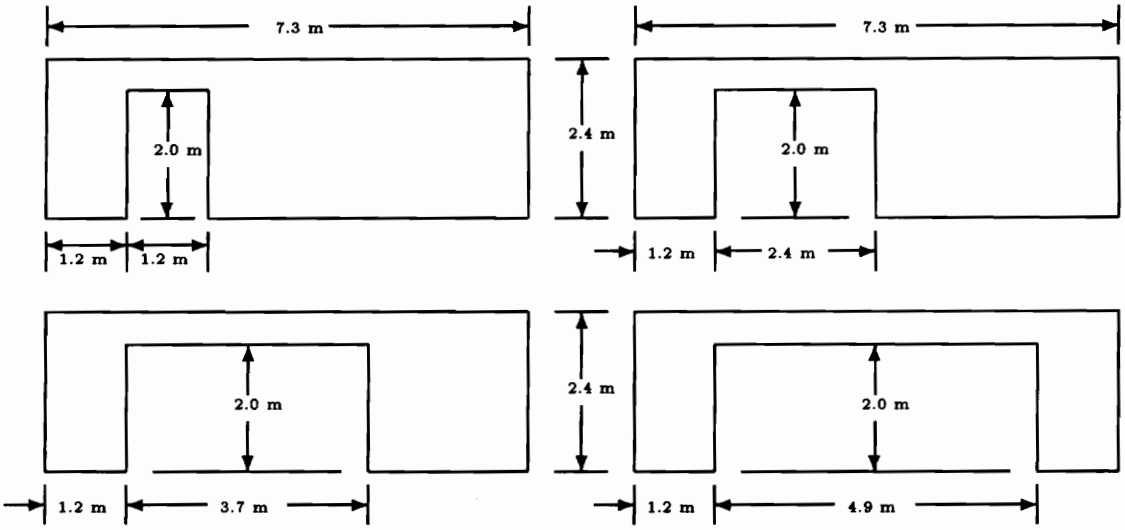

Figure 5.5: Dimensions of 2.4 m (8 ft) High Wall Models with Door Openings

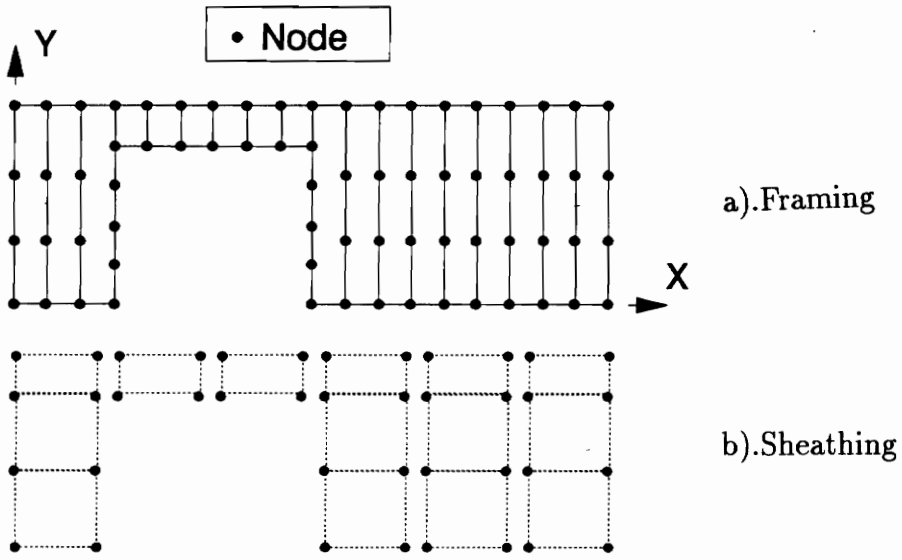

Figure 5.6: Configuration of 2.4 m (8 ft) High Shear Wall Model with 2.4 m (8 ft) Long Door Opening

opening were composed of one 49 cm (19.2 in) long framing element. Each sheathing panel in the solid portion of the wall consisted of three sheathing elements, the bottom two measuring 1.2 m by 1.0 m (4 ft by 3.2 ft) and the top element measuring 1.2 m by 0.5 m (4 ft by 1.6 ft), while each sheathing panel over the opening of the wall consisted of one 1.2 m by 0.5 m (4 ft by 1.6 ft) sheathing element. The spacing of the connector elements is 10 cm (4 in) along the exterior of the sheathing and 15 cm (6 in) along the interior of the sheathing for all of the sheathing panels.

The third group consists of three wall models, shown in Figure 5.7, that are

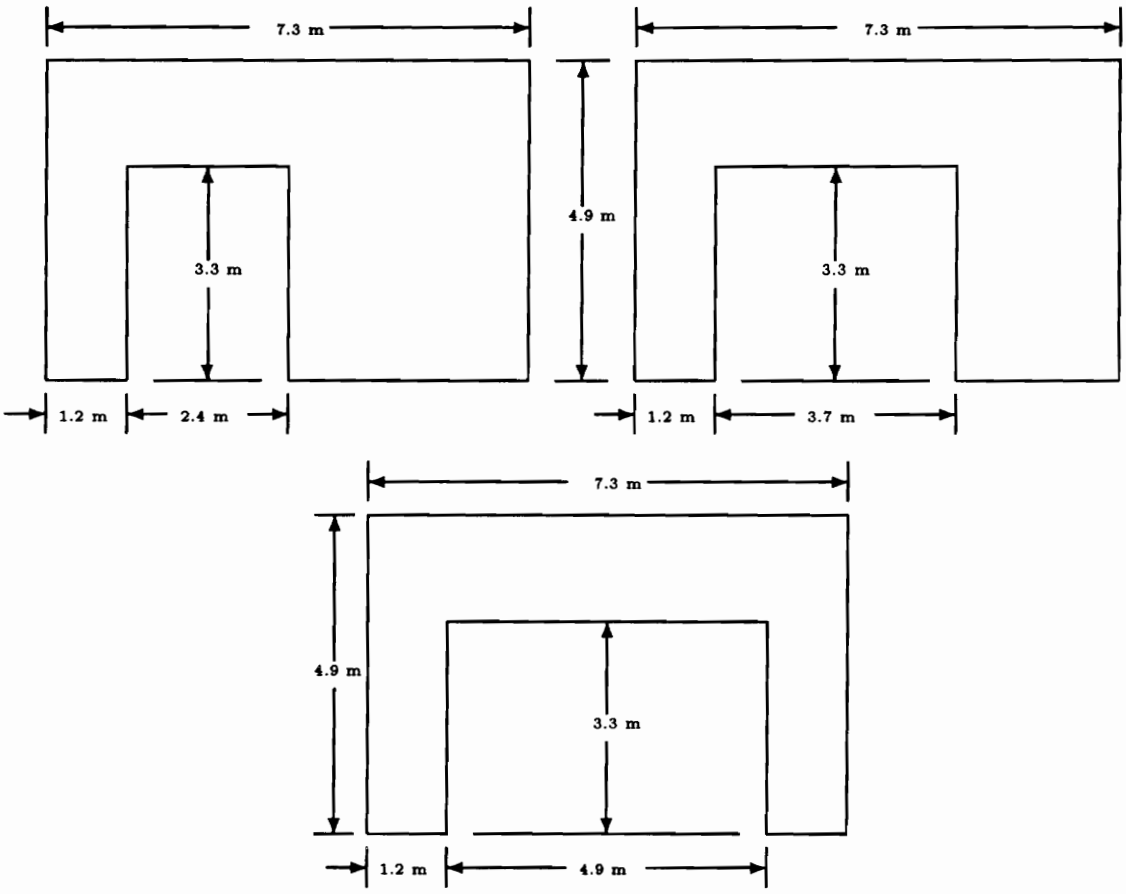

Figure 5.7: Dimensions of 4.9 m (16 ft) High Wall Models with Door Openings

4.9 m (16 ft) high and 7.3 m (24 ft) long with door openings. The openings extend

3.3 m (10.7 ft) in the positive Y–direction and from 2.4 m (8 ft) to 4.9 m (16 ft), in increments of 1.2 m (4 ft), in the positive X–direction from a location 1.2 m (4 ft) from the left edge of the wall. The layout of the framing and sheathing elements for these models adhere to the same general pattern, which is shown in Figure 5.8 for a model with a 2.4 m (8 ft) long door opening. The element length and arrangement for the

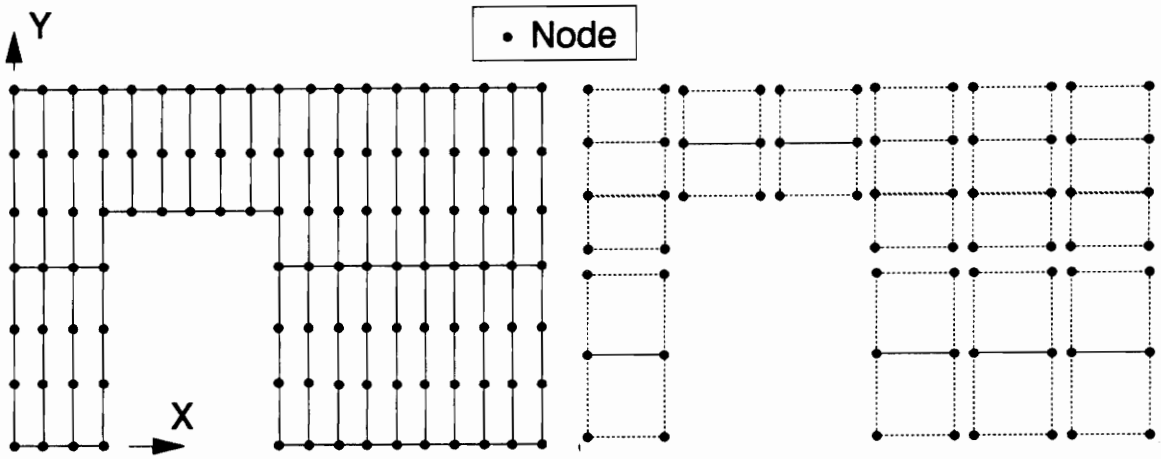

a).Framing b).Sheathing

Figure 5.8: Configuration of 4.9 m (16 ft) High Shear Wall Model with 2.4 m (8 ft) Long Door Opening

sill plate, sole plate, studs, and end chords are identical to those used for the 4.9 m (16 ft) high wall models without openings, with the exceptions that the sole plate and bracing exists only in the portion of the wall that does not contain the opening and the the studs over the opening were composed of two 81 cm (32 in) long framing elements. The window header, which is the framing located directly above and/or below the opening, consisted of a series of 41 cm (16 in) long framing elements. Each sheathing panel in the solid portion of the wall consisted of two 1.2 m by 1.2 m (4 ft by 4 ft) sheathing elements, while each sheathing panel over the opening of the wall consisted of two 1.2 m by 0.8 m (4 ft by 2.7 ft) sheathing elements. The connector

elements were spaced at intervals of 10 cm (4 in) along the exterior of the sheathing and 15 cm (6 in) along the interior of the sheathing for all of the sheathing panels.

5.2.3 Element Properties

The geometric and material properties assigned to the framing elements for all of the wall models, listed in Table 5.3, are identical to the properties assigned to

Table 5.3: Geometric and Material Properties of Framing Elements

Framing Component	Width	Depth	Modulus of Elasticity	Density
	cm (in)	cm (in)	N/cm^2 (lb/in^2)	kg/cm^3 ($slugs/in^3$)
Sole plate, Studs, Blocking	8.9 (3.5)	3.8 (1.5)	$1.09E^6$ ($1.58E^6$)	$2.07E^{-4}$ ($2.32E^{-4}$)
End chords, Opening chords	8.9 (3.5)	7.6 (3.0)	$1.09E^6$ ($1.58E^6$)	$2.07E^{-4}$ ($2.32E^{-4}$)
Sill plate	8.9 (3.5)	7.6 (3.0)	$1.09E^6$ ($1.58E^6$)	$*3.29E^{-1}$ ($3.70E^{-1}$)

*:The high density for the sill plate represents the inertial mass of the upper story.

the framing elements for the models without openings used to validate WALSEIZ for the sole plate, sill plate, studs, and end chords. The blocking, chords adjacent to the openings, and headers, which were not present in the validation models without openings, were assigned the properties listed in Table 5.3. The material properties and thickness assigned to the sheathing elements are identical to the properties assigned to the sheathing elements for the model without openings with plywood sheathing used to validate WALSEIZ, which represent 3/8 inch A–5 Exterior CF BC grade Canadian softwood (CSP) plywood. The constants used to define the shape of the load–deflection curves for all of the connectors subjected to monotonic and seismic loading are identical to the constants used for the validation wall model with plywood

sheathing, which represents 8d or 63.5 mm (2.5 in) nails attaching plywood to Spruce–Pine–Fir framing.

5.2.4 Loading

Each model was analyzed twice: once when subjected only to load–controlled monotonic loading and once when subjected only to seismic loading. The models were loaded in a manner similar to that shown in Figure 4.8. The monotonic loading was a distributed load applied parallel to the X–axis to the elements forming the sill plate of the wall. The load was increased at increments of 8.8 N/cm (5.0 lb/in) for the models without openings and 4.4 N/cm (2.5 lb/in) for the models with openings until "failure" (i.e. singular stiffness matrix or strength reduction of connectors) occurred. The increments were chosen so that a sufficient number of load–relative drift points would be calculated before failure.

The seismic loading consisted of the acceleration record from the S00E component of the 1940 El Centro earthquake record, shown in Figure 5.9, which has a maximum

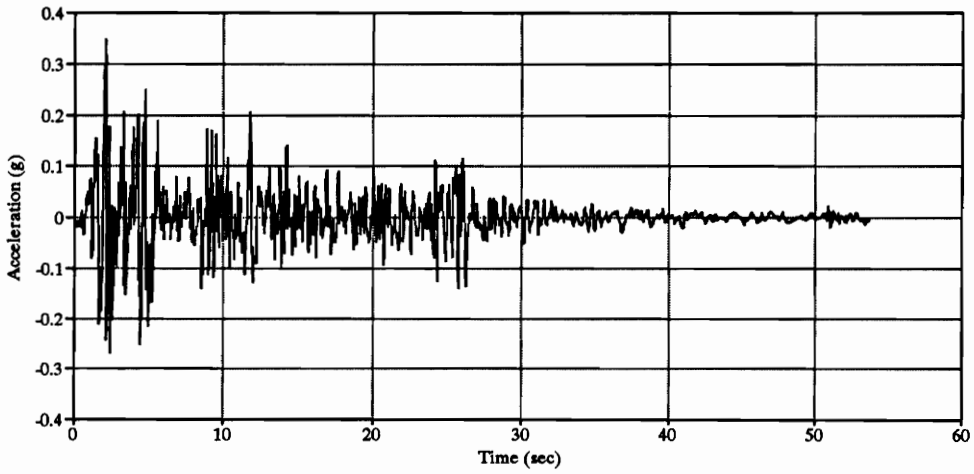

Figure 5.9: Acceleration Record for S00E Component of El Centro Earthquake

acceleration of 341.71 cm/sec^2 (134.53 in/sec^2), maximum velocity of 33.55 cm/sec

(13.17 in/sec), and maximum horizontal displacement of 10.9 cm (4.28 in). This particular record was used because it is the basis for the earthquake design used in some of the world's design codes and it has wide recognition in the design and research communities. The ground acceleration acts in the horizontal direction (i.e., parallel to the X–axis). The models were analyzed for the first 10 seconds of the record only Only the initial 10 seconds of the earthquake record were used in the analysis because the energy of the earthquake is relatively low after this point and was not considered to be significant to the primary response of a wall model and because of the significant amount of CPU time needed to analyze the larger wall models[1]. The record contained acceleration points taken every 0.02 seconds for a maximum of 500 points being used in the analysis.

5.3 Data Collected

The following information was recorded for each wall model subjected to monotonic loading: relative drift as a function of applied load (i.e. load–deflection or story drift curve) and maximum resistance, element forces, and forces at the reactions. Examination of the load–relative drift curves provides information concerning initial stiffness of a wall. Examination of the force and stress profile shows if there are any shear lag effects at the base of the wall and highlights any high stress regions in the wall.

The following information was recorded for each wall model subjected to dynamic loading: relative drift of the wall as a function of time and maximum relative displacement, base shear, element forces, and forces at the reactions. Examination of the time–relative drift history, and more importantly the maximum relative drift, was

[1]Three of the walls were analyzed for less than 10 seconds, but appeared to have sustained their peak displacement based on the results from the other models that were analyzed.

performed to determine how changes in wall configuration affects the displacement of a wall, which is a factor in the possibility of architectural damage (cracking, etc.) hapening in a shear wall. The purpose of examining the force and stress history was twofold and similar to the reasoning presented for the monotonic data. One purpose was to determine the magnitude of the base shear and whether or not there is a shear lag effect. The second purpose was to determine the state of loads in the wall, which would highlight any high stress regions in the wall and provide information useful for locating and designing anchorage connections.

5.4 Summary

A parametric study involving timber shear wall models developed using finite elements was outlined. The purpose of the study is to determine the effect that aspect ratio and openings have on the response of timber shear walls subjected to either static or dynamic loads. A total of twenty–five models that corresponded to shear walls framed with Spruce–Pine–Fir and sheathed with plywood were utilized in the study, fourteen models without openings with aspect ratios (ratio of wall length to height) ranging from 0.25 to 5 and eleven models of identical length with various opening sizes and configurations. Each model was analyzed twice using WALSEIZ, once when subjected to a distributed monotonic load acting along the elements composing the sill plate elements and once when subjected to a component of the acceleration record from the 1940 El Centro earthquake. The monotonic load–relative drift curve, dynamic time–relative drift curve, and maximum monotonic resistance, dynamic relative drift, base shear, and forces in the elements and reactions were recorded for each model.

Chapter 6

Results

6.1 Introduction

The results from the parametric study outlined in the previous chapter are presented. Shear wall models of different configurations, subjected to both monotonic and seismic loading, were analyzed using shear wall analysis program WALSEIZ in order to determine the effect that aspect ratio and openings have on the distribution of forces, initial stiffness, and maximum seismic base shear, relative drift, resistance, velocity, and acceleration of shear walls. The results are used to develop a new methodology for the design of timber shear walls.

6.2 Aspect Ratio

The results from the portion of the parametric study consisting of shear wall models without openings of various aspect ratios subjected to monotonic and dynamic loading are presented in this section. The results indicate the following concerning timber shear walls:

- The connectors, as opposed to the displacement of the elements, are the mechanisms by which most of the load is transferred to the sheathing and framing.

- The maximum monotonic resistance, initial stiffness, and maximum seismic base shear increase linearly as the aspect ratio increases for walls of a given height.
- The maximum monotonic and seismic relative drift and unit shear remain constant for walls of a given height.
- The shear force resisted by anchorages close to a stud where sheathing panels meet is higher than the shear force resisted by other anchorages.
- The force–couple resisted at the end chords is lower than the force–couple used for design because the vertical resistance at studs other than the end chords provide some resistance to uplift.
- The uplift force resisted by the anchorage connectors located in close proximity to a region in which two sheathing panels meet is lower than the uplift resisted by other anchorage connectors.
- The initial stiffness, maximum seismic base shear, and maximum monotonic and seismic relative drift and unit shear decrease as wall height increases for walls with the same length.

6.2.1 Monotonic Loading

A summary of the results from the parametric study for the wall models without openings of various aspect ratios subjected to monotonic loading is presented in Table 6.1. The load–relative drift plots generated from the analysis of these models are shown in Figures 7–11 of the Appendix. The results indicate that for shear walls of a given height, the maximum strength and initial stiffness of the walls increase linearly as aspect ratio increases while the maximum relative drift and unit shear remain constant, except for walls with a very low aspect ratio (i.e. very short length). The linear

Table 6.1: Results from Wall Models Without Openings Subjected to Monotonic Loading

Wall Height	Wall Length	Aspect Ratio	Initial Stiffness	Maximum[1] Load	Maximum Unit Shear	Maximum Relative Drift
m (ft)	m (ft)		kN/cm (kips/in)	kN (kips)	kN/m (lb/in)	cm/cm
2.4 (8)	0.6 (2)	0.25	2.91 (1.66)	7.5 (1.7)	12.3 (70)	0.045
	0.9 (3)	0.33	5.43 (3.10)	13.6 (3.1)	14.9 (85)	0.034
	1.2 (4)	0.5	8.41 (4.48)	18.1 (4.1)	14.9 (85)	0.028
	2.4 (8)	1	17.0 (9.09)	36.3 (8.2)	14.9 (85)	0.028
	4.9 (16)	2	33.8 (18.2)	72.6 (16.3)	14.9 (85)	0.029
	6.1 (20)	2.5	42.4 (22.9)	90.8 (20.4)	14.9 (85)	0.029
	7.3 (24)	3	50.8 (29.0)	108.9 (24.5)	14.9 (85)	0.029
	9.8 (32)	4	67.5 (37.5)	145.2 (32.6)	14.9 (85)	0.029
	12.2 (40)	5	84.8 (48.4)	181.6 (40.8)	14.9 (85)	0.029
4.9 (16)	1.2 (4)	0.25	4.72 (2.08)	13.9 (3.12)	11.4 (65)	0.012
	2.4 (8)	0.5	9.40 (5.37)	27.7 (6.24)	11.4 (65)	0.012
	4.9 (16)	1	18.7 (10.0)	51.2 (11.5)	10.5 (60)	0.010
	9.8 (32)	2	38.0 (20.0)	102.4 (23.0)	10.5 (60)	0.010
	12.2 (40)	2.5	47.8 (27.3)	128.0 (28.8)	10.5 (60)	0.010

[1]Maximum load calculated to nearest 0.88kN/m

relationship for maximum strength and initial stiffness, shown in Figures 6.1 and 6.2, occurs because the components that control the stiffness and resistance of a wall

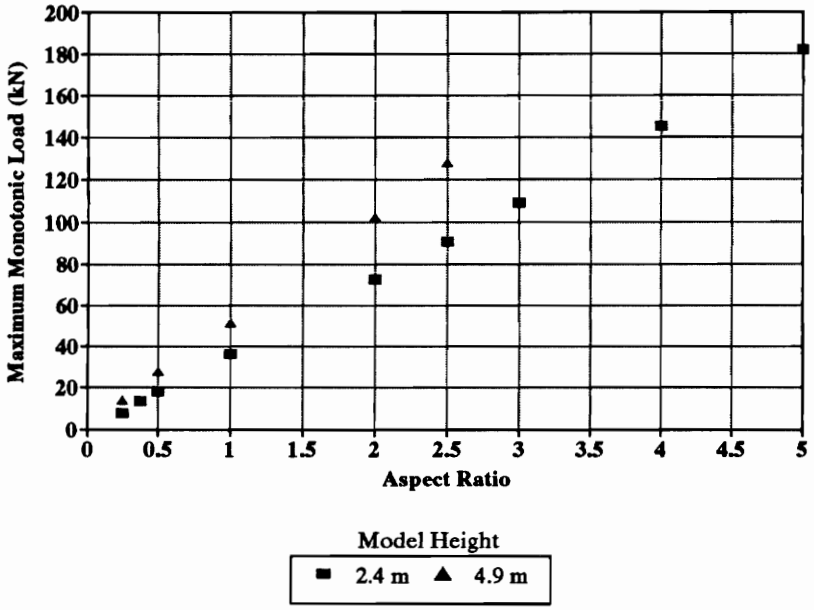

Figure 6.1: Maximum Strength of Wall Models Without Openings as a Function of Aspect Ratio

(i.e., the framing, sheathing, and connectors) increase linearly as the length of the wall increases. The constant maximum relative drift and unit shear occur because of the proportional increase in wall strength. The different characteristics of the 2.4 m high wall models with aspect ratios lower than 0.5, which are evident in the unit shear vs. relative drift curves shown in Figure 6.3, is due to their higher instance of bending deformation as opposed to shear deformation due to the "narrowness" of the sheathing panel.

Comparison of the wall models of different heights indicates that the maximum unit shear and relative drift is lower for taller walls and that for shear walls of identical aspect ratio, the maximum strength and initial stiffness increases as the height of the wall increases. The reduced maximum unit shear and relative drift occur because of

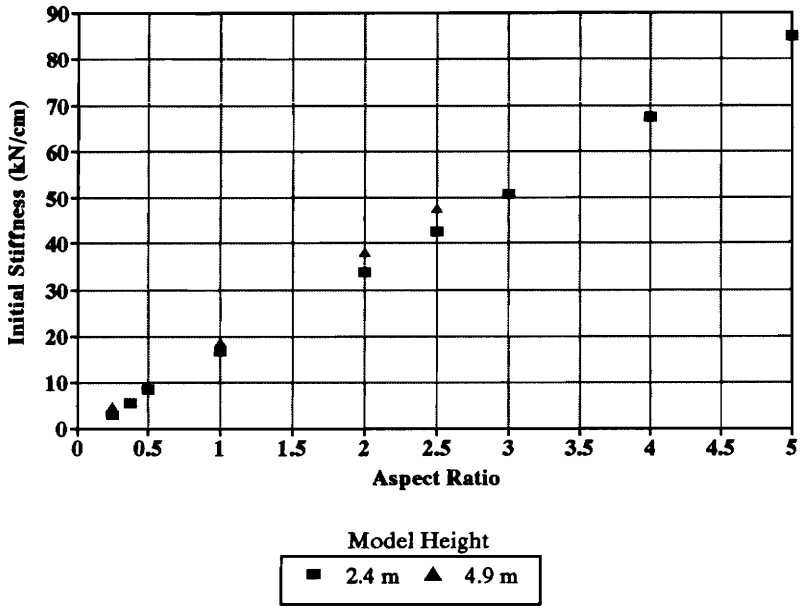

Figure 6.2: Initial Stiffness of Wall Models Without Openings as a Function of Aspect Ratio

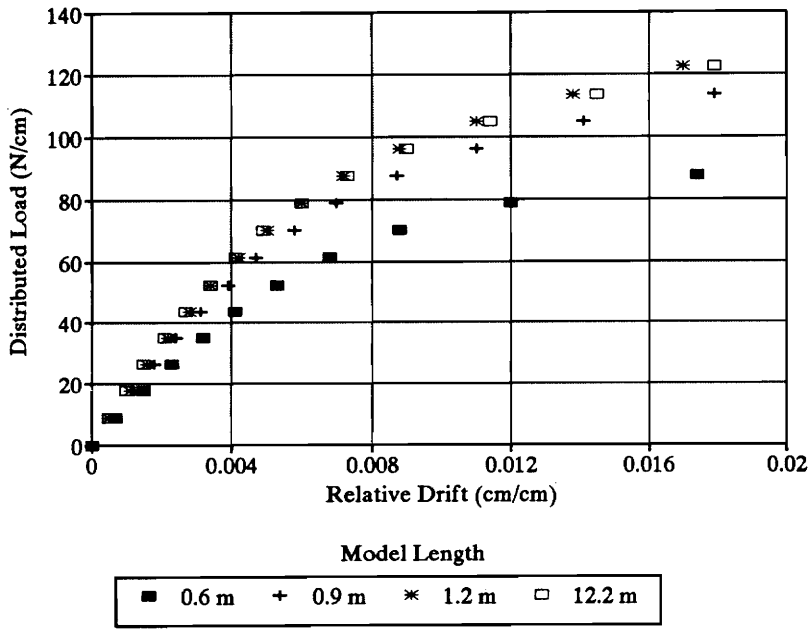

Figure 6.3: Unit Shear–Relative Drift Curves for Wall Models Without Openings

premature localized failure at the bottom of the end chords, which occurs because the overturning force–couple present in a shear wall increases as the height of the wall increases for walls subjected to an identical unit shear. As shown in Figure 6.3, the unit shear–relative drift curves for the wall models with different heights are almost identical up to failure of the 4.9 m high models. The increased maximum strength in the taller walls occurs because they are longer and therefore have more framing, sheathing, and connectors to provide resistance than a shorter wall with an identical aspect ratio. However, the maximum strength of a 4.9 m (16 ft) high model is not double that of a 2.4 m (8 ft) high model with an identical aspect ratio, as might be anticipated, because of the premature localized failure in the end chords. The increased initial stiffness in the taller walls also occurs because of their increased length. The initial stiffness of a 4.9 m high model, however, is lower than that of a 2.4 m high model of identical length because of the relatively slender configuration of the taller model.

The small displacements in the framing and sheathing of the wall models indicate that the majority of the force in the components are produced by the loads transferred through the connectors. The displacement pattern of the shear wall produces the following connector load distribution and resulting force distribution for the studs in a shear wall. The studs are relatively free to move at the top of the wall but not at the bottom, therefore having boundary conditions that are similar to a pinned reaction at the bottom and soft spring at the top. The connectors in the studs are each displaced approximately the same amount in the axial direction, thus transferring a series of loads of approximately the same magnitude, which is similar to a constant, distributed axial load. Therefore the member is loaded in a manner similar to that shown in Figure 6.4a, which results in a linear load distribution with the maximum load (tension or compression) at the reaction and a minimum load at the top, as shown in Figure 6.4b. The studs located where two sheathing panels meet have a

net axial load that approaches zero because the axial loading from the connectors of each sheathing panel are of equal magnitude and act in opposing directions. A

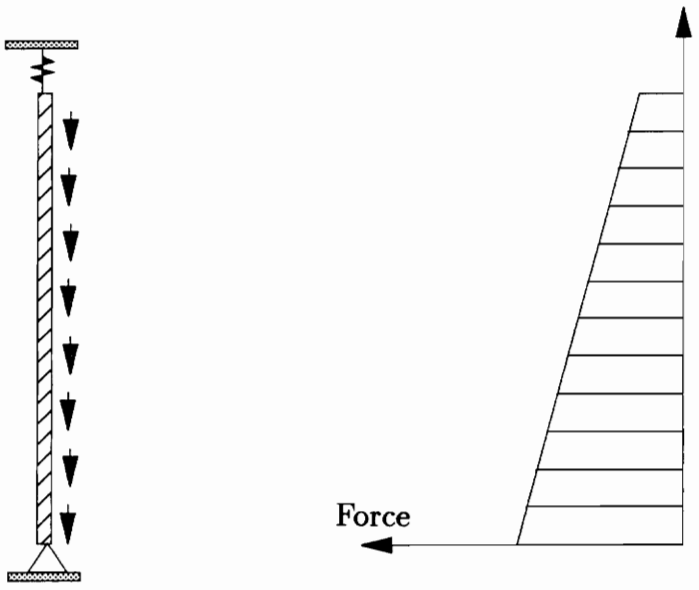

a).Equivalent System b).Axial Force Diagram

Figure 6.4: Distribution of Axial Force in Typical Stud

similar equivalent system and axial force diagram occur for the 4.9 m (16 ft) high wall models, with the difference being that a concentrated shear force is present at the studs in the blocking, which is transferred to the studs in the form of a concentrated axial force. The connectors in the studs displace a maximum distance at the top and bottom of the stud in the transverse direction, with the displacement of the connector varying linearly between these two points and points approximately 1/3 length of stud from the ends. This displacement results in a distribution of shear forces similar to the monotonic load–displacement curve of the connectors (see Figure 6.5a). This system results in the distribution of forces shown Figure 6.5b, with a high shear force at top and bottom of wall and a very low shear near the center of the member.

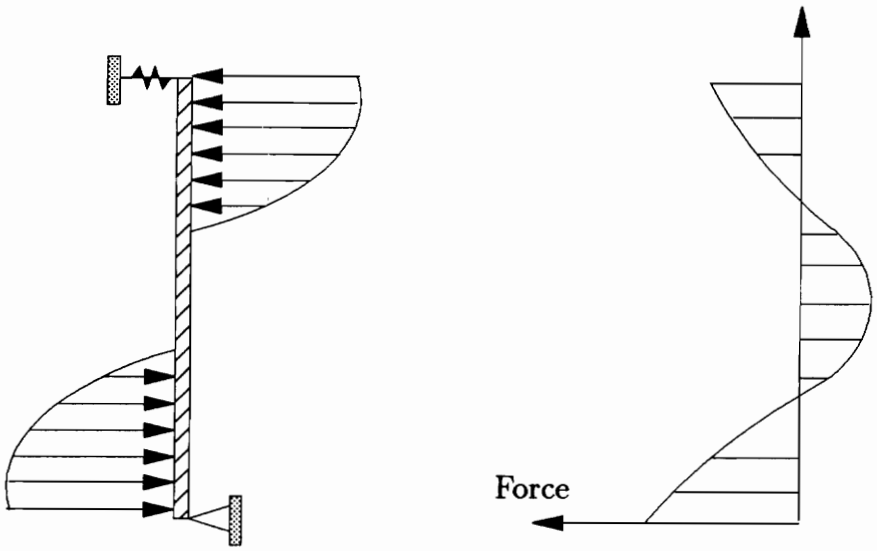

a).Equivalent System b).Shear Diagram

Figure 6.5: Distribution of Shear Force in Typical Stud

The equivalent system and shear force diagram for the 4.9 m (16 ft) walls models is similar to those for the 2.4 m (8 ft) high wall models placed above one another. The difference occurs because the sheathing panels above and below the blocking rotate independently, thereby producing two distributions of similar shape.

The displacement pattern of the shear wall produces the following connector load distribution and resulting force distribution for the sill plate in a shear wall. The majority of the resistance is provided by the end chords, with the interior studs providing some additional resistance. Therefore the member has boundary conditions similar to relatively rigid springs at the ends and soft springs located at each of the studs. The connectors in the sill plate are each displaced equally in the axial direction, producing a series of loads of approximately the same magnitude. (see Figure 6.6a). This displacement results in a force distribution analogous to that shown in Figure 6.6b, which is linear and varies from a maximum tensile force to a maximum

compressive force at the ends of the member with discrete increases in load at the interior reactions. The connectors in the sill plate have a linear displacement pattern

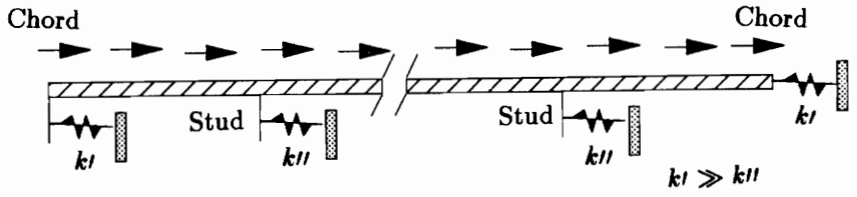

a).Equivalent System

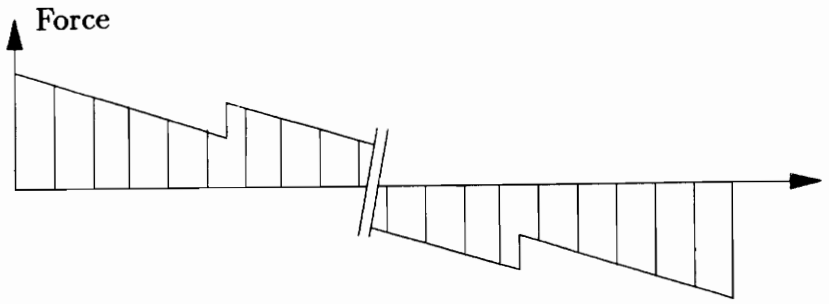

b).Axial Force Diagram

Figure 6.6: Distribution of Axial Force in Typical Sill Plate

in the transverse direction, with the maximum absolute displacements located at the studs in which two sheathing panels meet. This displacement results in a series of shear force distributions similar in shape to the monotonic load–displacement curve of the connectors. which is shown in Figure 6.7a. This system results in the distribution of forces shown Figure 6.7b, with the maximum force occurring where sheathing panels meet and the minimum force located at the mid–point of sheathing panels. The axial and shear force distribution are similar for the sole plate, the difference being that the reactions in the model provide unyielding support.

Traditionally, it has been assumed that the horizontal (or shear) force resisted at each anchorage is identical and equal to the total applied load divided by the number of anchorages. However, as shown in Table 6.2, which contains the magnitude of the horizontal force at the reactions divided by the average theoretical horizontal

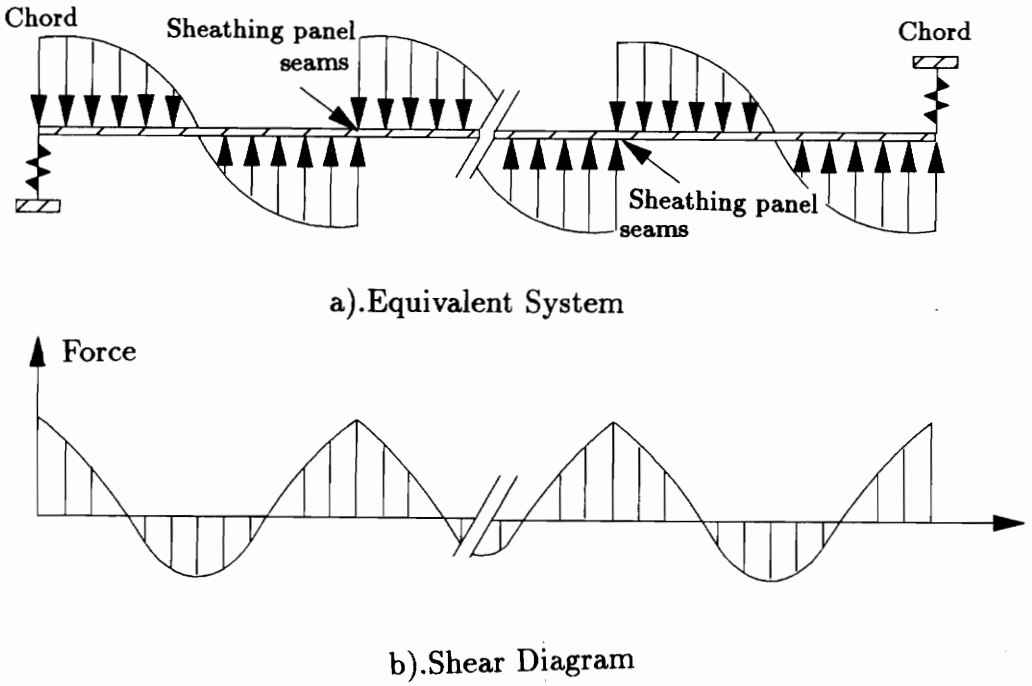

Figure 6.7: Distribution of Shear Force in Typical Sill Plate

Table 6.2: Ratio of Maximum Horizontal Force at Reaction to Average Horizontal Load Per Reaction for Wall Models Without Openings Subjected to Monotonic Loading

Wall		Distance from End Chord: cm (in)															
Length	Height																
m	m	0	41	81	122*	163	203	244*	284	325	366*	406	447	488*	528	569	610*
-	-	(0)	(16)	(32)	(48)	(64)	(80)	(96)	(112)	(128)	(144)	(160)	(176)	(192)	(208)	(224)	(240)
12.2	2.4	0.91	0.83	0.83	1.29	0.86	0.86	1.32	0.87	0.87	1.33	0.87	0.87	1.33	0.87	0.87	1.33
	4.9	0.92	0.87	0.87	1.29	0.90	0.90	1.32	0.91	0.91	1.32	0.91	0.91	1.33	0.91	0.91	1.33
9.8	2.4	0.92	0.83	0.83	1.29	0.87	0.87	1.33	0.88	0.88	1.34	0.88	0.88	1.34			
	4.9	0.93	0.88	0.88	1.30	0.91	0.91	1.33	0.92	0.92	1.33	0.92	0.92	1.33			
7.3	2.4	0.93	0.84	0.84	1.31	0.88	0.88	1.35	0.88	0.89	1.35						
6.1	2.4	0.93	0.85	0.85	1.32	0.88	0.89	1.36	0.89								
4.9	2.4	0.95	0.86	0.86	1.34	0.89	0.90	1.37									
	4.9	0.96	0.91	0.91	1.34	0.94	0.94	1.36									
2.4	2.4	0.99	0.90	0.91	1.38												
	4.9	1.01	0.95	0.95	1.39												
1.2	2.4	1.04	0.96														
	4.9	1.01	0.99														
0.9[1]	2.4	1.08	0.91														
0.6[1]	2.4	1.02	0.95														

SYM.

*:Indicates studs where sheathing panels meet.

[1]Distance between reactions is 30 cm (12 in).

force resisted at each reaction, anchorages located in close proximity to a stud where sheathing panels meet resist a shear force (approximately 30–35% greater for the wall models in the study) than the average load per anchorage. This phenomenon occurs because two sets of connectors are present along these studs and they transmit a higher shear force to the stud, which is in turn transferred to the closest anchorage. The closer nail spacing along the exterior of the sheathing panels also contributes to the higher shear force at these locations. The reduced spacing between nails along the exterior of the sheathing panels is also the reason that the shear force resisted at the end chords of a shear wall is higher than the shear resisted by anchorages located adjacent to the interior studs. Another trend exhibited in Table 6.2 is that the magnitude of the load at the reactions increases slightly as the center of the wall model is approached. This is similar to a shear lag effect, with the difference being that the shear wall is a system as opposed to an individual member. This effect is small ($\approx$ 3% change) and can be neglected in practice.

The results presented in Table 6.3, which contains the magnitude of the vertical force at a support divided by the theoretical overturning force–couple resisted at the end chords, indicate that the maximum vertical load at the end chords is lower than the overturning force–couple. The load at the end chords is approximately 86% of the force–couple for 2.4 m (8 ft) high wall models and 99% of the force–couple for the 4.9 m (16 ft) high wall models. The reduction occurs because the theoretical overturning force–couple is based on the assumption that no resistance is provided at the interior studs. However, as shown in Table 6.3, the axial load found at the interior reactions, except for those reactions at studs where sheathing panels meet, is approximately 40% of the theoretical force–couple for the 2.4 m (8 ft) high wall models and 27% of the theoretical force–couple for the 4.9 m (16 ft) high wall models. Therefore, the only resistance to the overturning moment is not provided at the end chords (assuming that sufficient resistance to vertical loading is provided along the

Table 6.3: Ratio of Maximum Absolute Vertical Force at Reaction to Theoretical Overturning Force–Couple at End Chords for Wall Models Without Openings Subjected to Monotonic Loading

Wall		Distance from End Chord: cm (in)															
Length	Height																
m	m	0	41	81	122*	163	203	244*	284	325	366*	406	447	488*	528	569	610*
–	–	(0)	(16)	(32)	(48)	(64)	(80)	(96)	(112)	(128)	(144)	(160)	(176)	(192)	(208)	(224)	(240)
12.2	2.4	0.87	0.42	0.40	0.00	0.39	0.39	0.00	0.39	0.39	0.00	0.39	0.39	0.00	0.39	0.39	0.00
	4.9	0.99	0.28	0.26	0.01	0.26	0.26	0.00	0.26	0.26	0.00	0.26	0.26	0.00	0.26	0.26	0.00
9.8	2.4	0.87	0.42	0.40	0.0	0.39	0.39	0.0	0.39	0.39	0.0	0.39	0.39	0.0			
	4.9	0.99	0.28	0.26	0.01	0.26	0.26	0.00	0.26	0.27	0.0	0.26	0.26	0.00			
7.3	2.4	0.87	0.42	0.40	0.0	0.39	0.39	0.0	0.39	0.39	0.0						
6.1	2.4	0.87	0.42	0.40	0.0	0.39	0.39	0.0	0.39								
4.9	2.4	0.86	0.42	0.40	0.0	0.39	0.39	0.0									
	4.9	0.99	0.28	0.26	0.01	0.26	0.26	0.00									
2.4	2.4	0.86	0.41	0.40	0.0												
	4.9	0.99	0.28	0.27	0.00												
1.2	2.4	0.86	0.42														
	4.9	0.99	0.28														
0.9[1]	2.4	0.88	0.37														
0.6[1]	2.4	1.01	0.0														

SYM.

*:Indicates studs where sheathing panels meet.

[1]Distance between reactions is 30 cm (12 in).

sole plate), which results in reduced axial load at these locations. The taller shear walls resist a higher percentage of the overturning force–couple at the end chords and a lower percentage at the interior studs because the increased height of the wall produces more bending deformation. The magnitude of vertical load transferred to the end chords and interior studs, however, is dependent on the configuration of the framing. This is because the axial load at the studs occurs primarily due to the vertical displacement of the connectors attaching the sheathing to the framing. The closer a stud is located towards the center of a sheathing panel, a location in which the vertical displacement of the connectors is negligible, the lower the load carried by the stud. Other trends involving the vertical forces at the reactions include the following. The studs located along the seams of the sheathing resist a net load of very low magnitude (essentially zero) because the axial load transferred from the connectors attaching the two sheathing panels act in opposite directions and cancel each other. Also, the percentage of the force resisted at the end chords does not vary significantly as a function of wall length because the relative vertical displacement between the sheathing and the end chords are displaced by approximately the same amount in all of the wall models, therefore providing a similar distribution of axial load from the connectors. There is also a slight increase in the magnitude of vertical load resisted at the reactions as the center of the wall is approached that seems to represent a system shear lag effect, although this effect is minor.

6.2.2 Seismic Loading

A summary of the results from the parametric study for the wall models without openings of various aspect ratios subjected to seismic loading is presented in Table 6.4. Representative plots of the first ten seconds of the time–relative drift curves are shown in Figure 6.8. The results indicate that the maximum base shear increases linearly

Table 6.4: Results from Wall Models Without Openings Subjected to Seismic Loading

Wall Height	Wall Length	Aspect Ratio	Maximum Relative Drift	Max. Top–of–Wall		Maximum Base Shear	Maximum Unit Shear
				Velocity	Acc.		
m (ft)	m (ft)		cm/cm	cm/sec (in/sec)	cm/sec^2 (in/sec^2)	kN (kips)	kN/m (lb/in)
2.4 (8)	0.6 (2)	0.25	0.038	50.8 (20.0)	552.2 (217.4)	9.7 (2.2)	15.9 (91)
	0.9 (3)	0.33	0.035	41.1 (16.2)	630.4 (248.2)	15.4 (3.5)	16.8 (96)
	1.2 (4)	0.5	0.029	32.6 (12.8)	664.1 (253.6)	21.6 (4.9)	17.7 (101)
	2.4 (8)	1	0.029	31.8 (12.5)	639.9 (251.9)	42.6 (9.6)	17.5 (100)
	4.9 (16)	2	0.029	31.5 (12.4)	636.6 (250.6)	84.5 (19.0)	17.3 (99)
	6.1 (20)	2.5	0.028	31.4 (12.3)	635.2 (250.1)	105.4 (23.7)	17.3 (99)
	7.3 (24)	3	0.028	31.3 (12.3)	634.0 (249.6)	126.7 (28.5)	17.3 (99)
	9.8 (32)	4	0.028	31.3 (12.3)	626.7 (249.7)	168.5 (37.9)	17.3 (98)
	12.2 (40)	5	0.028	31.3 (12.3)	635.5 (250.2)	209.9 (47.2)	17.2 (98)
4.9 (16)	1.2 (4)	0.25	0.023	57.8 (22.7)	564.3 (222.2)	19.2 (4.3)	15.7 (90)
	2.4 (8)	0.5	0.021	55.0 (21.7)	577.4 (227.3)	38.4 (8.6)	15.7 (90)
	4.9 (16)	1	0.021	54.1 (21.3)	590.2 (232.4)	76.7 (17.3)	15.7 (90)
	9.8 (32)	2	0.020	53.3 (21.0)	592.1 (233.1)	153.0 (34.4)	15.7 (90)
	12.2 (40)	2.5	0.020	53.2 (20.9)	592.7 (233.4)	191.7 (43.1)	15.7 (90)

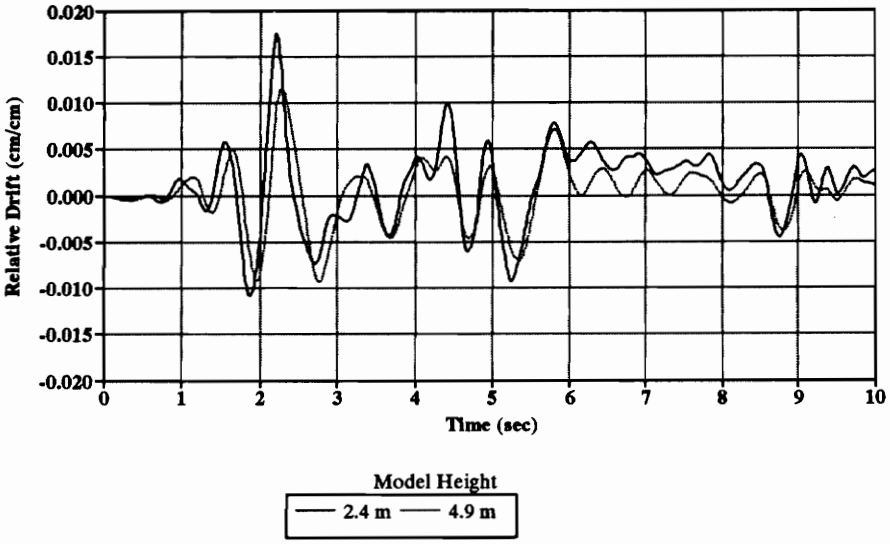

Figure 6.8: Time–Relative Drift Curves for Wall Models Without Openings

as the aspect ratio increases (i.e. the maximum unit shear remains constant) while the maximum relative drift as well as the maximum velocity and acceleration at the top of the wall remain constant, except for shear walls that have a short length (less than 1.2 m (4 ft) for the models in the study), for shear walls of a given height. The linear relationship for base shear, shown in Figure 6.9, occurs because a majority of the mass, which is directly proportional to the external loading, is concentrated at the top of the wall and therefore increases linearly as the length of the wall increases. This, along with the linearly increasing stiffness of the wall, would seem to result in a constant fundamental period of the walls as the length increases, which in turn leads to the constant relationship for the wall relative drift, velocity, and acceleration.

Comparison of the wall models of different heights indicates that the maximum relative drift and velocity and acceleration at the top of the wall are greater for taller shear walls of identical length. The differences between the properties of the walls of different heights occurs because of an anticipated difference in fundamental period, which occurs due to a difference in initial stiffness. Given two walls of equal length

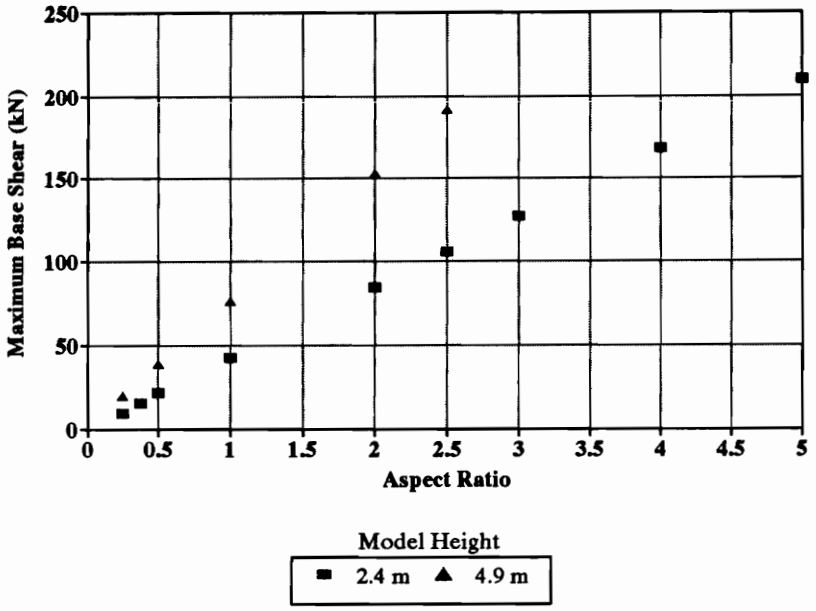

Figure 6.9: Maximum Base Shear of Wall Models Without Openings as a Function of Aspect Ratio

(and therefore roughly equal mass), a 2.4 m (8 ft) high wall has a significantly higher initial stiffness than a 4.9 m (16 ft) high wall (see Figure 6.2). The higher initial stiffness in the shorter wall would result in a higher frequency and therefore lower period for the wall. The lower period for the 2.4 m (8 ft) high walls thereby indicates that these walls will have a quicker response and therefore a greater maximum relative drift and top–of–wall acceleration than the taller wall. Comparison of the models also indicates that the maximum base shear increases as the height of the wall increases for shear walls with identical aspect ratios, as is shown in Figure 6.9. This occurs because the taller walls would be longer and therefore have a larger mass. However, the results of the study show that the maximum base shear for a 4.9 m (16 ft) high wall model is not twice as great the maximum base shear for a 2.4 m (8 ft) high wall model with the same aspect ratio, as might be anticipated because the 4.9 m high models have twice as much mass. This occurs because of the probable lower frequency of the 4.9 m high walls. The presence of blocking has some effect on the response of

the walls, although it is not considered to be significant.

The distribution of forces in the wall models without openings subjected to seismic loading is similar to the force distribution in the models without openings subjected to monotonic loading, with a linear force distribution in the axial direction and a nonlinear force distribution in the transverse direction for the studs, chords, and sill plate. This indicates that the distribution of forces in a shear wall is similar when monotonic or seismic loads are applied. The distribution of forces at the reactions for the models without openings subjected to seismic loads is also similar to force distribution at the reactions for the models subjected to monotonic loading. The results shown in Table 6.5, which contains the magnitude of the horizontal force at the reactions divided by the average theoretical horizontal force resisted at each reaction for the models without openings subjected to seismic loading, indicate that the base shear loading is significantly ($\approx$ 30–35%) greater at the locations in which sheathing panels meet than the average reaction force and the supports at the end chords resists a base shear load slightly ($\approx$ 0–5%) higher than the load resisted at the interior studs, which correspond to the findings for the models without openings subjected to monotonic loading.

The results shown in Table 6.6, which contains the magnitude of the vertical force at a support divided by the theoretical overturning force–couple at the end chords for the models without openings subjected to seismic loading, indicates that the reactions at the end chords resist an axial force lower than the theoretical overturning force–couple given that the reactions at the interior studs provide resistance to overturning, the net axial load in studs located at the seams of sheathing panels is essentially zero because of forces transferred from adjacent connectors opposing one another, and there is a small overall shear lag effect for both shear and axial loads, although this effect is small and negligible in a practical sense. These conclusions also correspond to the findings of the models subjected to monotonic loading.

Table 6.5: Ratio of Maximum Absolute Horizontal Force at Reaction to Average Horizontal Load Per Reaction for Wall Models Without Openings Subjected to Seismic Loading

Wall		Distance from End Chord: cm (in)															
Length	Height																
m	m	0	41	81	122*	163	203	244*	284	325	366*	406	447	488*	528	569	610*
–	–	(0)	(16)	(32)	(48)	(64)	(80)	(96)	(112)	(128)	(144)	(160)	(176)	(192)	(208)	(224)	(240)
12.2	2.4	0.87	0.85	0.85	1.27	0.88	0.88	1.30	0.89	0.89	1.31	0.89	0.89	1.31	0.89	0.89	1.31
	4.9	0.85	0.85	0.86	1.26	0.88	0.89	1.29	0.89	0.89	1.30	0.89	0.89	1.30	0.89	0.90	1.30
9.8	2.4	0.87	0.85	0.85	1.28	0.89	0.89	1.31	0.89	0.89	1.32	0.89	0.90	1.32			
	4.9	0.86	0.86	0.86	1.27	0.89	0.89	1.30	0.90	0.90	1.31	0.90	0.90	1.31			
7.3	2.4	0.88	0.86	0.86	1.29	0.90	0.90	1.33	0.90	0.90	1.34						
6.1	2.4	0.89	0.87	0.87	1.31	0.90	0.90	1.33	0.91								
4.9	2.4	0.90	0.88	0.89	1.32	0.91	0.92	1.35									
	4.9	0.89	0.89	0.89	1.31	0.92	0.92	1.34									
2.4	2.4	0.95	0.93	0.93	1.36												
	4.9	0.93	0.94	0.95	1.36												
1.2	2.4	1.00	1.00														
	4.9	0.99	1.01														
0.9[1]	2.4	1.04	0.96														
0.6[1]	2.4	1.03	1.09														

SYM.

*:Indicates studs where sheathing panels meet.

[1]Distance between reactions is 30 cm (12 in).

Table 6.6: Ratio of Maximum Absolute Vertical Force at Reaction to Theoretical Overturning Force-Couple at End Chords for Wall Models Without Openings Subjected to Seismic Loading

Wall		Distance from End Chord: cm (in)															
Length	Height																
m	m	0	41	81	122*	163	203	244*	284	325	366*	406	447	488*	528	569	610*
-	-	(0)	(16)	(32)	(48)	(64)	(80)	(96)	(112)	(128)	(144)	(160)	(176)	(192)	(208)	(224)	(240)
12.2	2.4	0.88	0.43	0.42	0.06	0.41	0.40	0.04	0.40	0.40	0.03	0.40	0.40	0.06	0.40	0.40	0.07
	4.9	0.90	0.26	0.21	0.06	0.22	0.21	0.06	0.21	0.21	0.06	0.21	0.21	0.05	0.21	0.21	0.05
9.8	2.4	0.87	0.43	0.42	0.08	0.40	0.40	0.08	0.40	0.40	0.06	0.40	0.40	0.07			
	4.9	0.90	0.26	0.21	0.06	0.22	0.21	0.06	0.21	0.21	0.05	0.21	0.21	0.05			
7.3	2.4	0.87	0.43	0.42	0.07	0.40	0.40	0.12	0.40	0.40	0.08						
6.1	2.4	0.89	0.43	0.41	0.06	0.40	0.40	0.08	0.40								
4.9	2.4	0.88	0.43	0.41	0.11	0.40	0.40	0.10									
	4.9	0.91	0.27	0.21	0.06	0.22	0.21	0.05									
2.4	2.4	0.89	0.44	0.41	0.08												
	4.9	0.91	0.26	0.21	0.05												
1.2	2.4	0.89	0.44														
	4.9	0.93	0.25														
0.9[1]	2.4	0.89	0.39														
0.6[1]	2.4	1.06	0.07														

SYM.

*:Indicates studs where sheathing panels meet.

[1]Distance between reactions is 30 cm (12 in).

6.3 Openings

The results of the portion of the parametric study consisting of shear wall models with various opening sizes and configurations subjected to monotonic and dynamic loading are presented in this section. The results indicate the following concerning timber shear walls:

- The deformation pattern of a typical shear wall with openings, shown in Figure 6.10 for a wall with a window opening, has the framing displaced as a

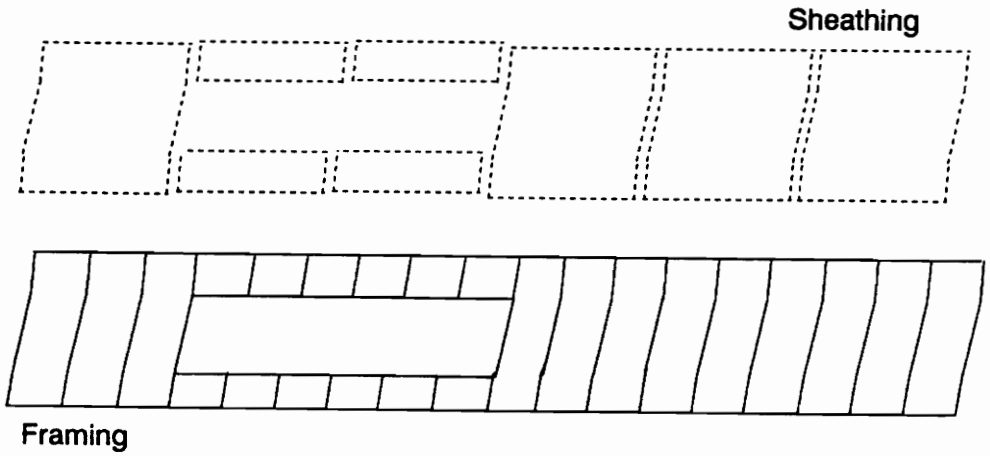

Figure 6.10: Typical Deflection Pattern of Shear Wall With Openings

parallelogram with a majority of the rotation occuring away from the openings and the sheathing rotating slightly while being distorted. The distortion of the sheathing and framing is greater when the length of the opening is greater because the resistance to rotation becomes concentrated in a small area.

- The relative drift increases as the opening length increases for walls subjected to both monotonic and seismic loading.

- The monotonic resistance, initial stiffness and maximum seismic base shear decrease as the opening length increases for walls of a given height.

- The horizontal member(s) adjacent to the openings (i.e. the header) sustains a significant axial load that in turn is applied to the studs adjacent to the opening.
- The current calculation of design overturning moments for use in determining the forces in the end chords overestimate the magnitude of the moments by a much as 48%.

6.3.1 Monotonic Loading

A summary of the results from the parametric study for the wall models with various opening sizes and configurations subjected to monotonic loading is presented in Table 6.7. The load–relative drift plots generated from the analysis of these models are shown in Figures 12–14 of the Appendix. The results indicate that for shear walls of identical overall length with openings, the resistance and initial stiffness decrease as the length of the opening increases. The relationship for strength and initial stiffness is evident in Figures 6.11 and 6.12 (where effective aspect ratio is the ratio of the effective length of the wall to the height) and also in the load–relative drift curves shown in the Appendix. The strength is compared at a relative drift of 0.006 because the displacement at which the maximum load was calculated by WALSEIZ had a wide variation. The decrease in stiffness and strength occurs because the components that provide stiffness and strength for a shear wall (namely the framing, sheathing, and connectors) are reduced as the length of the opening increases. The graphs shown in Figures 6.11 and 6.12 also indicate that the initial stiffness and maximum resistance is greater for the walls with window openings than for the wall with door openings. This occurs because the walls with window openings have slightly more wall material above and below the opening than the walls with door openings, which provide more stiffness and resistance.

Comparison of the wall models of different heights indicates that for shear walls of

Table 6.7: Results from Wall Models with Openings Subjected to Monotonic Loading

Opening Type	Wall Height m (ft)	Opening Length m (ft)	Effective[1] Aspect Ratio	Initial Stiffness kN/cm (kips/in)	Maximum[2] Load kN (kips)	Unit Load in Header N/cm (lb/in)
Window	2.4 (8)	1.2 (4)	2.5	48.0 (27.5)	89.7 (20.2)	56.6 (32.3)
		2.4 (8)	2	41.5 (23.7)	67.3 (15.1)	56.0 (32.0)
		3.7 (12)	1.5	33.8 (19.3)	64.1 (14.4)	58.5 (33.4)
		4.9 (16)	1	25.0 (14.3)	48.0 (10.8)	44.8 (25.6)
Door	2.4 (8)	1.2 (4)	2.5	44.7 (25.5)	60.9 (13.7)	57.6 (32.9)
		2.4 (8)	2	36.5 (20.9)	48.0 (10.8)	39.4 (22.5)
		3.7 (12)	1.5	28.0 (16.0)	38.4 (8.64)	30.6 (17.5)
		4.9 (16)	1	19.3 (11.0)	25.6 (5.76)	20.9 (11.9)
	4.9 (16)	2.4 (8)	1	20.8 (11.9)	41.6 (9.36)	56.4 (32.2)
		3.7 (12)	0.75	16.9 (9.62)	41.6 (9.36)	51.8 (29.6)
		4.9 (16)	0.5	10.6 (6.06)	25.6 (5.76)	31.7 (18.1)

[1]Effective aspect ratio is calculated using the total length of the wall less the length of the opening(s)

[2]Maximum load calculated to nearest 0.44kN/m

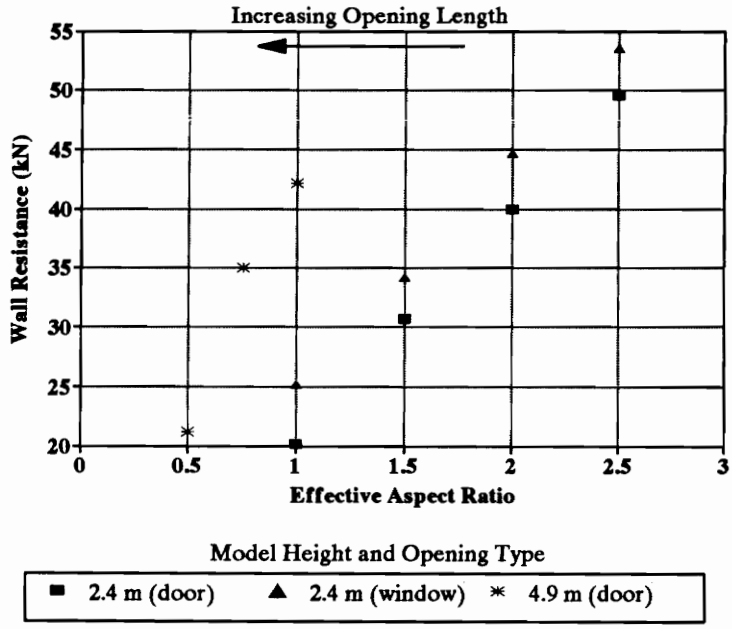

Figure 6.11: Strength of Wall Models with Openings at Relative Drift of 0.006 as a Function of Effective Aspect Ratio

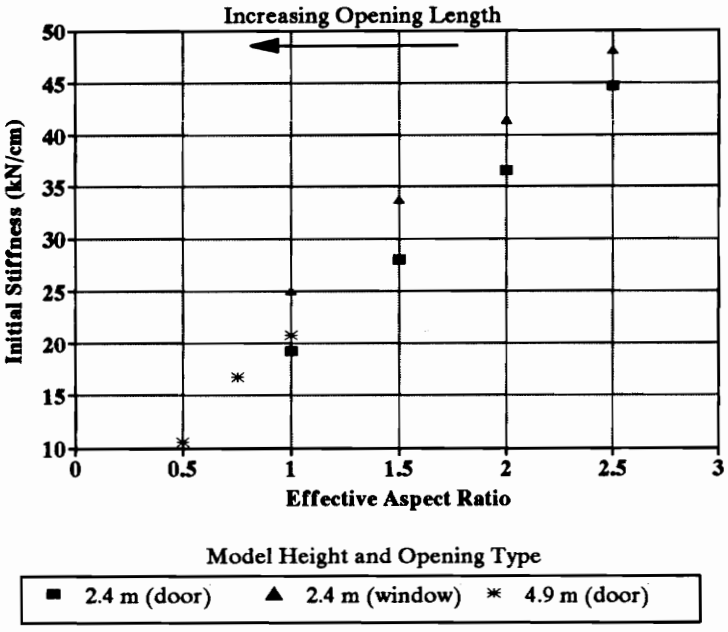

Figure 6.12: Initial Stiffness of Wall Models with Openings as Function of Effective Aspect Ratio

a given effective aspect ratio, the strength of a shear wall increases as the height of the wall increases and the initial stiffness remains relatively similar for walls of different heights. The increased strength of the taller walls occurs because of their greater length. However, the 4.9 m (16 ft) high wall models with openings had a higher resistance than the 2.4 m (8 ft) high wall models of identical effective length with door openings and the resistance of the models with window openings was greater than that of the 4.9 m high models of identical effective length with openings. These differences in strength are presumably influenced by the proportion of wall above and below the opening, therefore indicating that the height of an opening also has a significant effect on the strength of a shear wall. The initial stiffness for walls of different heights with the same aspect ratio, which is greatest for the wall models with window openings and lowest for the 2.4 m (8 ft) high wall models with door openings, is affected by the configuration of the walls and also presumably influenced by the proportion of wall above and below the opening. The presence of blocking also has an effect on the response, although this effect is presumed to be relatively minor.

The distribution of forces in a shear wall with openings is similar, but not identical, to the force distribution in a shear wall without openings. The distribution of forces in the end chords and studs is the same as the force distribution in a shear wall without openings. The displacement pattern of the shear wall produces the following connector load distribution and resulting force distribution for the header in a shear wall. The majority of the resistance is provided by the chords adjacent to the openings, with the studs above and/or below the opening providing some additional resistance. Therefore the member has boundary conditions similar to relatively rigid springs at the ends and soft springs located at each of the studs. The portion of the wall above/below the opening experiences rotation similar to that of the wall without openings. This results in constant relative displacement between the sheathing and framing, which causes the connectors in the header to displace approximately the same magnitude in the

axial direction and produces a series of loads of approximately the same magnitude (see Figure 6.13a). This displacement results in a force distribution analogous to that shown in Figure 6.13b, which is linear and varies from a maximum tensile force to a maximum compressive force at the ends of the member with discrete increases in load at the interior reactions. The displacement of the wall above/below the opening also

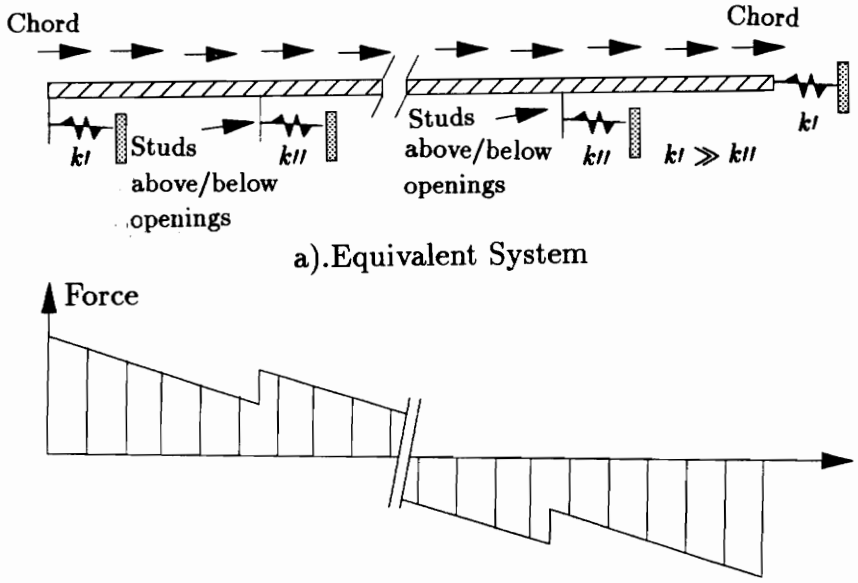

Figure 6.13: Distribution of Axial Force in Typical Header Above and/or Below Opening

produces a linear displacement pattern in the transverse direction of the header, with the maximum absolute displacements located at the studs in which two sheathing panels meet. This displacement pattern results in a series of shear force distributions, shown in Figure 6.14a, similar in shape to the monotonic load–displacement curve of the connectors. This system results in the distribution of forces shown Figure 6.14b, with the maximum force located where sheathing panels meet and the minimum force located at the mid–point of sheathing panels.

The axial and shear loads from the header impact the chords adjacent to the opening. The equivalent system for the chord adjacent to the openings are very similar

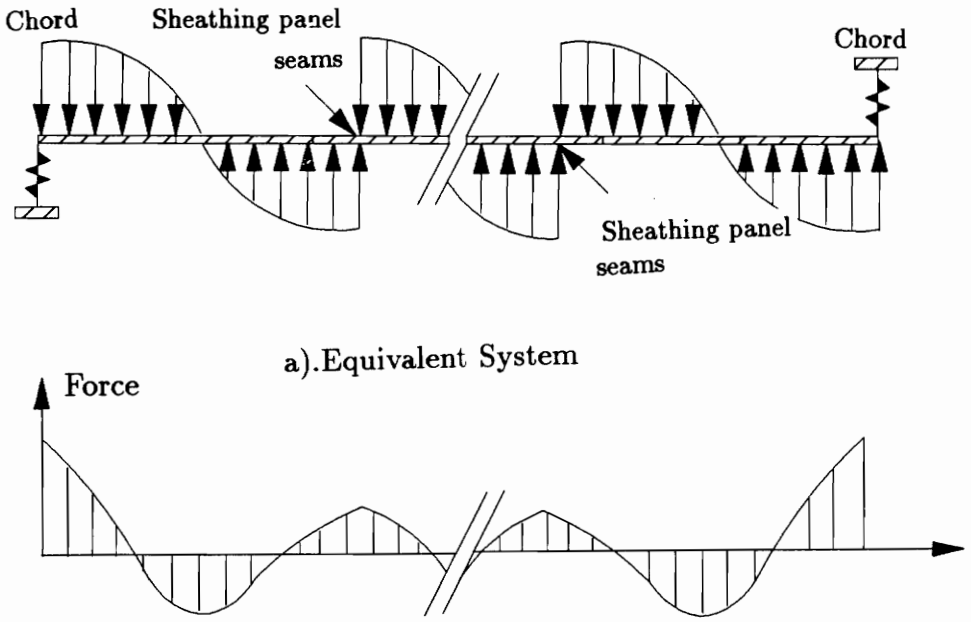

Figure 6.14: Distribution of Shear Force in Typical Header Above and/or Below Opening

those for the studs in the walls without openings. The difference occurs due to the contribution from the opening header. The shear force at the ends of the header are transferred to the adjacent chords. The addition of this force on the equivalent system for a stud subjected to axial forces, shown in Figure 6.4a, produces the modified equivalent system shown in Figure 6.15a, which results in the shear diagram shown in Figure 6.15b. The axial force at the ends of the header are transferred to the adjacent chords. The addition of this force on the equivalent system for a stud subjected to shear forces, shown in Figure 6.5a, produces the modified equivalent system shown in Figure 6.16a. This results in the shear diagram shown in Figure 6.16a, which has the same general shape as a typical stud except for the effect of the concentrated load.

Analogous to shear walls without openings, the shear force resisted at each anchorage is assumed to be identical and equal to the applied load divided by the number of anchorages. However, as shown in Table 6.8 which contains the magnitude of the

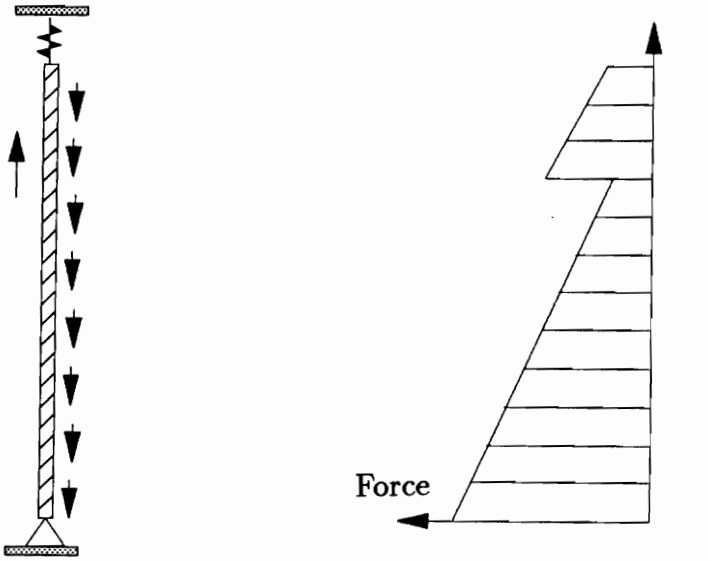

a).Equivalent System b).Axial Force Diagram

Figure 6.15: Distribution of Axial Force in Chord Adjacent to Opening

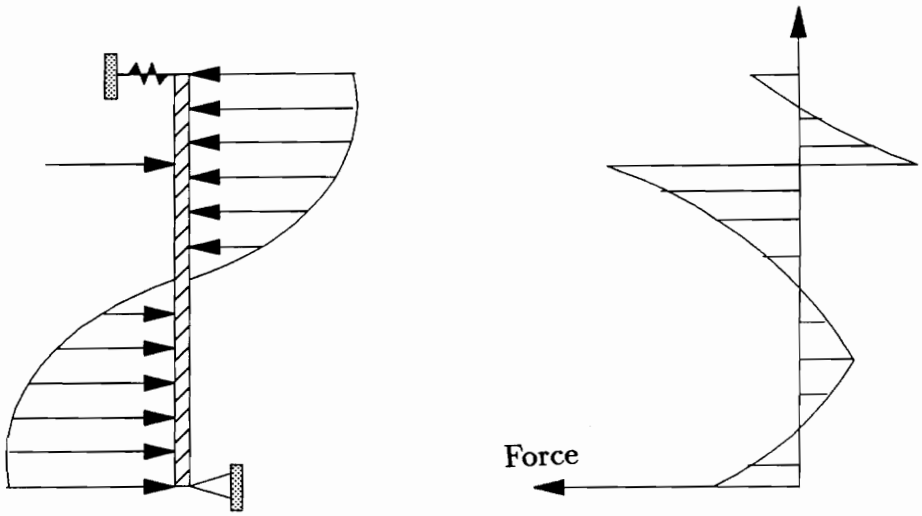

a).Equivalent System b).Shear Diagram

Figure 6.16: Distribution of Shear Force in Chord Adjacent to Opening

Table 6.8: Ratio of Maximum Horizontal Force at Reaction to Average Horizontal Load Per Reaction for Wall Models With Openings Subjected to Monotonic Loading

	Wall Height m –	Wall Length m –	Distance from End Chord: cm (in) 0 (0)	41 (16)	81 (32)	122* (48)	163 (64)	203 (80)	244* (96)	284 (112)	325 (128)	366* (144)	406 (160)	447 (176)	488* (192)	528 (208)	569 (224)
Wind.	2.4	6.1	0.41	0.48	0.44	0.99#	0.93	0.92	1.40#	0.95	0.90	1.46	1.00	1.00	1.52	1.00	1.00
		4.9	0.59	0.67	0.67	0.89#	0.46	0.46	0.65	0.46	0.46	1.26#	1.13	1.13	1.78	1.28	1.28
		3.7	1.06	1.08	1.08	1.31#	0.52	0.53	0.79	0.56	0.56	0.79	0.53	0.52	1.37#	1.20	1.20
		2.4	1.47	1.47	1.47	1.64#	0.53	0.54	0.80	0.58	0.59	0.83	0.59	0.58	0.80	0.54	0.53
Door	2.4	6.1	0.94	0.94	0.94	0.73#			0.74#	0.96	0.96	1.40	0.97	0.97	1.40	0.96	0.96
	2.4	4.9	0.96	0.97	0.97	0.75#						0.75#	0.98	0.98	1.42	0.99	0.99
	4.9	4.9	0.96	0.93	0.93	0.96#						0.95#	0.91	0.91	1.33	0.95	0.95
	2.4	3.7	1.01	0.99	1.00	0.77#									0.78#	1.01	1.01
	4.9	3.7	0.94	0.93	0.93	0.95#									0.97#	0.95	0.95
	2.4	2.4	1.09	1.09	1.09	0.73#											
	4.9	2.4	0.97	0.99	0.99	0.98#											

*:Indicates studs where sheathing panels meet.
#:Indicates location of chords adjacent to openings for walls with window openings.

	Wall Height m –	Wall Length m –	610* (240)	650 (256)	691 (272)	732 (288)
Wind.	2.4	6.1	1.52	1.00	1.00	1.09
		4.9	1.93	1.27	1.27	1.37
		3.7	1.87	1.31	1.31	1.40
		2.4	1.64#	1.47	1.47	1.48
Door	2.4	6.1	1.36	0.92	0.92	0.92
	2.4	4.9	1.40	0.95	0.95	0.94
	4.9	4.9	1.39	0.93	0.93	0.98
	2.4	3.7	1.45	0.99	0.99	1.00
	4.9	3.7	1.41	0.98	0.98	1.01
	2.4	2.4	0.73#	1.09	1.09	1.09
	4.9	2.4	1.01#	1.02	1.02	1.02

horizontal force at a reaction divided by the average theoretical horizontal force resisted at each reaction for the models with openings subjected to monotonic loading, the trend in which the shear force resisted by the anchorages in close proximity to studs in which sheathing panels meet resist a higher percentage of the base shear (up to 78% higher for the models with window openings and 45% higher for the models with door openings) than the average load per reaction. The large increase for the walls with window openings occurs because the reactions below the window resist a much lower percentage of the load, which is consistent with the old axiom that load follows stiffness, and therefore more load is distributed to the reactions in the portion of the walls without openings. The tendency of the reactions under the window opening to resist a lower percentage of the shear force is also why the percentage of load resisted by the reactions in the portion of the wall without openings increases as the opening length increases. Another trend that is evident is that a larger percentage of the shear resistance is shifted towards the right side of the wall models with window openings. This is believed to occur because the bottom sheathing panels bear against the left–side sheathing panels and therefore the shear load can be distributed between the panels.

The results presented in Table 6.9, which contains the magnitude of the vertical force at a support divided by the theoretical overturning force–couple at the chords for the models with openings subjected to monotonic loading, indicate that the vertical forces at the end chords are lower than the theoretical overturning force–couple. This occurs because some resistance to the overturning force–couple is provided at the interior studs (approximately 40% for the 2.4 m (8 ft) high wall models and 20% for the 4.9 m (16 ft) high wall models). The results also indicate that the chords along the exterior of the wall is subjected to a higher load than those chords adjacent to the openings; a very small percentage of the vertical load is resisted by reactions below the opening for walls with window openings, except for the reaction under the stud

Table 6.9: Ratio of Maximum Absolute Vertical Force at Reaction to Theoretical Overturning Force–Couple at Chords for Wall Models With Openings Subjected to Monotonic Loading

	Wall Height	Wall Length	Distance from End Chord: cm (in)														
	m –	m –	0 (0)	41 (16)	81 (32)	122* (48)	163 (64)	203 (80)	244* (96)	284 (112)	325 (128)	366* (144)	406 (160)	447 (176)	488* (192)	528 (208)	569 (224)
Wind.	2.4	6.1	0.61	0.26	0.36	0.24#	0.16	0.16	0.14#	0.48	0.24	0.04	0.38	0.38	0.00	0.38	0.38
		4.9	0.61	0.27	0.28	0.30#	0.04	0.04	0.00	0.04	0.03	0.71#	0.46	0.43	0.02	0.41	0.41
		3.7	0.75	0.37	0.38	0.58#	0.02	0.03	0.00	0.03	0.03	0.00	0.03	0.02	0.57#	0.37	0.34
		2.4	0.69	0.33	0.35	0.58#	0.01	0.02	0.00	0.02	0.02	0.00	0.02	0.02	0.00	0.02	0.01
Door	2.4	6.1	0.87	0.39	0.42	0.71#			0.70#	0.41	0.36	0.01	0.35	0.35	0.00	0.35	0.35
	2.4	4.9	0.86	0.38	0.40	0.75#						0.74#	0.39	0.34	0.01	0.33	0.33
	4.9	4.9	0.83	0.22	0.23	0.59#						0.69#	0.21	0.20	0.04	0.22	0.30
	2.4	3.7	0.83	0.38	0.41	0.75#									0.74#	0.40	0.36
	4.9	3.7	0.73	0.21	0.18	0.63#									0.66#	0.20	0.15
	2.4	2.4	0.75	0.37	0.40	0.65#											
	4.9	2.4	0.68	0.18	0.16	0.60#											

*:Indicates studs where sheathing panels meet.
#:Indicates location of chords adjacent to openings for walls with window openings.

	Wall Height	Wall Length				
	m –	m –	610* (240)	650 (256)	691 (272)	732 (288)
Wind.	2.4	6.1	0.00	0.38	0.40	0.80
		4.9	0.00	0.41	0.43	0.87
		3.7	0.01	0.33	0.35	0.72
		2.4	0.58#	0.35	0.33	0.69
Door	2.4	6.1	0.00	0.36	0.38	0.86
	2.4	4.9	0.00	0.34	0.36	0.84
	4.9	4.9	0.22	0.02	0.21	0.49
	2.4	3.7	0.00	0.35	0.37	0.82
	4.9	3.7	0.00	0.14	0.23	0.75
	2.4	2.4	0.65#	0.40	0.37	0.75
	4.9	2.4	0.59#	0.16	0.18	0.65

adjacent to the chords; and the axial load at the locations where sheathing panels meet occurs for the walls with openings is minuscule.

The analysis and design of a shear wall with openings is currently done by analyzing each portion of the wall without openings independently. The overturning moment and forces in the chords are determined by calculating the applied load acting on each of the free bodies and analyzing each one separately. It has already been shown that the chords of each free body are subjected to an axial load that is lower than the overturning force–couple (see Table 6.9). The results presented in Table 6.10, which show the ratio of the overturning moment calculated using the current design procedure and the moment calculated using the vertical loads at the reactions from the wall models, indicate that the overturning moment is overestimated by as much as 48% when the wall is separated into two free bodies. These results indicate that the aforementioned assumption is conservative. This is because some resistance to the overturning moment is provided at the interior studs and because the entire wall as a unit resists the overturning moment. As with the wall models without openings, the fact that vertical resistance was provided at the interior supports may influence the results, however, the assumption that all interior chords must have anchor connections for the wall to resist shear loads may also be more conservative than previously thought. The practice of leaving these connections out, frequently found in building construction in the Eastern United States, may not be as detrimental as currently believed.

6.3.2 Seismic Loading

A summary of the results from the parametric study for the wall models with various opening sizes and configurations subjected to seismic loading is presented in Table 6.11. The time–relative drift plots generated from the analysis of these

Table 6.10: Comparison of Overturning Moments for Walls with Openings[1]

	Wall Height	Opening Length	Effective Aspect Ratio	Magnitude of Overturning Moment					
				"Left" Free Body			"Right" Free Body		
				Design[2]	Study[3]		Design	Study	
	m (ft)	m (ft)		kN*m (kips*ft)	kN*m (kips*ft)	Ratio	kN*m (kips*ft)	kN*m (kips*ft)	Ratio
Window	2.4 (8)	1.2 (4)	2.5	43.9 (32.4)	23.0 (17.0)	0.52	175.7 (129.6)	121.2 (89.4)	0.69
		2.4 (8)	2	40.8 (30.1)	22.2 (16.4)	0.54	122.3 (90.2)	119.9 (88.4)	0.98
		3.7 (12)	1.5	51.9 (38.3)	40.9 (30.2)	0.79	104.0 (76.7)	79.9 (58.9)	0.77
		4.9 (16)	1	58.3 (43.0)	43.7 (32.2)	0.75	58.3 (43.0)	43.7 (32.2)	0.75
Door	2.4 (8)	1.2 (4)	2.5	29.2 (21.5)	27.0 (19.9)	0.93	116.6 (86.0)	107.7 (79.4)	0.92
		2.4 (8)	2	28.9 (21.3)	27.0 (19.9)	0.93	86.5 (63.8)	78.9 (58.2)	0.91
		3.7 (12)	1.5	31.2 (23.0)	28.7 (21.2)	0.92	62.5 (46.1)	57.2 (42.2)	0.92
		4.9 (16)	1	39.7 (29.3)	33.1 (24.4)	0.83	39.7 (29.3)	33.1 (24.4)	0.83
	4.9 (16)	2.4 (8)	1	70.0 (51.6)	54.8 (40.4)	0.78	209.8 (154.7)	160.4 (118.3)	0.76
		3.7 (12)	0.75	66.2 (48.8)	49.5 (36.5)	0.75	132.3 (97.6)	106.0 (78.2)	0.80
		4.9 (16)	0.5	61.8 (45.6)	43.1 (31.8)	0.69	61.8 (45.6)	41.9 (30.9)	0.68

[1]Comparison made to walls models subjected to monotonic loading.
[2]Design moments determined using current design methodology.
[3]Moments from parametric study determined using vertical forces at reactions.

Table 6.11: Results from Wall Models with Openings Subjected to Seismic Loading

Opening Type	Wall Height	Opening Length	Effective Aspect Ratio	Max. Relative Drift	Max. Top–of–Wall		Max. Base Shear	Max. Unit Shear
					Vel.	Acc.		
	m (ft)	m (ft)		cm/cm	cm/sec (in/sec)	cm/sec^2 (in/sec^2)	kN (kips)	kN/m (lb/in)
Window	2.4 (8)	1.2 (4)	2.5	0.034	40.3 (15.8)	622.9 (245.2)	122.3 (27.5)	20.1 (115)
		2.4 (16)	2	0.037	47.8 (18.8)	576.0 (226.8)	110.8 (24.9)	22.7 (130)
		3.7 (12)	1.5	0.039	50.3 (19.8)	510.1 (200.8)	89.0 (20.0)	24.3 (139)
		4.9 (16)	1	0.040	46.9 (18.5)	404.5 (159.3)	69.4 (15.6)	28.5 (163)
Door	2.4 (8)	1.2 (4)	2.5	0.036	43.9 (17.3)	611.7 (240.8)	114.9 (25.8)	18.8 (108)
		2.4 (8)	2	0.037	49.3 (19.4)	551.4 (217.1)	92.4 (20.8)	18.9 (108)
		3.7 (12)	1.5	0.039	49.5 (19.5)	478.4 (188.3)	70.9 (15.9)	19.4 (111)
		4.9 (16)	1	0.042	45.0 (17.7)	398.7 (157.0)	51.1 (11.5)	21.0 (120)
	4.9 (16)	2.4 (8)	1	0.021	49.0 (19.3)	427.5 (168.3)	58.6 (13.1)	12.0 (68)
		3.7 (12)	0.75	0.023	46.6 (18.3)	404.4 (159.2)	54.3 (12.2)	14.8 (85)
		4.9 (16)	0.5	0.027	40.3 (15.9)	409.8 (161.3)	40.0 (9.0)	16.4 (94)

models are shown in Figures 15–17 of the Appendix. The results indicate that the maximum acceleration and base shear decrease, maximum relative drift increases, and the maximum unit shear increases slightly as the length of the opening increases for shear walls of a given height with the same overall length. The decrease in maximum base shear as opening length increases, shown graphically in Figure 6.17, would seem

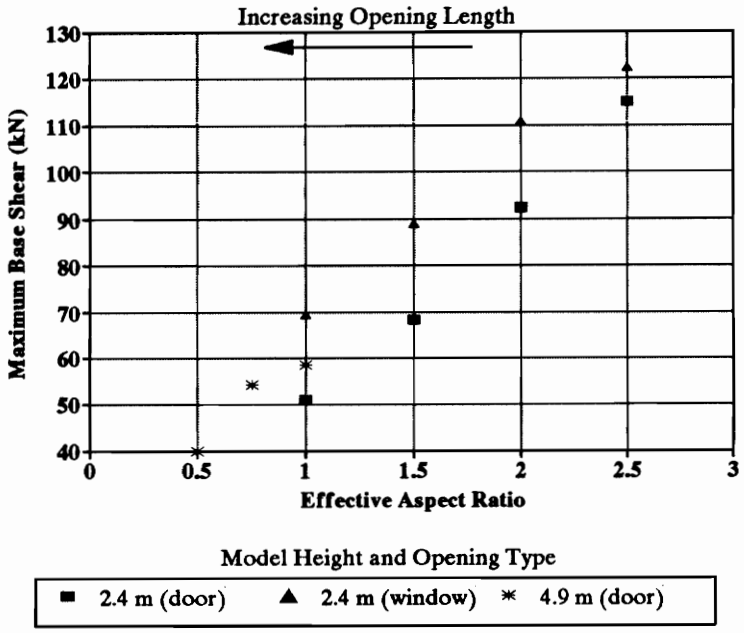

Figure 6.17: Maximum Base Shear of Wall Models With Openings as a Function of Effective Aspect Ratio

to occur primarily due to an increase in period as opening length increases. This is caused by the decreasing stiffness in a shear wall as the length of the opening of the wall increases coupled with a mass which remains essentially constant. The higher period for the walls as the length of the opening increases indicates that these walls will have a slower response and therefore a lower maximum acceleration and base shear. The increase in maximum relative drift of the wall with increasing opening length, shown graphically in Figure 6.18, is believed to occur because of the decrease in stiffness as the length of the wall increases. A comparison of the 2.4 m (8 ft)

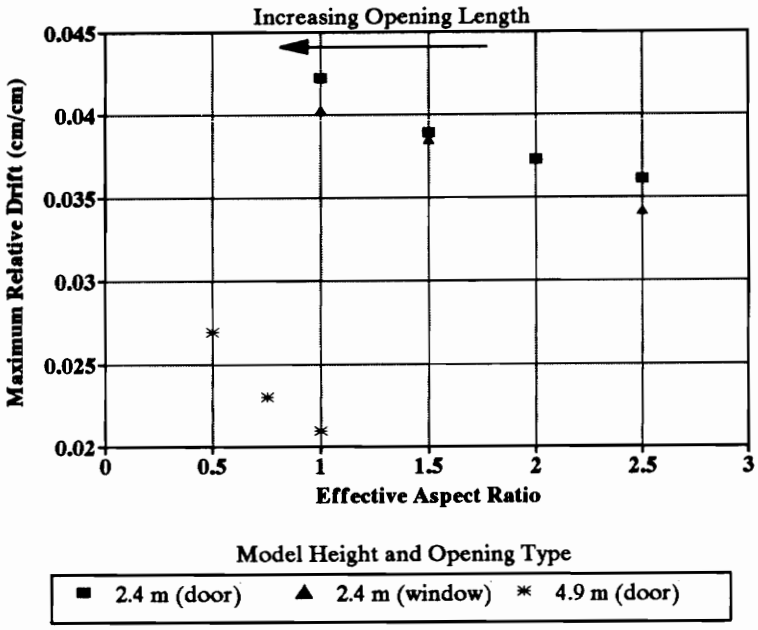

Figure 6.18: Maximum Relative Drift of Wall Models With Openings as a Function of Effect Length

high wall models indicates that the effects are more pronounced for the models with door openings because they have a greater reduction in stiffness than the models with window openings. The effects are more pronounced in the 4.9 m (16 ft) high wall models because of their greater change in stiffness as opening length increases. The slight increase in maximum unit shear as opening length increases most likely occurs because the portion of the wall above and/or below the wall provides extra stiffness, and the longer the opening, the larger the percentage of this added stiffness in the wall.

As with the wall models subjected to monotonic loading, the distribution of forces in the models with openings are similar for both monotonic and seismic loading. This indicates that the distribution of forces in a shear wall is similar when monotonic or seismic loads are applied. The distribution of forces at the reactions are also similar for the models with openings subjected to monotonic and seismic loadings.

The results shown in Table 6.12, which contains the magnitude of the horizontal force at a reaction divided by the average theoretical horizontal force resisted per reaction for the models with openings subjected to seismic loading, indicate that the shear force resisted by anchorages located in close proximity to the studs in which sheathing panels meet resist a higher percentage (up to 80% for the models in the study) of the base shear than the average load per anchorage and the shear force resisted at the reactions beneath a window opening are significantly lower than the shear force resisted by the reactions in the solid portion of the wall, which is consistent with the findings for the models with openings subjected to monotonic loading. The results shown in Table 6.13, which contains the magnitude of the vertical force at a support divided by the theoretical overturning force–couple at the end chords for the models with openings subjected to seismic loading, indicate that the end chords of each solid section of wall resists an overturning force–couple that is lower than the theoretical load, the chords along the exterior of the wall resist a higher load than those chords bordering the openings, studs located where the sheathing panels meet are subjected to a very low net vertical load because the axial forces from the connectors on the sheathing panels cancel, the percentage of overturning moment resisted at the studs beneath the window opening is negligible, and the overturning moment is overestimated by as much as 29% when the wall is seperated into two free bodies (see Table 6.14). These results also correspond to the findings for the models with openings subjected to monotonic loading.

6.4 Aspect Ratio vs. Openings

The design of shear walls with openings is currently performed by assuming that their resistance and initial stiffness is similar to that of shear walls without openings of identical effective length and that their seismic base shear force is identical to that of

Table 6.12: Ratio of Maximum Absolute Horizontal Force at Reaction to Average Horizontal Load Per Reaction for Wall Models With Openings Subjected to Seismic Loading

	Wall		Distance from End Chord: cm (in)														
	Height	Length															
	m	m	0	41	81	122*	163	203	244*	284	325	366*	406	447	488*	528	569
	–	–	(0)	(16)	(32)	(48)	(64)	(80)	(96)	(112)	(128)	(144)	(160)	(176)	(192)	(208)	(224)
W		6.1	0.59	0.66	0.67	1.18#	0.87	0.88	1.38#	0.90	0.90	1.36	0.96	0.96	1.42	0.97	0.97
i	2.4	4.9	0.59	0.72	0.67	1.16#	0.78	0.79	1.09	0.74	0.73	1.32#	0.98	0.98	1.50	1.07	1.07
n		3.7	0.66	0.75	0.76	1.27#	0.76	0.78	1.03	0.67	0.66	0.92	0.64	0.64	1.42#	1.18	1.19
d.		2.4	1.50	1.51	1.51	1.75#	0.67	0.67	0.94	0.67	0.67	0.99	0.73	0.74	1.19	0.93	0.91
	2.4	6.1	0.97	0.92	0.93	0.73#			0.75#	0.94	0.95	1.42	0.95	0.96	1.42	0.95	0.95
D	2.4	4.9	1.00	0.95	0.95	0.76#						0.76#	0.96	0.96	1.44	0.97	0.97
o	4.9	4.9	1.08	0.92	0.86	0.83#						0.81#	0.73	0.93	1.30	0.89	0.88
o	2.4	3.7	1.04	0.98	0.98	0.78#									0.78#	0.99	0.99
r	4.9	3.7	0.99	0.91	0.91	0.99#									1.02#	0.93	0.94
	2.4	2.4	1.11	1.03	1.03	0.83#											
	4.9	2.4	1.04	0.96	0.96	1.05#											

*:Indicates studs where sheathing panels meet.
#:Indicates location of chords adjacent to openings for walls with window openings.

	Wall					
	Height	Length				
	m	m	610*	650	691	732
	–	–	(240)	(256)	(272)	(288)
W		6.1	1.42	0.95	0.95	1.00
i	2.4	4.9	1.58	1.06	1.06	1.11
n		3.7	1.80	1.28	1.28	1.32
d.		2.4	1.49#	0.75	0.74	0.64
	2.4	6.1	1.38	0.91	0.91	0.95
D	2.4	4.9	1.42	0.94	0.94	0.98
o	4.9	4.9	1.58	1.04	1.03	1.11
o	2.4	3.7	1.47	0.98	0.98	1.04
r	4.9	3.7	1.42	0.93	0.93	1.02
	2.4	2.4	0.82#	1.03	1.03	1.11
	4.9	2.4	1.04#	0.95	0.95	1.05

Table 6.13: Ratio of Maximum Absolute Vertical Force at Reaction to Theoretical Overturning Force–Couple at Chords for Wall Models With Openings Subjected to Seismic Loading

	Wall Height m –	Wall Length m –	Distance from End Chord: cm (in) 0 (0)	41 (16)	81 (32)	122* (48)	163 (64)	203 (80)	244* (96)	284 (112)	325 (128)	366* (144)	406 (160)	447 (176)	488 (192)	528 (208)	569 (224)
Wind	2.4	6.1	0.83	0.43	0.43	0.53#	0.10	0.10	0.46#	0.42	0.40	0.06	0.37	0.38	0.08	0.37	0.37
		4.9	0.80	0.40	0.40	0.58#	0.07	0.07	0.11	0.06	0.05	0.50#	0.38	0.37	0.07	0.34	0.34
		3.7	0.70	0.37	0.38	0.53#	0.05	0.05	0.08	0.04	0.04	0.06	0.04	0.03	0.51#	0.36	0.34
		2.4	0.60	0.33	0.33	0.49#	0.02	0.03	0.04	0.02	0.02	0.04	0.03	0.03	0.04	0.04	0.04
Door	2.4	6.1	0.89	0.47	0.47	0.73#			0.63#	0.47	0.43	0.10	0.41	0.41	0.07	0.40	0.40
	2.4	4.9	0.95	0.46	0.47	0.80#						0.70#	0.46	0.43	0.10	0.40	0.40
	4.9	4.9	0.86	0.25	0.22	0.71#						0.64#	0.22	0.24	0.05	0.25	0.25
	2.4	3.7	0.85	0.43	0.46	0.80#									0.79#	0.45	0.41
	4.9	3.7	0.73	0.21	0.18	0.64#									0.67#	0.18	0.21
	2.4	2.4	0.80	0.42	0.44	0.74#											
	4.9	2.4	0.69	0.19	0.16	0.62#											

*:Indicates studs where sheathing panels meet.
#:Indicates location of chords adjacent to openings for walls with window openings.

	Wall Height m –	Wall Length m –	610* (240)	650 (256)	691 (272)	732 (288)
Wind	2.4	6.1	0.09	0.38	0.40	0.80
		4.9	0.05	0.35	0.36	0.79
		3.7	0.08	0.33	0.34	0.69
		2.4	0.47#	0.33	0.32	0.60
Door	2.4	6.1	0.08	0.42	0.43	0.87
	2.4	4.9	0.08	0.40	0.42	1.01
	4.9	4.9	0.06	0.25	0.27	0.90
	2.4	3.7	0.10	0.39	0.42	0.86
	4.9	3.7	0.06	0.21	0.22	0.76
	2.4	2.4	0.68#	0.44	0.42	0.79
	4.9	2.4	0.55#	0.16	0.19	0.69

Table 6.14: Comparison of Overturning Moments for Walls with Openings[1]

	Wall Height	Opening Length	Effective Aspect Ratio	Magnitude of Overturning Moment					
				"Left" Free Body			"Right" Free Body		
				Design[2]	Study[3]		Design	Study	
	m (ft)	m (ft)		kN*m (kips*ft)	kN*m (kips*ft)	Ratio	kN*m (kips*ft)	kN*m (kips*ft)	Ratio
Window	2.4 (8)	1.2 (4)	2.5	59.7 (44.0)	48.8 (36.0)	0.82	238.8 (176.1)	184.3 (135.9)	0.77
		2.4 (8)	2	67.5 (49.8)	55.5 (40.9)	0.82	202.6 (149.4)	155.7 (114.8)	0.77
		3.7 (12)	1.5	72.4 (53.4)	53.6 (39.5)	0.74	144.8 (106.8)	103.6 (76.4)	0.72
		4.9 (16)	1	75.7 (55.8)	55.7 (41.1)	0.74	75.7 (55.8)	54.8 (40.4)	0.72
Door	2.4 (8)	1.2 (4)	2.5	56.1 (41.3)	54.2 (39.9)	0.97	224.2 (165.4)	214.9 (158.5)	0.96
		2.4 (8)	2	56.4 (41.6)	58.2 (42.9)	1.03	169.1 (124.7)	173.8 (128.2)	1.03
		3.7 (12)	1.5	57.6 (42.5)	56.3 (41.5)	0.98	115.2 (85.0)	112.5 (83.0)	0.98
		4.9 (16)	1	62.2 (45.9)	56.7 (41.8)	0.91	62.2 (45.9)	56.7 (41.8)	0.91
	4.9 (16)	2.4 (8)	1	71.5 (52.7)	62.0 (45.7)	0.87	214.5 (158.2)	196.9 (145.2)	0.92
		3.7 (12)	0.75	88.3 (65.1)	66.4 (49.0)	0.75	176.7 (130.3)	137.0 (101.1)	0.78
		4.9 (16)	0.5	97.5 (71.9)	69.6 (51.3)	0.71	97.5 (71.9)	69.7 (51.4)	0.71

[1]Comparison made to walls models subjected to seismic loading.
[2]Design moments determined using current design methodology.
[3]Moments from study determined using vertical forces at reactions.

shear walls without openings of the same overall length. Therefore, it is assumed that the wall above and/or below an opening does not provide any additional resistance and that the presence of an opening does not affect the horizontal force "attracted" by a wall subjected to seismic loading. The results from the parametric study for the wall models with various opening configurations are compared to the results from the models without openings to determine the adequacy of the aforementioned design assumptions.

6.4.1 Monotonic Loading

Shear walls with openings exhibit greater strength and initial stiffness than walls without openings of identical effective aspect ratio. This phenomenon, shown in Figures 6.19 and 6.20, is particularly evident for the wall models with window openings,

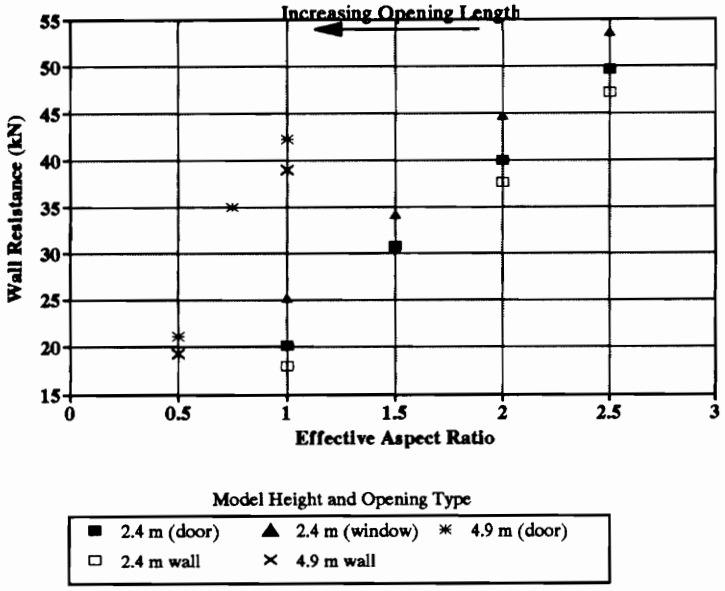

Figure 6.19: Resistance of Wall Models (at relative drift of 0.006) as a Function of Effective Aspect Ratio

which resist loads ranging from 11% to 46% greater and have an initial stiffness from

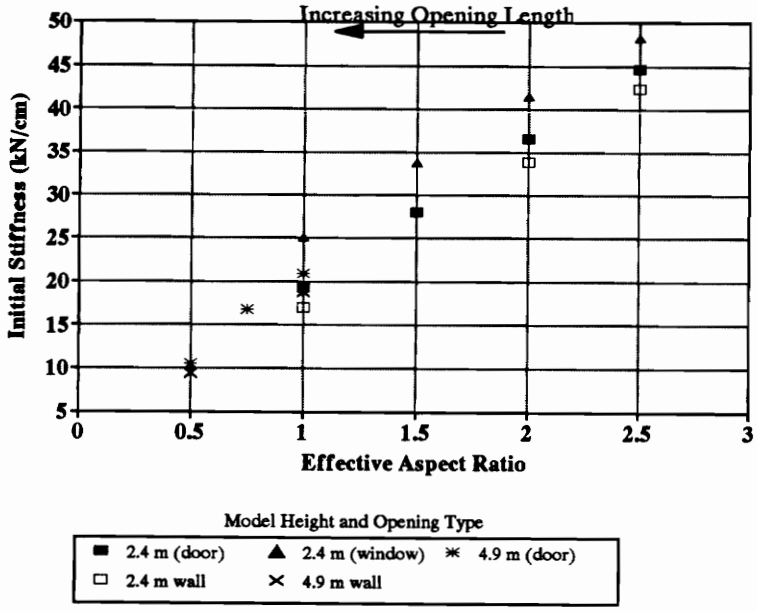

Figure 6.20: Initial Stiffness of Wall Models as a Function of Effective Aspect Ratio

13% to 47% greater than those of the models without openings of comparable effective aspect ratio. The phenomena is also present for the 2.4 m (8 ft) high wall models with door openings, which resist loads ranging from 5% to 12% greater and have an initial stiffness from 6% to 14% greater than those of the models without openings of comparable effective aspect ratio, and for the 4.9 m (16 ft) high models with door openings, which resist load ranging from 10% to 11% greater and have an initial stiffness from 11% to 13% greater than those of the wall models without openings of comparable effective aspect ratio. The increase for the walls with openings occurs because the portion of the wall above/below the openings provide added resistance and stiffness. The wall models with the window openings have a more pronounced increase in resistance because there is a greater area of wall present in the opening. The lines converge as the aspect ratio increases because the percentage of wall area located above and below the opening increases.

6.4.2 Seismic Loading

The design codes assume a shear wall with openings is subjected to a maximum base shear force equal to that of a wall without openings with an identical overall length. However, the wall models with openings experienced maximum base shear forces that were lower than those of the models of identical overall length without openings. The reduction in base shear ranged from 5% to 52% for the 2.4 m (8 ft) high models with window openings, 9% to 60% for the 2.4 m (8 ft) high models with door openings, and 49% to 65% for the 4.9 m (16 ft) high models with door openings. The decrease is believed to occur because the stiffness, and therefore natural frequency, of the walls decrease, which in turn reduces the base shear of the wall. The trend of the maximum base shear force corresponds more closely with the values for walls of similar effective length, as is shown in Figure 6.21, than for a wall of similar length

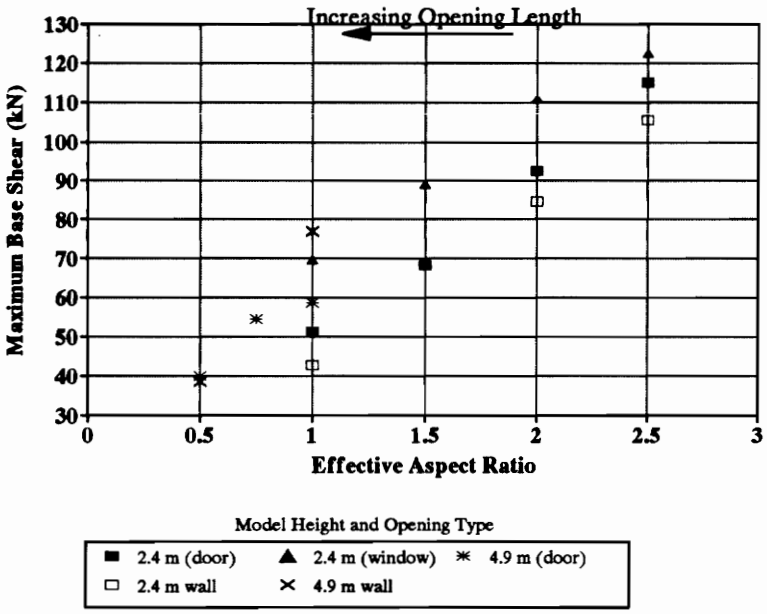

Figure 6.21: Maximum Base Shear for Wall Models as a Function of Effective Aspect Ratio

without openings.

The relative drift of a shear wall with an opening is greater than that of shear wall without openings of identical effective aspect ratio. The increase in relative drift ranged from 17% to 38% for the 2.4 m (8 ft) high wall models with window openings, 24% to 45% for the 2.4 m (8 ft) high wall models with door openings, and 0% to 29% for the 4.9 m (16 ft) high wall models with door openings. This relationship, shown in Figure 6.22, occurs because the greater mass (positioned above opening) produces

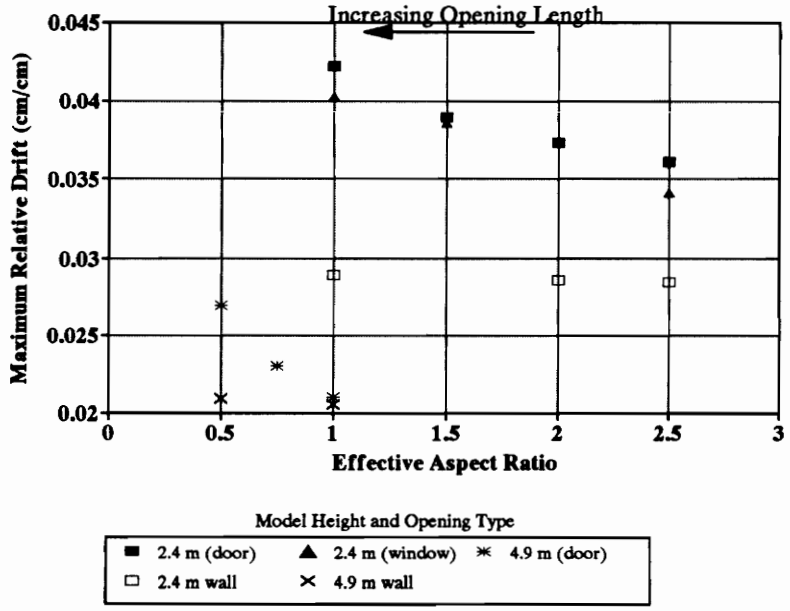

Figure 6.22: Maximum Relative Drift of Wall Models as a Function of Effective Aspect Ratio

a larger applied load and in turn a larger displacement. The increase in maximum displacement increases as the length of the opening increases because the stiffness of the wall is reduced.

6.5 Summary

The results of the parametric study outlined in Chapter 5 were presented. The results obtained from the wall models without openings of various aspect ratios indicated the following:

- The strength and stiffness of shear walls of a given height increase linearly as the aspect ratio of the wall increases, except for relatively tall, narrow walls (wall less than 1.2 m (4 ft) in length).
- The magnitude of the vertical force resisted at the end chords is lower than the theoretical overturning force–couple, provided that sufficient resistance to vertical loads is provided along the interior of the wall.
- The shear force is not evenly distributed at the anchorages, with the anchorages near the seams of the sheathing panels resisting a higher load ($\approx 35\%$) than the average load per anchorage.
- Wall length has no effect on the maximum relative drift, velocity, or acceleration at the top of the wall except for relatively tall, narrow walls,
- The base shear experienced by a shear wall subjected to seismic increases linearly as a function of aspect ratio, except for the aforementioned tall, narrow walls.

The results obtained from the wall models with varying opening configurations indicated the following:

- The strength and stiffness of a shear wall decrease as the length of the opening in the wall increases for walls of identical overall length.
- Shear walls with openings are slightly stiffer and stronger than walls of similar effective length without openings.

- The shear force is not evenly distributed at the anchorages, with the anchorages near the seams of the sheathing panels resisting a higher load than other anchorages.

- The magnitude of the vertical force resisted at the chords is lower than that of the theoretical overturning force–couple, provided that sufficient resistance to vertical loads is provided along the interior of the wall.

- The maximum relative drift increases and the maximum base shear and top–of–wall acceleration decrease as the length of the opening increases for shear walls of identical overall length subjected to seismic loading.

Chapter 7

Recommendations for Design Methodology

7.1 Introduction

The results of the parametric study indicate that the response of timber shear walls is affected by variations in aspect ratio and openings, and that the force distribution in a wall varies from the distribution assumed for current design practice. Unfortunately, these effects are not reflected in the current design methodology for shear walls or in provisions in some of the design codes. Therefore, modification of the current design methodology and design code specifications is necessary in order to accurately and efficiently design timber shear walls with various aspect ratios and opening configurations.

7.2 Current Design Methodology

The general procedure for the design of shear walls is to determine the magnitude of the applied load(s) acting on the wall and then select a wall and design the components of the wall and anchorages to resist the applied loading. The design load for a wall subjected to constant wind pressure, which has its line of action along the sill plate, is calculated by determining the wind pressure acting on a tributary area of the

wall and dividing it by the area. The design load for a shear wall subjected to seismic loading is an equivalent static load, which is calculated using the base shear equation. This equation varies between design codes but in most codes has the general form (UBC, 1991):

$$V = (\frac{ZIC}{R_w})W \tag{7.1}$$

where Z accounts for the seismic activity of the region in which the structure is located and is based on the peak ground acceleration for a specific, code–dependent recurrence interval (475-yr recurrence interval for UBC); I takes into account the importance of the structure in order to ensure that "essential" facilities remain functional after an earthquake; C accounts for the natural frequency of the structure and the soil conditions at the site; R_w accounts for the ductility and energy–dissipating capacity of the structure; and W is the weight of the structure. This equation is analogous to the equation governing Newton's second law, $F = a(W/g)$, where the applied force F is analogous to the base shear; the relative acceleration, a/g, is analogous to the $\frac{ZIC}{R_w}$ term; and the weight, W, is analogous to the weight of the structure.

Once the design load is determined, the design unit shear is calculated by dividing the design load by the effective length of the wall, which is the total length of the walls less the length of any openings. A shear wall of a given sheathing grade and thickness and sheathing–to–framing connector type and spacing is selected from Table 25–K–1 of the UBC (1991) based on the design unit shear.

The chords and header(s) are designed once the wall size is selected. The overturning moment produced by the load acting at the top of the wall is resolved into a force–couple with the forces acting at the chords of the wall. The chords, one of which is in tension and the other in compression, are then designed to resist these forces. In the presence of openings, each solid section of wall is treated as a separate free body with an overturning moment and resistant force–couple acting at the chords. A

solid header for a shear wall with an opening is designed by constructing a free body diagram of the sill plate and header that has the design distributed load (the design load divided by the total length of the wall) acting along the entire length of the wall and the design unit shear acting along the top of the solid sections of the wall. The header is designed to resist the maximum load that is present in the diagram at the location of the header. The number of anchorages is determined by dividing the design load by the strength of one anchor bolt. The spacing of the anchorages is then determined by dividing the effective length of the wall by the number of bolts. Finally, hold–down connector is designed and attached to the chords to prevent uplift of the wall. The magnitude of load resisted is the difference between the overturning moment and the resisting moment divided by the length of the wall.

7.3 Aspect Ratio

A modified design methodology was developed that takes into account the effect that aspect ratio has on the response of timber shear walls. The methodology incorporates the following modifications into the existing design methodology.

7.3.1 Monotonic Loading

The results from the parametric study indicated that shear walls less than 1.2 m (4 ft) in length do not provide the anticipated resistance due to their high incidence of bending deformation. Therefore, these walls should be avoided for use as shear walls or their increased drift must be taken into account. This would include the use of these walls as a portion of a wall with openings. The constant maximum unit shear load for shear walls of a given height, shown in Figure 7.1, indicates that use of unit shear to select adequate shear walls from Table 25–K–1 of the UBC (1991), which is consistent with the current design procedure, is valid, except for the aforementioned

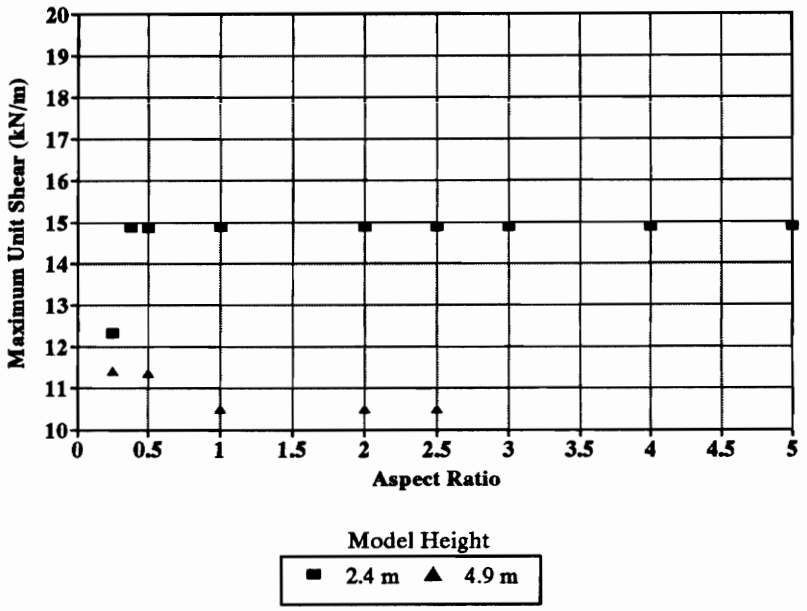

Figure 7.1: Maximum Unit Shear for Models Subjected to Monotonic Loading

walls of limited length. However, Table 25–K–1 should be updated to include the reduction of maximum unit shears for shear walls of different heights.

Current design procedure indicates that the end chords are to be designed based on a force–couple that is calculated based on the assumption that the interior studs do not provide any resistance to uplift. However, some resistance to uplift is provided at the interior studs, approximately 35–40% of the theoretical overturning force–couple for the 2.4 m (8 ft) high and 20–25% of the theoretical overturning force–couple for the 4.9 m (16 ft) high wall models examined in the study. This results in a force at the end chords which is approximately 85% of the theoretical overturning force–couple, assuming that adequate resistance to vertical loading is provided at the interior anchorages. Although this reduction occurs, the current method is adequate, albeit conservative, for the design of the end chords. However, the interior studs should be checked to ensure that they can withstand the load to which they are subjected and the connectors attaching the studs to the sole plate should be checked

to ensure that they can provide adequate resistance. The larger shear force resisted by the anchorages located adjacent to the studs at which sheathing panels meet should be accounted for by multiplying the design load by a factor (in the case of the wall models analyzed in the study, 1.4). Therefore, the design load for each of the anchorages, which is equal to the design load for the wall divided by the number of anchorages, would equal that of the anchorages resisting the higher loads. This would result in overdesign for the majority of anchorages, but it would ensure that all of the anchorages perform properly.

7.3.2 Seismic Loading

The results from the parametric study indicated that the maximum seismic unit shear is similar for shear walls of identical height regardless of the length of the wall (see Figure 7.2) except for walls with lengths less than 1.2 m (4 ft). The magnitude

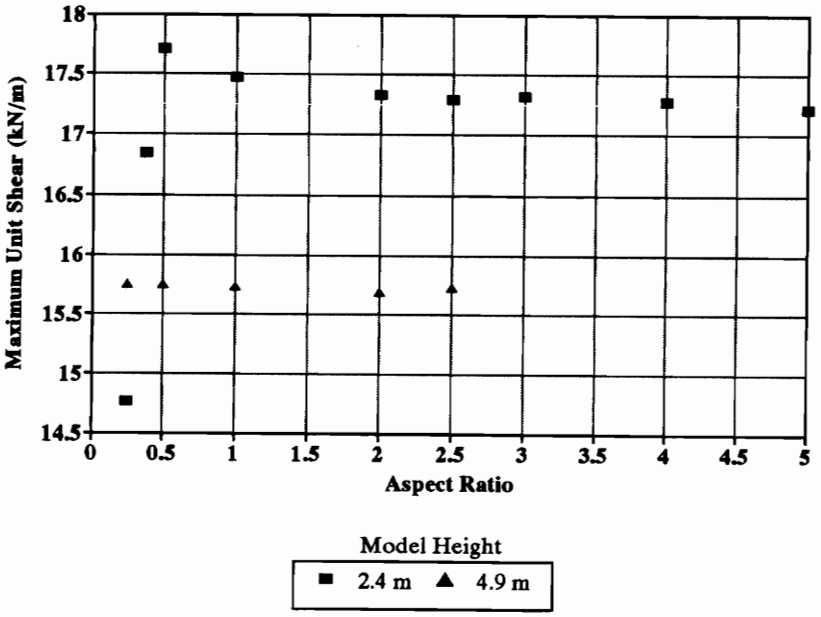

Figure 7.2: Maximum Unit Shear for Models Subjected to Seismic Loading

of the base shear, however, is greater than the design value calculated using the base shear equation from the Uniform Building Code. A comparison between the maximum base shear values from the study and the corresponding design base shear values calculated assuming values of $Z = 0.4$ (Zone 4 region), $I = 1.0$ (standard occupancy structure), $C = 2.75$ (assuming rock–like soil), $R_w = \sqrt{8}$ (code value for timber shear walls), and $W = 218.9$ N/cm (125.0 lb/in), is shown in Table 7.1. The

Table 7.1: Comparison of Base Shear Forces for Walls Without Openings Subjected to Seismic Loading

Wall Length	Wall Height	Aspect Ratio	Base Shear		Parametric Study/ Design Code Base Shear
			Parametric Study	1991 UBC (Factored)	
m (ft)	m (ft)		kN (kips)	kN (kips)	
0.6 (2)	2.4 (8)	0.25	9.7 (2.2)	7.8 (1.8)	1.24
1.2 (4)	2.4 (8)	0.5	21.6 (4.9)	15.6 (3.5)	1.38
	4.9 (16)	0.25	19.2 (4.3)		1.23
2.4 (8)	2.4 (8)	1	42.6 (9.6)	31.1 (7.0)	1.37
	4.9 (16)	0.5	38.4 (8.6)		1.23
4.9 (16)	2.4 (8)	2	84.5 (19.0)	62.3 (14.0)	1.36
	4.9 (16)	1	76.7 (17.3)		1.23
6.1 (20)	2.4 (8)	2.5	105.4 (23.7)	77.9 (17.5	1.35
7.3 (24)	2.4 (8)	3	126.7 (28.5)	93.4 (21.0)	1.36
9.8 (32)	2.4 (8)	4	168.5 (37.9)	124.6 (28.0)	1.35
	4.9 (16)	2	153.0 (34.4)		1.23
12.2 (40)	2.4 (8)	5	209.9 (47.2)	155.7 (35.0)	1.35
	4.9 (16)	2.5	191.7 (43.1)		1.23

results shown in the table indicate that the factored design base shear underestimates

the actual maximum base shear by as much as 38%. This discrepancy occurs because the design codes are based on the assumption that walls behave in a perfectly elastic–plastic manner, with purely plastic deformation occurring after yielding (Dolan, 1989). However, the walls behave in a non–linear manner, and therefore the walls provide added resistance until the maximum displacement is reached. This discrepancy can be alleviated by decreasing the ductility factor in the seismic base shear equation from the current value of $\sqrt{8}$ to 2 to account for the reduced ductility due to the non-linear behavior of the walls. This change would bring the magnitude of the design base shear in line with the actual base shear, although it must be noted that this proposed modification is based on the response of a component rather than that of a system. The recommendations outlined earlier in this section involving the design of anchorage connections, end chords, and interior studs also apply.

Incorporating the aforementioned modifications into the existing design methodology results in the following modified design methodology for shear walls without openings. The design load is determined by calculating the total monotonic load acting on the wall or calculating the equivalent seismic force acting on the wall using the base shear equation with the modifications outlined earlier in the section. The design load is divided by the wall length to obtain the design unit shear. A shear wall of a given sheathing grade and thickness and sheathing–to–framing connector type and spacing is selected from Table 25–K–1 of the UBC (1991) based on the design unit shear. The design load is then used to determine the overturning moment, which is resolved into a force–couple that is resisted at the end chords. The chords are then designed to resist this force–couple, and a percentage of the load, which is dependent on the configuration of the wall (40% of the force–couple for the 2.4 m (8 ft) models examined in the study), is used to check the adequacy of the interior studs and the connectors attaching the studs to the sole plate. The design load is multiplied by a factor of 1.4 to account for the increased load resisted by the connectors adjacent to

studs where sheathing panels meet. This factored design load is used to design the anchorages, which are placed at and attached directly to the studs for added resistance to overturning. Finally, the hold–down connectors are then designed by taking the difference between the overturning moment and the resisting moment divided by the length of the wall and are attached to the end chords.

7.4 Openings

A modified design methodology was developed that accounts for the effect that openings have on the response of timber shear walls. The methodology incorporates the following modifications into the existing design methodology.

7.4.1 Monotonic Loading

Current design for walls with openings is done by assuming that the resistance is provided only by the sections of the wall that do not contain openings, neglecting the resistance provided by the portion of the wall above and/or below the opening. The results from the parametric study indicate that this added resistance increases the total resistance of the wall and that the current design of the walls with openings is conservative. However, the use of the effective length for shear wall design should continue because more results are needed to develop an empirical relationship between opening size and wall strength and furthermore, using the effective length is a procedure that is relatively easy to implement for design. The results from the parametric study also indicate that the vertical forces at the chords are lower the load currently used in design, which occurs provided some additional resistance to vertical loads is provided along the interior of the wall. Although the method used to determine the loads in the chords is adequate, albeit conservative, and should continue to be used for design, the interior studs should be checked to ensure that they are capable of

resisting the applied loading and also the connector attaching the studs to the sole plate should be checked to ensure it is adequate.

The current design methodology for shear walls with solid headers specifies that a free body diagram of the sill plate and header be constructed with the applied distributed load acting along the entire length of the wall and the effective unit shear acting along the top of the solid sections of the wall. The axial force diagram is then constructed for the sill plate and header and a header is designed to withstand the applied load. This methodology assumes that the only load acting directly on the header is the applied distributed load. However, the distributed axial load developed in the header(s) adjacent to the openings is less than the applied distributed load, as is shown in Figure 7.3, indicating that this approach is conservative and therefore

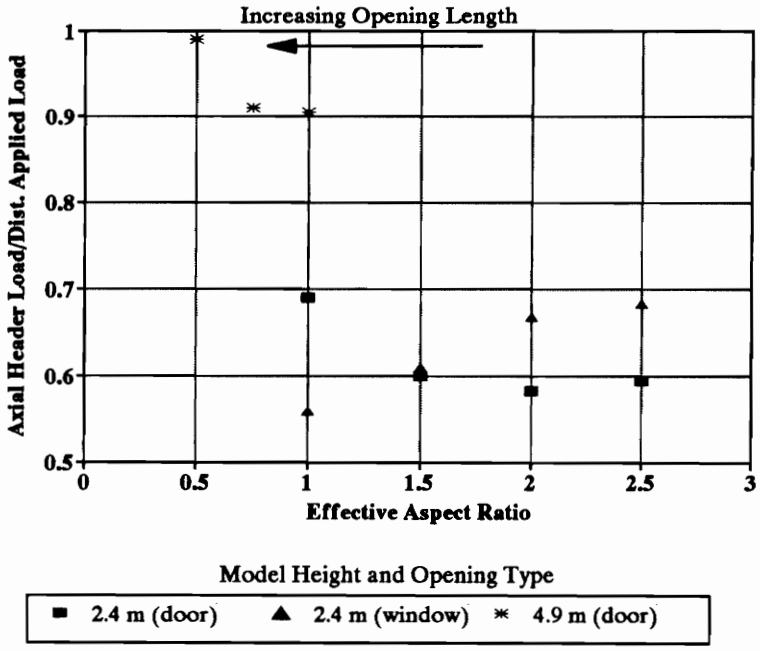

Figure 7.3: Ratio of Distributed Axial Force in Header to Applied Distributed Load for Models Subjected to Monotonic Loading

adequate. The connectors attaching the header to the adjacent studs should be designed to withstand the corresponding force. Also, some type of blocking should

be used adjacent to the region in which an opening header(s) exists in order to offset the large axial force transferred from the header(s) to the adjacent studs.

Analogous to shear walls without openings, the larger shear force resisted by the anchorages located adjacent to the studs at which sheathing panels meet should be accounted for by multiplying the design load by a factor, thereby making the design load for each of the anchorages equal to that of the anchorages resisting the higher loads. However, the ratio of the load resisted at these anchorages and the average load resisted by the anchorages is very dependent on the length and type of opening, thereby making it difficult to specify a single value for use with all shear walls with openings (in the case of the wall models analyzed in the study, the maximum factor would be 2.0).

7.4.2 Seismic Loading

The results from the parametric study indicate that the maximum seismic base shear experienced by a shear wall with openings is lower than the base shear experienced by a shear wall without openings of identical overall length. However, shear walls with openings are currently designed assuming that their maximum seismic base shear is equivalent to the maximum base shear of a wall with the same overall size without openings. This assumption results in overestimates of the design seismic base shear for shear walls with larger openings, as is shown in Table 7.2. A few of the wall models have a parametric study/design code base shear ratio greater than 1.0 because of the reduced ductility in the walls due to their inelastic behavior. The overestimation of the base shear occurs because of an assumed increase in period of the wall as the length of the opening increases, which is due to a decrease in stiffness coupled with a relatively constant mass. This effect can be rectified by modifying the

Table 7.2: Comparison of Base Shear Forces for Walls With Openings Subjected to Seismic Loading

Opening Type	Wall Height m (ft)	Opening Length m (ft)	Effective Aspect Ratio	Base Shear from Parametric Study kN (kips)	Parametric Study/ Design Code Base Shear[1]
Window	2.4 (8)	1.2 (4)	2.5	120.5 (27.1)	1.29
		2.4 (8)	2	101.5 (22.8)	1.09
		3.7 (12)	1.5	78.6 (17.7)	0.84
		4.9 (16)	1	61.0 (13.7)	0.65
Door	2.4 (8)	1.2 (4)	2.5	114.9 (25.8)	1.23
		2.4 (8)	2	92.4 (20.8)	0.99
		3.7 (12)	1.5	70.9 (15.9)	0.76
		4.9 (16)	1	51.1 (11.5)	0.55
	4.9 (16)	2.4 (8)	0.5	58.4 (13.2)	0.63
		3.7 (12)	0.75	54.3 (12.2)	0.58
		4.9 (16)	1	40.0 (9.0)	0.43

[1]Factored design base shear for all walls is 93.4 kN (21.0 kips)

response factor (C) to take the reduction of period into account. The modified response factor coupled with the modified ductility factor recommended in section 7.3.2 would result in a more accurate determination of the maximum design seismic base shear using the base shear equation (Equation 7.1). The force distribution is similar for the monotonic and dynamically loaded walls, including the distributed axial load found in the header(s) (see Figure 7.4), and therefore the recommendations concern-

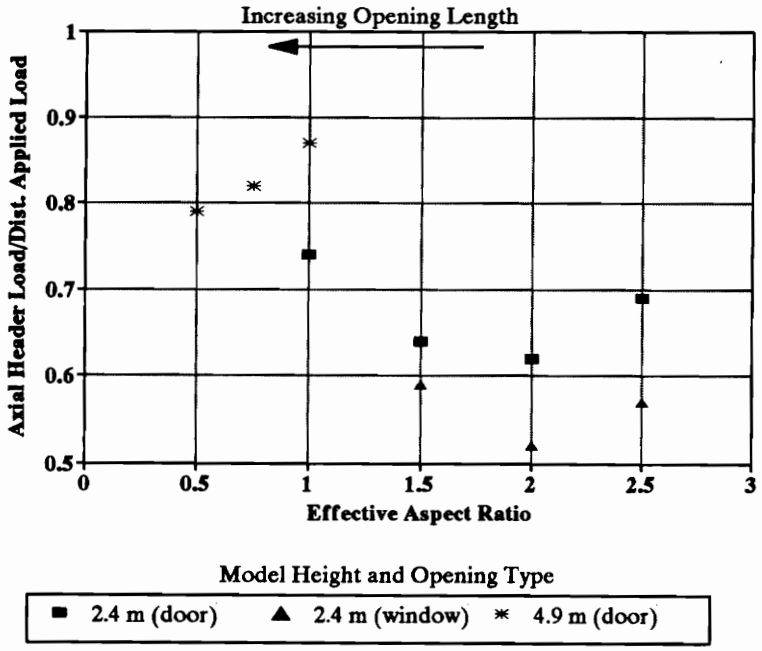

Figure 7.4: Ratio of Distributed Axial Force in Header to Applied Distributed Load for Models Subjected to Seismic Loading

ing the force distribution in the walls subjected to monotonic loading adheres to the walls subjected to dynamic loading.

Incorporating the aforementioned modifications into the existing design methodology results in the following modified design methodology for shear walls with openings. The design load is determined by calculating the total monotonic load acting on the wall or calculating the equivalent seismic force acting on the wall using the base shear equation with the modifications outlined earlier in the section. The design load

is divided by the effective wall length to obtain the design unit shear. A shear wall of a given sheathing grade and thickness and sheathing–to–framing connector type and spacing is selected from Table 25–K–1 of the UBC (1991) based on the design unit shear. Each shear panel (portion of shear wall not containing an opening) is then analyzed as a separate free–body, with the design unit shear acting along the sill plate. The unit shears are used to determine the overturning moment in each shear panel, which is resolved into a force–couple that is resisted by the chords at the ends of the shear panels. The chords are then designed to resist this force–couple, and a percentage of the force–couple is used to check the adequacy of the interior studs and the connectors attaching the studs to the sole plate. Next, the distributed load acting on the header(s) is calculated by dividing the design load by the total length of the shear wall. This load is used to calculate the forces at the ends of the header(s) by assuming the member is an axial member with pinned ends, which can then be used to determine the adequacy of the header(s) and the connectors attaching the header(s) to the adjacent stud. Blocking should be utilized adjacent to the header to offset the axial force transferred from the header(s) to the adjacent studs. The design load is multiplied by a factor, which is dependent on the configuration of the wall, to account for the increased load resisted by the connectors adjacent to studs where sheathing panels meet and the connectors located in the solid portion of the wall for walls with window openings. This factored design load is used to design the anchorages, which are placed at and attached directly to the studs for added resistance to overturning. Finally, the hold–down connectors are then designed by taking the difference between the overturning moment and the resisting moment divided by the length of the wall and are attached to the chords.

7.5 Summary

The results of the parametric study indicate that aspect ratio and openings affect the response of timber shear walls. However, these effects are not adequately addressed in the current design methodology. Therefore, the following modifications were incorporated into the current design methodology in order to develop a new design methodology that takes into account the effect of aspect ratio and openings.

- Avoid use of 2.4 m (8 ft) high walls with an aspect ratio less than 0.5 because they do not provide the anticipated resistance due to their higher incidence of bending deformation. Use of these walls requires special design considerations.

- Multiply the design load for the anchorages by a factor to account for the higher load resisted by the anchorages adjacent to studs where sheathing panels meet. The magnitude of the factor is dependent on the configuration of the wall.

- Check the adequacy of the interior studs and the connectors attaching these studs to the sole plate to resist a load that is a percentage of the theoretical overturning force–couple. The percentage is dependent on the configuration of the wall.

- Reduce the value of the ductility parameter in the base shear equation from $\sqrt{8}$ to 2 in order to better predict the value of the base shear experienced by a wall subjected to seismic loads, although it must be noted that this proposed modification is based on the response of a component rather than that of a system.

- Check the adequacy of the opening header(s) and the connectors attaching the header(s) to the stud to resist a load equal to the design distributed load.

- Use blocking in the regions adjacent to the opening header(s) to offset the axial force transferred from the header(s) to the adjacent studs.

- Modify the period calculation in the design spectrum response value of the seismic base shear equation to account for period increases for taller walls and walls with openings.

Chapter 8

Summary and Future Research

8.1 Introduction

Shear walls provide the resistance to lateral loads in many low–rise timber structures. They can vary in size depending on the dimensions of the structure and sometimes contain openings to accommodate windows and doors. These variations in configuration have an effect on the response of the wall. A parametric study that consisted of a set of shear wall models analyzed using a finite element program was performed to determine the effect that aspect ratio (ratio of wall length to height) and openings have on the response of timber shear walls subjected to monotonic and seismic loads.

8.2 Shear Wall Analysis Program

A program, WALSEIZ, that is capable of performing static, load–controlled monotonic, or dynamic analysis on shear wall models, was developed in order to analyze the shear wall models for the parametric study. The program is a modification of the shear wall analysis program DYNWALL, which was developed by Dolan (1989). WALSEIZ utilizes the finite–element method for analysis and uses four different elements to model a shear wall: a plane frame element to model the framing, a plane rectangular bilinear element to model the sheathing, two nonlinear spring elements

to model the connectors that attach the sheathing to the framing, and a bi–linear spring element to model the effect of bearing between adjacent sheathing panels. The program is capable of calculating the forces and stresses in the elements as a function of applied load or time; displacement at the nodes as a function of applied load or time; velocity and acceleration at the nodes as a function time; and the maximum and minimum forces, stresses, displacements, velocities, and accelerations.

Validation of WALSEIZ consisted of creating three wall models corresponding to two shear walls tested by Dolan (1989) and a shear wall tested by Kolba (unpublished), analyzing the models using WALSEIZ, and comparing those results to the experimental results. The models corresponding to the walls tested by Dolan (1989), which were subjected to monotonic and seismic loading, were 2.4 m by 2.4 m (8 ft by 8 ft) and did not contain openings. The model corresponding to the wall tested by Kolba (unpublished), which was subjected to monotonic loading only, was 2.4 m by 3.7 m (8 ft by 12 ft) with a window opening. The load–displacement curve, maximum load, and/or time–displacement curve calculated using WALSEIZ compared favorably to similar data from the experimental tests (except maximum load for the wall with an opening), indicating that WALSEIZ accurately models the response of a shear wall.

8.3 Parametric Study

The parametric study consisted of analyzing twenty–five shear wall models subjected to monotonic and seismic loading using WALSEIZ. The models corresponded to common light–frame shear walls with sheathing attached to one side of the framing using nails spaced 10 cm (4 in) along the perimeter of a sheathing panel and 15 cm (6 in) along the interior of a sheathing panel. Fourteen of the models had various aspect ratios and no openings. These models were both 2.4 m (8 ft) and 4.9 m (16 ft)

in height and had aspect ratios (ratio of wall length to height) ranging from 0.25 to 5 for the 2.4 m (8 ft) high models and 0.25 to 2.5 for the 4.9 m (16 ft) high models. The other eleven models were 7.3 m (12 ft) long and had openings corresponding to windows or doors. Four of the models were 2.4 m (8 ft) high with 1.2 m (4 ft) high window openings ranging in length from 1.2 m (4 ft) to 4.9 m (16 ft), another four models were 2.4 m (8 ft) high with 2.0 m (6.4 ft) high door openings ranging in length from 1.2 m (4 ft) to 4.9 m (16 ft), and the other three models were 4.9 m (16 ft) high with 3.3 m (10.7 ft) high door openings ranging in length from 2.4 m (8 ft) to 4.9 m (16 ft). Each model was analyzed twice, once when subjected to a distributed monotonic load acting along the sill plate of the wall model and once when subjected to the S00E component of the acceleration record from the El Centro earthquake. The initial stiffness and maximum resistance, relative drift, and element forces were examined for the models subjected to monotonic loading. The maximum relative drift, base shear, velocity and acceleration at the top of the wall, and element forces were examined for the models subjected to seismic loading.

8.3.1 Results

The results from the parametric study indicate the following concerning timber shear walls without openings of varying aspect ratio:

- The maximum strength, initial stiffness, and maximum seismic base shear increase linearly as the length of a shear wall increases for walls of the same height, except for walls of length shorter than 1.2 m (4 ft).

- The relative drift and maximum unit shear remain constant for shear walls of the same height except for the aforementioned walls of short length, and these properties decrease as the height of a wall increases for shear walls of the same total length.

- The shear force resisted by anchorages in close proximity to studs where sheathing panels meet is significantly larger ($\approx$ 30–35% larger for the models in the study) than average shear force resisted per anchorage.

- The vertical force resisted at the end chords is lower (upwards of 15% lower) than the theoretical overturning force–couple provided that sufficient resistance to vertical loading is provided along the length of the wall. The extent to which the force at the end chord is reduced depends on the location of the vertical resistance along the interior of the shear wall.

- A significant axial load ($\approx$ 25–40% of the theoretical overturning force–couple for the models in the study) is present at the interior studs not located where sheathing panels meet.

The results from the parametric study indicate the following concerning timber shear walls with various opening configurations with the same overall length:

- The strength, initial stiffness, and maximum seismic base shear decrease as the length of the opening increases for shear walls of the same height.

- Shear walls with openings are stronger and stiffer than walls without openings of the same height and effective length.

- Shear walls with openings have a higher relative drift than the walls without openings of the same height and effective length when subjected to seismic loading.

- The relative drift and unit shear increase as the length of the opening increases for shear walls of the same height.

- The shear force resisted by anchorages in close proximity to studs where sheathing panels meet is significantly larger (up to 93% larger for the models in the

study) than the average shear force resisted per anchorage, which is similar to what is found for shear walls without openings.

- The shear force resisted by anchorages located below an opening (such as an opening for a window) are significantly lower than the load resisted at the other anchorages.

- The reactions at the chords resist a vertical load lower than the theoretical overturning force–couple, the reactions at the studs resist a vertical load of some magnitude, the reactions at the studs where sheathing panels meet resist a negligible vertical load.

- The headers are subjected to a distributed axial load that is less than the distributed load applied at the top of the wall.

8.4 Design Methodology

The results from the parametric study were the basis for the development of a modified design methodology. The following modifications to the current design methodology are implemented based on the results from the study.

- The use of shear walls less than 1.2 m (4 ft) in length should be avoided or designed to account for their increased drift because their strength per unit length is substantially lower than that of other walls.

- The interior studs and the connectors attaching the studs to the sill and sole plates should be designed to withstand a load that is a percentage of the overturning force–couple because axial loading is present at the studs. The percentage is dependent on the configuration of the wall.

- The design load should be multiplied by a factor (1.4 for wall models without openings and 2.0 for wall models with openings in the study), and this modified design load used to design the anchorages. This factor accounts for the increased shear force resisted by the anchorages near the sheathing panel seams, and its value is dependent on the configuration of the wall. The factor is applied to all of the anchorages in order to simplify the design process.

- The value of the system response (ductility) factor in the seismic base shear equation is reduced from the current value of $\sqrt{8}$ to 2 to account for the lower ductility due to the nonlinear behavior of the walls; however, it must be remembered that this recommendation is based on the response of a single shear wall and does not account for system effects.

- The value for the period in the response factor in the seismic base shear equation should be modified to account for the higher period, and therefore the lower base shear, found in the taller walls and the walls with openings.

- The header(s) should be designed as a simply supported member sufficient to withstand a distributed load equal to the applied distributed load. The connectors attaching the header to the adjacent studs should be designed to withstand the resulting forces at the ends of the member.

- Blocking should be utilized adjacent to the region in which an opening header(s) exists to offset the large axial force transferred from the header(s) to the adjacent studs.

The incorporation of the aforementioned modifications into the existing design methodology produces the following modified design methodology. The design load is determined by calculating either the total applied load acting on the wall or using the base shear equation (UBC, 1991) with the aforementioned modifications. The

design unit shear is then calculated by dividing the design load by the effective wall length, and a shear wall of a given sheathing grade and thickness and sheathing–to–framing connector type and spacing is selected from Table 25–K–1 of the UBC (1991) that is that is sufficient to withstand the design unit shear. The chords in the shear wall are then designed by analyzing each shear panel (portion of shear wall not containing an opening) as a separate free–body subjected to the design unit shear acting along the sill plate. The unit shears are used to determine the overturning moment in each shear panel, which is resolved into a force–couple that is resisted by the chords at the ends of the shear panels. The chords are then designed to resist this force–couple, and a percentage of the force–couple, the magnitude of which is dependent on the configuration of the wall, is used to check the adequacy of the interior studs and the connectors attaching the studs to the sole plate. The header(s) and the connectors attaching the header(s) to the adjacent stud are then designed for shear walls with openings by assuming that they are a member pinned at each end subjected to an axial load equal to the design load divided by the total length of the shear wall. Blocking should be utilized for shear walls with openings adjacent to the header. The design load is multiplied by a factor, which is dependent on the configuration of the wall, to account for the increased load resisted by the connectors adjacent to studs where sheathing panels meet and the connectors located in the solid portion of the wall for walls with window openings. This factored design load is used to design the anchorages, which are placed at and attached directly to the studs for added resistance to overturning. Finally, the hold–down connectors are then designed by taking the difference between the overturning moment and the resisting moment divided by the length of the wall and are attached to the chords.

8.5 Future Research

Although there has been a significant amount of research concerning the behavior of timber shear walls, there remain some areas that require investigation, including:

- Experimental testing to supplement the results from this study and to further validate the model, especially for shear walls with openings.

- The effect that using adhesives to attach the sheathing to the framing has on the response of timber shear walls. Adhesives have exhibited higher strength and stiffness and lower ductility than the average nail connector and have been shown to have a pronounced effect on the response of a shear wall (Foschi and Filiatrault, 1989).

- The effect that the location of openings has on the response of shear walls. The openings in the wall models analyzed in the study all originated at the same location along the length of the wall. Variation of the location of an opening could have an effect on the response of a shear wall due to the different geometry.

- The effect that the adjacent components (i.e. adjacent walls, diaphragms, etc.) have on the response of shear walls. This effect, which could be substantial, is currently neglected in the design of timber shear walls.

- The development of a shear wall macro–element, based on WALSEIZ, which could eventually lead to the development of a 3D model to predict the behavior of an entire structure. This would greatly reduce the time and effort needed to analyze full–scale structures.

- The development of a graphical interface for WALSEIZ. This would provide a visual representation of the response of a shear wall subjected to monotonic

or dynamic loading, thereby allowing WALSEIZ to become a more valuable educational tool.

Bibliography

[1] Adeli, H., Gere, J.M., and Weaver, W., 1978. "Algorithms for Nonlinear Structural Dynamics," *Journal of the Structural Division, Proceedings of the American Society of Civil Engineers,* Vol. 104, No. ST2, pp. 263–280.

[2] Akerlund, S., 1987. "Behavior of Wood-Framed Shear Walls," *Journal of Structural Engineering,* Vol. 113, No. 11, pp. 2306–2309.

[3] *APA Design/Construction Guide – Diaphragms*, 1991. American Plywood Association, Tacoma, Washington.

[4] American Plywood Association, 1988. *Technical Note number N375 – Design Capacities of APA Performance–Rated Structural–Use Panels*, Tacoma, Washington.

[5] Anderson, K.R., 1988. "Design Considerations for Wind and Earthquake Resisting Wood Panel Diaphragms," *Proceedings of the International Conference on Timber Engineering.* Seattle, Washington, pp. 339–343.

[6] Anderson, G.A. and Reinhold, G., 1990. "A Simplified Shear Diaphragm Design Procedure for Practicing Engineers," *ASAE International Winter Meeting.* Chicago, Illinois, paper 904523, 16 pp.

[7] Arima, T., Okabe, M., Maruyama, N., and Hayamura, S., 1990. "Dynamic Behavior and Stiffness of Full–Scale Houses During Progressive Stages of Construction," *Proceedings of the International Timber Engineering Conference.* Tokyo, Japan, pp. 778–785.

[8] Bodig, J. and Parquhar, B.J.M., 1988. "Behavior of Mechanical Joints of Wood at Acelerated Strain Rates," *Proceedings of the International Conference on Timber Engineering.* Seattle, Washington, pp. 455–464.

[9] Boughton, G.N. and Reardon, G.F., 1984. "Simulated Cyclone Wind Test on a Timber Frame House," *Proceedings of the Pacific Timber Engineering Conference, Volume II - Timber Design Theory.* Auckland, New Zealand, pp.527–534.

[10] Brebbia, C.A. and Ferrante, A.J., 1978. *Computational Methods for the Solution of Engineering Problems.* Crane, Russak, & Company, Inc., New York, N.Y.

[11] Breyer, D.E., 1993. *Design of Wood Structures.* McGraw–Hill Book Company, New York, N.Y.

[12] Buchanan, A., 1984. "Wood Properties and Seismic Design of Timber Structures," *Proceedings of the Pacific Timber Engineering Conference, Volume II - Timber Design Theory.* Auckland, New Zealand, pp. 462–469.

[13] Bulleit, W.M., 1987. "Markov Model for Wood Structural Systems," *Journal of Structural Engineering,* Vol. 113, No. 9, pp. 2023–2031.

[14] Ceccotti, A. and Vignoli, A., 1986. "Engineered Timber Structures. An Evaluation of Their Seismic Behaviour," *Proceedings of the 1990 International Timber Engineering Conference.* Tokyo, Japan, pp. 946–953.

[15] Cheung, C.K. and Itani, R.Y., 1984. "Damping Characteristics of Sheathed Wood Diaphragms," *Proceedings of the Pacific Timber Engineering Conference, Volume II - Timber Design Theory.* Auckland, New Zealand, pp. 470–477.

[16] Clough, R.W., and Penzien, J., 1975. *Dynamics of Structures.* McGraw–Hill Book Company, New York, N.Y.

[17] Cook, R.D., Malkus, D.S., and Plesha, M.E., 1989. *Concepts and Applications of Finite Element Analysis.* John Wiley & Sons, New York, N.Y.

[18] Dean, J.A. and Moss, P.J., 1984. "A Design for Rectangular Openings in Shearwalls and Diaphragms," *Proceedings of the Pacific Timber Engineering Conference, Volume II - Timber Construction.* Auckland, New Zealand, pp. 513–518.

[19] Dean, J.A., Stewart, W.G., and Carr, A.J., 1986. "The Seismic Behavior of Plywood Sheathed Shearwalls," *The Bulletin of the New Zealand Society for Earthquake Engineering,* Vol. 19, No. 1, pp. 48-63.

[20] Diekmann, E.F., 1989. "Wood Shearwalls for Engineers," *Proceedings of the Second Pacific Timber Engineering Conference 1989, Volume 2.* Seattle, Washington, pp. 273–281.

[21] Dolan, J.D., 1989. *The Dynamic Response of Timber Shear Walls*, thesis submitted in partial fulfillment of the Doctor of Philosophy Degree at the Unversity of British Columbia, Vancouver, British Columbia.

[22] Dolan, J.D. and Foschi, R.O., 1991. "Structural Analysis Model for Static Loads on Timber Shear Walls," *Journal of Structural Engineering,* Vol. 117, No. 3, pp. 851–861.

[23] Dorwick, D.J. and Smith, P.C., 1986. "Timber Shear Walls for Wind and Earthquake Resistance," *Bulletin of the New Zealand National Society for Earthquake Resistance,* Vol 19, No. 2, pp. 123–134.

[24] Easley, J.T., Foomani, M., and Dodds, R.H., 1982. "Formulas for Wood Shear Walls," *Journal of the Structural Division, Proceedings of the American Society of Civil Engineers,* Vol. 108, No. ST11, pp. 2460–2478.

[25] Falk, R.H. and Itani, R.Y., 1987. "Dynamic Characteristics of Wood and Gypsum Diaphragms," *Journal of Structural Engineering,* Vol. 113, No. 6, pp. 1357–1370.

[26] Falk, R.H. and Itani, R.Y., 1989. "Finite Element Modeling of Wood Diaphragms," *Journal of Structural Engineering,* Vol. 115, No. 3, pp. 543–559.

[27] Filiatrault, A., 1990. "Seismic Response of Friction Damped Shear Walls," *Earthquake Engineering and Structural Dynamics,* Vol. 19, No. 2, pp. 259–273.

[28] Filiatrault, A., Foschi, R.O., and Folz, B., 1990. "Reliability of Timber Shear Walls Under Wind and Seismic Loads," *Proceedings of the 1990 International Timber Engineering Conference,* pp. 319–325.

[29] Foliente, G.C., McLain, T.E., and Singh, M.P., 1993. "A General Hysteresis Model for Wood Structures." *Paper Presented at the 1993 ASCE Structures Conference,* Irvine, CA.

[30] Foschi, R.O., 1977. "Analysis of Wood Diaphragms and Trusses: Part I: Diaphragms," *Canadian Journal of Civil Engineering,* Vol. 4, No. 3, pp. 345–352.

[31] Foschi, R.O. and Filiatrault, A., 1990. "Performance Evaluation of the 3M Scotch Grip Wood Adhesive 5230 for the Static and Dynamc Design of Timber Shear Walls and Diaphragms." *Final Report Prepared for 3M Corporation,* 43 pp.

[32] Freeman, S.A., 1977. "Racking Tests of High-Rise Building Partitions," *Journal of the Structural Division, Proceedings of the American Society of Civil Engineers,* Vol. 103, No. ST8, pp. 1673–1685.

[33] Ge, Y.Z., Gopalaratnam, V.S., and Liu, H., 1991. "Effect of Openings on the Stiffness of Wood-Frame Walls," *Forest Products Journal,* Vol. 41, No. 1, pp. 65–70.

[34] Girhammar, U.A. and Andersson, H., 1988. "Effect of Loading Rate on Nailed Timber Joint Capacity," *Journal of Structural Engineering,* Vol. 114, No. 11, pp. 2439–2456.

[35] Gray. R.G. and Zacher, E.G., 1988. "Dynamic Testing of Wood Shear Panels," *Architecture,* Vol. 77, No. 3, pp. 121–124.

[36] Griffiths, D.R., 1984. "Determining the Racking Resistance of Timber Framed Walls," *Proceedings of the Pacific Timber Engineering Conference, Volume I - Timber Construction.* Auckland, New Zealand, pp. 504–512.

[37] Gupta, A.K. and Kuo, G.P., 1985. "Behavior of Wood-Framed Shear Walls," *Journal of Structural Engineering,* Vol. 111, No. 8, pp. 1722–1733.

[38] Gupta, A.K. and Kuo, G.P., 1987. "Modeling of a Wood-Framed House," *Journal of Structural Engineering,* Vol. 113, No. 2, pp. 260–278.

[39] Gupta, A.K. and Kuo, G.P., 1987. "Wood Frame Shear Walls with Uplifting," *Journal of Structural Engineering,* Vol. 113, No. 2, pp. 241–259.

[40] Gutkowski, R.M. and Castillo, A.L., 1988. "Single- and Double- Sheathed Wood Shear Wall Study," *Journal of Structural Engineering,* Vol. 114, No. 6, pp. 1268–1284.

[41] Hayashi, K., 1989. "Studies on Methods to Estimate the Racking Resistance of Houses with Wooden Wall Panels," *Proceedings of the Second Pacific Timber Engineering Conference 1989, Volume 2.* Seattle, Washington, pp. 113–118.

[42] Hayashi, K., 1990. "Studies on Methods to Estimate the Racking Resistance of Houses With Wooden Wall Panel Sheathing," *Proceedings of the 1990 International Timber Engineering Conference.* Tokyo, Japan, pp. 633–640.

[43] Holzer, S.M., 1990. *Class notes from Finite Element Analysis course (CE5414).* Virginia Polytechnic Institute and State University, Blacksburg, Virginia.

[44] Hoyle, R.J., 1988. "Design of Wood Shear Joints Fastened with Nails and Structural Elastomeric Adhesives," *Proceedings of the 1988 International Conference of Timber Engineering, Volume 1.* Seattle, Washington, pp. 38–45.

[45] Isao, S., Ohashi, Y., and Yoshitaka, F., 1990. "Seismic Behavior of Base Isolated Two–Storied Wooden Building – Static Loading Tests and Earthquake Observations," *Proceedings of the 1990 International Timber Engineering Conference.* Tokyo, Japan, pp. 938–945.

[46] Itani, R.Y. and Cheung, C.K., 1984. "Nonlinear Analysis of Sheathed Wood Diaphragms," *Journal of Structural Engineering,* Vol. 110, No. 9, pp. 2137–2147.

[47] James, G.W. and Bryant, A.H., 1984. "Plywood Diaphragms and Shearwalls," *Proceedings of the Pacific Timber Engineering Conference, Volume II - Timber Design Theory.* Auckland, New Zealand, pp. 478–485.

[48] Jenkins, J.L., Polensek, A., and Bastendorff, K.M., 1979. "Stiffness of Nailed Wall Joints Under Short and Long Term Lateral Loads," *Wood Science,* Vol. 11, No. 3, pp. 145–154.

[49] Kalkert, R., 1992. "Hysteretic Action of Adhesive Connectors," *Unpublished Report.*

[50] Kamiya, F., 1987. "Buckling Theory of Sheathed Walls: Linear Analysis," *Journal of Structural Engineering,* Vol. 113, No. 9, pp. 2009–2022.

[51] Kasal, B. and Leichti, R.J., 1992. "Nonlinear Finite–Element Model for Light–Frame Stud Walls," *Journal of Structural Engineering,* Vol. 118, No. 11, pp. 3122–3134.

[52] Kawachi, T., Tominaga, H., and Sakaguchi, N., 1990. "Tests on Full–Scale Model of the Traditional Wooden Structure (Mutsubo) Subjected to Horizontal Load," *Proceedings of the 1990 International Timber Engineering Conference.* Tokyo, Japan, pp. 388–394.

[53] Kawai, N., Sugiyama, H., and Matsumoto, T., 1990. "The Hand Calculation Method Calculating the Distribution of Horizontal Force to Shear Walls by Considering the Effect of Shear Rigidity of Floor," *Proceedings of the 1990 International Timber Engineering Conference.* Tokyo, Japan, pp. 510–517.

[54] Koh, C.G. and Kelly, J.M., 1990. "Application of Fractional Derivates to Seismic Analysis of Base–Isolated Models," *Earthquake Engineering and Structural Dynamics,* Vol. 19, No. 2, pp. 229–241.

[55] Kolba, A.E., 1995. *Personal Correspondance.*

[56] Law, A.M. and Kelton, W.D., 1991. *Simulation Modeling & Analysis.* McGraw–Hill Book Company, New York, N.Y.

[57] Leichti, R. and Kasal, B., 1992. "Nonlinear Analysis of Load Sharing Among the Components of a Light–Frame Wood Building," *Presentation at the 1992 Forest Products Research Society Annual Meeting.* Charleston, SC.

[58] Mahaney, J.A. and Kehoe, B.E., 1988. "A Rational Design Procedure for Multistory Buildings with Wood Diaphragms," *Proceedings of the International Conference on Timber Engineering.* Seattle, Washington, pp. 306–316.

[59] McCutcheon, W.J., 1985. "Racking Deformations in Wood Shear Walls," *Journal of Structural Engineering,* Vol. 111, No. 2, pp. 257–269.

[60] McCutcheon, W.J., 1988. "Computer Program for Structural Analysis of Wood Walls and Floors," *Proceedings of the 1988 International Conference on Timber Engineering, Volume 2.* Seattle, Washington, pp. 909–914.

[61] McDowall, C.G., 1984. "Qualitative Assessment of Whole House Structural Response to Lateral Wind Loads," *Proceedings of the Pacific Timber Engineering Conference, Volume I - Timber Construction.* Auckland, New Zealand, pp. 519–526.

[62] McDowall, C.G. and Halligan, A.F., 1989. "Racking Resistance of Short Lengths of Particleboard Sheathed, Timber Framed Wall Panels," *Proceedings of the Second Pacific Timber Engineering Conference 1989, Volume 2.* Seattle, Washington, pp. 95–99.

[63] McLain, T.E., 1987. "Engineered Wood Connections and the 1991 National Design Specification," *Wood Design Focus,* Summer, 1991.

[64] Medearis, K., 1970. "Structural Dynamics of Plywood Shear Walls," *Wood Science,* Vol. 2, No. 2, pp. 106-110.

[65] *National Design Specification (NDS)*, 1991. National Forest Products Association, Washington, D.C.

[66] Nelson, E.L., Wheat, D.L., and Fowler, D.W., 1985. "Structural Behavior of Wood Shear Wall Assemblies," *Journal of Structural Engineering,* Vol. 111, No. 3, pp. 654–665.

[67] Patton-Mallory, M., Gutkowski, R.M., and Soltis, L.A., 1984. "Racking Performance of Light–Frame Walls Sheathed on Two Sides," *Research Paper FPL 448,* U.S. Department of Agriculture, Forest Service, Forest Products Laboratory, Madison, WI, 16 p.

[68] Patton-Mallory, M., Wolfe, R.W., Soltis, L.A., and Gutkowski, R.M., 1985. "Light-Frame Shear Wall Length and Opening Effects," *Journal of Structural Engineering,* Vol. 111, No. 10, pp. 2227–2239.

[69] Pellicane, P.J. and Schmidt, D., 1988. "Strength and Load–Slip Characteristics of Wood Joints with Elastomeric Construction Adhesives," *Proceedings of the International Conference on Timber Engineering.* Seattle, Washington, pp. 683–692.

[70] Pellicane, P.J., 1991a. "Modeling Nail/Glue Joints in Wood: Part I - Strength Behavior," *(No reference given).*

[71] Pellicane, P.J., 1991b. "Modeling Nail/Glue Joints in Wood: Part II - Load–Slip Behavior," *(No reference given).*

[72] Pellicane, P.J., 1991c. "Nail/Glue Joints in Wood," *Forest Products Journal,* Vol. 41, No. 11/12, pp. 33–35..

[73] Phillips. T.L., Itani, R.Y., and McLean, D.I., 1993. "Lateral Load Sharing by Diaphragms in Wood–Framed Buildings," *Journal of Structural Engineering,* Vol. 119, No. 5, pp. 1556–1571.

[74] Pidgeon, A.W. and Hons, B.E., 1984. "Fibrous Plaster on Timber Structures as Diaphragms," *Proceedings of the Pacific Timber Engineering Conference, Volume II - Timber Design Theory.* Auckland, New Zealand, pp. 75–80.

[75] *Plywood Design Specification (PDS)*, 1986. American Plywood Association, Tacoma, Washington.

[76] Polensek, A., 1978. "Properties of Components and Joints for Rational Design Procedure of Wood-Stud Walls," *Wood Science,* Vol. 10, No. 4, pp. 167–175.

[77] Polensek, A. and Schimel, B.D., 1986. "Rotational Restraint of Wood-Stud Wall Supports," *Journal of Structural Engineering,* Vol. 112, No. 6, pp. 1247–1262.

[78] Polensek, A. and Bastendorff, K.M., 1987. "Damping in Nailed Joints of Light-Frame Wood Buildings," *Wood and Fiber Science,* Vol. 19, No. 2, pp. 110–125.

[79] Potter, B.J., 1989. "MUTO Timber - Seismic Shear Distribution to Timber Shear Panels - A Computer Program," *Proceedings of the Second Pacific Timber Engineering Conference, Volume 2.* Seattle, Washington, pp. 269–272.

[80] Sakamoto, I., Ohashi, Y., and Shibata, M., 1984. "Theoretical Analysis of Seismic Response of Wooden Dwellings in Japan," *Proceedings of the Pacific Timber Engineering Conference, Volume II - Timber Design Theory.* Auckland, New Zealand, pp. 454–461.

[81] Sakamoto, I., Ohashi, Y., and Fujii, Y., 1990. "Seismic Behavior of Base Isolated Two–Storied Wooden Buildings–Static Loading Tests and Earthquake Observation," *Proceedings of the 1990 International Timber Engineering Conference.* Tokyo, Japan, pp. 938–945.

[82] Schmidt, R.J. and Moody, R.C., 1989. "Modeling Laterally Loaded Light-Frame Buildings," *Journal of Structural Engineering,* Vol. 115, No. 1, pp. 201–217.

[83] Sinha, S.C. and Guangning, L., 1994. "Optimal Design of Base–Isolated Structures with Dynamic Absorbers," *Journal of Structural Engineering,* Vol. 120, No. 1, pp. 221–231.

[84] Soltis, L.A., Wolfe, R.W., and Tuomi, R.L., 1981. "Design Approaches for Light-Frame Racking Walls," *Wall and Floor Systems - Design and Performance of Light–Frame Structures*, 1981, pp. 101–111.

[85] Soltis, L.A., 1984. "Seismic Performance of Low-Rise Light-Framed Wood Buildings," *Shock and Vibration Digest,* Vol. 16, No. 11, pp. 27–32.

[86] Soltis, L.A. and Mtenga, P.V.A., 1985. "Strength of Nailed Wood Joints Subjected to Dynamic Load," *Forest Products Journal,* Vol. 35, No. 11/12, pp. 14–18.

[87] Soltis, L.A. and Hanson, S., 1991. "Strength of Light–Gauge Steel Nailed Connections," *Forest Products Journal,* Vol. 41, No. 5, pp. 57–60.

[88] Soltis. L.A., 1991. "European Yield Model for Wood Connections," *Proceedings of the 1991 ASCE Structures Congress.* Indianapolis, IN, pp. 60–63.

[89] Stewart, W.G., Dean, J.A., and Carr, A.J., 1988. "The Earthquake Behavior of Plywood Sheathed Shearwalls," *Proceedings of the 1988 International Conference on Timber Engineering, Volume 2.* Seattle, Washington, pp. 248–261.

[90] Stewart, W.G. and Dean, J.A., 1989. "A Procedure for the Seismic Design of Timber Sheathed Shearwalls," *Proceedings of the Second Pacific Timber Engineering Conference 1989, Volume 2.* Seattle, Washington, pp. 273–281.

[91] Stewart, W.G., Dean, J.A., and Carr, A.J., 1984. "The Seismic Behavior of Plywood Sheathed Shearwalls," *Proceedings of the Pacific Timber Engineering Conference–Volume I Timber Construction.*, Auckland, New Zealand, pp. 486–495.

[92] Stewart, A.H., Kliewer, A., Goodman, J.R., and Salsbury, E.M., 1989. "Lateral Force Distribution in Manufactured Housing from Full–Scale Testing," *Proceedings of the Sessions Related to Design, Analysis, and Testing at Structures Congress '89.* ASCE, San Francisco, CA, pp. 112–123.

[93] Sugiyiama, H. and Suzuki, S., 1975a. "Experimental Study on the Effect of Racking Test Methods, Sheathing Materials and Nailing Upon the Strength Properties of the Platform Construction Wall Subjected to Lateral Force (Part 1)," *Trans. of A.I.J.*, No. 232, pp. 11–15.

[94] Sugiyiama, H. and Suzuki, S., 1975b. "Experimental Study on the Effect of Racking Test Methods, Sheathing Materials and Nailing Upon the Strength Properties of the Platform Construction Wall Subjected to Lateral Force (Part 2)," *Trans. of A.I.J.*, No. 233, pp. 48–50.

[95] Sugiyiama, H., Andoh, N., Hirano, S., Takayuki Uchisako, T., and Nakamura, N., 1988. "Full-Scale Test on a Japanese Type of Two-Story Wooden Frame House Subjected to Lateral Load," *Proceedings of the 1988 International Conference on Timber Engineering, Volume 2.* Seattle, Washington, pp. 55–61.

[96] Sugiyama, H., Kawai, N., Itoh, N., Takahasi, M., and Takaharu, O., 1990. "Earthquake–Proof Capacity of the Recently–Built Japaneese Conventional Wood Houses Estimated from the Arrangement of Shear Wall," *Proceedings of the 1990 International Timber Engineering Conference.* Tokyo, Japan, pp. 147–154.

[97] Sugiyama, H. and Matsumoto, T., 1993a. "A Simplified Method of Calculating the Shear Strength of a Plywood–Sheathed Shear Wall with Openings I. Evaluation of the racking load of shear walls without openings," *Mokuzai Gakkaishi,* Vol. 39, No. 1, pp. 75–79 (in Japanese).

[98] Sugiyama, H. and Matsumoto, T., 1993b. "A Simplified Method of Calculating the Shear Strength of a Plywood–Sheathed Shear Wall with Opening II. Analysis of the shear resistance and deformation of a shear wall with openings," *Mokuzai Gakkaishi,* Vol. 39, No. 8, pp. 924–929 (in Japanese).

[99] Sugiyama, H. and Matsumoto, T., 1994. "A Simplified Method of Calculating the Shear Strength of a Plywood–Sheathed Shear Wall with Openings III. Analysis of the shear resistance of a wall and of the strength behavior of panel elements," *Mokuzai Gakkaishi,* Vol. 40, No. 3, 7 pp (in Japanese).

[100] Suzuki, S., Sugiyama, H., and Takemura, Y., 1978. "Behavior of the Bearing Wall in the Wooden North–American–Type Full–Size Building (No. 1)," *Trans. of A.I.J.,* No. 269, pp. 58–59.

[101] Tembulkar, J.M. and Nau, J.M., 1987. "Inelastic Modeling and Seismic Energy Dissipation," *Journal of Structural Engineering,* Vol. 113, No. 6, pp. 1373–1377.

[102] Tezcan, S.S., 1963. "Simplified Formulation of Stiffness Matrices," by P.M. Wright, *Journal of the Structural Division, Proceedings of the American Society of Civil Engineers,* Vol. 89, No. ST6, pp. 445–449.

[103] Thorston, B.R., 1989. "Structural Design of Multistorey Buildings in Canada," *Proceedings of the Second Pacific Timber Engineering Conference.* Seattle, Washington, pp. 105–108.

[104] Thurston, S.J. and Hutchison, D.L., 1984. "Cyclic Load Testing of Timber–Sheathed Wall Panels," *Proceedings of the Pacific Timber Engineering Conference–Volume I Timber Construction.* Auckland, New Zealand, pp. 496–503.

[105] Tsai, C.S. and Lee, H.H., 1993. "Applications of Viscoelastic Dampers to High–Rise Buildings," *Journal of Structural Engineering,* Vol. 119, No. 4, pp. 1222–1233.

[106] Tuomi, R.L. and McCutcheon, W.J., 1978. "Racking Strength of Light-Frame Nailed Walls," *Journal of the Structural Division, Proceedings of the American Society of Civil Engineers,* Vol. 104, No. ST7, pp. 1131–1140.

[107] *Uniform Building Code (UBC)*, 1991. International Conference of Building Officials, Whittier, CA.

[108] Walford, G.B., 1976. "Derivation of Allowable Loads on Nailed Joints in Diaphragms," *Unpublished*

[109] Wernersson, H. and Gustafsson, P.J., 1988. "Strength and Constitutive Properties of Adhesive Joints," *Proceedings of the 1988 International Conference on Timber Engineering, Volume 1.* Seattle, Washington, pp. 673–682.

[110] Wolfe, R.W. and Moody, R.C., 1990. "North American Structural Performance Tests of Low–Rise Wood–Frame Building Systems," *Report prepared at the Forest Products Laboratory.* Madison, Wisconsin, 19 pp.

[111] Yasumura, M. and Sugiyama, H., 1984. "Shear Properties of Plywood–Sheathed Wall Panels with Opening," *Trans. of A.I.J,* No. 338, pp. 88–98.

[112] Yasumura, M., 1986. "Racking Resistance of Wooden Frame Walls with Various Openings," *International Council for Building Research Studies and Documentation, Working Commission W18 - Timber Structures, CIB - W18, IUFRO S5.02, Volume II, Meeting Nineteen.* Florence, Italy, 25 p.

[113] Yasumura, M. and Murota, T., 1992. "Design Procedures for Wood–Framed Shear Walls," *International Union of Forest Research Organizations Group S5.02–Timber Engineering.* Bordeau, France, pp. 363–381.

[114] Yasumura, M., 1992. "Mechanical Properties of Wood-Framed Shear Walls Subjected to Reversed Cyclic Lateral Loading," *International Council for Building Research Studies and Documentation, Working Commission W18 - Timber Structures.* Ahus, Sweden, Italy, 13 p.

[115] Zacher, E.G. and Gray, R.G., 1989. "Lessons Learned from Dynamic Test of Shear Panels," *Proceedings of the Sessions Related to Design, Analysis, and Testing at Structures Congress '89.* ASCE, San Francisco, CA, pp. 134–142.

[116] Zagajeski, S.W., Halvorsen, G.T., GangaRao, H.V.S., Luttrell, L.D., Jewell, R.B., Corda, D.N., and Roberts, J.D., 1983. "Theoretical and Experimental Studies on Timber Diaphragms Subject to Earthquake Loads," *NSF Earthquake Hazards Mitigation Program, Project No. CEE - 7804769.* Morgantown, West Virginia, 86 pp.

[117] Zahran, T.F. and Hall, W.J., 1984. "Earthquake Energy Absorption in SDOF Structures," *Journal of Structural Engineering,* Vol. 110, No. 8, pp. 1757–1772.

Appendix A

Additional Figures

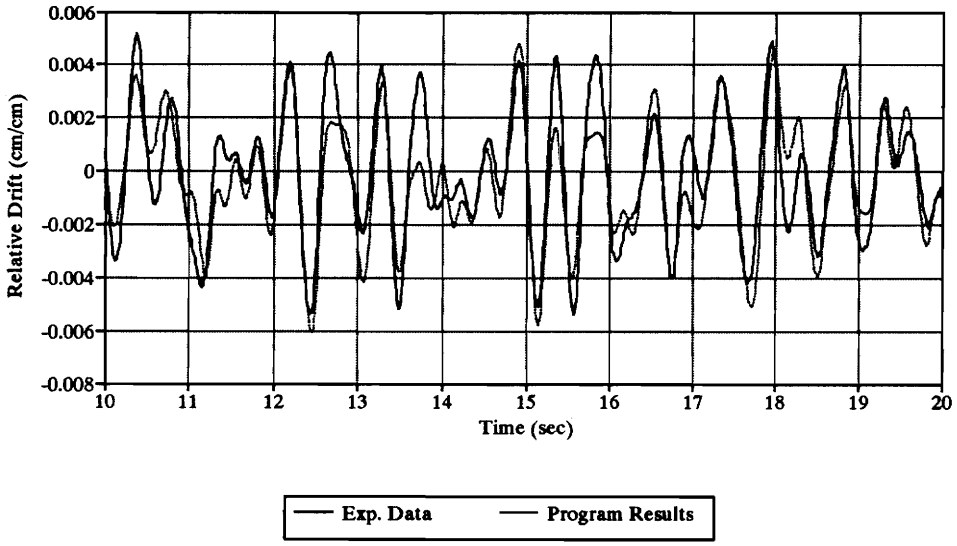

Figure A.1: Time–Relative Drift Curves for Walls With Plywood Sheathing Used to Validate WALSEIZ (10–20 sec)

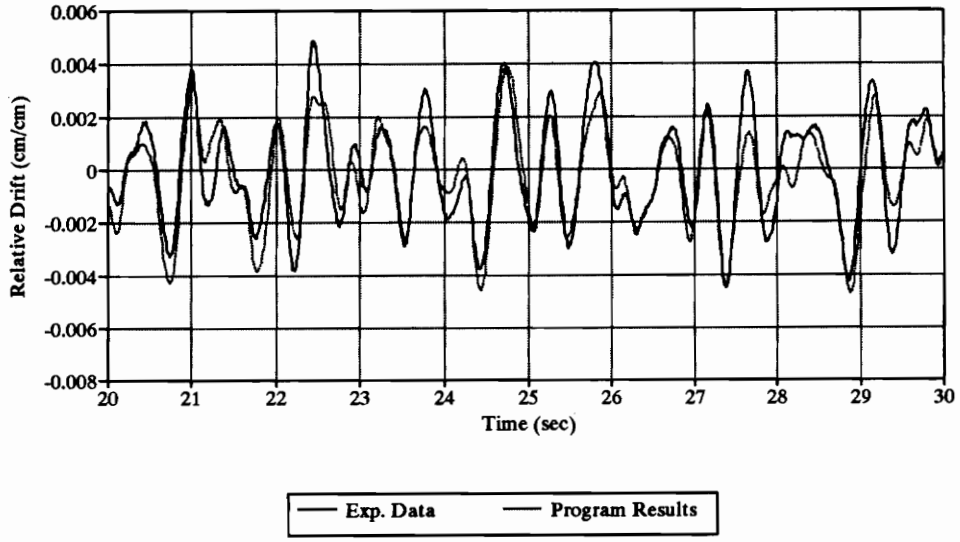

Figure A.2: Time–Relative Drift Curves for Walls With Plywood Sheathing Used to Validate WALSEIZ (20–30 sec)

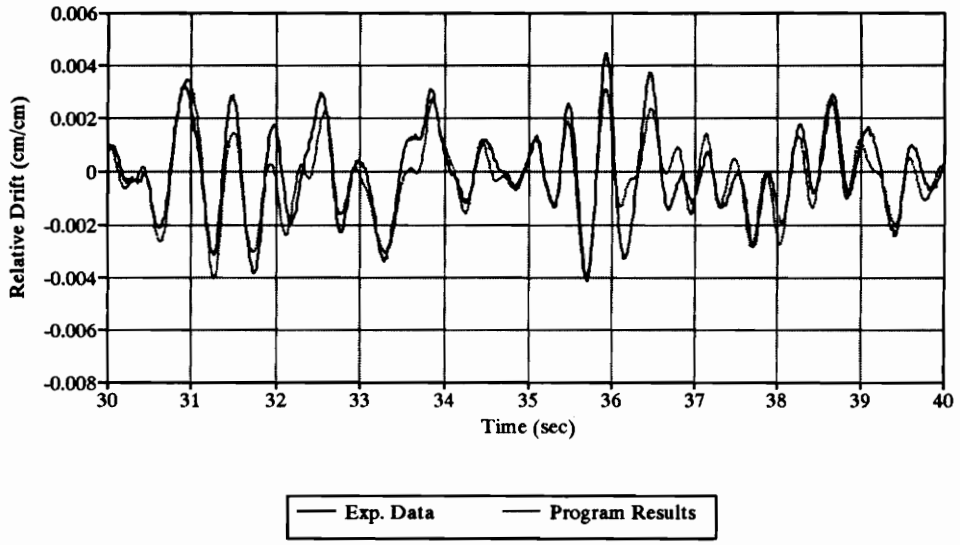

Figure A.3: Time–Relative Drift Curves for Walls With Plywood Sheathing Used to Validate WALSEIZ (30–40 sec)

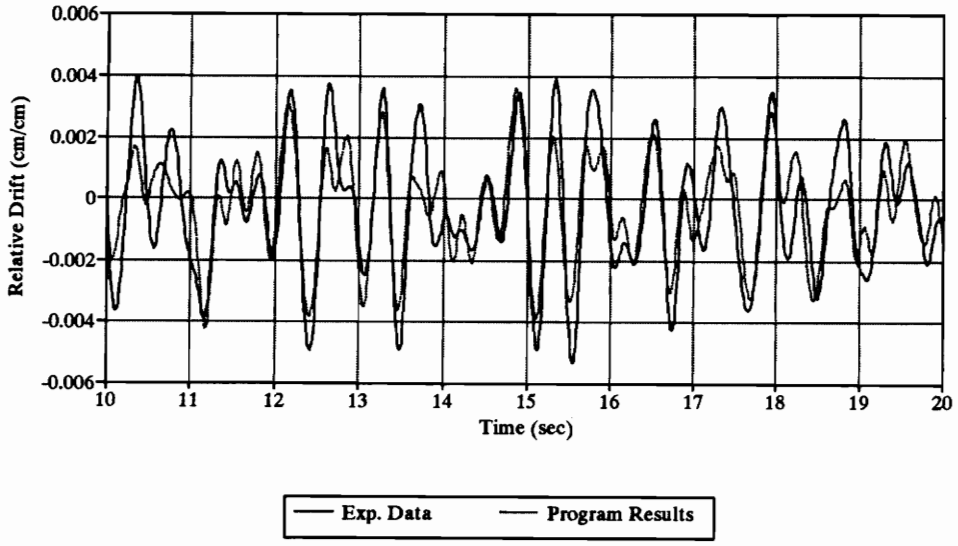

Figure A.4: Time–Relative Drift Curves for Walls With Waferboard Sheathing Used to Validate WALSEIZ (10–20 sec)

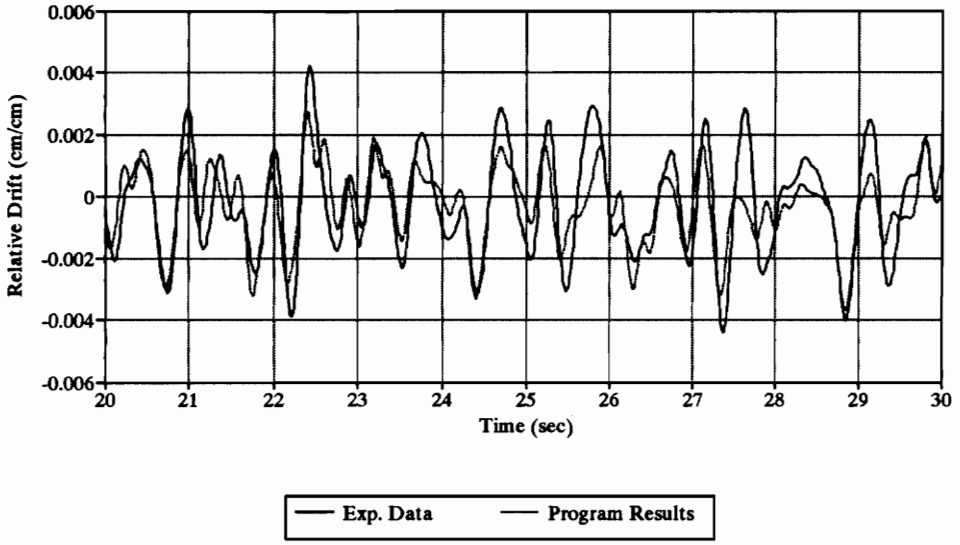

Figure A.5: Time–Relative Drift Curves for Walls With Waferboard Sheathing Used to Validate WALSEIZ (20–30 sec)

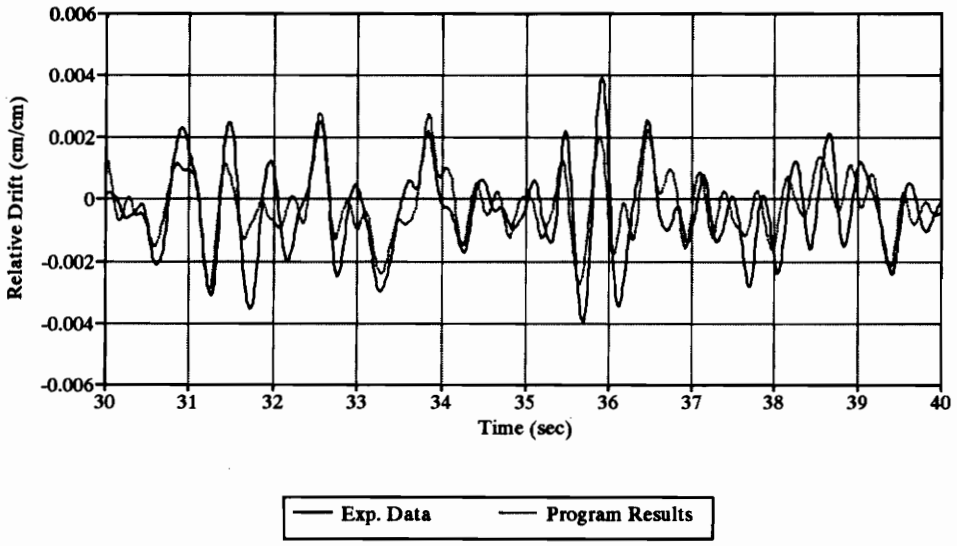

Figure A.6: Time–Relative Drift Curves for Walls With Waferboard Sheathing Used to Validate WALSEIZ (30–40 sec)

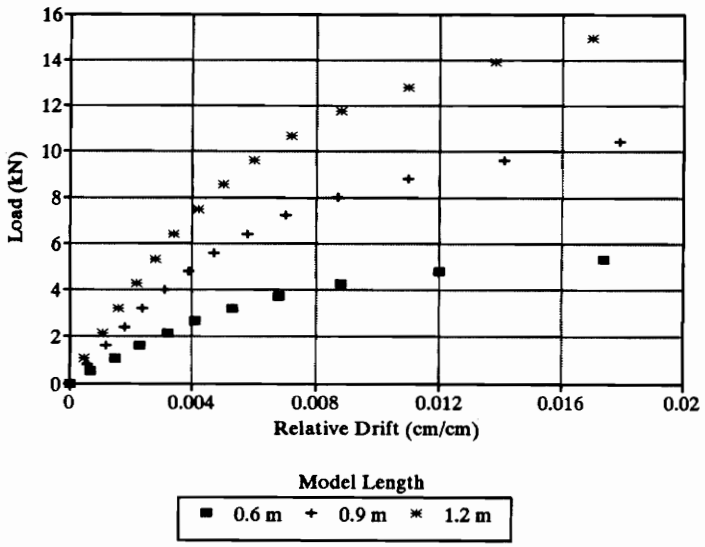

Figure A.7: Load–Relative Drift Curves for 2.4 m (8 ft) High Wall Models Without Openings

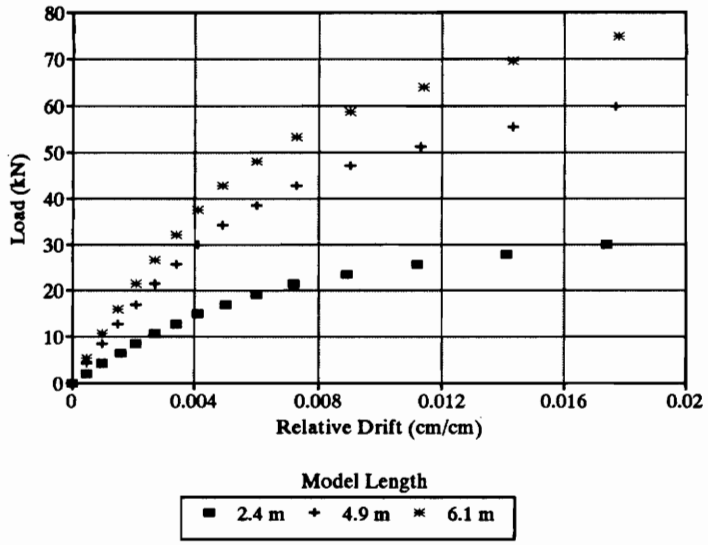

Figure A.8: Load–Relative Drift Curves for 2.4 m (8 ft) High Wall Models Without Openings

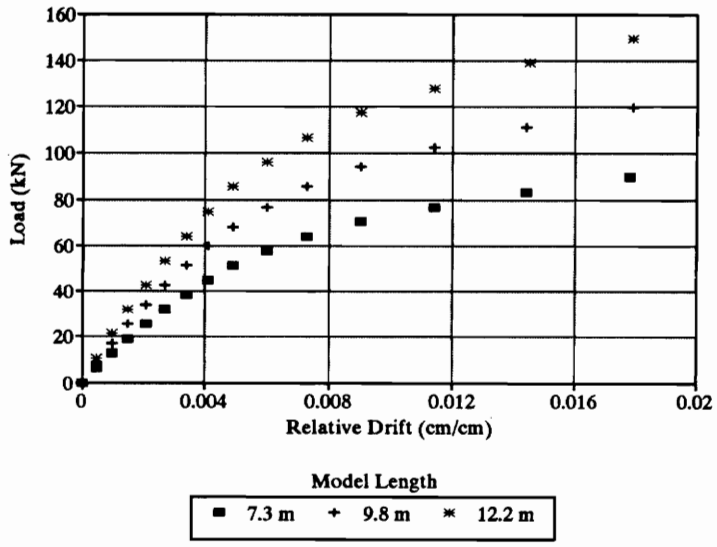

Figure A.9: Load–Relative Drift Curves for 2.4 m (8 ft) High Wall Models Without Openings

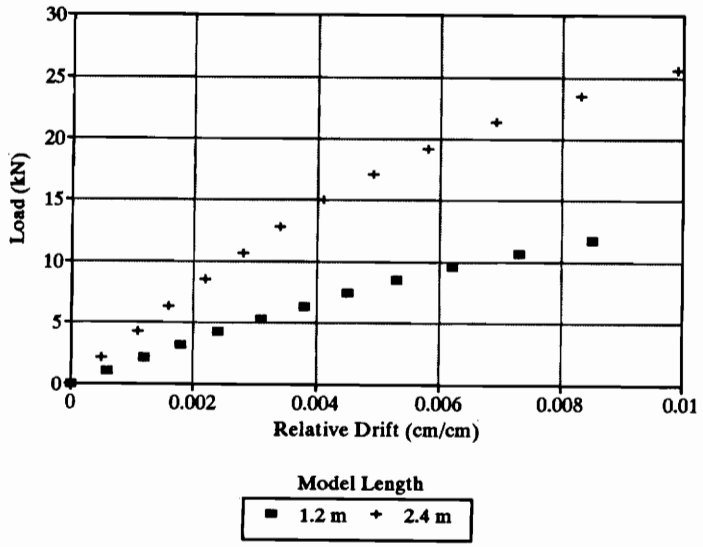

Figure A.10: Load–Relative Drift Curves for 4.9 m (16 ft) High Wall Models Without Openings

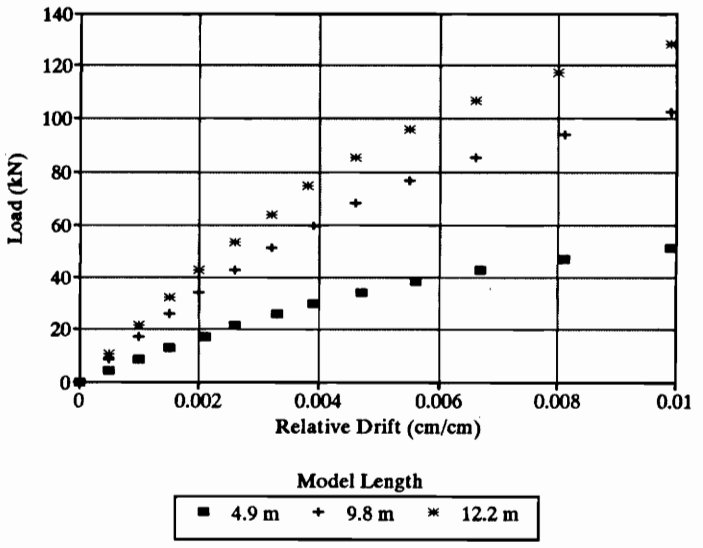

Figure A.11: Load–Relative Drift Curves for 4.9 m (16 ft) High Wall Models Without Openings

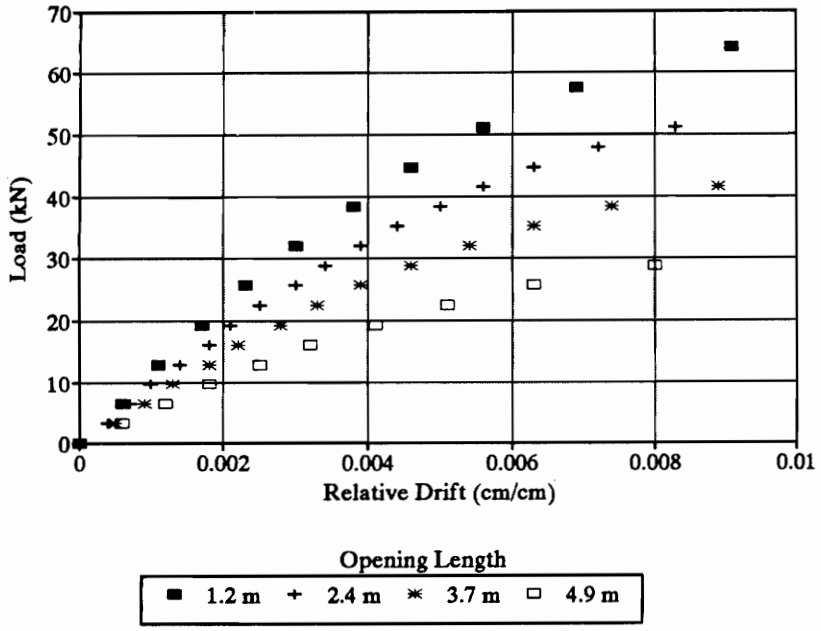

Figure A.12: Load–Relative Drift Curves for 2.4 m (8 ft) High Wall Models with Window Openings

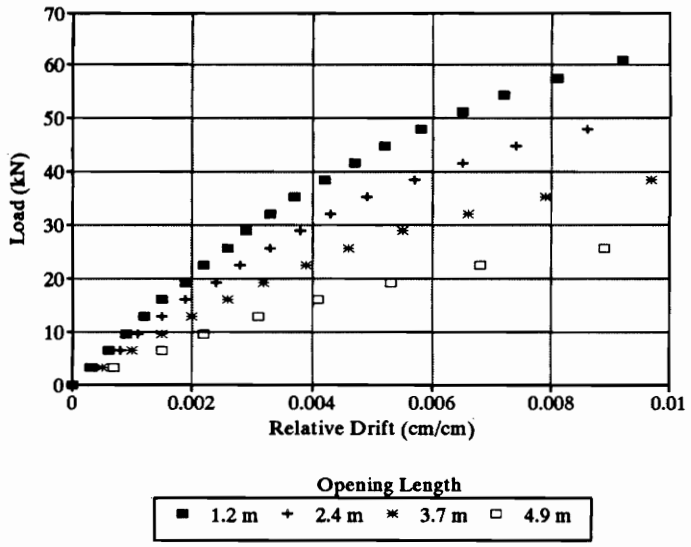

Figure A.13: Load–Relative Drift Curves for 2.4 m (8 ft) High Wall Models with Door Openings

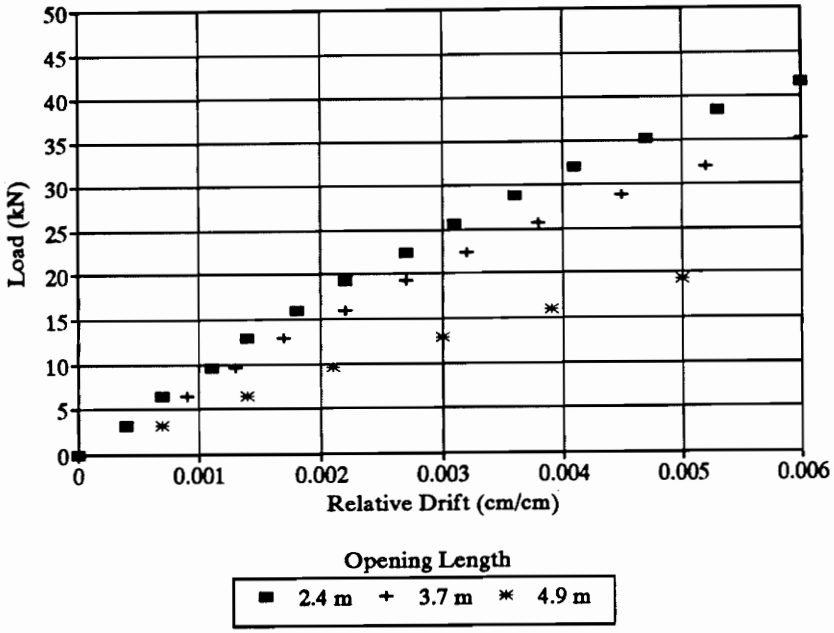

Figure A.14: Load–Relative Drift Curves for 4.9 m (16 ft) High Wall Models with Door Openings

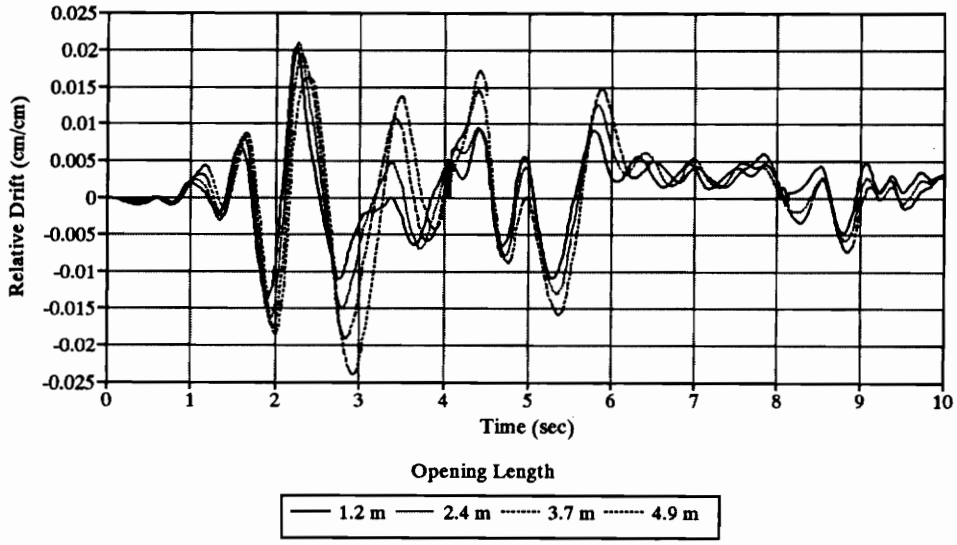

Figure A.15: Time–Relative Drift Curves for 2.4 m (8 ft) High Wall Models with Window Openings

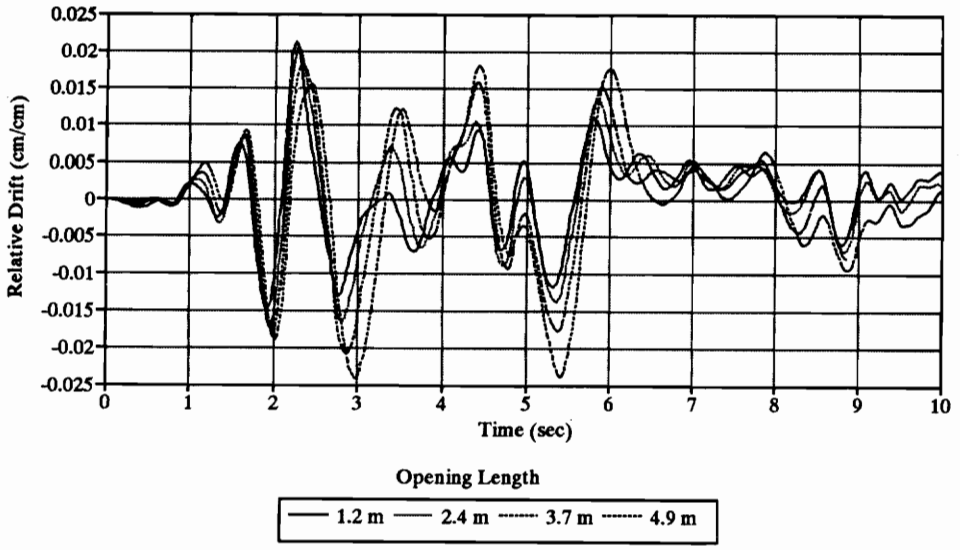

Figure A.16: Time–Relative Drift Curves for 2.4 m (8 ft) High Wall Models with Door Openings

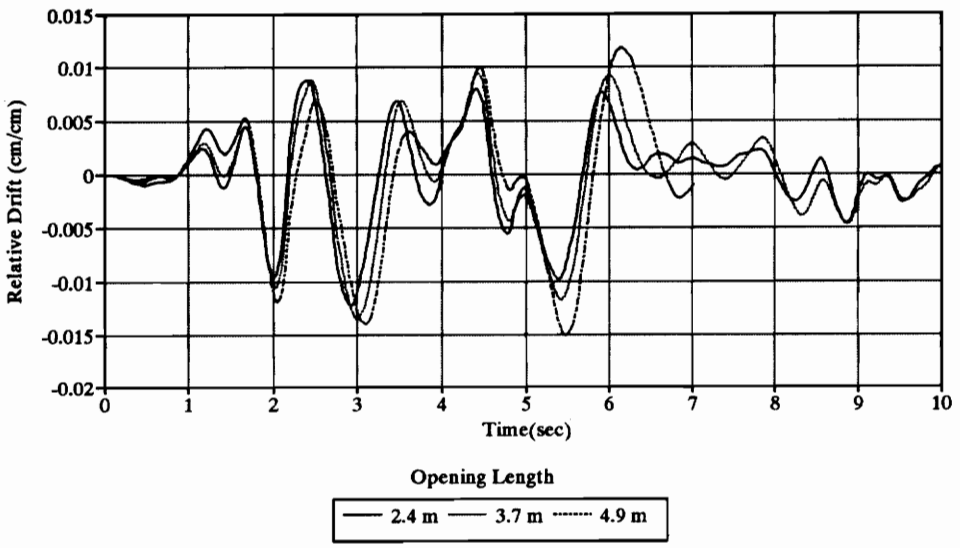

Figure A.17: Time–Relative Drift Curves for 4.9 m (16 ft) High Wall Models with Door Openings

Appendix B

Forces at Reactions

Table B.1: Maximum Horizontal Force at Reactions for Wall Models Without Openings Subjected to Monotonic Loading – kN (kips)

Wall		Distance from End Chord: cm (in)															
Length	Height																
m (ft)	m (ft)	0 (0)	41 (16)	81 (32)	122* (48)	163 (64)	203 (80)	244* (96)	284 (112)	325 (128)	366* (144)	406 (160)	447 (176)	488* (192)	528 (208)	569 (224)	610* (240)
12.2 (40)	2.4 (8)	5.32 (1.20)	4.83 (1.09)	4.84 (1.09)	7.52 (1.69)	5.04 (1.13)	5.04 (1.13)	7.74 (1.74)	5.09 (1.14)	5.09 (1.14)	7.79 (1.75)	5.10 (1.15)	5.10 (1.15)	7.80 (1.75)	5.10 (1.15)	5.11 (1.15)	7.80 (1.75)
	4.9 (16)	3.81 (0.86)	3.60 (0.81)	3.61 (0.81)	5.32 (1.20)	3.73 (0.84)	3.73 (0.84)	5.44 (1.22)	3.75 (0.84)	3.76 (0.84)	5.47 (1.23)	3.76 (0.85)	3.77 (0.85)	5.48 (1.23)	3.77 (0.85)	3.77 (0.85)	5.48 (1.23)
9.8 (32)	2.4 (8)	5.32 (1.20)	4.83 (1.09)	4.84 (1.09)	7.52 (1.69)	5.03 (1.13)	5.04 (1.13)	7.73 (1.74)	5.08 (1.14)	5.09 (1.14)	7.78 (1.75)	5.09 (1.15)	5.10 (1.15)	7.79 (1.75)			
	4.9 (16)	3.81 (0.86)	3.60 (0.81)	3.61 (0.81)	5.32 (1.20)	3.73 (0.84)	3.73 (0.84)	5.44 (1.22)	3.75 (0.84)	3.75 (0.84)	5.46 (1.23)	3.76 (0.84)	3.76 (0.85)	5.47 (1.23)			
7.3 (24)	2.4 (8)	5.31 (1.19)	4.82 (1.08)	4.83 (1.09)	7.51 (1.69)	5.02 (1.13)	5.03 (1.13)	7.76 (1.74)	5.07 (1.14)	5.08 (1.14)	7.75 (1.74)						
6.1 (20)	2.4 (8)	5.30 (1.19)	4.82 (1.08)	4.83 (1.09)	7.49 (1.68)	5.02 (1.13)	5.02 (1.13)	7.69 (1.73)	5.05 (1.14)								
4.9 (16)	2.4 (8)	5.29 (1.19)	4.81 (1.08)	4.82 (1.08)	7.47 (1.68)	4.99 (1.12)	5.00 (1.12)	7.63 (1.71)									
	4.9 (16)	3.78 (0.85)	3.59 (0.81)	3.60 (0.81)	5.29 (1.19)	3.70 (0.83)	3.71 (0.83)	5.38 (1.21)									
2.4 (8)	2.4 (8)	5.14 (1.16)	4.69 (1.05)	4.70 (1.06)	7.14 (1.61)												
	4.9 (16)	4.00 (0.90)	3.75 (0.84)	3.76 (0.85)	5.49 (1.23)												
1.2 (4)	2.4 (8)	4.70 (1.06)	4.35 (0.98)														
	4.9 (16)	3.50 (0.79)	3.44 (0.77)														
0.9[1] (2)	2.4 (8)	3.68 (0.83)	3.11 (0.70)														
0.6[1] (2)	2.4 (8)	2.55 (0.57)	2.36 (0.53)														

SYM.

*:Indicates studs where sheathing panels meet.

[1]Distance between reactions is 30 cm (12 in).

Table B.2: Maximum Absolute Vertical Force at Reactions for Wall Models Without Openings Subjected to Monotonic Loading – kN (kips)

Wall Length m (ft)	Wall Height m (ft)	Distance from End Chord: cm (in)															
		0 (0)	41 (16)	81 (32)	122* (48)	163 (64)	203 (80)	244* (96)	284 (112)	325 (128)	366* (144)	406 (160)	447 (176)	488* (192)	528 (208)	569 (224)	610* (240)
12.2 (40)	2.4 (8)	31.50 (7.08)	15.13 (3.40)	14.57 (3.23)	0.34 (0.08)	14.22 (3.20)	14.23 (3.20)	0.10 (0.02)	14.19 (3.19)	14.19 (3.19)	0.03 (0.00)	14.19 (3.19)	14.19 (3.19)	0.01 (0.00)	14.19 (3.19)	14.19 (3.19)	0.01 (0.00)
	4.9 (16)	50.90 (11.44)	14.19 (3.19)	13.21 (2.97)	0.51 (0.12)	13.20 (2.97)	13.19 (2.97)	0.06 (0.01)	13.15 (2.96)	13.15 (2.96)	0.02 (0.00)	13.14 (2.95)	13.14 (2.95)	0.01 (0.00)	13.14 (2.95)	13.13 (2.95)	0.01 (0.00)
9.8 (32)	2.4 (8)	31.35 (7.07)	15.12 (3.40)	14.56 (3.27)	0.34 (0.08)	14.21 (3.19)	14.22 (3.20)	0.10 (0.02)	14.19 (3.19)	14.19 (3.19)	0.03 (0.01)	14.19 (3.19)	14.18 (3.19)	0.01 (0.00)			
	4.9 (16)	50.88 (11.44)	14.18 (3.19)	13.21 (2.97)	0.52 (0.12)	13.19 (-2.97)	13.18 (2.96)	0.06 (0.01)	13.14 (2.95)	13.15 (2.96)	0.02 (0.00)	13.14 (2.95)	13.13 (2.95)	0.01 (0.00)			
7.3 (24)	2.4 (8)	31.42 (7.06)	15.11 (3.40)	14.55 (3.27)	0.34 (0.08)	14.20 (3.19)	14.21 (3.19)	0.10 (0.02)	14.18 (3.19)	14.17 (3.19)	0.01 (0.00)						
6.1 (20)	2.4 (8)	31.38 (7.06)	15.10 (3.39)	14.54 (3.27)	0.34 (0.08)	14.19 (3.19)	14.20 (3.19)	0.08 (0.02)	14.17 (3.19)								
4.9 (16)	2.4 (8)	31.33 (7.04)	15.08 (3.39)	14.52 (3.26)	0.31 (0.07)	14.18 (3.19)	14.18 (3.19)	0.01 (0.00)									
	4.9 (16)	50.80 (11.42)	14.16 (3.18)	13.17 (2.96)	0.56 (0.13)	13.18 (2.96)	13.16 (2.96)	0.01 (0.00)									
2.4 (8)	2.4 (8)	31.22 (7.02)	15.05 (3.38)	14.48 (3.25)	0.01 (0.00)												
	4.9 (16)	54.90 (12.34)	15.34 (3.45)	15.04 (3.38)	0.01 (0.00)												
1.2 (4)	2.4 (8)	31.32 (7.04)	15.31 (3.44)														
	4.9 (16)	54.88 (12.34)	15.49 (3.48)														
0.9[1] (2)	2.4 (8)	32.03 (7.20)	13.34 (2.99)														
0.6[1] (2)	2.4 (8)	30.13 (6.77)	0.01 (0.00)														

SYM.

*:Indicates studs where sheathing panels meet.

[1]Distance between reactions is 30 cm (12 in).

Table B.3: Maximum Absolute Horizontal Force at Reactions for Wall Models Without Openings Subjected to Seismic Loading – kN (kips)

Wall		Distance from End Chord: cm (in)															
Length	Height																
m (ft)	m (ft)	0 (0)	41 (16)	81 (32)	122* (48)	163 (64)	203 (80)	244* (96)	284 (112)	325 (128)	366* (144)	406 (160)	447 (176)	488* (192)	528 (208)	569 (224)	610* (240)
12.2 (40)	2.4 (8)	5.88 (1.32)	5.73 (1.29)	5.74 (1.29)	8.61 (1.94)	5.96 (1.34)	5.97 (1.34)	8.82 (1.98)	6.00 (1.35)	6.01 (1.35)	8.87 (2.00)	6.01 (1.35)	6.02 (1.35)	8.88 (2.00)	6.02 (1.35)	6.03 (1.36)	8.88 (2.00)
	4.9 (16)	5.25 (1.18)	5.27 (1.19)	5.29 (1.19)	7.81 (1.76)	5.47 (1.23)	5.47 (1.23)	7.98 (1.79)	5.51 (1.24)	5.52 (1.24)	8.02 (1.81)	5.52 (1.24)	5.53 (1.24)	8.04 (1.81)	5.53 (1.24)	5.54 (1.25)	8.04 (1.81)
9.8 (32)	2.4.8 (8)	5.89 (1.33)	5.75 (1.29)	5.76 (1.30)	8.63 (1.94)	5.96 (1.34)	5.97 (1.34)	8.82 (1.99)	6.02 (1.35)	6.03 (1.36)	8.88 (2.00)	6.03 (1.36)	6.04 (1.36)	8.89 (2.00)			
	4.9 (16)	5.24 (1.18)	5.25 (1.18)	5.27 (1.19)	7.76 (1.75)	5.46 (1.23)	5.47 (1.23)	7.95 (1.79)	5.51 (1.24)	5.51 (1.24)	8.01 (1.80)	5.52 (1.24)	5.52 (1.24)	8.02 (1.80)			
7.3 (24)	2.4 (8)	5.90 (1.33)	5.75 (1.29)	5.77 (1.30)	8.61 (1.94)	5.97 (1.34)	5.98 (1.35)	8.85 (1.99)	6.02 (1.36)	6.03 (1.36)	8.91 (2.00)						
6.1 (20)	2.4 (8)	5.89 (1.32)	5.74 (1.29)	5.75 (1.29)	8.62 (1.94)	5.95 (1.34)	5.96 (1.34)	8.79 (1.98)	5.99 (1.35)								
4.9 (16)	2.4 (8)	5.88 (1.32)	5.74 (1.29)	5.75 (1.29)	8.57 (1.93)	5.94 (1.34)	5.95 (1.34)	8.77 (1.97)									
	4.9 (16)	5.24 (1.18)	5.25 (1.18)	5.27 (1.19)	7.75 (1.74)	5.45 (1.23)	5.45 (1.23)	7.91 (1.78)									
2.4 (8)	2.4 (8)	5.79 (1.30)	5.67 (1.28)	5.67 (1.28)	8.31 (1.87)												
	4.9 (16)	5.10 (1.15)	5.18 (1.16)	5.20 (1.17)	7.45 (1.68)												
1.2 (4)	2.4 (8)	5.42 (1.22)	5.38 (1.21)														
	4.9 (16)	4.75 (1.07)	4.84 (1.09)														
0.9[1] (2)	2.4 (8)	4.01 (0.90)	3.67 (0.83)														
0.6[1] (2)	2.4 (8)	3.33 (0.75)	3.53 (0.80)														

SYM.

*:Indicates studs where sheathing panels meet.

[1]Distance between reactions is 30 cm (12 in).

Table B.4: Maximum Absolute Vertical Force at Reactions for Wall Models Without Openings Subjected to Seismic Loading – kN (kips)

Wall Length m (ft)	Wall Height m (ft)	Distance from End Chord: cm (in)															
		0 (0)	41 (16)	81 (32)	122* (48)	163 (64)	203 (80)	244* (96)	284 (112)	325 (128)	366* (144)	406 (160)	447 (176)	488* (192)	528 (208)	569 (224)	610* (240)
12.2 (40)	2.4 (8)	36.77 (8.27)	18.14 (4.08)	17.47 (3.93)	2.52 (0.57)	17.04 (3.83)	16.89 (3.80)	1.89 (0.42)	16.84 (3.79)	16.86 (3.79)	1.22 (0.27)	16.88 (3.80)	16.80 (3.78)	2.71 (0.61)	16.84 (3.79)	16.78 (3.77)	2.83 (0.64)
	4.9 (16)	69.31 (15.59)	20.01 (4.50)	15.86 (3.57)	4.69 (1.05)	16.55 (3.72)	16.05 (3.61)	4.31 (0.97)	16.16 (3.64)	16.35 (3.68)	4.27 (0.96)	16.01 (3.60)	16.19 (3.64)	3.78 (0.85)	16.16 (3.64)	16.20 (3.64)	3.93 (0.88)
9.8 (32)	2.4 (8)	36.69 (8.26)	18.10 (4.07)	17.55 (3.95)	3.24 (0.73)	16.93 (3.81)	16.95 (3.81)	3.30 (0.74)	16.82 (3.79)	16.89 (3.80)	2.71 (0.61)	16.82 (3.79)	16.84 (3.79)	3.01 (0.68)			
	4.9 (16)	69.10 (15.55)	19.93 (4.48)	15.85 (3.57)	4.49 (1.04)	16.59 (3.73)	16.29 (3.67)	4.28 (0.96)	16.25 (3.66)	16.43 (3.70)	4.10 (0.92)	16.06 (3.61)	16.26 (3.66)	3.92 (0.88)			
7.3 (24)	2.4 (8)	36.70 (8.26)	18.11 (4.07)	17.55 (3.95)	3.00 (0.67)	16.95 (3.81)	16.95 (3.81)	5.15 (1.16)	16.79 (3.78)	16.94 (3.81)	3.51 (0.79)						
6.1 (20)	2.4 (8)	37.52 (8.44)	18.12 (4.08)	17.28 (3.89)	2.74 (0.62)	16.93 (3.81)	17.00 (3.83)	3.30 (0.74)	16.80 (3.78)								
4.9 (16)	2.4 (8)	37.35 (8.40)	18.12 (4.08)	17.34 (3.90)	4.70 (1.06)	16.98 (3.82)	17.05 (3.84)	4.15 (0.93)									
	4.9 (16)	70.19 (15.79)	20.34 (4.58)	16.03 (3.61)	4.69 (1.05)	16.89 (3.80)	16.39 (3.69)	4.10 (0.92)									
2.4 (8)	2.4 (8)	37.87 (8.52)	18.58 (4.18)	17.59 (3.96)	3.38 (0.76)												
	4.9 (16)	69.65 (15.67)	20.25 (4.56)	15.91 (3.58)	4.11 (0.92)												
1.2 (4)	2.4 (8)	38.26 (8.61)	18.90 (4.25)														
	4.9 (16)	71.20 (16.02)	19.31 (4.35)														
0.9[1] (2)	2.4 (8)	36.64 (8.24)	16.07 (3.61)														
0.6[1] (2)	2.4 (8)	30.81 (6.93)	1.97 (0.44)														

SYM.

*:Indicates studs where sheathing panels meet.

[1]Distance between reactions is 30 cm (12 in).

Table B.5: Maximum Horizontal Force at Reactions for Wall Models With Openings Subjected to Monotonic Loading – kN (kips)

	Wall Height m (ft)	Wall Length m (ft)	Distance from End Chord: cm (in) 0 (0)	41 (16)	81 (32)	122* (48)	163 (64)	203 (80)	244* (96)	284 (112)	325 (128)	366* (144)	406 (160)	447 (176)	488* (192)	528 (208)	569 (224)
Window	2.4 (8)	6.1 (20)	1.92 (0.43)	2.26 (0.51)	2.10 (0.47)	4.70# (1.06)	4.38 (0.99)	4.37 (0.98)	6.61# (1.49)	4.51 (1.02)	4.27 (0.96)	6.93 (1.56)	4.72 (1.06)	4.73 (1.06)	7.18 (1.62)	4.73 (1.06)	4.74 (1.07)
		4.9 (16)	2.09 (0.47)	2.35 (0.53)	2.35 (0.53)	3.13# (0.70)	1.61 (0.36)	1.61 (0.36)	2.28 (0.51)	1.62 (0.36)	1.62 (0.37)	4.44# (1.00)	3.98 (0.90)	3.99 (0.90)	6.28 (1.41)	4.49 (1.01)	4.50 (1.01)
		3.7 (12)	3.56 (0.80)	3.62 (0.81)	3.62 (0.81)	4.41# (0.99)	1.75 (0.39)	1.77 (0.40)	2.64 (0.59)	1.90 (0.43)	1.90 (0.43)	2.65 (0.60)	1.78 (0.40)	1.76 (0.40)	4.62# (1.04)	4.04 (0.91)	4.05 (0.91)
		2.4 (8)	3.70 (0.83)	3.69 (0.83)	3.70 (0.83)	4.12# (0.93)	1.32 (0.30)	1.35 (0.30)	2.02 (0.45)	1.47 (0.33)	1.47 (0.33)	2.09 (0.47)	1.47 (0.33)	1.47 (0.33)	2.02 (0.45)	1.35 (0.30)	1.33 (0.30)
Door	2.4 (8)	6.1 (20)	3.29 (0.74)	3.30 (0.74)	3.31 (0.74)	2.55# (0.57)			2.60# (0.59)	3.38 (0.76)	3.38 (0.76)	4.91 (1.10)	3.41 (0.77)	3.42 (0.77)	4.91 (1.11)	3.38 (0.76)	3.38 (0.76)
	2.4 (8)	4.9 (16)	3.25 (0.73)	3.27 (0.74)	3.28 (0.74)	2.52# (0.57)						2.54# (0.57)	3.31 (0.74)	3.31 (0.75)	4.79 (1.08)	3.34 (0.75)	3.34 (0.75)
	4.9 (16)	4.9 (16)	3.92 (0.88)	3.79 (0.85)	3.79 (0.85)	3.93# (0.88)						3.87# (0.87)	3.71 (0.84)	3.72 (0.84)	5.43 (1.22)	3.88 (0.87)	3.88 (0.87)
	2.4 (8)	3.7 (12)	3.51 (0.79)	3.47 (0.78)	3.48 (0.78)	2.70# (0.61)									2.72# (0.61)	3.51 (0.79)	3.51 (0.79)
	4.9 (16)	3.7 (12)	3.49 (0.79)	3.44 (0.77)	3.45 (0.78)	3.50# (0.79)									3.59# (0.81)	3.52 (0.79)	3.53 (0.79)
	2.4 (8)	2.4 (8)	4.45 (1.00)	4.42 (0.99)	4.43 (1.00)	2.99# (0.67)											
	4.9 (16)	2.4 (8)	3.09 (0.69)	3.13 (0.70)	3.13 (0.70)	3.09# (0.70)											

*:Indicates studs where sheathing panels meet.
#:Indicates location of studs adjacent to openings for walls with window openings

	Wall Height m (ft)	Wall Length m (ft)	610* (240)	650 (256)	691 (272)	732 (288)
Window	2.4 (8)	6.1 (20)	7.18 (1.62)	4.73 (1.06)	4.73 (1.06)	5.17 (1.16)
		4.9 (16)	6.78 (1.53)	4.46 (1.00)	4.46 (1.00)	4.81 (1.08)
		3.7 (12)	6.30 (1.42)	4.40 (0.99)	4.40 (0.99)	4.72 (1.06)
		2.4 (8)	4.12# (0.93)	3.69 (0.83)	3.70 (0.83)	3.71 (0.83)
Door	2.4 (8)	6.1 (20)	4.78 (1.08)	3.25 (0.73)	3.24 (0.73)	3.22 (0.72)
	2.4 (8)	4.9 (16)	4.72 (1.06)	3.21 (0.72)	3.21 (0.72)	3.17 (0.71)
	4.9 (16)	4.9 (16)	5.69 (1.28)	3.82 (0.86)	3.82 (0.86)	4.03 (0.91)
	2.4 (8)	3.7 (12)	5.07 (1.14)	3.46 (0.78)	3.45 (0.78)	3.49 (0.79)
	4.9 (16)	3.7 (12)	5.20 (1.17)	3.61 (0.81)	3.61 (0.81)	3.74 (0.84)
	2.4 (8)	2.4 (8)	2.98# (0.67)	4.43 (1.00)	4.43 (1.00)	4.46 (1.00)
	4.9 (16)	2.4 (8)	3.21# (0.72)	3.23 (0.73)	3.23 (0.73)	3.22 (0.72)

Table B.6: Maximum Absolute Vertical Force at Reactions for Wall Models With Openings Subjected to Monotonic Loading – kN (kips)

	Wall Height m (ft)	Wall Length m (ft)	Distance from End Chord: cm (in) 0 (0)	41 (16)	81 (32)	122* (48)	163 (64)	203 (80)	244* (96)	284 (112)	325 (128)	366* (144)	406 (160)	447 (176)	488* (192)	528 (208)	569 (224)
Window	2.4 (8)	6.1 (20)	21.78 (4.90)	9.20 (2.07)	12.86 (2.89)	8.66# (1.95)	5.83 (1.31)	5.86 (1.32)	5.03# (1.13)	17.33 (3.90)	8.62 (1.94)	1.54 (0.35)	13.52 (3.04)	13.57 (3.05)	0.06 (0.01)	13.53 (3.04)	13.53 (3.05)
		4.9 (16)	20.30 (4.57)	8.94 (2.01)	9.38 (2.11)	10.15# (2.28)	1.27 (0.29)	1.20 (0.27)	0.08 (0.02)	1.30 (0.29)	0.85 (0.19)	23.76# (5.35)	15.32 (3.45)	14.28 (3.21)	0.79 (0.18)	13.61 (3.06)	13.65 (3.07)
		3.7 (12)	31.80 (7.15)	15.56 (3.50)	16.10 (3.62)	24.88# (5.60)	1.00 (0.22)	1.45 (0.33)	0.15 (0.03)	1.40 (0.32)	1.40 (0.32)	0.15 (0.03)	1.45 (0.33)	1.00 (0.22)	24.18# (5.44)	15.71 (3.54)	14.59 (3.28)
		2.4 (8)	33.06 (7.44)	15.96 (3.59)	16.62 (3.74)	27.70# (6.23)	0.68 (0.15)	1.11 (0.25)	0.11 (0.02)	1.04 (0.23)	1.03 (0.23)	0.00 (0.00)	1.04 (0.23)	1.03 (0.23)	0.11 (0.03)	1.11 (0.25)	0.68 (0.15)
Door	2.4 (8)	6.1 (20)	20.74 (4.67)	9.37 (2.11)	9.94 (2.24)	16.94# (3.81)			16.73# (3.76)	9.68 (2.18)	8.59 (1.93)	0.20 (0.05)	8.33 (1.87)	8.33 (1.87)	0.04 (0.01)	8.30 (1.87)	8.29 (1.87)
	2.4 (8)	4.9 (16)	20.26 (4.56)	8.93 (2.01)	9.49 (2.14)	17.77# (4.00)						17.53# (3.94)	9.26 (2.08)	8.14 (1.83)	0.23 (0.05)	7.88 (1.77)	7.88 (1.77)
	4.9 (16)	4.9 (16)	47.31 (10.64)	12.74 (2.87)	13.37 (3.01)	33.76# (7.60)						39.58# (8.91)	12.15 (2.73)	11.64 (2.62)	2.56 (0.58)	12.77 (2.87)	17.23 (3.88)
	2.4 (8)	3.7 (12)	21.14 (4.76)	9.85 (2.22)	10.36 (2.33)	19.17# (4.31)									18.95# (4.26)	10.14 (2.28)	9.09 (2.05)
	4.9 (16)	3.7 (12)	39.62 (8.91)	11.43 (2.57)	10.01 (2.25)	34.41# (7.74)									36.06# (8.11)	10.85 (2.44)	8.30 (1.87)
	2.4 (8)	2.4 (8)	24.47 (5.51)	11.97 (2.69)	13.14 (2.96)	21.31# (4.80)											
	4.9 (16)	2.4 (8)	34.29 (7.71)	9.19 (2.07)	8.29 (1.87)	30.57# (6.88)											

*:Indicates studs where sheathing panels meet.
#:Indicates location of studs adjacent to openings for walls with window openings

	Wall Height m (ft)	Wall Length m (ft)	610* (240)	650 (256)	691 (272)	732 (288)
Window	2.4 (8)	6.1 (20)	0.04 (0.01)	13.70 (3.08)	14.23 (3.20)	28.70 (6.46)
		4.9 (16)	0.02 (0.00)	13.86 (3.12)	14.39 (3.24)	29.18 (6.57)
		3.7 (12)	0.55 (0.12)	14.24 (3.21)	14.81 (3.33)	30.56 (6.88)
		2.4 (8)	27.68# (6.23)	16.63 (3.74)	15.95 (3.59)	33.07 (7.44)
Door	2.4 (8)	6.1 (20)	0.12 (0.03)	8.50 (1.91)	8.99 (2.02)	20.44 (4.60)
	2.4 (8)	4.9 (16)	0.07 (0.01)	8.00 (1.80)	8.53 (1.92)	19.91 (4.48)
	4.9 (16)	4.9 (16)	12.52 (2.82)	1.36 (0.30)	12.24 (2.75)	27.95 (6.29)
	2.4 (8)	3.7 (12)	0.13 (0.03)	8.98 (2.02)	9.45 (2.13)	20.89 (4.70)
	4.9 (16)	3.7 (12)	0.18 (0.04)	7.67 (1.73)	12.29 (2.77)	40.77 (9.17)
	2.4 (8)	2.4 (8)	21.31# (4.80)	13.14 (2.96)	11.97 (2.69)	24.48 (5.51)
	4.9 (16)	2.4 (8)	29.86# (6.72)	8.08 (1.82)	9.36 (2.10)	33.05 (7.44)

Table B.7: Maximum Absolute Horizontal Force at Reactions for Wall Models With Openings Subjected to Seismic Loading – kN (kips)

	Wall Height m (ft)	Wall Length m (ft)	Distance from End Chord: cm (in) 0 (0)	41 (16)	81 (32)	122* (48)	163 (64)	203 (80)	244* (96)	284 (112)	325 (128)	366* (144)	406 (160)	447 (176)	488* (192)	528 (208)	569 (224)
Window	2.4 (8)	6.1 (20)	3.82 (0.86)	4.26 (0.96)	4.34 (0.98)	7.59# (1.71)	5.60 (1.26)	5.67 (1.28)	8.88# (2.00)	5.78 (1.30)	5.78 (1.30)	8.78 (1.98)	6.17 (1.39)	6.17 (1.39)	9.17 (2.06)	6.22 (1.40)	6.24 (1.40)
		4.9 (16)	3.45 (0.78)	4.19 (0.94)	3.89 (0.87)	6.76# (1.52)	4.56 (1.03)	4.59 (1.03)	6.37 (1.43)	4.29 (0.96)	4.26 (0.96)	7.71# (1.74)	5.68 (1.28)	5.69 (1.28)	8.71 (1.96)	6.21 (1.40)	6.21 (1.40)
		3.7 (12)	3.08 (0.69)	3.52 (0.79)	3.54 (0.80)	5.92# (1.33)	3.57 (0.80)	3.64 (0.82)	4.80 (1.08)	3.13 (0.70)	3.11 (0.70)	4.33 (0.97)	2.99 (0.67)	2.99 (0.67)	6.67# (1.50)	5.53 (1.24)	5.55 (1.25)
		2.4 (8)	5.49 (1.24)	5.52 (1.24)	5.52 (1.24)	6.40# (1.44)	2.45 (0.55)	2.45 (0.55)	3.45 (0.78)	2.43 (0.55)	2.45 (0.55)	3.61 (0.81)	2.69 (0.60)	2.72 (0.61)	4.36 (0.98)	3.42 (0.77)	3.32 (0.75)
Door	2.4 (8)	6.1 (20)	6.56 (1.47)	6.24 (1.40)	6.25 (1.41)	4.96# (1.12)			5.05# (1.14)	6.37 (1.43)	6.39 (1.44)	9.61 (2.16)	6.44 (1.45)	6.46 (1.45)	9.63 (2.17)	6.40 (1.44)	6.40 (1.44)
	2.4 (8)	4.9 (16)	6.61 (1.49)	6.28 (1.41)	6.30 (1.42)	5.00# (1.12)						5.04# (1.13)	6.34 (1.43)	6.35 (1.43)	9.51 (2.14)	6.39 (1.44)	6.39 (1.44)
	4.9 (16)	4.9 (16)	4.51 (1.01)	3.87 (0.87)	3.58 (0.81)	3.47# (0.78)						3.41# (0.77)	3.07 (0.69)	3.88 (0.87)	5.45 (1.23)	3.70 (0.83)	3.70 (0.83)
	2.4 (8)	3.7 (12)	6.68 (1.50)	6.33 (1.42)	6.33 (1.42)	5.02# (1.13)									5.06# (1.14)	6.37 (1.43)	6.38 (1.44)
	4.9 (16)	3.7 (12)	4.88 (1.10)	4.50 (1.01)	4.50 (1.01)	4.89# (1.10)									5.02# (1.13)	4.61 (1.04)	4.62 (1.04)
	2.4 (8)	2.4 (8)	7.06 (1.59)	6.59 (1.48)	6.60 (1.48)	5.28# (1.19)											
	4.9 (16)	2.4 (8)	5.21 (1.17)	4.77 (1.07)	4.78 (1.07)	5.25# (1.18)											

*:Indicates studs where sheathing panels meet.
#:Indicates location of studs adjacent to openings for walls with window openings

	Wall Height m (ft)	Wall Length m (ft)	610* (240)	650 (256)	691 (272)	732 (288)
Window	2.4 (8)	6.1 (20)	9.13 (2.06)	6.12 (1.38)	6.13 (1.38)	6.41 (1.44)
		4.9 (16)	9.21 (2.07)	6.19 (1.39)	6.19 (1.39)	6.49 (1.46)
		3.7 (12)	8.43 (1.90)	6.00 (1.35)	6.00 (1.35)	6.18 (1.39)
		2.4 (8)	5.44# (1.22)	2.75 (0.62)	2.70 (0.61)	2.32 (0.52)
Door	2.4 (8)	6.1 (20)	9.33 (2.10)	6.15 (1.38)	6.15 (1.38)	6.45 (1.45)
	2.4 (8)	4.9 (16)	9.35 (2.10)	6.18 (1.39)	6.18 (1.39)	6.50 (1.46)
	4.9 (16)	4.9 (16)	6.63 (1.49)	4.33 (0.98)	4.33 (0.97)	4.66 (1.05)
	2.4 (8)	3.7 (12)	9.45 (2.13)	6.30 (1.42)	6.29 (1.42)	6.67 (1.50)
	4.9 (16)	3.7 (12)	7.03 (1.58)	4.61 (1.04)	4.60 (1.04)	5.03 (1.13)
	2.4 (8)	2.4 (8)	5.26# (1.18)	6.59 (1.48)	6.59 (1.48)	7.06 (1.59)
	4.9 (16)	2.4 (8)	5.20# (1.17)	4.76 (1.07)	4.77 (1.07)	5.22 (1.18)

Table B.8: Maximum Absolute Vertical Force at Reactions for Wall Models With Openings Subjected to Seismic Loading – kN (kips)

	Wall Height m (ft)	Wall Length m (ft)	Distance from End Chord: cm (in) 0 (0)	41 (16)	81 (32)	122* (48)	163 (64)	203 (80)	244* (96)	284 (112)	325 (128)	366* (144)	406 (160)	447 (176)	488* (192)	528 (208)	569 (224)
Window	2.4 (8)	6.1 (20)	40.44 (9.10)	20.81 (4.68)	20.94 (4.71)	25.69# (5.78)	4.97 (1.12)	4.97 (1.12)	22.39# (5.04)	20.48 (4.61)	19.57 (4.40)	2.84 (0.64)	18.29 (4.12)	18.52 (4.17)	4.10 (0.92)	18.18 (4.09)	18.18 (4.09)
		4.9 (16)	44.13 (9.93)	21.87 (4.92)	22.01 (4.95)	32.14# (7.23)	3.79 (0.85)	4.07 (0.92)	5.88 (1.32)	3.17 (0.71)	2.83 (0.64)	27.39# (6.16)	21.03 (4.73)	20.46 (4.60)	3.98 (0.89)	18.84 (4.24)	18.88 (4.25)
		3.7 (12)	41.63 (9.37)	21.83 (4.91)	22.29 (5.02)	31.53# (7.09)	2.74 (0.62)	3.05 (0.69)	4.58 (1.03)	2.13 (0.48)	2.12 (0.48)	3.70 (0.83)	2.27 (0.51)	1.86 (0.42)	30.02# (6.75)	21.29 (4.79)	20.29 (4.57)
		2.4 (8)	41.84 (9.41)	22.69 (5.11)	22.76 (5.12)	34.36# (7.73)	1.58 (0.35)	1.81 (0.41)	2.46 (0.55)	1.70 (0.38)	1.69 (0.38)	2.47 (0.56)	1.78 (0.40)	1.80 (0.40)	2.73 (0.61)	2.93 (0.66)	2.71 (0.61)
Door	2.4 (8)	6.1 (20)	40.67 (9.15)	21.64 (4.87)	21.57 (4.85)	33.69# (7.58)			28.99# (6.52)	21.40 (4.82)	19.73 (4.44)	10.97 (2.47)	18.83 (4.24)	18.66 (4.20)	9.39 (2.11)	18.60 (4.19)	18.43 (4.15)
	2.4 (8)	4.9 (16)	43.84 (9.86)	21.35 (4.80)	21.72 (4.89)	37.09# (8.34)						32.13# (7.23)	21.47 (4.83)	19.79 (4.45)	10.89 (2.45)	18.40 (4.14)	18.45 (4.15)
	4.9 (16)	4.9 (16)	50.62 (11.39)	14.77 (3.32)	12.98 (2.92)	41.73# (9.39)						37.51# (8.44)	12.90 (2.90)	14.16 (3.19)	6.38 (1.43)	14.92 (3.36)	14.77 (3.32)
	2.4 (8)	3.7 (12)	40.34 (9.08)	20.28 (4.56)	21.87 (4.92)	37.76# (8.50)									34.32# (7.72)	20.98 (4.72)	19.13 (4.30)
	4.9 (16)	3.7 (12)	53.13 (11.95)	15.22 (3.43)	12.99 (2.92)	46.25# (10.41)									41.36# (9.31)	13.15 (2.96)	15.11 (3.40)
	2.4 (8)	2.4 (8)	40.59 (9.13)	21.56 (4.85)	22.40 (5.04)	37.60# (8.46)											
	4.9 (16)	2.4 (8)	55.14 (12.41)	15.19 (3.42)	12.81 (2.88)	49.60# (11.16)											

*:Indicates studs where sheathing panels meet.
#:Indicates location of studs adjacent to openings for walls with window openings.

	Wall Height m (ft)	Wall Length m (ft)	610* (240)	650 (256)	691 (272)	732 (288)
Window	2.4 (8)	6.1 (20)	4.44 (1.00)	18.58 (4.18)	19.40 (4.37)	39.26 (8.83)
		4.9 (16)	2.76 (0.62)	19.42 (4.37)	19.92 (4.48)	43.76 (9.85)
		3.7 (12)	4.55 (1.02)	19.56 (4.40)	19.95 (4.49)	40.71 (9.16)
		2.4 (8)	32.88# (7.40)	23.08 (5.19)	22.51 (5.06)	41.78 (9.40)
Door	2.4 (8)	6.1 (20)	9.64 (2.17)	19.20 (4.32)	19.84 (4.46)	40.19 (9.04)
	2.4 (8)	4.9 (16)	9.32 (2.10)	18.61 (4.19)	19.46 (4.38)	46.68 (10.50)
	4.9 (16)	4.9 (16)	7.79 (1.75)	14.78 (3.33)	15.74 (3.54)	53.00 (11.93)
	2.4 (8)	3.7 (12)	11.08 (2.49)	18.59 (4.18)	19.88 (4.47)	40.51 (9.12)
	4.9 (16)	3.7 (12)	7.93 (1.78)	15.28 (3.44)	16.02 (3.60)	54.74 (12.32)
	2.4 (8)	2.4 (8)	34.80# (7.83)	22.40 (5.04)	21.56 (4.85)	40.51 (9.11)
	4.9 (16)	2.4 (8)	44.34# (9.98)	12.94 (2.91)	15.27 (3.44)	55.31 (12.44)

Vita

Maurice Walter White was born July 12, 1967 in Harve de Grace, Maryland. He attended school in Aberdeen, Maryland and graduated from Aberdeen High School in the spring of 1985. The author then attended the University of Delaware, beginning in the summer of 1985, and graduated with a Bachelor's of Science degree in Civil Engineering from the University of Delaware in the spring of 1989. While at Delaware, he successfully completed the Engineer–in–Training (EIT) examination. The author began pursuit of a masters degree in Civil Engineering at Virginia Tech beginning in the fall of 1989, culminating with the acquisition of the degree in the spring of 1991. Research performed for the degree involved evaluation of the MicasPlus structural analysis and design software package. The author then began to pursue his doctorate degree at Virginia Tech during the summer of 1991, performing research in the area of wood structures.